Universidade Federal Do Rio Grande Do Sul
Escola de Engenharia
Programa de Pós-Graduação em Engenharia Civil: Construção e Infraestrutura

José da Silva Andrade Neto

HYDRATION AND INTERACTIONS BETWEEN C_3S AND C_3A POLYMORPHS IN THE PRESENCE OF DIFFERENT CALCIUM SULFATES

Porto Alegre
2021

JOSÉ DA SILVA ANDRADE NETO

HYDRATION AND INTERACTIONS BETWEEN C_3S AND C_3A POLYMORPHS IN THE PRESENCE OF DIFFERENT CALCIUM SULFATES

Master Dissertation presented to the Postgraduate Program in Civil Engineering: Construction and Infrastructure at the Universidade Federal do Rio Grande do Sul, as part of the requirements for obtaining the title of Master's in civil engineering

Prof. Ana Paula Kirchheim
Dr. for the Federal University of Rio Grande do Sul, Brazil
Supervisor

Prof. M. Ángeles Gómez de la Torre
PhD for the University of Malaga, Spain
Co-Supervisor

Porto Alegre
2021

JOSÉ DA SILVA ANDRADE NETO

HYDRATION AND INTERACTIONS BETWEEN C_3S AND C_3A POLYMORPHS IN THE PRESENCE OF DIFFERENT CALCIUM SULFATES

MASTER'S IN CIVIL ENGINEERING, research area Materials, and approved in its final form by the Supervisor Professor and the Postgraduate Program in Civil Engineering: Construction and Infrastructure at the Universidade Federal do Rio Grande do Sul.

Porto Alegre, June of 2021

Prof. Ana Paula Kirchheim
Dr. for the Federal University of Rio Grande do Sul, Brazil
Supervisor

Prof. M. Ángeles Gómez de la Torre
PhD for the University of Malaga, Spain

Co-Supervisor

Prof. Ângela de Moura Ferreira Danilevicz
Coordinator of PPGCI/UFRGS

BANCA EXAMINADORA

Prof. Denise C. C. Dal Molin (UFRGS)
Dr. by Universidade de São Paulo

Prof. Paulo J. M. Monteiro (UC-Berkeley)
PhD for University of California at Berkeley (United States)

Prof. Sandro Marden Torres (UFPB)
PhD for University of Leeds (England)

Prof. Erich D. Rodríguez (UFSM)
Dr. for Universitat Politécnica de Valência (Spain)

Porto Alegre

2021

I dedicate this work to my girlfriend, family, and
friends, for the support during this period

ACKNOWLEDGEMENTS

I would like to thank God for all the blessings in my life and in the lives of my family, especially in this difficult moment.

To my girlfriend, Natália, thank you for all the love, support, incentive, and understanding. Thank you for being my safe place, where I recover my strength to continue.

To my mom, Ana Karine, for all the love, care, incentive, and support. To my father, Marcos Brito, for all the advice, love, incentive, and support. To my sister Isabella, for all the love.

To my family, especially my grandfather, José Andrade, and my grandmothers, Irma Lemos and Edilce Figueira, for all the support, love, and to be my examples in life.

To Ana Cristina, Ronaldo, and Leonardo to be my family in Porto Alegre. Thank you for receiving me so well.

To my guinea pig, Stark, for the company, so important during the pandemic.

To my supervisor, Ana Paula Kirchheim. Thank you for the ideas, countless advice, knowledge, and willingness to help. Thank you for being this wonderful person, very kind, and comprehensive. Thank you for opening many doors, and for believing in me. I hope to be a fraction of a researcher/professor that you are one day.

To my supervisor, Angeles de la Torre. Thank you for receiving me so well in Malaga. Thank you for all the discussion and teaching moments, you were always very kind to me. It was my honor to have you as my supervisor.

To Paulo Monteiro, who kindly accepted to participate in the examination board and as co-author of some of the papers that are the basis of this dissertation. Thank you for the thorough correction and also for the kindly provided resources for the purchase of the pure phases used in this study.

To Sandro Torres thank you for receiving me so well in João Pessoa, and also for accepting to be an examiner for this dissertation, giving important advice, and bring important discussions.

To Erich Rodriguez, who is an example of a researcher for me. Thank you for having accepted to participate in the examination board of this dissertation and for all the guidance, shared knowledge, and (VERY!) detailed corrections.

To Denise Dal Molin for accepting to participate in the examination board, it is an honor. Thank you for the knowledge shared in your classes.

To Paulo de Matos, whom I had the pleasure to become a friend in the last months. Thank you for the valuable help with all the *in-situ* XRD and rheometry experiments and analysis. Without your collaboration, this study would not be the same. Thank you for sharing such enthusiasm with science, which is contagious and makes me want to work harder.

To Marlon Longhi to be a friend and also to be very helpful during all my dissertation, especially with the MAS-NMR analysis.

To Tiago, Henrique, Gessivaldo, Nilson, and Silas thank you for the friendship, and thanks for the many meetings on Zoom/Google Meetings, which were a relief throughout the Master's degree. Thanks for all the shared knowledge and to the partnership in several studies.

To the group LINCE for the valuable weekly meetings, in which great discussions on different topics in the cement area were raised, including some which were used in this study. Especially, thanks to Camila, Micael, Matheus, Py, Rayara, Paula, Vinicius, and Samile for the friendship and funny moments in the lab.

To Jéssica, Thaís, Aline, Thainá, Luis, and Marcelo for the friendship and the partnership on several works and study meetings for the master´s subjects.

To PPGCI/UFRGS and all Professors for the teaching and support. Thanks to the family NORIE/UFRGS for the pleasant atmosphere and moments of fraternization, which were very important to me.

To LEDMA/UFBA, especially Daniel Véras, Cleber Dias, and Paulo Sant'anna who were extremely helpful in my first steps in science.

To Professor Carlos Campos, from UFSC, for providing the infrastructure for the *in-situ* XRD, and for helping in its analysis and discussion. To Philippe Gleize from UFSC, for providing the infrastructure for the rheological analysis.

To the Cement Science group (CemSciG) at the University of Malaga (UMA) for receiving me so well during three months in Malaga. Thanks to Alejandro Morales Cantero for the help in the calorimetry and TGA tests, and to Laura León Reina, Ana Lucena, and María Dolores for the help with the XRD, NMR-MAS, and BET analyses.

To the Servicios Centrales de Apoyo a la Investigación (SCAI) at University of Malaga for the infrastructure.

To Fábio Mariz Maia Neto and Isaque Jerônimo Porto for receiving me so well in João Pessoa and for helping me with the SEM analyzes.

To Elizabeth Cimentos for the help with the preparation of the polished samples for the SEM-BSE analyzes.

To INTERCEMENT, especially to Seiiti Suzuki, for the several meetings with very important and enlightening discussion about cement.

To CAPES for the financial support [88882.439908/2019-01] during the Master's degree.

To junta de Andalucia research project for the research stage the at University of Malaga.

“We ourselves feel that what we are doing is just a drop in the ocean. But the ocean would be less because of that missing drop.”

Mother Teresa

ABSTRACT

ANDRADE NETO, J. S. **Hydration and interactions between C_3S and C_3A polymorphs in the presence of different calcium sulfates**. 2021. Dissertation (Master of Science in Civil Engineering) - Postgraduate Program in Civil Engineering: Construction and Infrastructure, Engineering School, Federal University of Rio Grande do Sul, Porto Alegre, 2021.

Calcium sulfate is an important constituent in Portland cement nowadays. It is used to control the setting time of Portland cement. However, many questions about the role of calcium sulfate on the cement phases (C_3A and C_3S) hydration and its mechanisms persist. A critical overview of the effect of sulfates on Portland cement hydration and properties is presented here in a review manuscript form. In this sense, several knowledge gaps, such as the influence of C_3S and C_3A polymorphs and the calcium sulfate composition on the sulfate balance in Portland cement, were identified. To address some of the questions identified in the review three different experimental studies were executed. The first one was focused to understand how gypsum accelerates the C_3S hydration and whether aluminum incorporated in its structure plays an essential role or not. The effects of gypsum on the hydration of C_3S and aluminum-doped C_3S (Al-C_3S) hydration were assessed. Calorimetry, XRD, TGA, and ^{27}Al and ^{29}Si MAS-NMR were performed to analyze gypsum's influence on the hydration of C_3S and Al-C_3S. The results showed that the inclusion of gypsum retarded the initial hydration (first 3 h) for both C_3S and Al-C_3S, due to the interaction between the sulfate ions and C_3S. In contrast, gypsum enhanced the hydration of both C_3S and Al-C_3S afterward. This acceleration effect occurred earlier for the Al-C_3S due to the removal of aluminum from the solution. However, this is not the main mechanism behind the acceleration of C_3S by gypsum, which mainly results from changes in C-S-H morphology and increases in the ionic strength. Secondly, the mechanism responsible for the higher reactivity of orthorhombic C_3A (ort-C_3A) in sulfate-containing solutions, compared with cubic C_3A (cb-C_3A), which was previously related to either the difference in crystal structure or the sodium in ort-C_3A pore solution were investigated. The hydration of cb-C_3A (in water and NaOH solution) and Na-doped ort-C_3A in the presence of gypsum and hemihydrate were analyzed using isothermal calorimetry, *in-situ* XRD, TGA, SEM, and rheological tests. The results showed that NaOH accelerated the hydration of cb-C_3A, but ort-C_3A still presented a higher hydration rate. Ort-C_3A pastes revealed more and larger ettringite crystals at 30-120 minutes, resulting in higher viscosities and yield stresses than cb-C_3A pastes. The replacement of gypsum with hemihydrate accelerated ort-C_3A hydration but retarded cb-C_3A hydration. Overall, the higher reactivity of ort-C_3A is related to differences in crystal structure rather than the sodium in pore solution. Finally, the hydration of three-phase systems (C_3S-C_3A-calcium sulfate) was analyzed. Two C_3S (T1 pure C_3S and M1 aluminum-doped C_3S), two C_3A polymorphs (cubic and orthorhombic), and two calcium sulfates (gypsum and hemihydrate) were evaluated. For each system, the hydration of four different SO_3 contents was evaluated by calorimetry. From the calorimetry results, a 1.5 wt.% SO_3 content was fixed, and the mixtures were evaluated by *in-situ* XRD and TGA. The C_3S type was the factor that most affected the sulfate balance of the systems. The mixes with Al-C_3S presented higher ettringite formation in the first hours, resulting in much earlier sulfate depletions when compared to the mixes with C_3S. The mixes with ort-C_3A also presented faster sulfate depletions, due to its higher reactivity compared with cb-C_3A. Finally, the replacement of gypsum by hemihydrate, also resulted in faster sulfate depletions, which is the consequence of the higher solubility of hemihydrate.

Keywords: Portland cement;C_3A; C_3S; Calcium sulfate; Hydration.

FIGURES

TABLES

LIST OF ABBREVIATIONS AND ACRONYMS

SCM: Supplementary Cementitious Materials

PC: Portland cement

PCE: Polycarboxylate-eter

NSF: Naphtalene sulfonate formaldehyde polycondensate

C-S-H: Calcium silicate hydrate

OH-AFm: Hydroxy-AFm

SO_4-AFm: calcium monosulfoaluminate

IC: Isothermal calorimetry

XRD: X-ray Diffraction

XRF: X-ray Fluorescence

TGA: Thermogravimetry analysis

DTG: Derivative thermogravimetry

NMR: Nuclear Magnetic Resonance

SEM: Scanning Electron Microscopy

cb-C_3A: Cubic tricalcium aluminate

ort-C_3A: Orthorhombic tricalcium aluminate

C_3S: Tricalcium silicate

Al-C_3S: Aluminum-doped Tricalcium silicate

GYP: Gypsum

HEM: Hemihydrate

SUMMARY

Chapter 1

Introduction

1 INTRODUCTION

This chapter presents the context and justification of the proposed theme, research objectives, limitations, and delimitations.

1.1 CONTEXT AND JUSTIFICATION

Portland cement (PC) is the most consumed building material worldwide, having been used for almost 200 years and the use of calcium sulfate (gypsum, hemihydrate, and/or anhydrite) to regulate the setting of the cement began at the end of the 19^{th} [1,2]. It is known that the calcium sulfate delays the tricalcium aluminate (C_3A) hydration, retarding the setting of the cement paste, providing a period in which the mixtures have fluidity and workability to be used.

The mechanism by which the calcium sulfate retards the C_3A hydration is still not fully understood. The early theories had related this delay with a barrier of ettringite [3,4] or a "gel-like" layer [5]. However, recent experimental evidence supports the theory that the retard is due to the adsorption of S ions and/or Ca-S ion pairs on the C_3A surface [6–10].

Depending on the alkali content incorporated in the C_3A crystalline structure during clinker production, two different polymorphs can be present: cubic or orthorhombic [11]. In studies conducted with pure clinker phases produced in laboratories, the calcium sulfate retards the hydration of cubic C_3A but is ineffective to retard the orthorhombic C_3A hydration [12,13]. The reason for this is not yet clear, but it is possibly associated with the greater solubility of the alumina rings in the orthorhombic C_3A structure [9,14] or with the presence of sodium ions in the solution, released in the dissolution of orthorhombic C_3A [15].

In addition, some industrial clinkers have more orthorhombic C_3A than cubic C_3A. However, usually they do not present problems of workability and reactivity, which would be expected due to the almost instantaneous reaction of the orthorhombic C_3A synthesized in the laboratory. The explanation for this may be associated with the presence of alkaline sulfates or the presence of alite, which will alter the composition of the aqueous solution, which seems to impact the reactivity of orthorhombic C_3A [9].

Calcium sulfate enhances the tricalcium silicate (C_3S) hydration and modifies the phase assemblage, influencing in the shrinkage and strength [16–19]. However, this is usually neglected, and few studies focus on that. The reason for this enhancement is poorly understood. Some theories related this with the formation of ettringite [18,20], from the reactions between the sulfate ions and the alumina which may be incorporated in the C_3S structure. Withal the calcium sulfate also enhances pure C_3S [19,21–24], where the formation of ettringite does not occur. Therefore, the enhancement of C_3S hydration by gypsum is probably a result of the interaction between this phase and C_3S and/or C-S-H, rather than interactions that involve the aluminates [19].

The amount of calcium sulfate is extremely important and influences the properties of cement. If the amount of calcium sulfate is too low, a hydroxy-AFm-type meta-stable product (C_4AH_{13} and C_2AH_8) is formed, which is subsequently converted to katoite ($Ca_2Al_2(OH)_{12}$ or C_3AH_6) [12,25,26]. The formation of these products leads to "Flash-set", *i.e.*, stiffening and loss of workability in few minutes, making most practical applications of Portland cement unfeasible [27]. Besides that, if the amount of sulfate is not enough to delay the C_3A hydration until after the main C_3S hydration peak, the C_3S hydration is inherited, lowering the mechanical performance at the early ages [19,20,28].

On the other hand, the excess of calcium sulfate can impair the workability due to the high amount of ettringite formed, besides lowering the mechanical strength [19,20]. In mortars and/or concretes submitted to high-temperature curing (above 70°C), the excess of calcium sulfate can also lead to the delayed ettringite formation (DEF), which is deleterious to the durability of the material [29,30].

There is an optimum calcium sulfate content for each clinker, which will result in the lowest shrinkage and porosity, and the highest mechanical performance, in addition to good workability and proper setting times. Thus, for a worthy performance of the cement, the optimum sulfate content must be known.

Many factors as clinker and the sulfate source characteristics, the presence of supplementary cementitious materials (SCMs) and admixture, the water/cement ratio, and temperature may influence the sulfate demand. Despite the great importance of this theme, as it has a considerable influence on cement properties, many open questions regarding the influence of some parameters on the optimum sulfate content still exist.

Among these factors, the C_3A and C_3S polymorphism/ions doping, which greatly influence on their hydration and in the hydration products formation rate, and the calcium sulfate type, which has different solubilities and will impact the supply rate of sulfate ions into the pore solution, need more explanation. Therefore, these factors probably will influence the sulfate balance of the system.

1.2 JUSTIFICATION

Inherent in Portland concrete and cement research, studies on Portland clinker are the basis for understanding and developing material properties through investigations, often of its structural elements and defects that influence its mechanical behavior and durability properties in the nano or micrometric scale.

During the clinker manufacturing process, depending on the composition of the raw material and the fuel, some ions can be incorporated into the crystalline structure of the clinker phases. In this sense, sodium (and potassium) is usually incorporated into the structure of C_3A and aluminum in the structure of C_3S, which alters the reactivity of these phases and, consequently, the hydration of Portland cement. However, it is not yet understood the mechanism of the change in the reactivity of these phases due to the incorporation of these ions. In addition, it is not known the impact of these changes in the sulfate demand of PC. Furthermore, during cement milling, gypsum ($CaSO_4 \cdot 2H_2O$) may dehydrate into hemihydrate ($CaSO_4 \cdot 1/2H_2O$) and/or soluble anhydrite ($CaSO_4$), which are much more soluble than gypsum or natural anhydrite. This changes the rate of sulfates supply into the solution, accelerating the ettringite formation. However, there is a lack of studies regarding the impact of different calcium sulfate types on the hydration of C_3A and C_3S polymorphs and its impact on the sulfate demand of PC.

The correct understanding of these ions influence on the optimization of sulfates is essential to ensure that the cements meet the performance requirements. In this sense, the proposed research aims to determine the influence of the incorporation of aluminum in C_3S and sodium in C_3A in their hydration in the presence of calcium sulfate. In addition, it will be analyzed how the incorporation of these ions influences the sulfate balance, from the analysis of C_3S-C_3A mixtures (92% C_3S and 8% C_3A) hydration with different amounts of gypsum/hemihydrate. This understanding will assist in determining the

optimum sulfate content, avoiding cements with inadequate quantities that can cause problems of setting and workability, low mechanical resistance, and DEF.

1.3 RESEARCH OBJECTIVES

The general objective of the research is to evaluate the hydration and interactions between C_3S and C_3A polymorphs in the presence of different calcium sulfates.

The secondary research objectives are:

a) To present a review of the state-of-the-art of sulfate optimization.

b) To evaluate the effect of gypsum on the C_3S and Al-doped C_3S hydration.

c) To analyze the impact of NaOH on C_3A-gypsum hydration and compare it to the Na-doped C_3A-gypsum hydration.

d) To analyze the influence of calcium sulfate type (gypsum/hemihydrate) on the hydration of C_3A and Na-doped C_3A.

e) To investigate the interactions between the different C_3S and C_3A polymorphs.

f) To analyze the effect of the C_3S and C_3A polymorphism and calcium sulfate type on the sulfate balance of a three-phase systems (C_3S-C_3A-calcium sulfate).

1.4 DELIMITATIONS AND LIMITATIONS

Within the current proposal, the infrastructure, time, and materials available, some delimitations were established, and some limitations were identified.

As for delimitations:

a) only pure phases, synthesized in the laboratory, were evaluated, which inherently differ from the phases found in Portland clinker.

b) the C_3S and C_3A were synthesized separately and then mixed, a different situation from Portland clinker in which C_3A is the interstitial phase of the clinker, which impacts on availability during hydration and, therefore, on the hydration rate.

c) the other clinker phases (C_2S, C_4AF) were not evaluated, which, although less reactive, may impact the hydration of C_3S and C_3A and the optimum sulfate content.

As for limitations, there are:

a) in the analysis of C_3A, only one sulfate content was used due to limitation of the available materials.

b) in the three-phase systems only a C_3S/C_3A ratio (92%/8%) was used due to the limitation of materials.

1.5 RESEARCH STRUCTURE

The present work is organized into chapters. In this chapter (chapter 1) a brief contextualization of the optimization of sulfates and its importance was presented, as well as the justification, objectives, delimitations, and limitations, and the structure of the present study. In the next chapter (chapter 2) the structure of which chapter is presented, in order to facilitate the compression of research development.

Chapters 3, 4, 5, and 6 are composed of articles published/submitted/to be submitted for publication in international journals. Chapter 3 is a review of the state of the art of sulfate optimization, presenting the theory, the factors that interfere and the methods used to determine the optimal sulfate content. Finally, knowledge gaps about this topic are identified, which served as a basis for the development of subsequent chapters.

The need for investigations regarding the role of doping ions in the hydration of C_3S and C_3A, specifically aluminum (Al) for C_3S and sodium (Na) for C_3A, in the presence of calcium sulfate and their interactions and impact on the sulfate demand of cement was identified in chapter 3. Therefore, chapter 4 presents the study of the effects of gypsum on C_3S and Al-C_3S hydration. In chapter 5, the investigation about how the sodium (present in C_3A crystalline structure or in solution) and the sulfate type (gypsum and hemihydrate) affects the C_3A hydration is presented. Finally, chapter 6 presents the study of the hydration of three-phase systems (C_3S-C_3A-calcium sulfate).

1.6 REFERENCES

[1] J. Bensted, Gypsum in cements, in: J. Bensted, P. Barnes (Eds.), Structure and Perfomance of Cements, Spon Press, 2002: pp. 253–265.

[2] A. Bentur, Cementitious Materials — Nine Millennia and A New Century : Past , Present , and Future, (2002) 2–22.

[3] M. Collepardi, G. Baldini, M. Pauri, M. Corradi, Tricalcium aluminate hydration in the presence of lime, gypsum or sodium sulfate, Cement and Concrete Research. 8 (1978) 571–580. https://doi.org/10.1016/0008-8846(78)90040-6.

[4] J. Pommersheim, J. Chang, Kinetics of hydration of tricalcium aluminate in the presence of gypsum, Cement and Concrete Research. 18 (1988) 911–922.

[5] K.L. SCRIVENER, Microstructure Development During the Hydration of Portland Cement., 1984.

[6] H. Minard, S. Garrault, L. Regnaud, A. Nonat, Mechanisms and parameters controlling the tricalcium aluminate reactivity in the presence of gypsum, Cement and Concrete Research. 37 (2007) 1418–1426. https://doi.org/10.1016/j.cemconres.2007.06.001.

[7] G. Geng, R.J. Myers, Y.S. Yu, D.A. Shapiro, R. Winarski, P.E. Levitz, D.A.L. Kilcoyne, P.J.M. Monteiro, Synchrotron X-ray nanotomographic and spectromicroscopic study of the tricalcium aluminate hydration in the presence of gypsum, Cement and Concrete Research. 111 (2018) 130–137. https://doi.org/10.1016/j.cemconres.2018.06.002.

[8] R.J. Myers, G. Geng, J. Li, E.D. Rodríguez, J. Ha, P. Kidkhunthod, G. Sposito, L.N. Lammers, A.P. Kirchheim, P.J.M. Monteiro, Role of adsorption phenomena in cubic tricalcium aluminate dissolution, Langmuir. 33 (2016) 45–55. https://doi.org/10.1021/acs.langmuir.6b03474.

[9] R.J. Myers, G. Geng, E.D. Rodriguez, P. da Rosa, A.P. Kirchheim, P.J.M. Monteiro, Solution chemistry of cubic and orthorhombic tricalcium aluminate hydration, Cement and Concrete Research. 100 (2017) 176–185. https://doi.org/10.1016/j.cemconres.2017.06.008.

[10] X. Liu, P. Feng, C. Lyu, S. Ye, The role of sulfate ions in tricalcium aluminate hydration: New insights, Cement and Concrete Research. 130 (2020) 105973. https://doi.org/10.1016/j.cemconres.2020.105973.

[11] H.F.W. Taylor, Cement chemistry, 2nd ed., Thomas Telford, 1997. https://doi.org/10.1680/cc.25929.

[12] A.P. Kirchheim, E.D. Rodríguez, R.J. Myers, L.A. Gobbo, P.J.M. Monteiro, D.C.C. Dal Molin, R.B. de Souza, M.A. Cincotto, Effect of gypsum on the early hydration of cubic and Na-doped orthorhombic tricalcium aluminate, Materials. 11 (2018) 1–16. https://doi.org/10.3390/ma11040568.

[13] M.M. Alonso, F. Puertas, Adsorption of PCE and PNS superplasticisers on cubic and orthorhombic C3A. Effect of sulfate, Construction and Building Materials. 78 (2015) 324–332. https://doi.org/10.1016/j.conbuildmat.2014.12.050.

[14] F.P. Glasser, M.B. Marinho, Early stages of the hydration of tricalcium aluminate and its sodium-cotaining solid solutions, Proceedings of the British Ceramic Society. 35 (1984) 221–236.

[15] D. Stephan, S. Wistuba, Crystal structure refinement and hydration behaviour of doped tricalcium aluminate, Cement and Concrete Research. 36 (2006) 2011–2020. https://doi.org/10.1016/j.cemconres.2006.06.001.

[16] A. Bentur, Effect of Gypsum on the Hydration and Strength of C3S Pastes, Journal of the American Ceramic Society. 59 (1976) 210–213. https://doi.org/10.1111/j.1151-2916.1976.tb10935.x.

[17] D. Ménétrier, I. Jawed, J. Skalny, EFFECT OF GYPSUM ON C3S HYDRATION, CEMENT and CONCRETE RESEARCH. 10 (1980) 697–701.

[18] A. Quennoz, K.L. Scrivener, Interactions between alite and C3A-gypsum hydrations in model cements, Cement and Concrete Research. 44 (2013) 46–54. https://doi.org/10.1016/j.cemconres.2012.10.018.

[19] F. Zunino, K. Scrivener, Factors influencing the sulfate balance in pure phase C3S/C3A systems, Cement and Concrete Research. 133 (2020) 106085. https://doi.org/10.1016/j.cemconres.2020.106085.

[20] S.T. Bergold, F. Goetz-Neunhoeffer, J. Neubauer, Interaction of silicate and aluminate reaction in a synthetic cement system: Implications for the process of alite hydration, Cement and Concrete Research. 93 (2017) 32–44. https://doi.org/10.1016/j.cemconres.2016.12.006.

[21] P.W. Brown, C.L. Harner, E.J. Prosen, The effect of inorganic salts on tricalcium silicate hydration, Cement and Concrete Research. 16 (1986) 17–22. https://doi.org/10.1016/0008-8846(86)90063-3.

[22] Y. Zhang, X. Zhang, Research on effect of limestone and gypsum on C3A, C3S and PC clinker system, Construction and Building Materials. 22 (2008) 1634–1642. https://doi.org/10.1016/j.conbuildmat.2007.06.013.

[23] S. Gunay, S. Garrault, A. Nonat, P. Termkhajornkit, Influence of calcium sulphate on hydration and mechanical strength of tricalcium silicate, in: Proceedings of 13th International Congress on the Chemistry of Cement, Madrid, 2011: pp. 1–6.

[24] W. da S. Barbosa, INFLUÊNCIA FÍSICO-QUÍMICA DAS FASES DO CLÍNQUER NO COMPORTAMENTO REOLÓGICO DE PASTAS CIMENTÍCIAS, 2019.

[25] A. Quennoz, K.L. Scrivener, Hydration of C 3A-gypsum systems, Cement and Concrete Research. 42 (2012) 1032–1041. https://doi.org/10.1016/j.cemconres.2012.04.005.

[26] S. Joseph, J. Skibsted, Ö. Cizer, A quantitative study of the C3A hydration, Cement and Concrete Research. 115 (2019) 145–159. https://doi.org/10.1016/j.cemconres.2018.10.017.

[27] K.L. Scrivener, A. Nonat, Hydration of cementitious materials, present and future, Cement and Concrete Research. 41 (2011) 651–665. https://doi.org/10.1016/j.cemconres.2011.03.026.

[28] K. Scrivener, A. Ouzia, P. Juilland, A. Kunhi Mohamed, Advances in understanding cement hydration mechanisms, Cement and Concrete Research. 124 (2019) 105823. https://doi.org/10.1016/j.cemconres.2019.105823.

[29] K. Tosun, Effect of SO3 content and fineness on the rate of delayed ettringite formation in heat cured Portland cement mortars, Cement and Concrete Composites. 28 (2006) 761–772. https://doi.org/10.1016/j.cemconcomp.2006.06.003.

[30] S. Horkoss, G. Escadeillas, T. Rizk, R. Lteif, The effect of the source of cement SO3 on the expansion of mortars, Case Studies in Construction Materials. 4 (2016) 62–72. https://doi.org/10.1016/j.cscm.2015.12.004.

Chapter 2

Dissertation structure

2 DISSERTATION STRUCTURE

This chapter presents the dissertation structure in order to facilitate the compression of the research development. Each following chapter is composed of an article published, submitted, or to be submitted for publication in international journals. The research schedule and the state of experimental development of each of the subsequent chapters are also presented.

Figure 2.1 shows a schematic structure of the research, where the title of each article/chapter is presented, and further explanation can be seen in the following items.

Figure 2.1 – Organizational structure of the research.

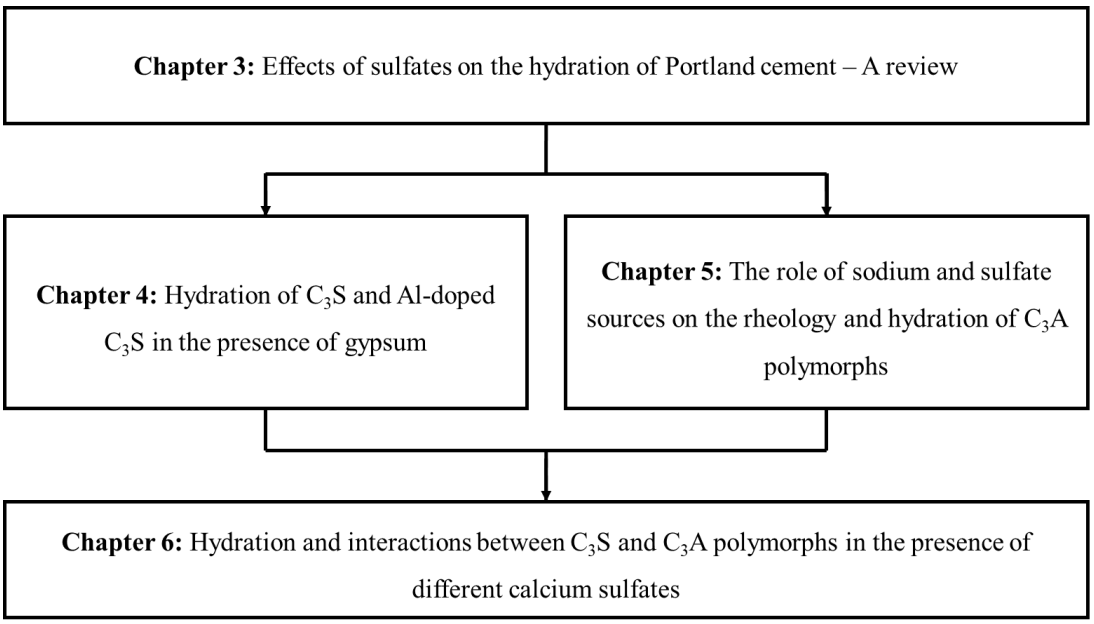

2.1 CHAPTER 3: EFFECTS OF SULFATES ON THE HYDRATION OF PORTLAND CEMENT – A REVIEW

Chapter 3 presents an extensive review regarding the effect of sulfates – especially calcium sulfates - on the hydration of Portland cement. The impact of calcium sulfate on C_3A and C_3S hydration are discussed, as well as its impact on cement hydration. The effects of sulfate on the cement properties are present and the optimum sulfate content is defined. Then, the main factors (clinker and sulfate source characteristics, supplementary cementitious materials, admixtures, among others) which influence the sulfate demand and the methods used to determine the optimum sulfate content are presented. Finally, the knowledge gaps and the perspectives for future research are discussed.

In this chapter, it was noted that the calcium sulfate enhances the C_3S hydration, but the mechanism it is not clear yet. The two main theories relate this enhance to the formation of ettringite, from the reaction between the aluminum present in alite and the calcium sulfate. However, this enhance was also observed in pure C_3S, without alumina and therefore without ettringite formation. Thus, further investigations on how calcium sulfate influences C_3S hydration are needed, which motivated the study presented in chapter 4.

From this review, it was also observed that although the calcium sulfate delays the pure cubic C_3A hydration, it is ineffective to retard the Na-doped C_3A (orthorhombic) hydration. However, the reason for this behavior is not clear yet and may be related to the difference in crystalline structure or to the presence of sodium in solution. Furthermore, the impact of calcium sulfate type on C_3A hydration is not well known – especially for ort-C_3A. Thus, the study presented in chapter 5 deals with the understanding of the role of sodium and sulfate sources (gypsum and hemihydrate) on the rheology and hydration of C_3A polymorphs.

Finally, it was concluded that further investigations regarding the impact of C_3S and C_3A polymorphism and calcium sulfate type on the sulfate balance of the systems are needed. Therefore, the study presented in chapter 6 was performed to enlighten these questions.

2.2 CHAPTER 4: HYDRATION OF C_3S AND Al-DOPED C_3S IN THE PRESENCE OF GYPSUM

In chapter 4, the hydration of C_3S (Triclinic 1) and aluminum-doped C_3S (Monoclinic 1) in the absence and in the presence of gypsum was analyzed. Pastes with 0.0%, 2.5% and 5.0% of gypsum (in relation to C_3S wt.%) were evaluated by isothermal calorimetry (IC). In addition, the hydration of the pastes with 0.0% and with 2.5% of gypsum was stopped at 10 h, 1, 3, and 7 d and thermogravimetric analysis (TGA/DTG), X-ray diffractometry (XRD), and ^{27}Al nuclear magnetic resonance (NMR) were performed. Figure 2.2 presents a summary of the analyzes carried out in chapter 4.

Figure 2.2 – Organization chart of the formulations and analyzes performed in chapter 4.

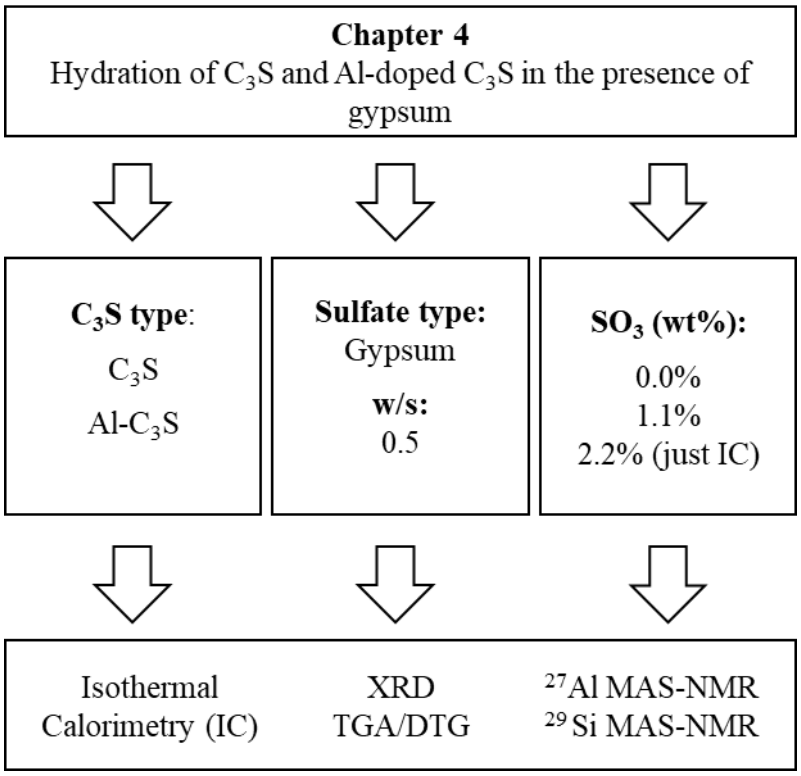

2.3 CHAPTER 5: THE ROLE OF SODIUM AND SULFATE SOURCES ON THE RHEOLOGY AND HYDRATION OF C_3A POLYMORPHS

In chapter 5, the rheology and hydration of cb-C_3A, cb-C_3A + NaOH, and ort-C_3A (Na-doped) with gypsum or hemihydrate, are analyzed. The method used in this study is presented in Figure 2.3. Mixtures of cubic and orthorhombic (Na-doped) C_3A with gypsum or hemihydrate were compared to mixtures with cubic C_3A plus NaOH solution. The concentration of the NaOH solution (0.99 M) was chosen to result in the same amount of Na^+ ions liberated with the orthorhombic C_3A dissolution, as determined by ICP-OES analysis. IC, *in-situ* XRD, TGA/DTG, SEM, and rheological analyses were done.

Figure 2.3 – Organization chart of the formulations and analyzes performed in chapter 5.

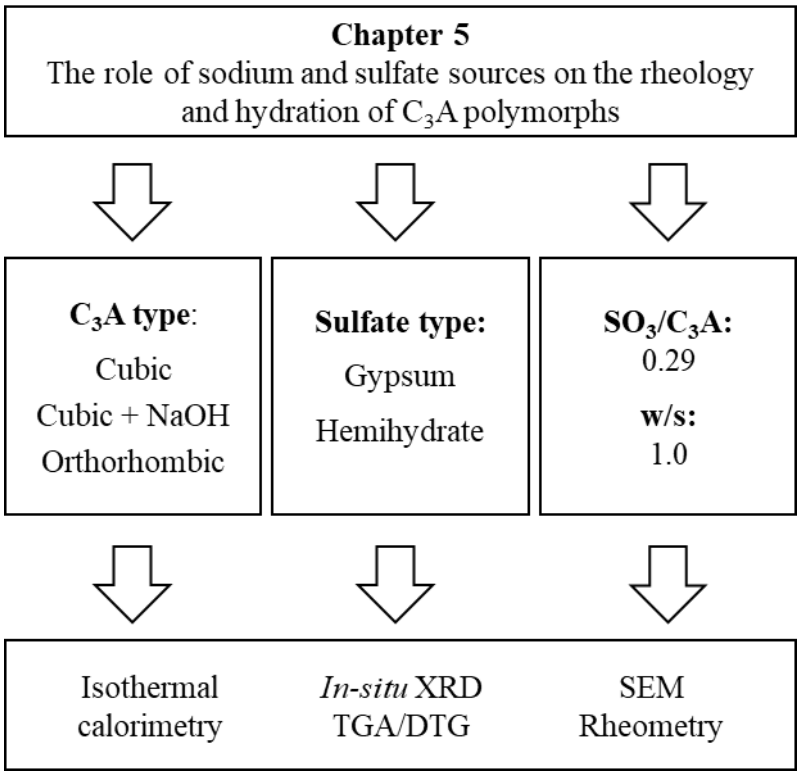

2.4 CHAPTER 6: HYDRATION AND INTERACTIONS BETWEEN C_3S AND C_3A POLYMORPHS IN THE PRESENCE OF DIFFERENT CALCIUM SULFATES

Finally, chapter 6 details the study of the mixtures of the different C_3S (C_3S and Al-C_3S) and C_3A (cubic and orthorhombic) with different amounts of gypsum or hemihydrate. First, the hydration of both C_3S without and with gypsum and hemihydrate (wt% SO_3 of 1.5) was analyzed by isothermal calorimetry. Then, the hydration of cb- and ort-C_3A without and with gypsum and hemihydrate (wt% SO_3 of 0%, 2.72%, 5.36%, and 9.84% - SO_3/C_3A wt% equals 0, 0.03, 0.06, and 0.13) were also analyzed by isothermal calorimetry. Finally, the hydration of three-phase systems (C_3S-C_3A-calcium sulfate) was analyzed. Two C_3S (T1 pure C_3S and M1 aluminum-doped C_3S), two C_3A polymorphs (cubic and orthorhombic), and two calcium sulfates (gypsum and hemihydrate) were evaluated. For each system, the hydration of four different SO_3 contents was evaluated by calorimetry. From the calorimetry results, a 1.5 wt.% SO_3 content was fixed, and the mixtures were evaluated by *in-situ* XRD, TGA, and SEM. Figure 2.4 presents the method of the study presented in chapter 6. Table 2.1 summarizes all the mixtures analyzed in chapters 4, 5, and 6 and the respective tests that were done.

Figure 2.4 – Organization chart of the formulations and analyzes performed in chapter 6.

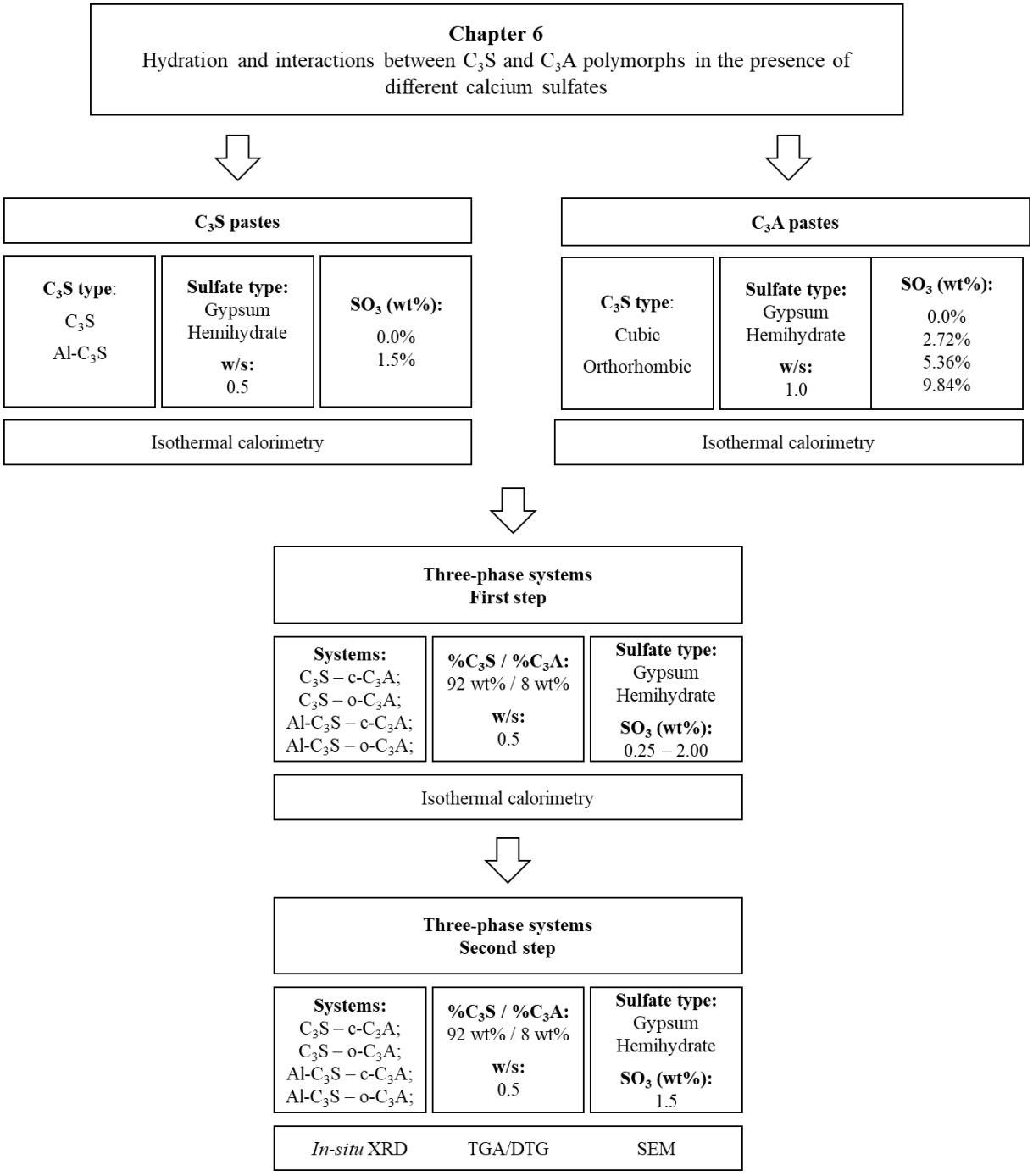

Table 2.1 – Mixtures analyzed, and tests performed in each study.

Chapter	Mixture	Sulfate	wt% SO_3 (SO_3/C_3A wt%)	Solution	w/c	Tests
4	C_3S	Gypsum	0%; 1.1%; 2.2% (-)	Distilled water	0.5	IC
	C_3S	Gypsum	0%; 1.1% (-)	Distilled water	0.5	XRD, TGA, ^{29}Si NMR, ^{27}Al NMR
5	C_3A	Gypsum / Hemihydrate	17.92% (0.29)	Distilled water/ 0.99 M NaOH	1.0	IC, *in-situ* XRD, TGA, SEM, Rheometry
6	C_3S	Gypsum / Hemihydrate	1.5% (-)	Distilled water	0.5	IC
	C_3A	Gypsum / Hemihydrate	0%, 2.72%, 5.36%, 9.84% (0, 0.03, 0.06, 0.13)	Distilled water	1.0	IC
	C_3S/C_3A (92/8 wt%)	Gypsum / Hemihydrate	0.25%, 0.50%, 1.0%, 1.5%, 2.0% (0.03, 0.06, 0.13, 0.19, 0.26)	Distilled water	0.5	IC
	C_3S/C_3A (92/8 wt%)	Gypsum / Hemihydrate	1.5% (0.19)	Distilled water	0.5	*In-situ* XRD, TGA, SEM

Chapter 3

Effects of sulfates on the hydration of Portland cement – A review

Chapter 3 is based on the article:

José S. Andrade Neto, Angeles G. de la Torre, Ana Paula Kirchheim. Effects of sulfates on the hydration of Portland cement – A review. **Construction and Building Materials**, v. 279, paper 122428, 2021.

3 EFFECTS OF SULFATES ON THE HYDRATION OF PORTLAND CEMENT – A REVIEW

ABSTRACT

Presented within is a critical overview of the effect of sulfates on cement hydration, properties, and optimum sulfate content in Portland cement. Calcium sulfate is used in Portland cement to control the C_3A reaction to induce the optimum hydration of C_3S to occur. The amount of calcium sulfate in the Portland cement influences the hydration, rheology, setting, phase assemblage, porosity distribution, and strength in cementitious materials. If added in excess, it can also lead to durability problems, thus a better understanding is needed about the mechanisms of sulfate on C_3A and C_3S hydration. The optimum sulfate content is well known as a key pathway to produce workable, good strength and durable concretes. Despite many years of research, questions regarding sulfate optimization remain. Further investigation on the influence of clinker and calcium sulfate characteristics, the use of different supplementary cementitious materials and chemical admixtures, and the curing conditions on the sulfate demand of Portland cement are needed. The main methods used to determine the optimum SO_3 content are reported, and the advantages and disadvantages are examined. Finally, recommendation for future research is also discussed.

Keywords: *Optimum sulfate content; Sulfate balance; Cement; Hydration; Supplementary Cementitious Materials*

DOI: https://doi.org/10.1016/j.conbuildmat.2021.122428

3.1 INTRODUCTION

Portland cement is the most consumed building material worldwide; it has been in use for almost 200 years. The use of calcium sulfate to control the duration of the setting of cement began at the end of the 19th century and universally adopted by cement producers around 1930 [1,2]. Nowadays, the inclusion of calcium sulfate is an integral ingredient in Portland cement. Despite thousands of studies over several decades, many questions about the role of calcium sulfate on the cement phases (C_3A and C_3S) hydration, its mechanisms, and the so-called "optimum sulfate content" persists.

Gypsum ($CaSO_4.2H_2O$) and/or natural anhydrite ($CaSO_4$) are usually added to clinker in the grinding stage. Depending on the temperature reached on the mill, the gypsum may dehydrate in hemihydrate ($CaSO_4.1/2H_2O$) and/or soluble anhydrite ($CaSO_4$), which are more soluble and, therefore, will influence the cement hydration [3]. In this paper, the term "calcium sulfate" is used regardless of its composition; otherwise, the specific composition is mentioned.

Calcium sulfate is added to control the hydration of C_3A to avoid flash setting and extending the period in which the mixtures have fluidity and workability [1,4,5]. When all the sulfate from the solution is consumed–this moment is known as sulfate depletion–the renewed hydration of C_3A begins [6–9]. The amount of calcium sulfate to be added will determine when the renewed hydration of C_3A will occur. The amount required must be sufficient enough to delay the C_3A hydration until after the main C_3S hydration peak. Otherwise, the C_3S hydration is hindered, reducing the mechanical performance at early ages [10–13]. On the other hand, if too much calcium sulfate is added, the mechanical performance suffers [14–16]. Furthermore, increasing the sulfate content may lead to durability problems due to delayed ettringite formation (DEF), especially in cements submitted to high curing temperatures [14–16].

Although not as heavily investigated as C_3A-calcium sulfate systems, calcium sulfate also changes the C_3S hydration, the morphology of its hydration products, and its mechanical strength [6,8,11,17–19]. The effect of calcium sulfate on C_3S hydration needs to be properly understood as it can influence the sulfate optimization in Portland cements and, therefore, can influence cement properties.

Lerch [20] noted there is an optimum sulfate content for each cement, which results in the highest mechanical performance and lowest shrinkage. The optimum sulfate content (optimum SO_3 content or sulfate demand) is usually obtained empirically through isothermal calorimetry and compressive strength tests with cements with different amounts of calcium sulfate, as described in the ASTM C563 [21] standard.

Many questions regarding the effect of calcium sulfate in C_3A and C_3S hydration and the factors that may influence the optimum sulfate content remain. As discussed herein, many factors may influence this content, including clinker and calcium sulfate characteristics (fineness, chemical, and mineralogical composition), presence of supplementary cementitious materials (SCMs) and chemical admixtures, temperature, and time of hydration. Understanding of the sulfate demand on the system can address several problems in the fresh and hardened state and long-term performance (durability), a problem still quite common in the construction field. Without a complete understanding of the mechanism driving sulfate demand on the system, these problems might become increasingly common as the use of different SCMs and chemical admixtures on cementitious materials increases. Recent investigations have provided insight on this subject. In this paper, the effect of calcium sulfate on C_3A, C_3S and Portland clinker hydration are reviewed, as well as the influence of the amount of sulfate on cement properties. Presented within are the main factors that may influence the optimum sulfate content and the methods that can be used to determine the sulfate demand. To the best of the authors' knowledge, a review focusing on the role of sulfate on Portland cement hydration and the optimization of the sulfate content is still NOT extant. Despite the increase in such research, there remains several issues to be resolved and recommendations for future research is discussed.

3.2 EFFECT OF CALCIUM SULFATE ON CEMENT HYDRATION

To properly understand the sulfate optimization, it is fundamental to comprehend the influence of calcium sulfate on cement hydration. To lay the groundwork, first we present its influence on the two most important Portland cement phases concerning the initial hydration and sulfate optimization: C_3A and C_3S, focusing on studies using pure phases synthesized in laboratory. Next, we present the influence of calcium sulfate on cement hydration.

3.2.1 Effect of calcium sulfate on C_3A hydration

Without the addition of calcium sulfate, C_3A reacts instantaneously once in contact with water, releasing a great amount of heat and resulting in the formation of a OH-AFm-type meta-stable product (C_4AH_{13} and C_2AH_8) (see Eq. 3.1 [22], which is subsequently converted to katoite ($Ca_2Al_2(OH)_{12}$ or C_3AH_6) [22–24]. The formation of these products leads to "Flash-set," i.e., stiffening and loss of workability in few minutes, making most practical Portland cement applications unfeasible [1,4].

$$2C_3A + 21H \rightarrow C_4AH_{13} + C_2AH_6 \quad \text{(Eq. 3.1)}$$

To avoid Flash-set, gypsum ($CaSO_4 \cdot 2H_2O$) and natural anhydrate ($CaSO_4$) are usually added. Depending on temperature of the cement mill, gypsum may be dehydrated to hemihydrate ($CaSO_4 \cdot 1/2H_2O$) and soluble anhydrite ($CaSO_4$) [3]. The addition of calcium sulfate completely alters the C_3A reaction, and ettringite ($C_6A\bar{S}_3H_{32}$) is formed in the first few minutes; see Eq. 3.2 [22,24]. The ettringite formation consumes the sulfates in the solution. When the sulfates are exhausted, the ettringite becomes unstable and reacts with the remaining C_3A to form a SO_4-AFm phase - monosulfate ($C_4A\bar{S}H_{12}$); see Eq. 3.3 [22,24]. Pourchet et al. [25] has reported the presence of OH-AFm phases in the first few minute when gypsum is used as calcium sulfate source; the presence of these phases is not observed when hemihydrate is used [25].

$$C_3A + 3C\bar{S}H_2 + 26H \rightarrow C_6A\bar{S}_3H_{32} \quad \text{(Eq. 3.2)}$$

$$2C_3A + C_6A\bar{S}_3H_{32} + 4H \rightarrow 3C_4A\bar{S}H_{12} \quad \text{(Eq. 3.3)}$$

Figure 3.1 shows the typical heat flow curve resulting from the hydration of C_3A in the presence of calcium sulfate, divided into three stages. In stage I, an exothermic peak of heat release is observed, followed by a sharp reduction. The heat released at this stage results from the wetting of the particles, the dissolution of ions, and the formation of ettringite [24].

Then the reaction rate decreases dramatically, and the induction period (stage II) begins. The duration of this period of low heat release depends on the amount of calcium sulfate in the system. The higher the calcium sulfate content, the longer the duration of this period [25–27]. Finally, when all the added calcium sulfate is consumed, a new exothermic peak is observed due to the renewed C_3A dissolution and the formation of monosulfate (stage

III) [24,26,28]. The peak shape has an almost vertical acceleration part, followed by an exponentially decaying shoulder [28]. Minard et al. [26] proposed that the hydrations kinetics of this period is controlled by dissolution. Quennoz and Scrivener [22] disagree and have suggested that it is related to the nucleation and growth of SO_4-AFm. Further studies regarding this issue are needed to clarify the mechanism that controls the renewed C_3A dissolution and SO_4-AFm formation.

The mechanism responsible for this delay is not yet fully understood. Several hypotheses have been proposed. The oldest theory is that the delay occurs due to the formation of an ettringite barrier on the particles of C_3A [29–31]; however, due to the needle-like crystalline morphology of the ettringite, it is improbable that this layer is responsible for hindering the diffusion of ions and the transport of water [4,32,33].

Other authors have suggested that the reason for the delaying of the reaction would be a "gel like" layer on the surface of C_3A [34]. This hypothesis is disputed according to the study of Minard et al. [26], this layer is an OH-AFm type phase, which also forms when C_3A is hydrated in the absence of calcium sulfate, in which the delay in the reaction is *not* observed. As noted earlier, this hydrate does not form when hemihydrate is used, but the reaction remains delayed [25]. Furthermore, the finer the C_3A, the greater the quantity of precipitated AFm, and the shorter the time for the sulfate ions to be consumed [26]. Finally, as shown by Geng et al. [32] ettringite forms after a few minutes of hydration when the C_3A surface is already covered by OH-AFm or SO_4-AFm and, therefore, these phases do not retard C_3A hydration to any extent.

Joseph et al. [24] proposed that the C_3A hydration in the presence of gypsum is inhered by the surface coverage of ettringite on the active surface of C_3A. The authors suggest that the retardation is governed by a dissolution-controlled mechanism instead of a diffusion-controlled mechanism of the ettringite barrier hypothesis [24]. As recently showed by Liu et al. [27], however, the extraction of the sulfate of the solution (by adding $Ba(NO_3)_2$) leads to an abrupt end of the induction period (stage II), although ettringite is still present. Also, ettringite is more abundant in C_3A-gypsum systems, but the C_3A-$MgSO_4$ systems show the highest induction period [27]; thus the ettringite formation cannot explain the delay in C_3A hydration.

Another theory proposed by Minard et al. [26] is that the delay in hydration of C_3A occurs due to the adsorption of sulfate ions on its surface. According to Bullard et al. [28] the sulfates may be adsorbed at defect sites and inhibit the formation of etch pits, delaying the dissolution of C_3A. This theory may also explain why the reaction decreases more quickly in the presence of the highly soluble hemihydrate than in the presence of gypsum (which is less soluble) [28], as observed by Pourchet et al. [25].

Myers et al. [35] proposed that an Al-rich leached layer is formed at the partially dissolved C_3A surface, and Ca-S ion-pair complexes are adsorbed onto this layer, decreasing the active dissolution sites and the undersaturation of calcium ions, delaying the C_3A hydration. Recent experimental data reported in the literature [27,32,36,37] agrees with the theory that the adsorption of S and/or Ca-S ion-pair complexes is correct mechanism that accurately describes the retardation on C_3A hydration.

In addition, the alkaline of the sulfate seems to play an important role in the retardation of C_3A hydration. As observed by Ye et al. [38], there is a cation-specific effect of sulfates on the delay of C_3A hydration. While most studies agree that calcium sulfate retards the C_3A hydration, there are contradictory results regarding the effect of other sulfate salts. Some authors have observed that magnesium sulfate retards the C_3A hydration [27,37,38], while others have noted an increase in C_3A hydration rate when adding magnesium sulfate [39]. The addition of sodium sulfate (Na_2SO_4) either does not result in a delay [29,40] or delays to a less extent compared to calcium sulfate [27,38]. Further studies regarding the effect of different sulfate salts on C_3A hydration are necessary.

Figure 3.5 – Typical calorimetry curve of C_3A-calcium sulfate mixtures.

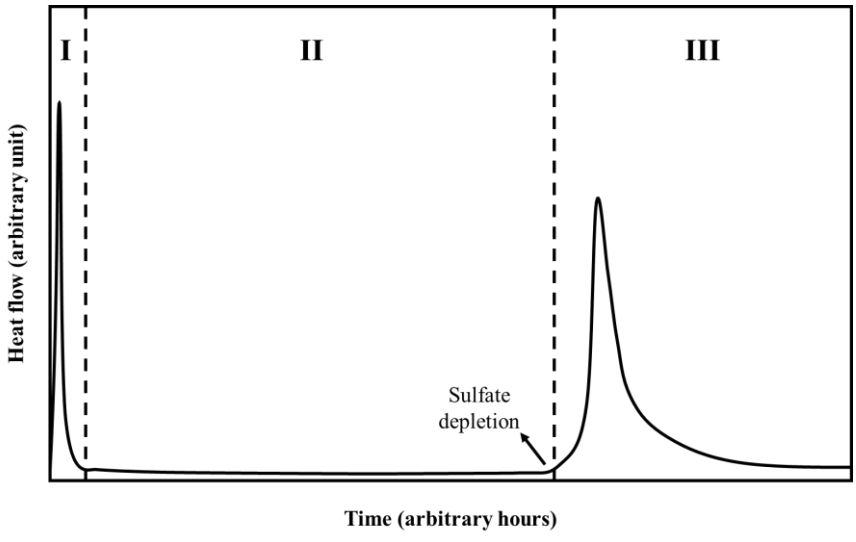

The crystalline structure of C_3A in the clinker depends on the alkali content present in the raw materials and on the alkali content incorporated during the clinker process (which is dependent on the fuel used). When Na^+ ions are incorporated into the crystalline structure of C_3A—thus replacing Ca^{2+} ions—the formation of a solid solution with a general form of $Na_{2x}Ca_{3-x}Al_2O_3$ occurs, where x is the amount of Ca^{2+} that has been replaced by Na^+. x values of up to 0.10 (2.4 wt% of Na_2O) result in only cubic C_3A, while values of x between 0.10 and 0.16 (2.4 – 3.7 wt% of Na_2O) result in the co-existence of the cubic and the orthorhombic polymorph. As the value of x increases to 0.16-0.20 (3.7 – 4.6 wt% of Na_2O), only the orthorhombic C_3A is presented. x values above 0.20 (4.6 wt% of Na_2O) result in a monoclinic polymorph [31,41–43]. In OPC, the monoclinic polymorph is not observed, and the clinker usually presents cubic and orthorhombic C_3A [31,44].

The crystalline structure has a great influence on the C_3A hydration process and, consequently, in the rheological properties (workability) of the cement paste. In the absence of calcium sulfate, both cubic and orthorhombic C_3A react with water, resulting in the formation of metastable hydroxy-AFm phases, which then convert to katoite (C_3AH_6) [5,23]; however, cubic C_3A is more reactive than the orthorhombic C_3A [23,45,46].

In the presence of calcium sulfate, the behavior is inverted, and the orthorhombic C_3A is more reactive than the cubic one [5,23,36,45,47–49]. This is because despite retarding the cubic C_3A hydration, calcium sulfate accelerates the hydration process of orthorhombic C_3A [5,23,36,50]. As shown in Figure 3.2, the addition of gypsum decreases the heat released during the first hours of the hydration of cubic C_3A, indicating a delay in the reactions, while adding the same amounts of gypsum increase the heat released by the orthorhombic C_3A hydration.

Figure 3.6 – Total heat released during the first 24 h of hydration for (A) cubic C_3A and (B) orthorhombic C_3A with different amounts of gypsum, normalized by wt.% of dry solid (C_3A + gypsum). Source: adapted from Kirchheim et al. [23].

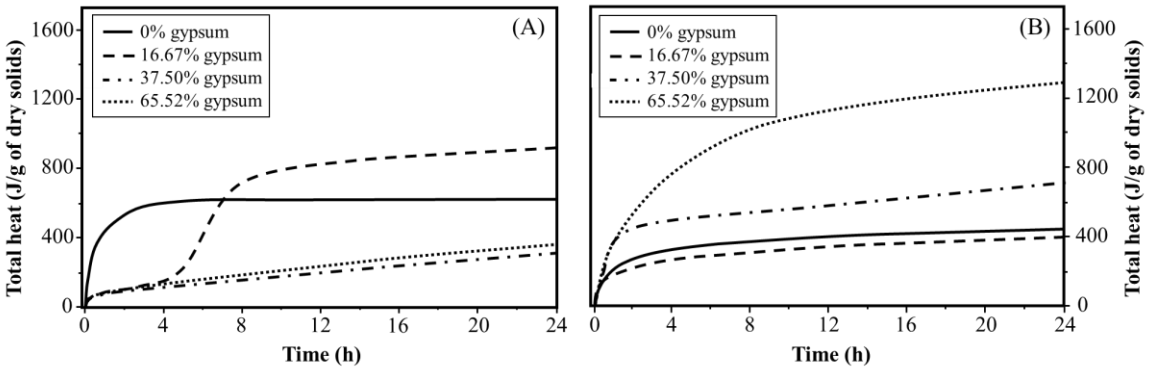

To date, it is not known why calcium sulfate is effective in delaying hydration of cubic C_3A but not orthorhombic C_3A. This may be related to the greater solubility of the ring structures of $Al_6O_{18}^{18-}$ in orthorhombic C_3A, which impacts the formation of the amorphous alumina layer on the C_3A particles, and thus affects the dissolution rate [23,36,46]. It may also be related to the sodium ions released in the dissolution of the orthorhombic C_3A, destabilizing the amorphous alumina layer [45] where the Ca-S ion-pair complexes are adsorbed according to the hypothesis of Myers et al. [35]. Further studies regarding the role of calcium sulfate on the hydration of the different C_3A polymorphisms are needed.

3.2.2 Effect of calcium sulfate on C_3S hydration

As calcium sulfate is normally added to control the C_3A hydration, their impact on C_3S hydration and strength are normally neglected. This ignores that fact that it has a great influence on C_3S hydration, which needs to be properly understood as it can influence the sulfate optimization in Portland cements, influencing the properties of the cement.

The addition of gypsum does not change the products formed during C_3S hydration, with the exception of the aluminum-doped C_3S where ettringite is formed [8,51]. The sulfate ions released from the gypsum dissolution are specifically absorbed on C-S-H, changing their morphology [51,52]. As illustrated in Figure 3.3, a cloud of sulfate ions could be physically adsorbed by charge affinity in the positive charged C-S-H needles [51]. According to Mota et al. [51] this would result in the repulsion of the C-S-H needles and

lead to a more divergent needle-structure instead of the convergent morphology observed in plain C_3S pastes.

Figure 3.7 – Schematic representation of the impact of sulfate ions on C-S-H morphology. Source: adapted from Mota et al. [51].

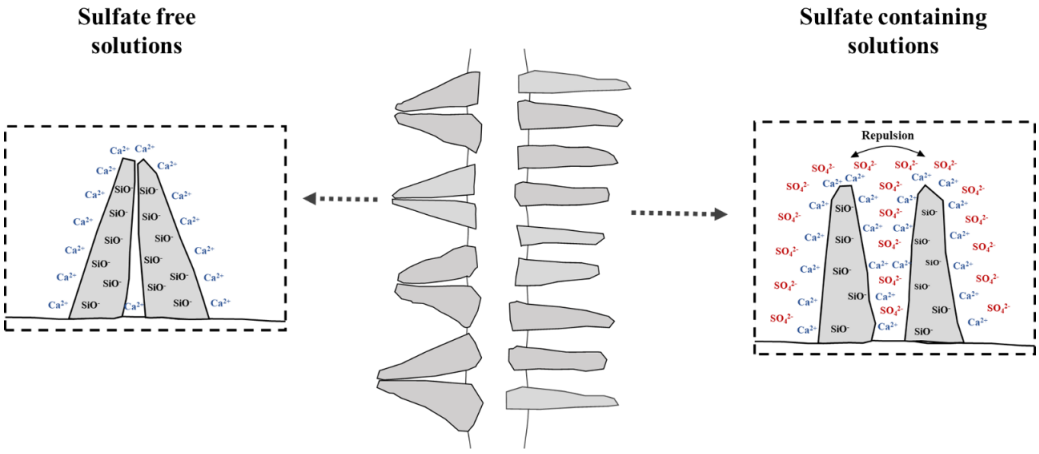

In addition, gypsum (and other soluble sulfates salts as Na_2SO_4) influence the C_3S hydration. Gypsum retards the initial hydration of C_3S, and a more extended induction period is observed [6,8,11,17]. According to Nicoleau et al. [11] and Juilland et al. [17] the sulfate ions are physically adsorbed on C_3S surface, decreasing the surface charge and lowering its dissolution rate.

After the induction period, the behavior changes and gypsum enhance the C_3S hydration [6,8,18,51–58]; see Figure 3.4. Yamashita et al. [59] have observed that increasing the clinker SO_3 content also accelerated the alite reaction but why it accelerates the reaction is still not known. Quennoz and Scrivener [8] proposed that the enhancement in C_3S hydration by gypsum is due to reactions between the sulfates and the aluminum present in C_3S structure, thus forming ettringite. These reactions remove the aluminum (which is known to retard C_3S hydration) of the solution and accelerate its hydration. Bergold et al. [60] suggest that this enhancement in aluminum-doped C_3S hydration is due to the seeding effect of very fine (nano-)ettringite, which might provide a suitable surface for heterogeneous nucleation of C-S-H, leading to a faster dissolution of C_3S.

As observed by many researchers [6,53,55,58,61], however, including the example given in Figure 3.4, gypsum also accelerates the hydration of C_3S without alumina, where the formation of ettringite is not observed. Therefore, these hypotheses cannot explain the

increase of C_3S hydration in the presence of calcium sulfate. According to Zunino and Scrivener [6], the enhancement of C_3S hydration by gypsum is probably a result of the interaction between this phase and C_3S and/or C-S-H, rather than interactions associated with the aluminates.

Due to the acceleration in C_3S hydration, the addition of gypsum usually increases the initial mechanical strength of C_3S pastes [18,56] but with a decrease in mechanical performance at later ages [18,56]. This is probably related to the decrease in C_3S content when gypsum is incorporated into the mixture, resulting in a lower amount of C-S-H at higher hydration degrees [56]. Besides, the intrinsic strength of the C-S-H gel is linearly related to its C/S mole ratio, and when gypsum is added, the C/S decreases as well as the intrinsic strength of C-S-H [18,62].

The enhancement in C_3S hydration by gypsum may be related to the change in morphology mentioned before. According to simulations performed by Gunay et al. [56], gypsum increases the C-S-H growth rate, but its mechanism is unknown as yet. Further studies on the impact of calcium sulfate on C_3S hydration are needed.

Note that all these studies were performed with gypsum. Therefore, it is also essential to study the effect of other calcium sulfate composition, e.g., hemihydrate and anhydrite, on C_3S hydration.

Figure 3.8 – Heat flow curves of C_3S and C_3S + 1.0% of gypsum pastes (w/c = 0.5) during the first 24 hours of hydration. Source: adapted from Zunino and Scrivener [6].

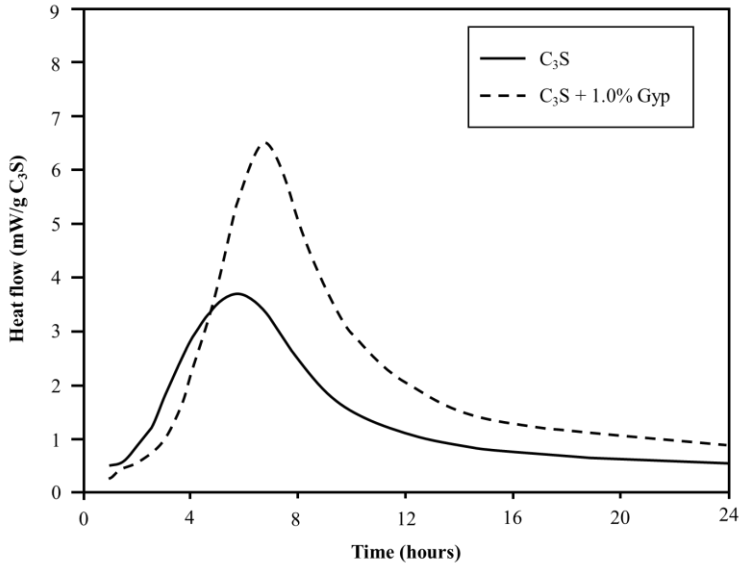

The C_3S can present in seven different polymorphs: (1) triclinic (T1, T2, and T3); (2) monoclinic (M1, M2, and M3); and (3) rhombohedral (R), which will depend on the temperature and doping with foreign ions [31,63–65]. Pure C_3S is T1, while the OPC usually presents M1 and/or M3 [31,63,65]. The SO_3 seems to stabilize the M1 polymorph, while the MgO favors the formation of M3 C_3S [66–69].

The change in C_3S crystalline structure might influence its hydration. The M1 polymorph seems to present a higher reactivity when compared to M3, resulting in higher mechanical strength [70]. This difference might be related to the higher non-bonding electrons in the M1-C_3S when compare to M3-C_3S [71]. Bazzoni et al. [72] has stated that there is no clear link between the polymorphism and reactivity, as the same polymorph can present completely different reactivities depending on the foreign ion used to stabilize it. Thus, this difference between the M1 and M3 hydration rate might be related to the foreign ions usually incorporated in the alite structure during the clinker production, which can greatly influence C_3S hydration. The aluminum [73,74] and iron [74] doping decreases the C_3S hydration rate, while zinc increases the main hydration peak [72,75]. A study the effect of C_3S polymorphs (or the doping of foreign ions) on the interaction with gypsum remains to be conducted, despite some theories relating the presence of aluminum with the enhancement due to the presence of gypsum [8,60], as mentioned before. Further investigations on this topic are strongly recommended, as the interaction between C_3S and calcium sulfate might be a key factor to understand sulfate optimization.

3.2.3 Effect of calcium sulfate on Portland cement hydration

Figure 3.5 shows schematically the role of sulfate ions during Portland cement hydration. In the first few minutes, the dissolution of the calcium and alkaline sulfates release sulfate ions into the solution. A part of these ions reacts with the C_3A to form ettringite, while the other part is adsorbed—as $CaSO_3$ complexes—by the C-S-H needles. When all the solid sulfate has dissolved and the concentration of sulfates in solution decreases, reached the moment known as “sulfate depletion point,” the sulfate ions are desorbed from the C-S-H, leading to a renew dissolution of C_3A with a new and rapid formation of ettringite [8,76,77]. Then, the SO_3/Al_2O_3 ratio of the solution decreases, and the ettringite reacts with the remaining C_3A to form AFm phases [76,77].

Figure 3.9 – The role of sulfate on Portland cement hydration.

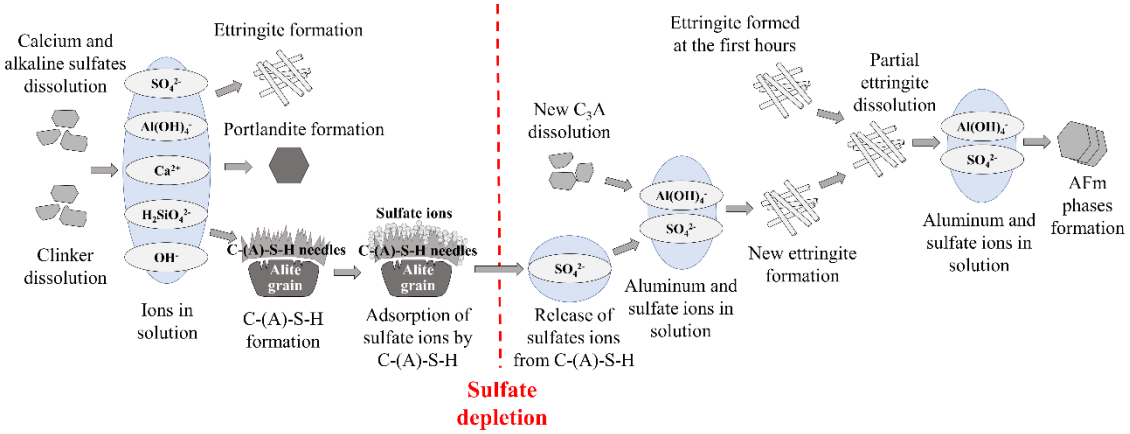

As discussed in Section 3.2.2, the morphology of C-S-H is influenced by the sulfate ions and changes with the sulfate depletion; see Bérodier et al. [78]. During the first hours of hydration of the OPC, the sulfate ions are adsorbed on C-S-H, resulting in a divergent needle-like morphology (similar to the C-S-H formed in C_3S pastes with gypsum, shown schematically in Figure 3.3) [78]. After the sulfate depletion, the sulfate ions previously adsorbed on C-S-H are released into the solution, resulting in a change in C-S-H morphology that becomes “agglomerated” [78].

Figure 3.6 presents some examples of heat flow curves of ternary cements (OPC, blast furnace slag, and limestone) undersulfated, properly sulfated and supersulfated [79]. Figure 3.7 presents heat flow curves of undersulfated and properly sulfated pure C_3S-C_3A mixtures (92-8 wt%) [6]. The SD point shown in Figures 3.6 and 3.7 corresponds to the sulfate depletion point, leading to a renewed C_3A dissolution with a new and rapid formation of ettringite, followed by the begging of AFm phases formation [6–9,80,81].

In the undersulfated systems, the sulfate depletion happens before or just after the main C_3S hydration peak, as shown in Figure 3.6. In the undersulfated sample, the amount of calcium sulfate added is not enough to delay the renewed C_3A hydration until after the main C_3S hydration peak. When this happens, the C_3S hydration is hindered and the peak becomes smaller and broader, influencing the strength development [6,33,60,80]. The heat flow curve from ternary cement pastes (Figure 3.6) differs from the heat curves of undersulfated pure C_3S-C_3A mixtures (Figure 3.7), where a higher and narrower peak (from the C_3A hydration) is observed, followed by a smaller and broader peak of heat (from the C_3S hydration) [8,81]. These differences are probably due to the C_3A

availability (which will be higher in pure monophase mixtures) [8] and the presence of iron in OPC (which decreases the reactivity of the aluminates). The reason for the delay of C_3S hydration in OPC pastes where the renewed C_3A hydration occurs early is not yet understood. This may be related to the release of aluminum ions into the solution due to the renewed C_3A dissolution, as the C_3S hydration in the aluminum containing solution is hindered [10–13]. There are several different hypotheses to explain this behavior.

In Al-contain solutions, aluminum incorporates to the bridging site and in the interlayer of C-S-H, resulting in C-A-S-H [82,83]. According to Garrault et al. [10] and Begarin et al. [84], C-A-S-H is not a suitable substrate for the C-S-H growth C-S-H nuclei themselves, and this may be the reason why the C_3S hydration is delayed. Another hypothesis is that the condensation of an alumino-silicate species at the C_3S surface, linked via hydrogen bonds to silicate surface groups, may be the reason for the inhibition of C_3S reaction [11,12]. Finally, Bergold et al. [60] suggest that this slow-down in C_3S hydration is due to AFm precipitation. These AFm phases could coagulate with the C-S-H and occupy C-S-H surface, which would become unavailable as a substrate for further C-S-H precipitation [60].

In the proper sulfated cements, the sulfate depletion point needs to be after the main C_3S hydration peak; see Figure 3.6. In these cements, the C_3S hydration occurs normally and the matrix has a proper mechanical performance.

In supersulfated cements, the sulfate depletion point occurs many hours later than the main peak of C_3S hydration. In these cements, the C_3S hydration is not negatively affected, but the mechanical performance is lower than in the proper sulfated systems, and the excess of calcium sulfate may lead to durability problems, as will be discussed in Section 3.4.

Figure 3.10 – Heat flow curves of ternary cements (OPC, slag and limestone). Undersulfated, proper sulfated, and supersulfated. SD represents the sulfate depletion point. Source: adapted from Adu-Amankwah et al. [79].

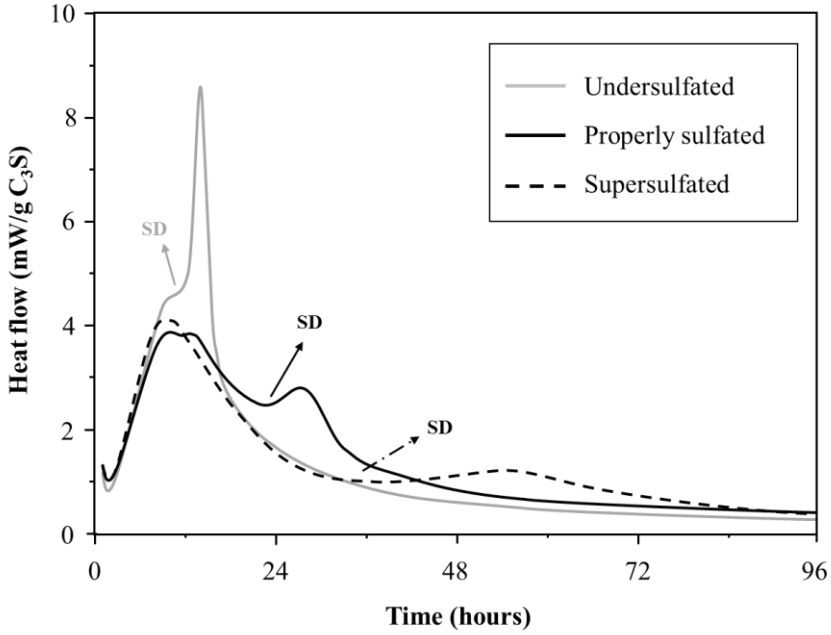

Figure 3.11 – Heat flow curves of C_3S-C_3A pastes (92-8 wt%) undersulfated and properly sulfated. SD represents the sulfate depletion point. Source: adapted from Quennoz and Scrivener [8].

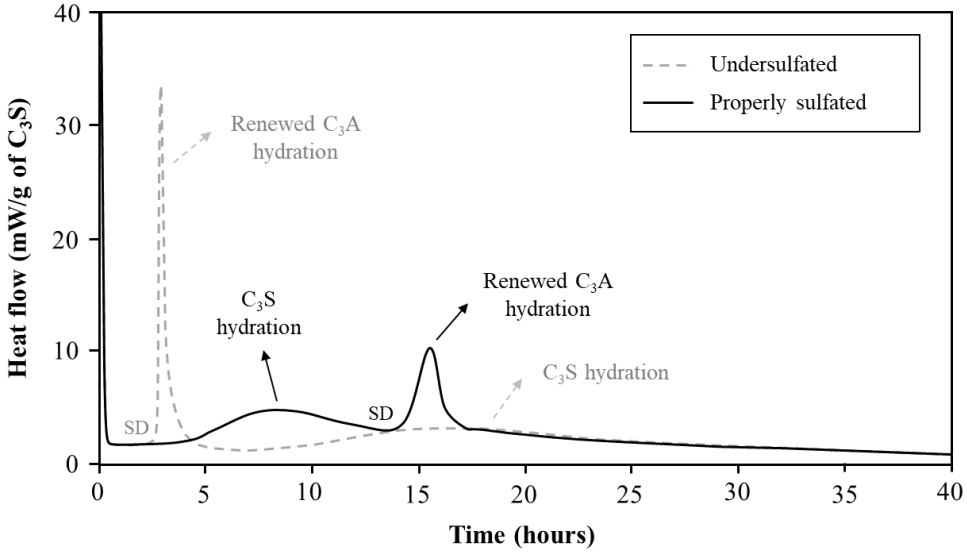

3.3 FACTORS THAT INFLUENCE THE SULFATE DEMAND

As mentioned earlier, good mechanical strength in concrete requires obtaining proper C_3S hydration; sulfate depletion needs to occur after the main alite hydration peak. Any factor that changes the sulfate supply to the solution and/or the sulfate consumption will change the optimum sulfate content. The sulfates in solution come mainly from the sulfate source

(gypsum, hemihydrate, anhydrate, alkaline sulfates, etc.) dissolution. If the dissolution is accelerated, more sulfate will be supplied, increasing its depletion and the optimum sulfate content will rise and vice versa. The sulfate of the solution is consumed by ettringite formation and C-S-H adsorption [6]. Thus, factors that increase the ettringite and/or C-S-H formation will increase the sulfate consumption, thus increasing the optimum sulfate content.

3.3.1 Physic-chemical and mineralogic properties of clinker

The fineness of cement has a significant influence on sulfate demand. Increasing the C_3A fineness increases the ettringite formation [6]. Increasing the C_3S fineness results in higher C-S-H precipitation in the first hours of curing [6]. Thus, sulfate consumption is enhanced, and sulfate depletion is accelerated. Therefore, the higher the cement fineness, the higher the amount of sulfate needed to obtain a proper sulfated system [6,85].

The C_3A content of the clinker also influences the sulfate demand. The higher the C_3A content, the higher the ettringite formation, which consumes more sulfate ions from the solution and, therefore, will increase the demand for sulfate [6,86]. According to Damidot et al. [86], in cements with more than 10 wt% of C_3A, the optimum sulfate content for maximum strength often exceed the limits of cement standards (e.g., 3.5 wt% in ASTM C150 [87], and 4.5 wt% in Brazilian standard NBR 16697 [88]). The C_4AF content excites a similar behavior as the C_3A content, but its influence is lower due to its lower reactivity [89].

The C_3S content also has a significant role in sulfate demand. More C_3S results in more C-S-H formed and more sulfate adsorbed [8]. Therefore, an increase in C_3S content might lead to a higher optimum sulfate content.

Another factor, which influences the sulfate demand, is the alkali content of cement. The higher the alkali content, the higher the amount of sulfate needed [89,90]. The alkali in cement occurs as alkali sulfates and/or are incorporated in the cement phases, mainly in C_3A and in the silicate phases. Among the alkali sulfates, different phases can be present in clinker, as thenardite (Na_2SO_4), arcanite (K_2SO_4), aphthitalite ($3K_2SO_4{\cdot}Na_2SO_4$), syngenite ($CaSO_4{\cdot}K_2SO_4.H_2O$), and calcium langbeinite ($2CaSO_4{\cdot}K_2SO_4$) [91,92].

In the presence of alkali sulfates, which are very soluble, the hydration of C_3S is accelerated in the first few days, increasing the amount of C-S-H formed [91,93], which increases the amount of sulfate absorbed by C-S-H and thus increases the sulfate demand. As observed by Fu et al. [94], the addition of 2.5% of Na_2SO_4 anticipated the sulfate depletion in two hours.

Conversely, alkaline sulfate might retard the C_3A hydration (to a lesser extent compared to calcium sulfate), thereby decreasing the sulfate demand. This delay in C_3A hydration will depend on the alkaline sulfate polymorph. Calcium langbeinite seems to greatly retard the C_3A hydration, followed by syngenite, and thenardite. Arcanite and aphthitalite also result in lower delays on C_3A hydration [91,92,95]. With the increase of calcium langbeinite content, the amount of calcium sulfate necessary for obtaining proper sulfated mixtures decreases [91]. Therefore, the higher the SO_3 of the clinker, the lower the amount of calcium sulfate that needs to be added to obtain proper sulfated cements.

On the other hand, as observed by Wistuba et al. [47] an increase in the alkali content of clinker favors an increase in orth-C_3A/cub-C_3A ratios, which anticipates the sulfate depletion. The crystalline structure of C_3A depends on the alkali content incorporated. High alkali contents favor the orthorhombic phase rather than the cubic one. As mentioned in Section 3.2.1, when studying pure phases, orthorhombic C_3A reacts much faster than cubic C_3A in the presence of calcium sulfate, increasing the amount of ettringite formed and increasing the consumption the sulfate of solution. Thus, the orth-C_3A/cub-C_3A ratio of clinker probably influences the optimum sulfate content, but further studies are needed to verify this assumption, as there are differences between pure C_3A polymorphs and C_3A polymorphs from industrial clinker, which might influence its reactivity.

The C_3S polymorphism and/or the ions doping changes its reactivity [70,74,84]. As discussed in Section 3.2.2, the M1 polymorph seems to be more reactive than the M3 polymorph [70]. Regarding ion doping, Al_2O_3 [74,84] and Fe_2O_3 [74] retards the C_3S hydration, while the MgO slightly increases it [74]. Therefore, these factors will influence the C-S-H formation rate and affect the sulfate consumption by its adsorption. Thus, it will probably alter the optimum sulfate content.

3.3.2 Physics, chemical, and mineralogic properties of the sulfate source

The optimum sulfate content is related to the SO_3 content rather than to the solid sulfate content. Therefore, the higher the SO_3 content of the sulfate source, the lower the amount of the solid sulfate source needed to obtain proper sulfated cements. Sulfate solubility plays a huge role in the sulfate demand. Generally, the higher the calcium sulfate solubility, the higher the optimum sulfate content. The solubility of calcium sulfate varies with its fineness (surface area) and its chemical/mineralogical composition. The higher the sulfate source surface area, the higher its solubility. Therefore, as observed by Barbosa et al. [96], the increase in gypsum fineness anticipates the sulfate depletion and renewed C_3A hydration. Thus, a higher calcium sulfate fineness tends to increase the sulfate demand of the cement.

Regarding the calcium sulfate source, gypsum ($CaSO_4 \cdot 2H_2O$) and natural anhydrate ($CaSO_4$) are commonly used in cement production; however, depending on temperature of the cement mill, gypsum may be dehydrated to hemihydrate ($CaSO_4 \cdot 1/2H_2O$) and soluble anhydrite ($CaSO_4$) [3]. The crystal structure and composition of calcium sulfate impact its solubility [25,97], as shown in Figure 3.8; hemihydrate and the soluble anhydrite are the most soluble, followed by gypsum and then natural anhydrite [3].

Mixtures with hemihydrate form more ettringite in the first hours, increasing the sulfate consumption and anticipating sulfate depletion [6,25,98]. Thus, from these observations, it is expected that the use of a more soluble calcium sulfate polymorph (i.e., hemihydrate and/or soluble anhydrite) will increase the optimum sulfate content. The use of natural anhydrite or gypsum, which have similar solubility, seems to result in the same optimum SO_3 content [99].

Note: it is essential to have a correct adjustment between C_3A reactivity and sulfate solubility. If gypsum or natural anhydrite is used to control the hydration of cements with high C_3A activities (high content and/or the orthorhombic form), a flash set may occur due to the insufficient amount of sulfate in solution, causing the formation of OH-AFm or SO_3-AFm [86,100,101]. On the other hand, if a more soluble calcium sulfate (hemihydrate or soluble anhydrite) is used in cements with low C_3A activity, false set may occur due to the formation of gypsum [100,101]. Therefore, to obtain properly sulfated mixtures, a rule of thumb would be to use more soluble calcium sulfates

(hemihydrate or soluble anhydrite) in cements with high C_3A reactivity and less soluble calcium sulfates (gypsum or natural anhydrite) in cements with low C_3A reactivity. Further studies on this subject are required to fully understand this mechanism.

Figure 3.12 – Dissolution rates of gypsum, hemihydrate, soluble anhydrite, and natural anhydrite. Source: adapted from Dodson and Hayden [3].

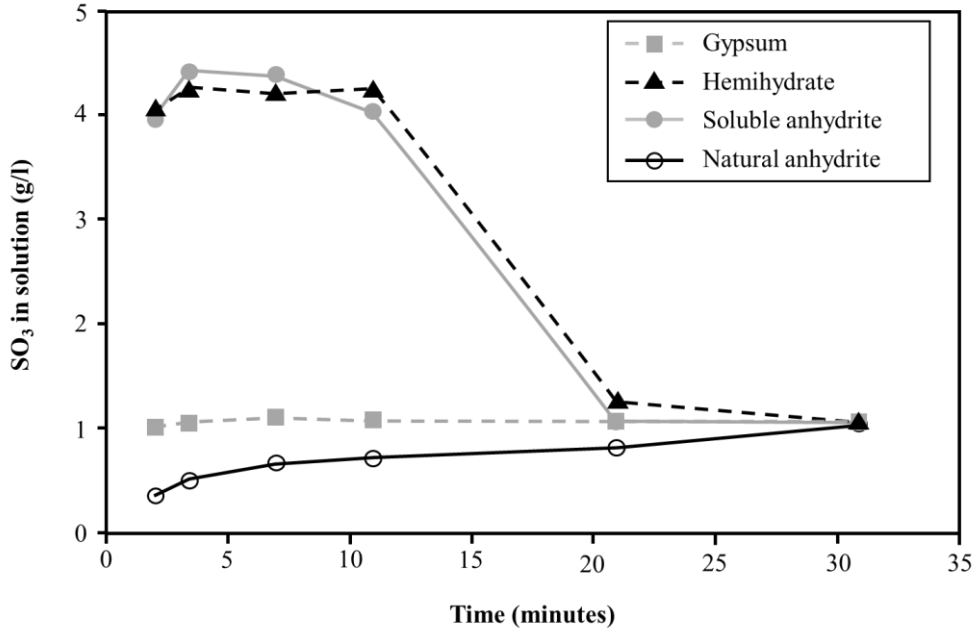

The influence of sulfate ions on pure cubic C_3A hydration depends on the type of cation (Na, Mg or Ca). Liu et al. [27] have shown that $MgSO_4$ causes the most significant retardation, followed by $CaSO_4 \cdot 2H_2O$, and Na_2SO_4. In addition, Fu et al. [94] observed that the addition of Na_2SO_4 anticipates the sulfate depletion point in slag-cement mixtures, thus increasing the sulfate demand. This probably occurs due to the increase in alite hydration and, as a result, in C-S-H formation in the presence of Na_2SO_4. Therefore, the cation in sulfate probably influences the optimum sulfate content in Portland cements, as observed by He et al. [102] when studying $MgSO_4$, $CaSO_4 \cdot 2H_2O$, Na_2SO_4 and K_2SO_4. Further investigations are needed to verify and provide more information regarding this process.

Many studies also have shown the potential of using phosphogypsum as a replacement for gypsum [103–105]; however, the presence of impurities (P_2O_5) in phosphogypsum delays the C_3S hydration [105], changing the sulfate consumption rate, which may influence the optimal sulfate content. A study Radwan and Heikal [106] phosphogypsum

impurities actually accelerate C_3A hydration. To the best of the authors' knowledge, no systematic study regarding the sulfate optimization with phosphogypsum has been published yet. This is an area that should be studied without delay as phosphogypsum as a setting regulator seems to be a future trend. It is also essential to verify Radwan and Heikal [106] results regarding the effect of phosphogypsum impurities on C_3A hydration and shed light on this mechanism.

The distribution of sulfates seems to be as important as the other factors already mentioned. As showed by Tang and Gartner [92], the C_3A hydration rate is much lower in cements where clinker and gypsum were interground when compared to cements which they were interblend. Intergrinding increases the sulfate supply rate by reducing the diffusion distances between the sulfate and aluminate phases [92]. Thus, when testing to determine the optimum sulfate content is important to intergrind the calcium sulfate with clinker (as is typically done by the cement industry), as the intergrinding results in lower sulfate demand, and the results obtained with interblend will not be representative of the intergrinding cements [92].

3.3.3 Supplementary Cementitious Materials (SCMs)

As reported by many researchers, replacing cement (clinker + calcium sulfate) by SCMs as slags [107,108], fly ash [100,109–112] (especially high calcium fly ashes [109,112]), silica fume [113], calcined clay [9,114–117], limestone [9,118], red mud [119,120], zeolite [121], and ground waste expanded perlite (highly reactive pozzolan) [113], usually anticipate sulfate depletion, thus increasing the sulfate demand per clinker. Because of the high amounts of calcined clay and limestone, LC^3 cements usually require more gypsum in comparison with plain Portland cement [9,122–127]. As demonstrated by Zunino and Scrivener [9] (Figure 3.9), replacing approximately 50% of the OPC with a mixture of calcined clay and limestone (2:1), i. e. the LC^3 50 cement, anticipates sulfate depletion and, in this case, the mixture became slightly undersulfated. To adjust the sulfate balance here, required adding 3 wt% of gypsum to the LC^3 50 cement [9].

Figure 3.13 – Heat flow curves of OPC and LC^3 50 cement. SD is the sulfate depletion point. Source: adapted from Zunino and Scrivener [9].

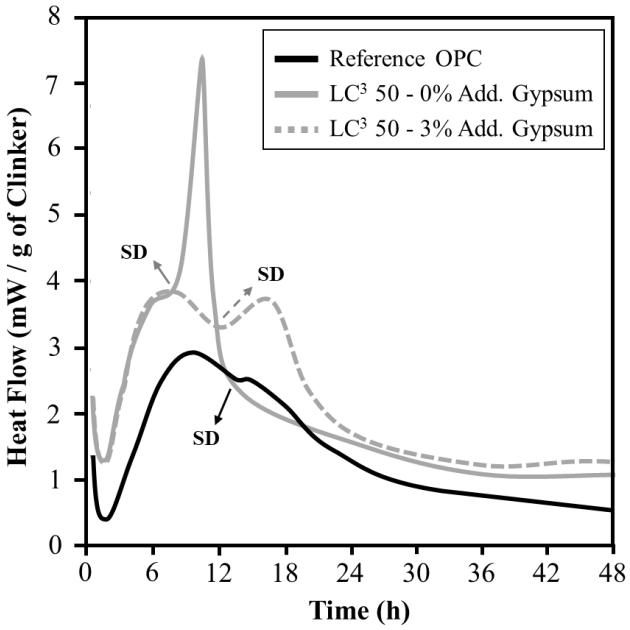

Note that by replacing OPC (cement + calcium sulfate) with SCMs, the content of calcium sulfate concerning cement mass decreases, but remains the same in regard to clinker. Usually, this anticipates sulfate depletion, and the mixture could become undersulfated, requiring more sulfate. In these situations, the optimum sulfate content per clinker will be higher than the OPC, but the optimum sulfate content per cement will be lower. The lower optimum sulfate content in relation to cement mass is expected and by replacing clinker with SCMs will result in the mixture having less C_3A and less C_3S. Note: the increase of the optimum sulfate per clinker by SCMs is possibly related to two main factors: filler effect and alumina content.

First, when SCM replaces a portion of clinker, the C_3S hydration is accelerated due to more space available for the hydrates of clinker phases to form in and adhere to the surface of the SCM particles, which act as sites for heterogeneous precipitation and growth of hydrates [9,80]. Thus, as more C-S-H is formed, more sulfate is adsorbed, increasing the sulfate demand per clinker [9,80].

Generally, C_3S hydration increases with the increase in SCM content, directly influencing the sulfate demand. Also, the higher the SCM surface area, the higher the enhancement in C_3S hydration and C-S-H formation [9,80]. Thus, SCMs with higher surfaces areas have a higher sulfate demand [80,108,110,114,116,119,120,125].

The aluminum content of the SCMs may also influence sulfate demand [9]. Using SCMs with higher aluminum contents, increases the amount of ettringite formed, which increases the sulfate consumption and anticipating sulfate depletion. Using SCMs with higher amounts of alumina seems to increase the sulfate demand. Zunino and Scrivener [9] disagree despite the majority of the studies indicating that the alumina content influences the optimum sulfate content. They contend that the aluminum content of calcined clay does not influence the sulfate demand. They studied two different clays with different aluminum contents and different surfaces areas. The clay with higher aluminum content and lower surface area presented a lower sulfate requirement than the other clay [9]. Although this clearly shows the great impact of surface area on sulfate demand, it is impossible to conclude that aluminum content does not influence the optimum sulfate content as SCMs with higher aluminum content usually increase the amount of ettringite formed.

Whittaker et al. [108] studied slags with similar particle size distribution but different alumina contents. The sulfate depletion occurred early in the cement with slag with the higher alumina content, indicating that the alumina content influences sulfate demand. In a study by Avet et al. [125], the sulfate depletion occurred early in the mixture with the calcined clay, which contained 95.0 wt% of kaolinite (43.8 wt% of Al_2O_3) when compared to the mixture with the calcined clay, which contained 50.3 wt% (32.3 wt% of Al_2O_3), despite its much lower B.E.T. surface area (9.6 m^2/g for the clay with higher alumina content and 45.7 m^2/g for the other). Based on these results, the alumina content seems to have significant influence on the sulfate demand. Additional study on the role of SCM aluminum content on the optimal sulfate content is required to confirm the finding of Zunino and Scrivener [9].

The effect of limestone on optimum sulfate content is also not clear. Some authors [9] state that an increase in limestone increases the optimum sulfate content due to filler effect for the other SCMs. The enhancement in cement hydration is generally higher when using limestone compare to others SCMs, as the limestone surface seems to have a stronger bond interaction with calcium ions [9,115]. According to Campiteli et al. [85] the limestone actually decreases the optimum sulfate content for maximum strength. This behavior may be related to the change in phase assembly when using limestone, which stabilizes hemicarboaluminate and monocarboaluminate instead of monosulfate, thus increasing the ettringite formation [54,128]. This changes the volumes of solid and,

therefore, the strength. Thus, the optimum SO_3 content for maximum strength may differ in cements with limestone compared to plain cements. Further investigations are needed to verify the results postulated by Campiteli et al. [85] and understand why a decrease in the sulfate demand occurs in the presence of limestone.

Some SCMs—e.g., fly ash [109,112] and in particular circulating fluidized bed combustion (CFBC) fly ashes [129,130]—contains sulfates in their composition. The sulfates from SCM, if available in the early hours of hydration, will help control C_3A hydration by reducing the amount of calcium sulfate and obtaining a properly sulfated mixture. Unfortunately, as sulfates are present in different phases of the chemical reaction, with different solubilities, the decrease in the calcium sulfate to obtain maximum performance is not straightforward. Sulfates can be found in fly ash and other SCMs as alkali sulfates and calcium sulfate (dihydrate, hemihydrate, or anhydrous), which are relatively soluble and will contribute to the sulfate demand of cement. Alternatively, sulfates can be present in the glassy phase, which would not be necessarily be soluble at the early ages; therefore they could not contribute to the sulfate demand of the cement [109,112]. More investigation on this subject is encouraged to properly understand the effect of the sulfates from SCMs on the sulfate demand of OPC.

Note that the influence of SCMs on the sulfate demand of Portland cement is not straightforward, as it may depend on the particle size, chemical composition, and solubility, among other factors. Therefore, when analyzing a new SCM, it is important to verify its impact on the sulfate demand of the cement in order to obtain the best performance and avoid incompatibilities.

In some countries, such as the United States, it is common to add the SCMs in the concrete stage instead of during cement production [131]. This can become problematic as the SCM may increase the sulfate demand of the cement, which would render the mixture undersulfated and cause problems such as setting, workability, and strength development. When added to the mix during cement production, the industry can control the sulfate demand and adjust the sulfate content in a much better way.

3.3.4 Chemical admixtures

Many chemical admixtures used in mortars and concrete influence the reactivity of cement phases and the dispersion and wetting of cement grains. In addition, they may affect the dissolution of sulfates [100], i.e., the optimum sulfate content.

Water reducers, plasticizers, or superplasticizers affect cement hydration. Polycarboxylate-ether (PCE), naphthalene sulfonate formaldehyde polycondensate (NSF) and lignosulfonate (LS) admixtures result in retarding alite hydration, thus prolonging the induction period and lowering the C-S-H formation rate [132–135]. According to Kishar et al. [136] however, the NSF accelerates the conversion of ettringite to monosulfate. The same behavior was observed by Rosa [137] and by Jiang et al. [138] when studying pure C_3A pastes with PCE admixtures. As observed by Ng and Justnes [134] and Jansen et al. [135], the presence of PCE, NSF, or LS admixtures approaches the sulfate depletion point from the main hydration peak of alite, as shown in Figure 3.10 [134], indicating that these chemical admixtures increase the sulfate demand.

Figure 3.14 – Heat flow curves of reference OPC without chemical admixture and with 0.2 wt% (in relation to OPC) of naphthalene sulphonate-formaldehyde (NSF), lignosulfonate (LS), and polycarboxylate superplasticizers of short side chains (PCE-1), long side chains (PCE-2), and long and very long side chains (PCE-3). Source: adapted from Ng and Justnes [134].

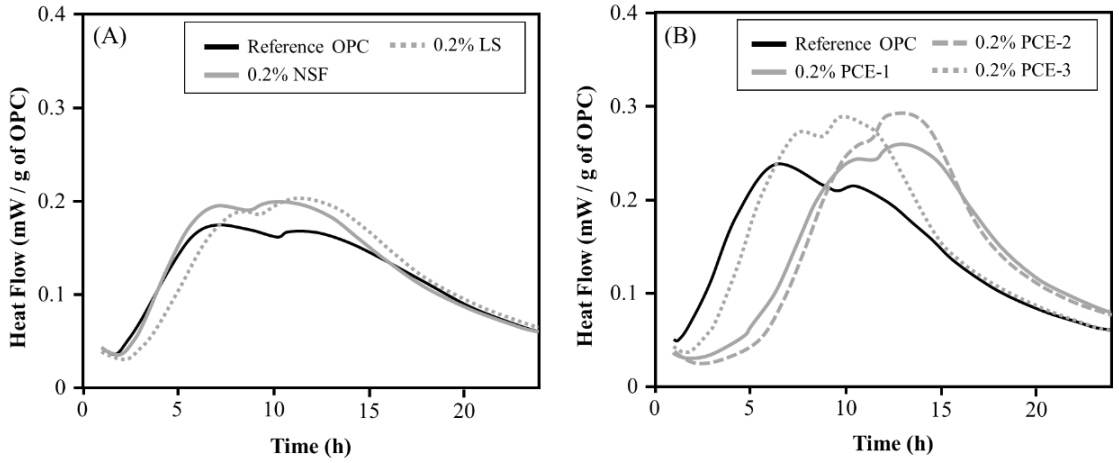

There are three main hypotheses to explain this behavior [139]. First, the adsorption of the superplasticizer on the sulfates may slow down the dissolution of the calcium sulfate, thereby decreasing the supply of sulfate ions to the solution [3,135,139,140]. The lower the rate of sulfate ions supplies into the chemical admixture solution might not be enough to “feed” the dissolution of C_3A, creating a “false” sulfate depletion [135,139].

The second hypothesis is that the presence of superplasticizer leads to a faster sulfate consumption due to the better dispersion of anhydrous particles [139]. The third hypothesis is that the PCEs-based admixtures enhance ettringite nucleation, providing a large surface area for the growth of the hydration products, resulting in faster consumption of sulfates [139]. Why PCE admixtures enhance ettringite nucleation is not well understood [139]. Additional investigations are needed to understand this mechanism and the chemical admixture's influence (e.g., chain length, etc.) on the optimum SO_3 content.

Also worth mentioning is that the sulfate amount added may interfere with the efficiency of the chemical admixture. At the optimum SO_3 content, C_3A reacts with the sulfates in solution, forming ettringite, and the superplasticizer admixtures adsorb onto aluminate hydrates and silicates phases, increasing the fluidity of the mixture [133,141]. That said, the superplasticizer effect of PCE decreases with an increase in the content of sulfate added, being most significantly influenced by the alkali sulfates (Na_2SO_4 and K_2SO_4) when compared to gypsum and $MgSO_4$ [102,141]. When the content of sulfate in cement paste increases, the amount of sulfate ions in solution increases and is competitively adsorbed onto cement surfaces, thereby reducing the adsorption of PCE and decreasing its superplasticizer effect [49,102]. If the soluble sulfate/C_3A ratio is too low, hydration of C_3A occurs, resulting in the formation of aluminate hydrates that adsorb the chemical admixtures and form organo-mineral phases, thus reducing the superplasticizer effect of PCE [49,133,141]. These "incompatibilities" between superplasticizer and cement can be avoided if the amount of calcium sulfate and the solubility of the sulfate source is well adjusted.

The use of accelerators and retarders also changes the sulfate demand of the cement. The accelerators enhance the C_3S and C_3A hydration, increasing the sulfate consumption and accelerating the sulfate depletion [100,142,143]. This effect is higher in aluminum-containing accelerators with high Al_2O_3/SO_4^{2-} due to the reaction between the sulfate and the alumina from the chemical admixture [142]. Salvador et al. [143] have observed this behavior in mixtures with both main types of accelerators, alkaline and alkali-free. Note: the sulfate depletion occurs early in the mixtures with alkaline accelerators. The accelerators compositions explain this result. As the alkali-free accelerator is based on an aluminum sulfate solution (while the alkaline type is based on sodium aluminate solution), the sulfates from the chemical admixture provide more sulfate to the solution

even though the sulfate concentration in solution was always lower than that in the reference paste [143].

As for other chemical admixtures, the amount and composition of calcium sulfate added might influence the accelerator efficiency. Maltese et al. [144] have observed that the lower the dissolution rate of the calcium sulfate, the more efficient is the accelerator.

Retarders might also influence the sulfate demand for cement. Although all retarders delay the C_3S hydration, the effect on C_3A hydration is different depending on the type of retarder used. As observed by Bishop and Barron [145], while tartaric acid retards the C_3A hydration and ettringite formation, sucrose and the lignosulfonate-based admixture accelerate it. Thus, retarders probably have different effects on optimum sulfate content. Studies on this subject are quite scarce and this should be the subject of future research.

Grinding aids are commonly used during the comminution of clinker to reduce electrostatic forces and minimize agglomeration between clinker and SCM grains [146,147]. The chemical composition of the grinding aids includes glycols–propylene glycol (PG), monoethylene glycol (MEG), and diethylene glycol (DEG); alkanolamines-triethanolamine (TEA), triisopropanolamine (TIPA), and diethylisopropanolamine (DEIPA); and polycarboxylate ethers (PCEs) [146]. The use alkanolamines promotes the reaction of C_3A, thus increasing the amount of ettringite formed (which anticipates the sulfate depletion) and enhancing the aluminate reaction [146,148]. More investigations are needed to fully understand the effect of the alkanolamines on the sulfate demand and investigate the impact of other types of grinding aids (such as the glycols) on cement hydration and sulfate optimization.

3.3.5 Water/binder ratio

The water/binder ratio (or water/cement ratio) influences cement hydration. Generally, when the w/c ratio decreases, the concentration of alkalis in the solution increases, increasing the cement hydration rate [149]; however, due to the lower space available for the hydrates to grow and the lower amount of water available to hydrate, the long-term degree of hydration is decreased [90,100,111,150]. If the water/binder (w/b) ratio alters cement hydration, it probably influences the sulfate demand. In the study Wyrzykowsky and Lura [151] the OPC that was properly sulfated at a w/b ratio of 0.30 became under-sulfated at a w/b ratio of 0.16. As observed by Zunino and Scrivener [126], the sulfate

depletion occurred slightly early in the LC^3 system, with a w/b ratio of 0.4 compared to the mixture w/b ratio of 0.8. Despite delaying the sulfate depletion, the increase in w/b ratio enhanced the aluminate peak of LC^3 systems [126]. More investigation on this subject is needed to properly understand the effect of w/b ratio on the sulfate demand of OPC.

3.3.6 Hydration age

At later ages, although the optimum sulfate content seems to be higher [149,152], it is less pronounced [13] (see Figure 3.11 [111], demonstrating that there is a different optimum sulfate content for each age. The reason for this is not clear and is counterintuitive. The opposite effect would be expected, i.e., the optimum sulfate content decreases with age, as calcium sulfate enhances the hydration of C_3S, resulting in higher initial strength, but lowers the final strength due to the decrease in C-S-H density and the lower amount of C-S-H formed as less clinker (hence less C_3S and C_2S) is present in the cement. It is speculated that this behavior might be related to the SO_3 content needed to result in the maximum volume of aluminate phases at each age, which impacts the volume of solids, the porosity, and the strength. As observed by Cottin and Vibert (1976) [1] and cited by Kurdowski [152], the gypsum content needed for the maximum volume of aluminate phases increases with time, which could explain the higher optimum sulfate content at later ages. Further studies regarding the variation of optimum sulfate content with the age are required to understand this phenomenon properly.

Figure 3.15 – Mechanical strengths vs sulfate factor. Example of the procedure to determine the optimum sulfate content. Source: adapted from Tsamatsoulis and Nikolakakos [111].

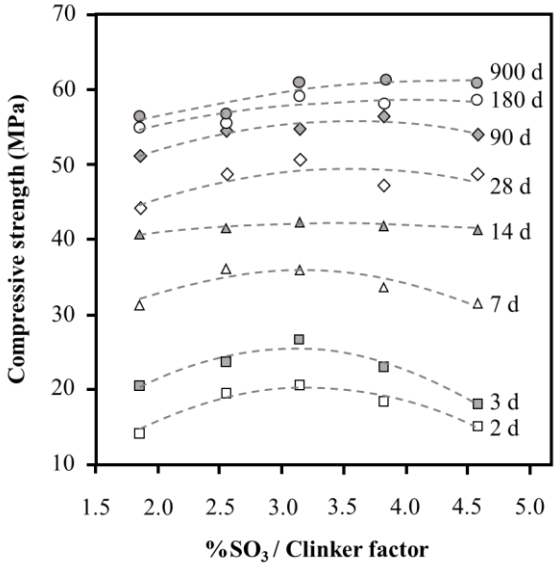

1 B. Cottin, C. Vibert. Poisoning of tricalcium silicate hydration by soluble alumina Cement-Wapno-Gips, 7 (1976) 193-196.

3.3.7 Curing conditions

The dissolution of gypsum [153] and anhydrous cement, and the precipitation of hydrates increases with the temperature [154,155], prompting the rapid consumption of sulfates from the solution and anticipating sulfate depletion [152,156]; simply, high curing temperatures results in higher optimum sulfate content [89,111,152,156].

The relative humidity (RH) also plays a vital role in cement hydration, especially when low water/binder ratios (w/b < 0.30) are used. As observed by Wyrzykowsky and Lura [151], water-saturated cement pastes hydrate faster than the sealed ones. It stands to reasons that a change in RH might influence sulfate demand. Further investigations are needed to fully understand this mechanism.

As discussed in Section 3.4.5, DEF formation occurs in mortars and concretes that have been cured at high temperatures (> 65 °C) and in moist environments. As observed by Al Shamaa et al. [157], RH greatly influences the probability of DEF. Clearly, as the curing temperature and RH are predominant factors in DEF; they should be considered together with the sulfate content to prevent durability problems.

3.3.8 Summary of the effects that influence sulfate optimization

Table 3.1 summarizes the main factors that may influence the optimum sulfate content in Portland cement (direct, inverse, or unknown) and the state-of-knowledge (well known or needs further investigation).

Table 3.2 – Main factors that may influence the optimum sulfate content.

Type	Sub-type	Relationship	Status
Clinker	Fineness	Direct	Well known
	Alkali content	Direct	Well known
	SO_3 content	Inverse	Well known
	C_3A and C_4AF content	Direct	Well known
	C_3S content	Direct	Well known
	C_3A polymorphism	Unknown	Needs further investigation
	C_3S polymorphism	Unknown	Needs further investigation
Sulfate source	SO_3 content	Inverse	Well known
	Fineness	Inverse	Well known
	Composition (solubility)	Inverse	Needs further investigation
	Impurities (phosphogypsum)	Unknown	Needs further investigation
	Cation	Unknown	Needs further investigation
	Distribution in cement	Inverse	Well known
SCMs	Content	Inverse	Well known
	Fineness	Direct	Well known
	Aluminum content	Uncertain	Needs further investigation
	Sulfate content	Uncertain	Needs further investigation
Admixtures	Plasticizers	Direct	Needs further investigation
	Setting accelerators	Direct	Needs further investigation
	Retarders	Unknown	Needs further investigation
	Grinding aids - alkalonamines	Direct	Needs further investigation
	Grinding aids - glycols	Unknown	Needs further investigation
Water/binder ratio		Inverse	Needs further investigation
Hydration age		Direct	Needs further investigation
Curing conditions	Temperature	Direct	Well known
	Relative humidity	Unknown	Needs further investigation

3.4 INFLUENCE OF SULFATE CONTENT ON THE CEMENTITIOUS MATRIX PROPERTIES

As discussed in Section 3.2.3, the sulfate content has a significant effect on cement hydration kinetics. It also changes the composition of the phase assemblage and influences other properties, e.g., setting time, workability and rheology, mechanical performance, and drying shrinkage, and may impact a cement's long-term performance, i.e., durability.

3.4.1 Effect of sulfate content on setting time

The increase of calcium sulfate content delays the initial and final setting times until a limit is reached. Further addition of calcium sulfate does not influence the setting time [158]. In addition, the inadequate amount/type of sulfate may lead to two types of premature setting: flash set and false set.

Undersulfated systems may present a "flash set" due to the quick reaction of C_3A, with the formation of calcium-alumina hydrates, making most practical applications of Portland cement unfeasible [4]. When the flash set occurs, further mixing cannot break apart the microstructure that has formed, and subsequent strength development is poor [31,159].

The presence of hemihydrate ($CaSO_4 \cdot 1/2H_2O$) in OPCs—that can be formed from the dehydration of gypsum during grinding—can result in premature stiffing known as "false set," in the first few minutes due to its rehydration and formation of gypsum ($CaSO_4 \cdot 2H_2O$) [159,160]. Stiffing results from interlocking needle-like gypsum crystals and the reduction in free water available to lubricate the system and promote fluidity [31]. Further mixing can overcome this premature stiffing, and the subsequent strength development is not greatly affected [31,159].

3.4.2 Effect of sulfate content on workability and rheology

Typically, increasing the sulfate content of the cement increases the water demand [158], the viscosity [102], and the yield stress [102] of cementitious mixtures. Gypsum is softer than clinker; therefore, when it is interground with clinker it usually shows a higher surface area, which is responsible for the increase in the water demand [158]. In addition, more ettringite is formed at higher sulfate contents, which has a prismatic/needle shape and high surface area, and greatly impacts the viscosity of cement paste [97].

The composition of the calcium sulfate added also influences the rheology of the cement paste. The use of hemihydrate, which has a higher solubility than gypsum, increases the amount of sulfate on the solution and changes the ettringite morphology from spherical or stubby rod to elongated ettringite [161]. According to Mbasha et al. [161], this change in the ettringite morphology is responsible for increasing the yield stress and plastic viscosity of the cement pastes.

3.4.3 Effect of sulfate content on the degree of hydration and chemical shrinkage

As discussed in Section 3.2.3, the amount of sulfate greatly influences the cement hydration and, consequently, the degree of hydration. Usually, the degree of hydration of the cement increases with the increase of the amount of sulfate until a certain content is reached—the optimum SO_3 content—and then decreases. In this sense, chemical shrinkage related to the degree of the hydration of the cement is influenced in the same way by the sulfates; i.e., the cement with the optimum SO_3 content presents the highest chemical shrinkage [79].

3.4.4 Effect of sulfate content on porosity and mechanical strength

The sulfate content also influences the porosity and the mechanical strength of the cement. The optimum sulfate content shows the lowest porosity with the highest strength [62,79,158]. As mentioned in Section 3.2.3, in undersulfated systems, the C_3S hydration is inhered, greatly impacting the porosity and the strength mainly in the first days. Adding more calcium sulfate increases the SO_3/Al_2O_3 ratio in the cement, resulting in relatively more ettringite and less monosulfate [86]. Ettringite has a higher volume compared with monosulfate; therefore, as the volume of solids increases, it modifies the porosity distribution, lowers the total porosity and increases the mechanical strength [62,79]. The higher the sulfate content, the higher the solid volumes, and, until a determined value (i.e., the optimum sulfate content), the lower the porosity and the higher the strength.

Further additions of calcium sulfate—over the optimum content—increase the porosity and thus decrease the mechanical strength. This behavior probably is due to the decrease in the C-S-H amount, as the clinker content is lower. Moreover, it may also be related to the reduction of density and increase of C-S-H gel porosity with an increase of sulfate added and the consequent decrease in C/S mole ratio [79], leading to a decrease in the intrinsic strength of C-S-H gel [18,62].

A higher volume of solids means there is less liquid available to evaporate. Thus, an increase in the sulfate content usually decreases drying shrinkage until a certain value is reached. The optimum SO_3 content for maximum cement mortar strength usually coincides with the optimum sulfate level for minimum concrete shrinkage under normal curing conditions [100].

3.4.5 Effect of sulfate content on long-term performance (durability)

The excess of sulfate can be deleterious to a concrete's durability, as the increase in the SO_3 content of cements increases the risk of delayed ettringite formation (DEF) [14–16], which is the formation of ettringite in a cementitious material after the concrete has set. This formation may occur in cementitious materials that have been cured at elevated temperatures (above 65 °C) or in massive concrete structures [162–164]. Delayed ettringite formation causes expansion and cracking, increasing the porosity and permeability, facilitating the entry of aggressive agents as CO_2 and chlorides, and reducing the lifetime of concrete structures [157,162,163]. Thus, cement standards usually limit the maximum content of SO_3 in cements, depending on the type of cement. The threshold of 5 to 6% SO_3 is commonly accepted in the literature for expansion [31].

3.4.6 Summary of the effects of sulfates on cement properties

It is important to keep in mind that the amount needed to optimize each property (rheology, setting time, porosity, drying shrinkage, and mechanical strength) may not be the same, and different "optimum sulfate content" can exist for each cement [31,158]. Table 3.2 summarizes the effects of sulfate content on the properties of cementitious mixtures.

Table 3.3 – Effects of sulfate content on the properties of cementitious mixtures.

Property		Effect	References
Setting time	Increase of SO_3 content	Increase of initial and final setting times until a plateau value	[158]
	Insufficient amount of SO_3 (undersulfated systems)	Flash set	[4,31,159]
	Use of hemihydrate ($CaSO_4 \cdot 1/2H_2O$)	False set	[31,159]
Rheology	Increase of sulfate content	Increase of viscosity, yield stress and water demand	[102,158]
	Use of hemihydrate ($CaSO_4 \cdot 1/2H_2O$)	Increase of viscosity, yield stress and water demand	[161]
Porosity	Increase of sulfate content	Decreases until an optimum content and then increases	[62,79]
Mechanical strength	Insufficient amount of SO_3	Poor mechanical strength	[62,79,158]
	Increase of sulfate content	Increases until an optimum content and then decreases	[62,79,158]
Chemical shrinkage	Increase of sulfate content	Increases until an optimum content and then decreases	[79]
Drying shrinkage	Increase of sulfate content	Decreases until an optimum content and then increases	[100]
Durability	Increase of sulfate content	Increases the risk of DEF	[14–16]

3.5 METHODS TO DETERMINE THE OPTIMUM SULFATE CONTENT

The determination of the initial and final setting times by the Vicat needle [165] is the most popular method used by the cement industry to adjust the calcium sulfate content. This method can verify setting problems as flash set or false set, and if the amount of calcium sulfate added provides an adequate setting time. As discussed in Section 3.4.1, the setting times increase with the increase in calcium sulfate content until a plateau value. In this test, the amount of SO_3 is chosen as the amount that results in a specific initial and final setting time. This method cannot determine the optimum sulfate content, which will result in the highest mechanical strength and lowest shrinkage.

There are some empirical equations in the literature to determine the optimum SO_3 content [31,152]. Because many factors influence the optimum sulfate content (as discussed in Section 3.3), these formulae have limited practical importance [13]. The best and most used way to determine the optimum sulfate content is to test different mixtures and varying the sulfate content.

The optimum sulfate content is usually defined by measuring the mechanical strength or the heat released by mixtures of the same components (clinker or SCM) with different calcium sulfate contents. ASTM C563 [21] describes the method to determine the optimum sulfate content by using either isothermal calorimetry and/or measuring mechanical strength. This standard [21] recommends that at least five mixtures with different SO_3 contents should be tested. The SO_3 should differ more than 0.20 wt% between the individual mixes, and the maximum and minimum SO_3 content of the blended samples must differ by at least 2.0 wt%. The higher the number of samples with different SO_3 contents tested, the more accurate the optimum sulfate content will be. The cement fineness should be as similar as practically possible [13,149,166].

Isothermal calorimetry is a simple, convenient, and rapid way of determining the optimum sulfate content [13,109,166]. The optimum sulfate content is determined by plotting the cumulative heat at determined age (i.e., 1, 3, or 7 days) as a function of the SO_3 content in the cement; see Figure 3.12. The heat recorded before the end of the induction period should not be considered in this cumulative heat due to the lower reproducibility of the initial peak [13]. Due to the low amount of heat released after 7 days, the calorimetry should not be used to determine the optimum sulfate content at later ages.

Measuring mechanical strength, the most common method to gauge the optimal sulfate content, is widely used by the cement industry. It is simple and does not need expensive equipment. It does demand a higher amount of material, which can be problematic for some studies with limited materials. The strength of each formulation is plotted, and a parabolic least square fit is realized in a similar method to isothermal calorimetry. The optimum sulfate will then be the x values that provide the highest strength; see Figure 3.12.

Although not as popular compared to isothermal calorimetry and compressive strength tests, ASTM C563 [21] describes the determination of the optimum sulfate content by the drying shrinkage of mortars. In this case, the optimum content is usually defined as the content of

calcium sulfate, resulting in the lowest drying shrinkage. Similarly, the chemical shrinkage test, described by Geiker [167], can also be used to optimize the amount of sulfate in Portland cement [79]. In this test, the optimum SO_3 content is that which results in the highest chemical shrinkage at a specific age—indicating the highest degree of hydration.

Figure 3.16 – Example of the procedure to determine the optimum sulfate content.

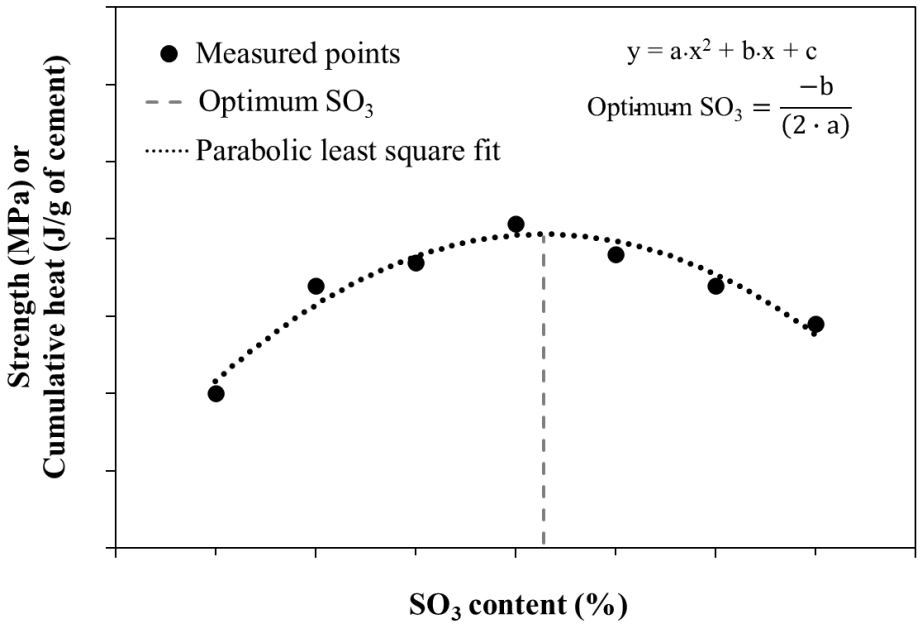

Note: none of the previous tests assess the long-term performance/durability of the cement paste, mortar, and/or concrete. As discussed in Section 3.4.5, the sulfate content might significantly influence the durability of the cement matrix, especially when an excess of sulfate in used that can lead to delayed ettringite formation (DEF). Therefore, the determination of the optimum sulfate content should be combined with durability tests that evaluate the probability of DEF, per the Duggan test [15,168] or similar method [16,169].

Table 3.3 summarizes the different methods that can be used to optimize sulfate content, in addition to the advantages and disadvantages of each method. The optimum sulfate content may not be a specific number but rather a range of SO_3. In addition, the optimum sulfate content might vary according to the performance criteria (mechanical strength, shrinkage, etc.) and with the age; see Section 3.3.6. Therefore, the optimum SO_3 content should be a compromise between the different performance criteria and the different ages.

Table 3.4 – Methods to determine the optimum sulfate content.

Method	Advantages	Disadvantages
Mechanical strength	• Quite common. • Do not require expensive equipment.	• Requires more material than calorimetry (600 g of cement per SO_3 content per age). • Time-consuming. • Do not evaluate long-term performance (durability).
Calorimetry	• Easy to test. • Rapid. • Can be carried out at a wide range of temperatures. • Requires less material than the other tests (depend on the equipment used, but usually between 5-50 g of cement per content of SO_3).	• Inaccurate in determining the optimum SO_3 content at later ages (> 7 d). • Require a calorimeter, which may not be available in all laboratories. • Do not evaluate long-term performance (durability).
Setting time	• Most common. • Verifies setting problems (flash set or false set).	• More laborious than the other techniques (as calorimeter). • Do not determine an optimum SO_3 content (only determines the SO_3 content, resulting in a specific setting time). • Requires more material than calorimetry (at least 1000 g of cement per SO_3 content). • Do not evaluate long-term performance (durability).
Chemical shrinkage	• Do not require expensive equipment. • Requires less material than the other tests (depend on the setup used, but usually between 5-30 g of cement per content of SO_3).	• Time-consuming. • Do not evaluate long-term performance (durability).
Shrinkage	• Do not require expensive equipment.	• Requires more material than calorimetry (750 g of cement per SO_3 content). • Time-consuming. • Do not evaluate long-term performance (durability).
Probability of DEF	• Evaluates the probability of occurrence of DEF, which will influence the long-term performance (durability).	• Time-consuming. • Do not determine optimum SO_3 content.

3.6 SUMMARY AND PERSPECTIVES FOR FUTURE RESEARCH

Calcium sulfate greatly influences C_3A, C_3S, and OPC hydration, influencing the properties of the concrete. This paper has summarized the most important research findings to date on this topic. Further investigation regarding the effect of calcium sulfate on C_3A and C_3S hydration is needed, especially with the C_3A and C_3S polymorphs, as the mechanism by which calcium sulfate influences the hydration is not yet fully understood.

The calcium sulfate content added to the cement influences the properties of the cement. An optimum SO_3 content results in concrete with the highest strength and lowest shrinkage. This content will depend on many factors, including the characteristics of the clinker and calcium sulfate, the presence of SCMs and admixtures, the water/binder ratio, curing conditions, and the age of hydration. Many knowledge gaps remain on this subject, and further investigation is high recommended.

Despite being used for more than a century and the subject of hundreds of studies, many questions on the influence of calcium sulfate on cement properties remain. Additional studies on this subject are required to provide a completely understanding of its influence on the rheology, setting, mechanical performance, and durability of OPC.

3.7 ACKNOWLEDGEMENTS

JSAN thanked the financial support of CAPES [88882.439908/2019-01]. The participation APK was sponsored by CNPq (Brazilian National Council for Scientific and Technological Development) through the research fellowships PQ2017 305530/2017- 8. JSAN also thanked the Spanish Junta de Andalucía [UMA18-FEDERJA-095] research project for the research stage at University of Málaga (Spain).

3.8 REFERENCES

[1] J. Bensted, Gypsum in cements, in: J. Bensted, P. Barnes (Eds.), Structure and Perfomance of Cements, Spon Press, 2002: pp. 253–265.

[2] A. Bentur, Closure to “cementitious materials— nine millennia and a new century: Past, present, and future,” Journal of Materials in Civil Engineering. 15 (2003) 412. https://doi.org/10.1061/(ASCE)0899-1561(2003)15:4(412).

[3] V.H. Dodson, T.D. Hayden, Another look at the Portland cement/chemical admixture incompatibility problem, Cement, Concrete and Aggregates. 11 (1989) 52–56. https://doi.org/10.1520/cca10102j.

[4] K.L. Scrivener, A. Nonat, Hydration of cementitious materials, present and future, Cement and Concrete Research. 41 (2011) 651–665. https://doi.org/10.1016/j.cemconres.2011.03.026.

[5] A.P. Kirchheim, D.C. Dal Molin, P. Fischer, A.H. Emwas, J.L. Provis, P.J.M. Monteiro, Real-time high-resolution X-ray imaging and nuclear magnetic resonance study of the hydration of pure and Na-doped C3A in the presence of sulfates, Inorganic Chemistry. 50 (2011) 1203–1212. https://doi.org/10.1021/ic101460z.

[6] F. Zunino, K. Scrivener, Factors influencing the sulfate balance in pure phase C3S/C3A systems, Cement and Concrete Research. 133 (2020) 106085. https://doi.org/10.1016/j.cemconres.2020.106085.

[7] D. Jansen, Ch. Naber, D. Ectors, Z. Lu, X.-M. Kong, F. Goetz-Neunhoeffer, J. Neubauer, The early hydration of OPC investigated by in-situ XRD, heat flow calorimetry, pore water analysis and 1H NMR: Learning about adsorbed ions from a complete mass balance approach, Cement and Concrete Research. 109 (2018) 230–242. https://doi.org/10.1016/j.cemconres.2018.04.017.

[8] A. Quennoz, K.L. Scrivener, Interactions between alite and C3A-gypsum hydrations in model cements, Cement and Concrete Research. 44 (2013) 46–54. https://doi.org/10.1016/j.cemconres.2012.10.018.

[9] F. Zunino, K. Scrivener, The influence of the filler effect on the sulfate requirement of blended cements, Cement and Concrete Research. 126 (2019) 105918. https://doi.org/10.1016/j.cemconres.2019.105918.

[10] S. Garrault, A. Nonat, Y. Sallier, L. Nicolaeau, On the Origin of the Dormant Period of Cement Hydration, in: 13th International Congress on the Chemistry of Cement., Madrid, 2011: pp. 1–7.

[11] L. Nicoleau, E. Schreiner, A. Nonat, Ion-specific effects influencing the dissolution of tricalcium silicate, Cement and Concrete Research. 59 (2014) 118–138. https://doi.org/10.1016/j.cemconres.2014.02.006.

[12] E. Pustovgar, R.K. Mishra, M. Palacios, J.B. d'Espinose de Lacaillerie, T. Matschei, A.S. Andreev, H. Heinz, R. Verel, R.J. Flatt, Influence of aluminates on the hydration kinetics of tricalcium silicate, Cement and Concrete Research. 100 (2017) 245–262. https://doi.org/10.1016/j.cemconres.2017.06.006.

[13] T. Matschei, P. Kruspan, P. Sandberg, L. Wadso, Sulphate optimization of binders containing portland cement clinker using isothermal calorimetry, in: Proceedings of 15th International Congress on the Chemistry of Cement, Prague, 2019.

[14] S. Horkoss, G. Escadeillas, T. Rizk, R. Lteif, The effect of the source of cement SO3 on the expansion of mortars, Case Studies in Construction Materials. 4 (2016) 62–72. https://doi.org/10.1016/j.cscm.2015.12.004.

[15] K. Tosun, Effect of SO3 content and fineness on the rate of delayed ettringite formation in heat cured Portland cement mortars, Cement and Concrete Composites. 28 (2006) 761–772. https://doi.org/10.1016/j.cemconcomp.2006.06.003.

[16] A. Pavoine, X. Brunetaud, L. Divet, The impact of cement parameters on Delayed Ettringite Formation, Cement and Concrete Composites. 34 (2012) 521–528. https://doi.org/10.1016/j.cemconcomp.2011.11.012.

[17] P. Juilland, L. Nicoleau, R.S. Arvidson, E. Gallucci, Advances in dissolution understanding and their implications for cement hydration, RILEM Technical Letters. 2 (2017) 90. https://doi.org/10.21809/rilemtechlett.2017.47.

[18] A. Bentur, Effect of Gypsum on the Hydration and Strength of C3S Pastes, Journal of the American Ceramic Society. 59 (1976) 210–213. https://doi.org/10.1111/j.1151-2916.1976.tb10935.x.

[19] B. Mota, T. Matschei, K. Scrivener, The influence of sodium salts and gypsum on alite hydration, Cement and Concrete Research. 75 (2015) 53–65. https://doi.org/10.1016/j.cemconres.2015.04.015.

[20] W. Lerch, The Influence of Gypsum on the Hydration and Properties of Portland Cement Pastes, Research Bulletin - Portland Cement Association, Chicago, IL. USA. 12 (1946) 1–48.

[21] American Society for Testing and Materials., ATSM C563-19: Standard Guide for Approximation of Optimum SO3 in Hydraulic Cement, (2019) 1–8.

[22] A. Quennoz, K.L. Scrivener, Hydration of C 3A-gypsum systems, Cement and Concrete Research. 42 (2012) 1032–1041. https://doi.org/10.1016/j.cemconres.2012.04.005.

[23] A.P. Kirchheim, E.D. Rodríguez, R.J. Myers, L.A. Gobbo, P.J.M. Monteiro, D.C.C. Dal Molin, R.B. de Souza, M.A. Cincotto, Effect of gypsum on the early hydration of cubic and Na-doped orthorhombic tricalcium aluminate, Materials. 11 (2018) 1–16. https://doi.org/10.3390/ma11040568.

[24] S. Joseph, J. Skibsted, Ö. Cizer, A quantitative study of the C3A hydration, Cement and Concrete Research. 115 (2019) 145–159. https://doi.org/10.1016/j.cemconres.2018.10.017.

[25] S. Pourchet, L. Regnaud, J.P. Perez, A. Nonat, Early C3A hydration in the presence of different kinds of calcium sulfate, Cement and Concrete Research. 39 (2009) 989–996. https://doi.org/10.1016/j.cemconres.2009.07.019.

[26] H. Minard, S. Garrault, L. Regnaud, A. Nonat, Mechanisms and parameters controlling the tricalcium aluminate reactivity in the presence of gypsum, Cement and Concrete Research. 37 (2007) 1418–1426. https://doi.org/10.1016/j.cemconres.2007.06.001.

[27] X. Liu, P. Feng, C. Lyu, S. Ye, The role of sulfate ions in tricalcium aluminate hydration: New insights, Cement and Concrete Research. 130 (2020) 105973. https://doi.org/10.1016/j.cemconres.2020.105973.

[28] J.W. Bullard, H.M. Jennings, R.A. Livingston, A. Nonat, G.W. Scherer, J.S. Schweitzer, K.L. Scrivener, J.J. Thomas, Mechanisms of cement hydration, Cement and Concrete Research. 41 (2011) 1208–1223. https://doi.org/10.1016/B978-0-08-100693-1.00008-4.

[29] M. Collepardi, G. Baldini, M. Pauri, M. Corradi, Tricalcium aluminate hydration in the presence of lime, gypsum or sodium sulfate, Cement and Concrete Research. 8 (1978) 571–580. https://doi.org/10.1016/0008-8846(78)90040-6.

[30] J. Pommersheim, J. Chang, Kinetics of hydration of tricalcium aluminate in the presence of gypsum, Cement and Concrete Research. 18 (1988) 911–922.

[31] H.F.W. Taylor, Cement chemistry, 2nd ed., Thomas Telford, 1997. https://doi.org/10.1680/cc.25929.

[32] G. Geng, R.J. Myers, Y.S. Yu, D.A. Shapiro, R. Winarski, P.E. Levitz, D.A.L. Kilcoyne, P.J.M. Monteiro, Synchrotron X-ray nanotomographic and spectromicroscopic study of the tricalcium aluminate hydration in the presence of gypsum, Cement and Concrete Research. 111 (2018) 130–137. https://doi.org/10.1016/j.cemconres.2018.06.002.

[33] G. Artioli, J.W. Bullard, Cement hydration: The role of adsorption and crystal growth, Crystal Research and Technology. 48 (2013) 903–918. https://doi.org/10.1002/crat.201200713.

[34] K.L. Scrivener, Microstructure Development During the Hydration of Portland Cement, phD Thesis (Department of Metallurgy and Materials Science, University of London), 1984, 215p.

[35] R.J. Myers, G. Geng, J. Li, E.D. Rodríguez, J. Ha, P. Kidkhunthod, G. Sposito, L.N. Lammers, A.P. Kirchheim, P.J.M. Monteiro, Role of adsorption phenomena in cubic tricalcium aluminate dissolution, Langmuir. 33 (2016) 45–55. https://doi.org/10.1021/acs.langmuir.6b03474.

[36] R.J. Myers, G. Geng, E.D. Rodriguez, P. da Rosa, A.P. Kirchheim, P.J.M. Monteiro, Solution chemistry of cubic and orthorhombic tricalcium aluminate hydration, Cement and Concrete Research. 100 (2017) 176–185. https://doi.org/10.1016/j.cemconres.2017.06.008.

[37] A.S. Brand, S.B. Feldman, P.E. Stutzman, A. v. Ievlev, M. Lorenz, D.C. Pagan, S. Nair, J.M. Gorham, J.W. Bullard, Dissolution and initial hydration behavior of tricalcium aluminate in low activity sulfate solutions, Cement and Concrete Research. 130 (2020) 105989. https://doi.org/10.1016/j.cemconres.2020.105989.

[38] S. Ye, P. Feng, Y. Liu, J. Liu, J.W. Bullard, Dissolution and early hydration of tricalcium aluminate in aqueous sulfate solutions, Cement and Concrete Research. 137 (2020) 2–7. https://doi.org/10.1016/j.cemconres.2020.106191.

[39] B.A. Clark, P.W. Brown, Formation of ettringite from tricalcium aluminate and magnesium sulphate, Advances in Cement Research. 12 (2000) 137–142. https://doi.org/10.1680/adcr.2000.12.4.137.

[40] M. Collepardi, G. Baldini, M. Pauri, Retardation of Tricalcium Aluminate Hydration by Calcium Sulfate, Journal of The American Ceramic Society. 62 (1979) 33–35.

[41] K. Fukuda, S. Inoue, H. Yoshida, Cationic substitution in tricalcium aluminate, Cement and Concrete Research. 33 (2003) 1771–1775. https://doi.org/10.1016/S0008-8846(03)00172-8.

[42] P. Mondal, J.W. Jeffery, The Crystal Structure of Triealeium Aluminate, Ca3Al2O6, Acta Crystallographica. (1975) 689.

[43] Y. Takéuchi, F. Nishi, Crystal-chemical characterization of the 3 CaO.Al2O3 solid-solution series, Zeitschrift Für Kristallographie. 152 (1980) 259–307.

[44] L. Gobbo, L. Sant'Agostino, L. Garcez, C3A polymorphs related to industrial clinker alkalies content, Cement and Concrete Research. 34 (2004) 657–664. https://doi.org/10.1016/j.cemconres.2003.10.020.

[45] D. Stephan, S. Wistuba, Crystal structure refinement and hydration behaviour of doped tricalcium aluminate, Cement and Concrete Research. 36 (2006) 2011–2020. https://doi.org/10.1016/j.cemconres.2006.06.001.

[46] F.P. Glasser, M.B. Marinho, Early stages of the hydration of tricalcium aluminate and its sodium-cotaining solid solutions, Proceedings of the British Ceramic Society. 35 (1984) 221–236.

[47] S. Wistuba, D. Stephan, G. Raudaschl-Sieber, J. Plank, Hydration and hydration products of two-phase Portland cement clinker doped with Na2O, Advances in Cement Research. 19 (2007) 125–131. https://doi.org/10.1680/adcr.2007.19.3.125.

[48] A.P. Kirchheim, V. Fernàndez-Altable, P.J.M. Monteiro, D.C.C. Dal Molin, I. Casanova, Analysis of cubic and orthorhombic C3A hydration in presence of gypsum and lime, Journal of Materials Science. 44 (2009) 2038–2045. https://doi.org/10.1007/s10853-009-3292-3.

[49] J. Cheung, A. Jeknavorian, L. Roberts, D. Silva, Impact of admixtures on the hydration kinetics of Portland cement, Cement and Concrete Research. 41 (2011) 1289–1309. https://doi.org/10.1016/j.cemconres.2011.03.005.

[50] M.M. Alonso, F. Puertas, Adsorption of PCE and PNS superplasticisers on cubic and orthorhombic C3A. Effect of sulfate, Construction and Building Materials. 78 (2015) 324–332. https://doi.org/10.1016/j.conbuildmat.2014.12.050.

[51] B. Mota, T. Matschei, K. Scrivener, The influence of sodium salts and gypsum on alite hydration, Cement and Concrete Research. 75 (2015) 53–65. https://doi.org/10.1016/j.cemconres.2015.04.015.

[52] D. Ménétrier, I. Jawed, J. Skalny, Effect of gypsum on C3S hydration, Cement and Concrete Research. 10 (1980) 697–701.

[53] Y. Zhang, X. Zhang, Research on effect of limestone and gypsum on C3A, C3S and PC clinker system, Construction and Building Materials. 22 (2008) 1634–1642. https://doi.org/10.1016/j.conbuildmat.2007.06.013.

[54] M. Zajac, A. Rossberg, G. le Saout, B. Lothenbach, Influence of limestone and anhydrite on the hydration of Portland cements, Cement and Concrete Composites. 46 (2014) 99–108. https://doi.org/10.1016/j.cemconcomp.2013.11.007.

[55] W. da S. Barbosa, Influência físico-química das fases do clínquer no comportamento reológico de pastas cimentícias, PhD thesis (Programa de Pós-Graduação em Engenharia e Ciência dos Materiais – PIPE. Setor de Tecnologia, Universidade Federal do Paraná), 2019, 234 p (in portuguese).

[56] S. Gunay, S. Garrault, a Nonat, P. Termkhajornkit, Influence of calcium sulphate on hydration and mechanical strength of tricalcium silicate, 13th International Congress on the Chemistry of Cement. (2011) 1–7.

[57] C. Li, X. Lu, G. Jing, Z. Ye, S. Wang, X. Cheng, The effect of gypsum on the hydration of alite–belite–ferrite phase system, Journal of Thermal Analysis and Calorimetry. 136 (2019) 717–724. https://doi.org/10.1007/s10973-018-7643-7.

[58] P.W. Brown, C.L. Harner, E.J. Prosen, The effect of inorganic salts on tricalcium silicate hydration, Cement and Concrete Research. 16 (1986) 17–22. https://doi.org/10.1016/0008-8846(86)90063-3.

[59] M. Yamashita, T. Harada, E. Sakai, K. Tsuchiya, Influence of sulfur trioxide in clinker on the hydration heat and physical properties of Portland cement, Construction and Building Materials. 250 (2020) 118844. https://doi.org/10.1016/j.conbuildmat.2020.118844.

[60] S.T. Bergold, F. Goetz-Neunhoeffer, J. Neubauer, Interaction of silicate and aluminate reaction in a synthetic cement system: Implications for the process of alite hydration, Cement and Concrete Research. 93 (2017) 32–44. https://doi.org/10.1016/j.cemconres.2016.12.006.

[61] S. Gunay, S. Garrault, A. Nonat, P. Termkhajornkit, Influence of calcium sulphate on hydration and mechanical strength of tricalcium silicate, in: Proceedings of 13th International Congress on the Chemistry of Cement, Madrid, 2011: pp. 1–6.

[62] M. Zajac, J. Skocek, A. Müller, M. ben Haha, Effect of sulfate content on the porosity distribution and resulting performance of composite cements, Construction and Building Materials. 186 (2018) 912–919. https://doi.org/10.1016/j.conbuildmat.2018.07.247.

[63] H.M. Ludwig, W. Zhang, Research review of cement clinker chemistry, Cement and Concrete Research. 78 (2015) 24–37. https://doi.org/10.1016/j.cemconres.2015.05.018.

[64] F. Dunstetter, M.-N. de Noirfontaine, M. Courtial, Polymorphism of tricalcium silicate, the major compound of Portland cement clinker, Cement and Concrete Research. 36 (2005) 54–64. https://doi.org/10.1016/j.cemconres.2004.12.004.

[65] W. v. Fernandes, S.M. Torres, C.A. Kirk, A.F. Leal, M.R. Lima Filho, D. Diniz, Incorporation of minor constituents into Portland cement tricalcium silicate: Bond valence assessment of the alite M1 polymorph crystal structure using synchrotron XRPD data, Cement and Concrete Research. 136 (2020) 106125. https://doi.org/10.1016/j.cemconres.2020.106125.

[66] I. Maki, K. Goto, Factors Influencing the Phase Constitution of Alite in Portland cement clinker, Cement and Concrete Research. 12 (1982) 301–308.

[67] H. Zhou, X. Gu, J. Sun, Z. Yu, H. Huang, Q. Wang, X. Shen, Research on the formation of M1-type alite doped with MgO and SO3—A route to improve the quality of cement clinker with a high content of MgO, Construction and Building Materials. 182 (2018) 156–166. https://doi.org/10.1016/j.conbuildmat.2018.06.078.

[68] X. Li, H. Huang, J. Xu, S. Ma, X. Shen, Statistical research on phase formation and modification of alite polymorphs in cement clinker with SO3 and MgO, Construction and Building Materials. 37 (2012) 548–555. https://doi.org/10.1016/j.conbuildmat.2012.07.099.

[69] M. Segata, N. Marinoni, M. Galimberti, M. Marchi, M. Cantaluppi, A. Pavese, Á.G. de la Torre, The effects of MgO, Na2O and SO3 on industrial clinkering process: phase composition, polymorphism, microstructure and hydration, using a multidisciplinary approach, Materials Characterization. 155 (2019). https://doi.org/10.1016/j.matchar.2019.109809.

[70] T. Staněk, P. Sulovský, The influence of the alite polymorphism on the strength of the Portland cement, Cement and Concrete Research. 32 (2002) 1169–1175. https://doi.org/10.1016/S0008-8846(02)00756-1.

[71] Q. Wang, X. Gu, H. Zhou, X. Chen, X. Shen, Cation substitution induced reactivity variation on the tricalcium silicate polymorphs determined from first-principles calculations, Construction and Building Materials. 216 (2019) 239–248. https://doi.org/10.1016/j.conbuildmat.2019.05.005.

[72] A. Bazzoni, M. Suhua, Q. Wang, X. Shen, M. Cantoni, K.L. Scrivener, The effect of magnesium and zinc ions on the hydration kinetics of C3S, Journal of the American Ceramic Society. 97 (2014) 3684–3693. https://doi.org/10.1111/jace.13156.

[73] D. Wagner, F. Bellmann, J. Neubauer, Influence of aluminium on the hydration of triclinic C3S with addition of KOH solution, Cement and Concrete Research. 137 (2020) 106198. https://doi.org/10.1016/j.cemconres.2020.106198.

[74] D. Stephan, S. Wistuba, Crystal structure refinement and hydration behaviour of 3CaO·SiO2 solid solutions with MgO, Al2 O3 and Fe2O3, Journal of the European Ceramic Society. 26 (2006) 141–148. https://doi.org/10.1016/j.jeurceramsoc.2004.10.031.

[75] A. Ouzia, K. Scrivener, The needle model: A new model for the main hydration peak of alite, Cement and Concrete Research. 115 (2019) 339–360. https://doi.org/10.1016/j.cemconres.2018.08.005.

[76] K.L. Scrivener, P. Juilland, P.J.M. Monteiro, Advances in understanding hydration of Portland cement, Cement and Concrete Research. 78 (2015) 38–56. https://doi.org/10.1016/j.cemconres.2015.05.025.

[77] E. Gallucci, P. Mathur, K. Scrivener, Microstructural development of early age hydration shells around cement grains, Cement and Concrete Research. 40 (2010) 4–13. https://doi.org/10.1016/j.cemconres.2009.09.015.

[78] E.M.J. Bérodier, A.C.A. Muller, K.L. Scrivener, Effect of sulfate on C-S-H at early age, Cement and Concrete Research. 138 (2020) 106248. https://doi.org/10.1016/j.cemconres.2020.106248.

[79] S. Adu-Amankwah, L. Black, J. Skocek, M. ben Haha, M. Zajac, Effect of sulfate additions on hydration and performance of ternary slag-limestone composite cements, Construction and Building Materials. 164 (2018) 451–462. https://doi.org/10.1016/j.conbuildmat.2017.12.165.

[80] K. Scrivener, A. Ouzia, P. Juilland, A. Kunhi Mohamed, Advances in understanding cement hydration mechanisms, Cement and Concrete Research. 124 (2019) 105823. https://doi.org/10.1016/j.cemconres.2019.105823.

[81] S. Joseph, J. Skibsted, Ö. Cizer, Hydration of polyphase Ca3SiO5-Ca3Al2O6 in the presence of gypsum and Na2SO4, Journal of the American Ceramic Society. 103 (2020) 1–30. https://doi.org/10.1111/jace.17321.

[82] G.K. Sun, J.F. Young, R.J. Kirkpatrick, The role of Al in C-S-H: NMR, XRD, and compositional results for precipitated samples, Cement and Concrete Research. 36 (2006) 18–29. https://doi.org/10.1016/j.cemconres.2005.03.002.

[83] J. Li, W. Zhang, K. Garbev, G. Beuchle, P.J.M. Monteiro, Influences of cross-linking and Al incorporation on the intrinsic mechanical properties of tobermorite, Cement and Concrete Research. 136 (2020) 106170. https://doi.org/10.1016/j.cemconres.2020.106170.

[84] F. Begarin, S. Garrault, A. Nonat, L. Nicoleau, Hydration of alite containing aluminium, Advances in Applied Ceramics. 110 (2011) 127–130. https://doi.org/10.1179/1743676110Y.0000000007.

[85] V.C. Campiteli, M.C. Florindo, Influence of limestone additions on optimum sulfur trioxide content in Portland cements, in: P. Klieger, R. Hooton (Eds.), Carbonate Additions to Cement, ASTM International, 1990: pp. 30–40.

[86] D. Damidot, B. Lothenbach, D. Herfort, F.P. Glasser, Thermodynamics and cement science, Cement and Concrete Research. 41 (2011) 679–695. https://doi.org/10.1016/j.cemconres.2011.03.018.

[87] American Society for Testing and Materials, ASTM C 150/ C150M-20 Standard specification for portland cement, (2020) 1–9. https://doi.org/10.1520/C0150.

[88] Associação Brasileira de Normas Técnicas, NBR 16697: Portland cement - Requirements (in portuguese), (2018).

[89] H.A. Ewadh, P. Karbalauniversity, Statistical Analysis for optimum sulphate content of Sulphate Resisting Cement (SRC), Journal of Kerbala University. 11 (2013) 31–37.

[90] I. Jelenić, A. Panović, A. Bezjak, Hydration and strength development in alite-C3A-CSH2-quartz pastes containing readily soluble alkalies, Cement and Concrete Research. 10 (1980) 463–466. https://doi.org/10.1016/0008-8846(80)90123-4.

[91] Y. Ma, J. Qian, Influence of alkali sulfates in clinker on the hydration and hardening of Portland cement, Construction and Building Materials. 180 (2018) 351–363. https://doi.org/10.1016/j.conbuildmat.2018.05.196.

[92] F.J. Tang, E.M. Gartner, Influence of sulphate source on Portland cement hydration, Advances in Cement Research. 1 (1988) 67–74. https://doi.org/10.1680/adcr.1988.1.2.67.

[93] B. Mota, T. Matschei, K. Scrivener, Impact of NaOH and Na2SO4 on the kinetics and microstructural development of white cement hydration, Cement and Concrete Research. 108 (2018) 172–185. https://doi.org/10.1016/j.cemconres.2018.03.017.

[94] J. Fu, A.M. Jones, M.W. Bligh, C. Holt, L.M. Keyte, F. Moghaddam, S.J. Foster, T.D. Waite, Mechanisms of enhancement in early hydration by sodium sulfate in a slag-cement blend – Insights from pore solution chemistry, Cement and Concrete Research. 135 (2020) 106110. https://doi.org/10.1016/j.cemconres.2020.106110.

[95] Y. Ma, X. Li, J. Qian, X. Shen, Effect of protogenetic alkali sulfates on the hydration and hardening of cement with different tricalcium aluminate content, Construction and Building Materials. 256 (2020) 119475. https://doi.org/10.1016/j.conbuildmat.2020.119475.

[96] W. Barbosa, R.D.P. Ramalho, K.F. Portella, Influence of gypsum fineness in the first hours of cement paste: Hydration kinetics and rheological behaviour, Construction and Building Materials. 184 (2018) 304–310. https://doi.org/10.1016/j.conbuildmat.2018.06.235.

[97] M. García-Maté, A.G. de La Torre, L. León-Reina, E.R. Losilla, M.A.G. Aranda, I. Santacruz, Effect of calcium sulfate source on the hydration of calcium sulfoaluminate eco-cement, Cement and Concrete Composites. 55 (2015) 53–61. https://doi.org/10.1016/j.cemconcomp.2014.08.003.

[98] S.A. Farrington, B.J. Christensen, Hydration behavior of portland cements with different hemihydrate/gypsum ratios in the presence of common chemical admixtures, Journal of ASTM International. 2 (2005) 51–62. https://doi.org/10.1520/JAI12478.

[99] G. Tzouvalas, N. Dermatas, S. Tsimas, Alternative calcium sulfate-bearing materials as cement retarders: Part I. Anhydrite, Cement and Concrete Research. 34 (2004) 2113–2118. https://doi.org/10.1016/j.cemconres.2004.03.020.

[100] P.J. Sandberg, L.R. Roberts, Cement-admixture interactions related to aluminate control, Journal of ASTM International. 2 (2005) 219–232. https://doi.org/10.1520/jai12296.

[101] P.K. Mehta, P.J.M. Monteiro, Concrete: Microstructure, Properties, and Materials, 4th ed., McGraw-Hill Professional Publishing, 2014.

[102] Y. He, X. Zhang, S. Liu, R.D. Hooton, T. Ji, Y. Kong, Impacts of sulphates on rheological property and hydration performance of cement paste in the function of polycarboxylate superplasticizer, Construction and Building Materials. 256 (2020) 119428. https://doi.org/10.1016/j.conbuildmat.2020.119428.

[103] A.M. Rashad, Phosphogypsum as a construction material, Journal of Cleaner Production. 166 (2017) 732–743. https://doi.org/10.1016/j.jclepro.2017.08.049.

[104] J. Rosales, S.M. Pérez, M. Cabrera, M.J. Gázquez, J.P. Bolivar, J. de Brito, F. Agrela, Treated phosphogypsum as an alternative set regulator and mineral addition in cement production, Journal of Cleaner Production. 244 (2020). https://doi.org/10.1016/j.jclepro.2019.118752.

[105] F. do C. Holanda, H. Schmidt, V.A. Quarcioni, Influence of phosphorus from phosphogypsum on the initial hydration of Portland cement in the presence of superplasticizers, Cement and Concrete Composites. 83 (2017) 384–393. https://doi.org/10.1016/j.cemconcomp.2017.07.029.

[106] M.M. Radwan, M. Heikal, Hydration characteristics of tricalcium aluminate phase in mixes containing β-hemihydate and phosphogypsum, Cement and Concrete Research. 35 (2005) 1601–1608. https://doi.org/10.1016/j.cemconres.2004.06.037.

[107] S. Adu-Amankwah, M. Zajac, C. Stabler, B. Lothenbach, L. Black, Influence of limestone on the hydration of ternary slag cements, Cement and Concrete Research. 100 (2017) 96–109. https://doi.org/10.1016/j.cemconres.2017.05.013.

[108] M. Whittaker, M. Zajac, M. ben Haha, F. Bullerjahn, L. Black, The role of the alumina content of slag, plus the presence of additional sulfate on the hydration and microstructure of Portland cement-slag blends, Cement and Concrete Research. 66 (2014) 91–101. https://doi.org/10.1016/j.cemconres.2014.07.018.

[109] M.D. Niemuth, L. Barcelo, J. Weiss, Effect of Fly Ash on Optimum Sulfate Levels Measured Using Heat and Strength at Early Ages, Advances in Civil Engineering Materials. 1 (2012) 20120012. https://doi.org/10.1520/acem20120012.

[110] I. de la Varga, J. Castro, D.P. Bentz, F. Zunino, J. Weiss, Evaluating the hydration of high volume fly ash mixtures using chemically inert fillers, Construction and Building Materials. 161 (2018) 221–228. https://doi.org/10.1016/j.conbuildmat.2017.11.132.

[111] D. Tsamatsoulis, N. Nikolakakos, Optimizing the sulphates content of cement using multivariable modelling and uncertainty analysis, Chemical and Biochemical Engineering Quarterly. 27 (2013) 133–144.

[112] M.D. Niemuth, Effect of Fly Ash on Optimum sulfate of Portland Cement, 2012. https://doi.org/10.1016/s0008-8846(99)00153-2.

[113] E. Kapeluszna, Ł. Kotwica, G. Malata, P. Murzyn, W. Nocuń-Wczelik, The effect of highly reactive pozzolanic material on the early hydration of alite – C3A – gypsum synthetic cement systems, Construction and Building Materials. 251 (2020). https://doi.org/10.1016/j.conbuildmat.2020.118879.

[114] M. Antoni, J. Rossen, F. Martirena, K. Scrivener, Cement substitution by a combination of metakaolin and limestone, Cement and Concrete Research. 42 (2012) 1579–1589. https://doi.org/10.1016/j.cemconres.2012.09.006.

[115] C. Rodriguez, J.I. Tobon, Influence of calcined clay/limestone, sulfate and clinker proportions on cement performance, Construction and Building Materials. 251 (2020) 119050. https://doi.org/10.1016/j.conbuildmat.2020.119050.

[116] J. Tang, S. Wei, W. Li, S. Ma, P. Ji, X. Shen, Synergistic effect of metakaolin and limestone on the hydration properties of Portland cement, Construction and Building Materials. 223 (2019) 177–184. https://doi.org/10.1016/j.conbuildmat.2019.06.059.

[117] J. da S. Andrade Neto, T.A. Santos, S. de A. Pinto, C.M.R. Dias, D.V. Ribeiro, Effect of the combined use of carbon nanotubes (CNT) and metakaolin on the properties of cementitious matrices, Construction and Building Materials. 271 (2021) 121903. https://doi.org/10.1016/j.conbuildmat.2020.121903.

[118] D.P. Bentz, C.F. Ferraris, S.Z. Jones, D. Lootens, F. Zunino, Limestone and silica powder replacements for cement: Early-age performance, Cement and Concrete Composites. 78 (2017) 43–56. https://doi.org/10.1016/j.cemconcomp.2017.01.001.

[119] R.C.O. Romano, H.M. Bernardo, M.H. Maciel, R.G. Pileggi, M.A. Cincotto, Hydration of Portland cement with red mud as mineral addition, Journal of Thermal Analysis and Calorimetry. 131 (2018) 2477–2490. https://doi.org/10.1007/s10973-017-6794-2.

[120] R.C. de O. Romano, H.M. Bernardo, M.H. Maciel, R.G. Pileggi, M.A. Cincotto, Using isothermal calorimetry, X-ray diffraction, thermogravimetry and FTIR to monitor the hydration reaction of Portland cements associated with red mud as a supplementary material, Journal of Thermal Analysis and Calorimetry. 137 (2019) 1877–1890. https://doi.org/10.1007/s10973-019-08095-x.

[121] R. Snellings, G. Mertens, R. Adriaens, J. Elsen, In situ synchrotron X-ray powder diffraction study of the early age hydration of cements blended with zeolitite and quartzite fines and water-reducing agent, Applied Clay Science. 72 (2013) 124–131. https://doi.org/10.1016/j.clay.2012.12.002.

[122] F. Avet, K. Scrivener, Effect of temperature on the water content of C-A-S-H in plain Portland and blended cements, Cement and Concrete Research. 136 (2020) 106124. https://doi.org/10.1016/j.cemconres.2020.106124.

[123] F. Avet, R. Snellings, A. Alujas Diaz, M. ben Haha, K. Scrivener, Development of a new rapid, relevant and reliable (R3) test method to evaluate the pozzolanic reactivity of calcined kaolinitic clays, Cement and Concrete Research. 85 (2016) 1–11. https://doi.org/10.1016/j.cemconres.2016.02.015.

[124] F. Avet, E. Boehm-Courjault, K. Scrivener, Investigation of C-A-S-H composition, morphology and density in Limestone Calcined Clay Cement (LC3), Cement and Concrete Research. 115 (2019) 70–79. https://doi.org/10.1016/j.cemconres.2018.10.011.

[125] F. Avet, K. Scrivener, Investigation of the calcined kaolinite content on the hydration of Limestone Calcined Clay Cement (LC3), Cement and Concrete Research. 107 (2018) 124–135. https://doi.org/10.1016/j.cemconres.2018.02.016.

[126] F. Zunino, K. Scrivener, The reaction between metakaolin and limestone and its effect in porosity refinement and mechanical properties, Cement and Concrete Research. 140 (2021) 106307. https://doi.org/10.1016/j.cemconres.2020.106307.

[127] K. Scrivener, F. Martirena, S. Bishnoi, S. Maity, Calcined clay limestone cements (LC3), Cement and Concrete Research. 114 (2018) 49–56. https://doi.org/10.1016/j.cemconres.2017.08.017.

[128] T. Matschei, B. Lothenbach, F.P. Glasser, The role of calcium carbonate in cement hydration, Cement and Concrete Research. 37 (2007) 551–558. https://doi.org/10.1016/j.cemconres.2006.10.013.

[129] P. Šiler, P. Bayer, T. Sehnal, I. Kolářová, T. Opravil, F. Šoukal, Effects of high-temperature fly ash and fluidized bed combustion ash on the hydration of Portland cement, Construction and Building Materials. 78 (2015) 181–188. https://doi.org/10.1016/j.conbuildmat.2015.01.032.

[130] H.A. Nguyen, T.P. Chang, J.Y. Shih, C.T. Chen, T.D. Nguyen, Influence of circulating fluidized bed combustion (CFBC) fly ash on properties of modified high volume low calcium fly ash (HVFA) cement paste, Construction and Building Materials. 91 (2015) 208–215. https://doi.org/10.1016/j.conbuildmat.2015.05.075.

[131] M.C.G. Juenger, J.L. Provis, J. Elsen, W. Matthes, R.D. Hooton, J. Duchesne, L. Courard, H. He, F. Michel, R. Snellings, N. de Belie, Supplementary Cementitious Materials for Concrete: Characterization Needs, Materials Research Society Symposium Proceedings. 1488 (2012). https://doi.org/10.1557/opl.2012.1536.

[132] Y. Zhang, X. Kong, Correlations of the dispersing capability of NSF and PCE types of superplasticizer and their impacts on cement hydration with the adsorption in fresh cement pastes, Cement and Concrete Research. 69 (2015) 1–9. https://doi.org/10.1016/j.cemconres.2014.11.009.

[133] M.M. Alonso, M. Palacios, F. Puertas, Compatibility between polycarboxylate-based admixtures and blended-cement pastes, Cement and Concrete Composites. 35 (2013) 151–162. https://doi.org/10.1016/j.cemconcomp.2012.08.020.

[134] S. Ng, H. Justnes, Influence of plasticizers on the rheology and early heat of hydration of blended cements with high content of fly ash, Cement and Concrete Composites. 65 (2016) 41–54. https://doi.org/10.1016/j.cemconcomp.2015.10.005.

[135] D. Jansen, J. Neubauer, F. Goetz-Neunhoeffer, R. Haerzschel, W.D. Hergeth, Change in reaction kinetics of a Portland cement caused by a superplasticizer - Calculation of heat flow curves from XRD data, Cement and Concrete Research. 42 (2012) 327–332. https://doi.org/10.1016/j.cemconres.2011.10.005.

[136] E.A. Kishar, W.S. Hegazy, D.A. el Monem Ahmed, Hydration reactions of the system C3A-CaSO4:2H 2O (1:1 mole ratio) at 30 and 50°C. Part II: Effect of naphthalene formaldehyde sulfonate, Advances in Cement Research. 23 (2011) 123–128. https://doi.org/10.1680/adcr.9.00025.

[137] P. Rosa, Hidratação do C3A cúbico e ortorrômbico na presença de aditivos policarboxilato de abertura e manunteção, 2019.

[138] Y. Jiang, S. Zhang, D. Damidot, Ettringite and monosulfoaluminate in polycarboxylate type admixture dispersed fresh cement paste, Advanced Science Letters. 5 (2012) 663–666. https://doi.org/10.1166/asl.2012.1798.

[139] D. Marchon, R.J. Flatt, Impacts of chemical admixtures on cement hydration, in: P.-C. Aïtcin, R.J. Flatt (Eds.), Science and Technology of Concrete Admixtures, Woodhead Publishing, Cambridge, 2016: pp. 279–304.

[140] C. Rößler, B. Möser, J. Stark, Influence of Superplasticizers on C3A Hydration and Ettringite Growth in Cement Paste, in: Proceedings of the 12th International Congress on The Chemistry of Cement, Montreal, 2007: pp. 1–12.

[141] S.G. Erzengin, K. Kaya, S. Perçin Özkorucuklu, V. Özdemir, G. Yıldırım, The properties of cement systems superplasticized with methacrylic ester-based polycarboxylates, Construction and Building Materials. 166 (2018) 96–109. https://doi.org/10.1016/j.conbuildmat.2018.01.088.

[142] R.P. Salvador, S.H.P. Cavalaro, M.A. Cincotto, A.D. de Figueiredo, Parameters controlling early age hydration of cement pastes containing accelerators for sprayed concrete, Cement and Concrete Research. 89 (2016) 230–248. https://doi.org/10.1016/j.cemconres.2016.09.002.

[143] R.P. Salvador, S.H.P. Cavalaro, I. Segura, A.D. Figueiredo, J. Pérez, Early age hydration of cement pastes with alkaline and alkali-free accelerators for sprayed concrete, Construction and Building Materials. 111 (2016) 386–398. https://doi.org/10.1016/j.conbuildmat.2016.02.101.

[144] C. Maltese, C. Pistolesi, A. Bravo, F. Cella, T. Cerulli, D. Salvioni, Effects of setting regulators on the efficiency of an inorganic acid based alkali-free accelerator reacting with a Portland cement, Cement and Concrete Research. 37 (2007) 528–536. https://doi.org/10.1016/j.cemconres.2007.01.002.

[145] M. Bishop, A.R. Barron, Cement hydration inhibition with sucrose, tartaric acid, and lignosulfonate: Analytical and spectroscopic study, Industrial and Engineering Chemistry Research. 45 (2006) 7042–7049. https://doi.org/10.1021/ie060806t.

[146] F. Zunino, K. Scrivener, Assessing the effect of alkanolamine grinding aids in limestone calcined clay cements hydration, Construction and Building Materials. 266 (2020) 121293. https://doi.org/10.1016/j.conbuildmat.2020.121293.

[147] J.J. Assaad, C.A. Issa, Effect of clinker grinding aids on flow of cement-based materials, Cement and Concrete Research. 63 (2014) 1–11. https://doi.org/10.1016/j.cemconres.2014.04.006.

[148] V.S. Ramachandran, Action of triethanolamine on the hydration of tricalcium aluminate, Cement and Concrete Research. 3 (1973) 41–54. https://doi.org/10.1016/0008-8846(73)90060-4.

[149] L. Wadsö, F. Winnefeld, K. Riding, P. Sandberg, Calorimetry, in: K. Scrivener, R. Snellings, B. Lothenbach (Eds.), A Practical Guide to Microstructural Analysis of Cementitious Materials, 1st ed., CRC Press, 2016.

[150] I. Odler, S. Abdul-Maula, Investigations on the relationship between porosity structure and strength of hydrated portland cement pastes III. Effect of clinker composition and gypsum addition, Cement and Concrete Research. 17 (1987) 22–30. https://doi.org/10.1016/0008-8846(87)90054-8.

[151] M. Wyrzykowski, P. Lura, Effect of relative humidity decrease due to self-desiccation on the hydration kinetics of cement, Cement and Concrete Research. 85 (2016) 75–81. https://doi.org/10.1016/j.cemconres.2016.04.003.

[152] W. Kurdowski, Cement and concrete chemistry, Springer, 2014. https://doi.org/10.1007/978-94-007-7945-7.

[153] Q. Jin, L.K.N. Perry, J.W. Bullard, Temperature dependence of gypsum dissolution rates, Cement and Concrete Research. 129 (2020) 105969. https://doi.org/10.1016/j.cemconres.2019.105969.

[154] H.C. Pedrosa, O.M. Reales, V.D. Reis, M. das D. Paiva, E.M.R. Fairbairn, Hydration of Portland cement accelerated by C-S-H seeds at different temperatures, Cement and Concrete Research. 129 (2020) 105978. https://doi.org/10.1016/j.cemconres.2020.105978.

[155] Z. Zhang, F. Han, P. Yan, Modelling the dissolution and precipitation process of the early hydration of, Cement and Concrete Research. 136 (2020) 106174. https://doi.org/10.1016/j.cemconres.2020.106174.

[156] H. Zhang, Z. Lin, D. Tong, Influence of the type of calcium sulfate on the strength and hydration of portland cement under an initial steam-curing condition, Cement and Concrete Research. 26 (1996) 1505–1511. https://doi.org/10.1016/0008-8846(96)00149-4.

[157] M. al Shamaa, S. Lavaud, L. Divet, G. Nahas, J.M. Torrenti, Influence of relative humidity on delayed ettringite formation, Cement and Concrete Composites. 58 (2015) 14–22. https://doi.org/10.1016/j.cemconcomp.2014.12.013.

[158] S. Mohammed, O. Safiullah, Optimization of the SO3 content of an Algerian Portland cement: Study on the effect of various amounts of gypsum on cement properties, Construction and Building Materials. 164 (2018) 362–370. https://doi.org/10.1016/j.conbuildmat.2017.12.218.

[159] C.W. Chung, P. Suraneni, J.S. Popovics, L.J. Struble, Using ultrasonic wave reflection to monitor false set of cement paste, Cement and Concrete Composites. 84 (2017) 10–18. https://doi.org/10.1016/j.cemconcomp.2017.08.010.

[160] R.M. Mota, A.S. Silva, V.H.S. Ramos, J.C.T. Rezende, E. de Jesus, Effects of storage temperature and time on false setting behavior of CPI-S Portland cement, Ceramica. 66 (2020) 321–329. https://doi.org/10.1590/0366-69132020663792842.

[161] W. Mbasha, R. Haldenwang, I. Masalova, The influence of sulfate availability on rheology of fresh cement paste, Applied Rheology. 30 (2020) 54–63. https://doi.org/10.1515/arh-2020-0106.

[162] M. Collepardi, A state-of-the-art review on delayed ettringite attack on concrete, Cement and Concrete Composites. 25 (2003) 401–407. https://doi.org/10.1016/S0958-9465(02)00080-X.

[163] R.J. Flatt, G.W. Scherer, Thermodynamics of crystallization stresses in DEF, Cement and Concrete Research. 38 (2008) 325–336. https://doi.org/10.1016/j.cemconres.2007.10.002.

[164] Y. Gu, R.P. Martin, O. Omikrine Metalssi, T. Fen-Chong, P. Dangla, Pore size analyses of cement paste exposed to external sulfate attack and delayed ettringite formation, Cement and Concrete Research. 123 (2019) 1–11. https://doi.org/10.1016/j.cemconres.2019.05.011.

[165] American Society for Testing and Materials., ASTM C191 − 19 Standard Test Methods for Time of Setting of Hydraulic Cement by Vicat Needle, (2019) 1–8. https://doi.org/10.1520/C0191-19.2.

[166] P. Sandberg, S. Bishnoi, Sulphate optimization of binders with calcined clay using isothermal calorimetry, in: F. Martirena, A. Favier, K. Scrivener (Eds.), Calcined Clays for Sustainable Concrete. Proceedings of the 2nd International Conference on Calcined Clays for Sustainable Concrete, RILEM, 2018: pp. 422–426. https://doi.org/10.1007/978-94-024-1207-9_68.

[167] M. Geiker, Development of cement hydration using chemical shrikage, in: K. Scrivener, R. Snellings, B. Lothenbach (Eds.), A Practical Guide to Microstructural Analysis of Cementitious Materials, 1st ed., CRC Press, 2016: pp. 75–105.

[168] E.; Grabowski, B.; Czarnecki, J.E.; Gillott, C.R.; Duggan, J.F. Scott, Rapid test of concrete expansivity due to internal sulfate attack, ACI Materials Journal. 89 (1992) 469–480.

[169] A. Pichelin, M. Carcassès, F. Cassagnabère, S. Multon, G. Nahas, Sustainability, transfer and containment properties of concrete subject to delayed ettringite formation (DEF), Cement and Concrete Composites. 113 (2020). https://doi.org/10.1016/j.cemconcomp.2020.103738.

Chapter 4

Hydration of C_3S and Al-doped C_3S in the presence of gypsum

Chapter 4 is based on the article:

José S. Andrade Neto, Erich D. Rodríguez, Paulo J. M. Monteiro, Angeles G. de la Torre, Ana Paula Kirchheim. Hydration of C_3S and Al-doped C_3S in the presence of gypsum. Accepted for publication in **Cement and Concrete Research**.

4 THE HYDRATION OF C_3S AND Al-DOPED C_3S IN THE PRESENCE OF GYPSUM

ABSTRACT

A full understanding of how gypsum accelerates the C_3S hydration, and the role of aluminum has not been achieved. The effects of gypsum (at 2.5 wt.% and 5.0 wt.%) on the hydration of tricalcium silicate (C_3S) and aluminum-doped C_3S (Al-C_3S) hydration are assessed. Isothermal calorimetry, thermodynamic modeling, XRD, TGA, and ^{27}Al and ^{29}Si MAS-NMR were performed to analyze gypsum's influence on the hydration of C_3S and Al-C_3S. The inclusion of gypsum retarded the initial hydration (first 3 h) for both C_3S and Al-C_3S, due to the interaction between the sulfate ions and C_3S. In contrast, gypsum enhanced the hydration of both C_3S and Al-C_3S afterward. This acceleration effect occurred earlier for the Al-C_3S due to the removal of aluminum from the solution. However, this is not the main mechanism behind the acceleration of C_3S by gypsum, which mainly results from changes in C-S-H morphology and increases in the ionic strength.

Keywords: C_3S; Sulfate; Gypsum; Aluminum; Hydration.

4.1 INTRODUCTION

Calcium sulfate, like gypsum, hemihydrate, and/or anhydrite, is added in Portland cement (PC) to control the C_3A hydration and subsequently improve its industrial application feasibility [1,2]. However, despite the much fewer studies, when compared to C_3A-calcium sulfate systems, calcium sulfate also modifies the C_3S/alite hydration and the morphology of its hydration products [3–12]. Also, as observed by Zunino and Scrivener [13], the C-S-H precipitation rate and, consequently, the alite reaction influences the sulfate demand of PC and, mainly, of blended cements. Therefore, the interactions between gypsum and alite may have an essential role in sulfate optimization of Portland cements, influencing the setting, workability, mechanical performance, and shrinkage of these cementitious materials [2]. This is particularly important for blended cements, which present different sulfate demands compared to PC [2,13]. Thus, the effects of calcium sulfate on alite reaction might influence the sulfate balance of a more complex system.

In clinker, C_3S usually forms solid solutions, containing several foreign elements as Mg^{2+}, Al^{3+}, Fe^{3+}, S^{6+}, Na^{+}, K^{+}, and P^{5+} [14,15]. The presence of these elements changes the C_3S structure and might influence its reactivity [14]. Therefore, it is important to differentiate C_3S as a single phase from the C_3S present in industrial clinkers. Because of this, the C_3S-solid solution present in the clinker is usually referred to as alite. In this study, the term alite is used when referred to the C_3S present in industrial clinker. Furthermore, the term "C_3S" is used to referred stoichiometric C_3S or C_3S with some incorporation of Mg^{2+}. Finally, the term "Al-C_3S" refers to the C_3S that contains Al^{3+} (and also Mg^{2+}). It is also important to define the nomenclature adopted to refer to changes in the C_3S hydration. Here, acceleration/retardation are related to time (when the main heat flow curve shifts left or right). At the same time, enhancement/suppression are related to the height/intensity of the main heat flow peak (when the main heat flow peak increases or decreases).

The initial C_3S dissolution is retarded (*i.e.*, the main heat flow peak is delayed) in the presence of gypsum, prolonging the induction period -the period where the initial rapid rate of hydration decreases within the first few minutes and remains at a low rate until the nucleation and growth period [16]. According to Nicoleau *et al.* [3] and Juilland *et al.* [4], this behavior occurs due to electrostatic interactions between the sulfate ions and the C_3S surface. The authors postulated that neutral $CaSO_4^0$ species are formed at the surface, reducing the charge screening created by calcium cations and resulting in a more negative surface charge, slowing the C_3S dissolution

rate. However, after the induction period, during the nucleation and growth period – the period in which the hydration rate increases again [16]-, the presence of calcium sulfate enhances the C_3S hydration rate, resulting in higher main heat flow peaks [2,5–12].

Some authors [6–8] state that this enhancement is due to ettringite- $[Ca_3Al(OH)_2 \cdot 12H_2O]_2 \cdot (SO_4)_3 \cdot 2H_2O$ -formation (Eqs. 4.1-4.3 [17]), which occurs when C_3A is presented or when the C_3S contains aluminum (such as Al-doped laboratory prepared C_3S and alite of industrial clinker-which typically contains 1.0 wt.% of Al_2O_3 [14]). According to Quennoz and Scrivener [6], the ettringite formation decreases the aluminum concentration on the solution, which is known to retard the Al-C_3S/alite hydration [3,18,19], and therefore increasing the hydration rate. Bergold *et al.* [8] suggested that the enhancement on alite hydration (by the inclusion of gypsum) is due to the seeding effect of very fine (nano-)ettringite, which might provide a suitable surface for heterogeneous nucleation of C-S-H and thus to a faster dissolution of alite.

$$AlO_2^- + 2OH^- + 2H_2O = [Al(OH)_6]^{3-} \quad (4.1)$$

$$2[Al(OH)_6]^{3-} + 6Ca^{2+} + 24H_2O = \{Ca_6[Al(OH)_6]_2 \cdot 24H_2O\}^{6+} \quad (4.2)$$

$$\{Ca_6[Al(OH)_6]_2 \cdot 24H_2O\}^{6+} + 3SO_4^{2-} + 2H_2O = \{Ca_6[Al(OH)_6]_2 \cdot 24H_2O\} \cdot [3SO_4^{2-} \cdot 2H_2O] \quad (4.3)$$

However, other authors report that gypsum also enhances the aluminum-free C_3S hydration [9–12], where no ettringite formation is observed. These hypotheses would not be enough to explain the effect of gypsum on C_3S hydration without consensus on the mechanism by which calcium sulfate enhances the C_3S hydration and whether aluminum ions have any influence or not. Therefore, the reason for that is not yet clearly understood.

The presence of gypsum also changes the C-S-H morphology [2,7,20,21]. According to Mota *et al.* [7], a cloud of sulfate ions is physically adsorbed in the positively charged C-S-H surface, which results in the electrical repulsion of C-S-H needles. This leads to a more divergent needle structure instead of the convergent morphology formed in C_3S pastes without sulfates.

In summary, there is no consensus on the mechanism by which calcium sulfate enhances the C_3S/alite hydration and whether aluminum ions have any influence or not. Therefore, this study aims to verify if the aluminum presented in aluminum-doped C_3S plays a crucial role in enhancing C_3S hydration due to gypsum and quantitatively compare the effects of gypsum on

C_3S and Al-C_3S hydration. The results obtained here are expected to advance understanding the mechanism by which gypsum influences C_3S hydration and, therefore, in the sulfate optimization of Portland and blended cements.

In this study, we assessed the hydration of C_3S and aluminum-doped C_3S (Al-C_3S) in the presence and absence of gypsum. Isothermal calorimetry (IC), thermodynamic modeling, X-ray diffractometry (XRD), thermogravimetry analysis (TGA), and ^{27}Aluminum and ^{29}Silicon magic angle spinning nuclear magnetic resonance spectroscopy (^{27}Al and ^{29}Si MAS-NMR) were performed to follow the C_3S and Al-C_3S hydration up to 7 days of curing.

4.2 MATERIALS AND METHODS

4.2.1 Materials

Powder samples of C_3S and aluminum-doped C_3S (Al-C_3S) were obtained from Mineral Research Processing (M.R.PRO, France). Both phases were synthesized in a laboratory by heating at 1450 °C, a stoichiometric mixture of reagent grade $CaCO_3$ and SiO_2. Approximately 0.8 wt.% of Al_2O_3 was used in the synthesis of Al-C_3S. In order to stabilize the intended polymorphs, ~0.5 and 1.0 wt.% of MgO were added to synthesize C_3S and Al-C_3S, respectively. Besides, high purity natural gypsum (> 96 wt.%) was used.

The samples were characterized by X-ray diffractometry (XRD), using an X'Pert MPD PRO diffractometer from PANalytical (Almelo, Netherlands). Monochromatic Cu-Kα_1 radiation, λ = 1.54059 Å obtained by a Ge (111) monochromator and an X'Celerator detector were used. The X-ray tube operated at 45 kV and 40 mA, and the samples were measured between 5º to 70º (2θ) with a step size of 0.016º, using a spinning sample-holder (16 rpm) to enhance particle statistics. The crystalline phases were identified using the X'Pert Highscore software (PANalytical) and quantified by the Rietveld method using the GSAS II software. The fitting process was adjusted to obtain an R_{WP} lower than 12% and a goodness-of-fit (GOF) lower than 5.

Figure 4.1 presents the X-ray patterns for the anhydrous materials. The C_3S sample presented 95.7 wt.% of triclinic C_3S (T1, Ca_3SiO_5, Inorganic Crystal Database - ICSD# 4331), 1.5 wt.% of magnesite ($MgCO_3$, ICSD# 40117), 1.5 wt.% of calcite ($CaCO_3$, ICSD# 73446), and 1.3 wt.% of portlandite ($Ca(OH)_2$, ICSD# 202220) (final agreement factor R_{WP} of 10.7% and GOF of 3.8 were obtained). The Al-C_3S consist of 98.7 wt.% of monoclinic C_3S (M1, Ca_3SiO_5, de

Noirfontaine *et al*. [22]), 0.9 wt.% of magnesite ($MgCO_3$, ICSD# 40117), 0.4 wt.% of calcite ($CaCO_3$, ICSD# 73446) and 0.1 wt.% of portlandite ($Ca(OH)_2$, ICSD# 202220) (final agreement factor R_{WP} of 11.4% and GOF of 4.1 were obtained). The natural gypsum contains 96.1 wt.% of gypsum ($CaSO_4 \cdot 2H_2O$, ICSD# 151692), 3.4% of dolomite ($CaMg(CO_3)_2$, ICSD# 66333), and 0.5% of quartz (SiO_2, ICSD# 200721) (final agreement factor R_{WP} of 11.7% and GOF of 3.1).

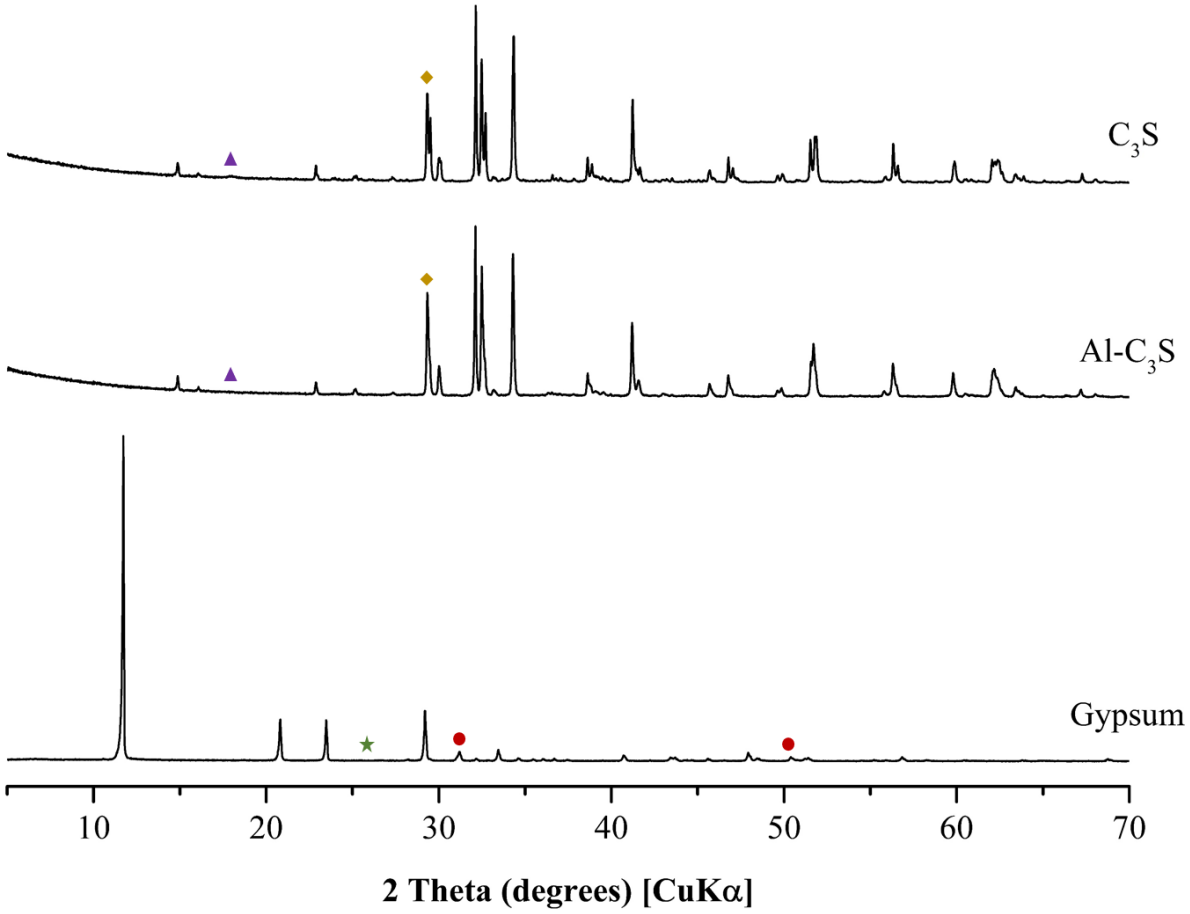

Figure 4.17 – X-ray diffractograms for the anhydrous materials. Symbols indicate the main reflections of the minor phases. Triangle: Portlandite; Rhombus: Calcite; Star: Quartz; Circle: Dolomite. Note that in some cases – such as calcite – the peaks overlap with the peak of the main phases.

The raw materials' BET surface area was obtained using an ASAP 2420 equipment from Micromeritics (Georgia, USA), according to the guidelines presented in Palacios et al. [23]. The particle size distribution was determined by laser diffraction, using PSA 1090 equipment from Anton Paar (Graz, Austria), isopropanol as the dispersant, and considering Mie theory [23]. Finally, the raw materials' density was determined through gas helium pycnometry, using

an AccuPyc II 1340 pycnometer from Micromeritics (Georgia, USA). The physical characterization results are presented in Table 4.1, and Figure 4.2 shows the particle size distribution of the raw materials. The Al-C_3S has a larger particle size and a slightly lower BET surface area (5.3% lower than C_3S).

Table 4.5 – Physical characterization of the raw materials.

Property	C_3S	Al-C_3S	Gypsum
BET surface area* (m^2/g)	1.14	1.08	1.33
D_v 90 (μm)	16.9	32.4	51.8
D_v 50 (μm)	6.7	11.6	16.9
D_v 10 (μm)	1.5	1.7	3.6
Density (kg/m^3)	3130	3150	2350

*Brunauer-Emmett-Teller theory surface area

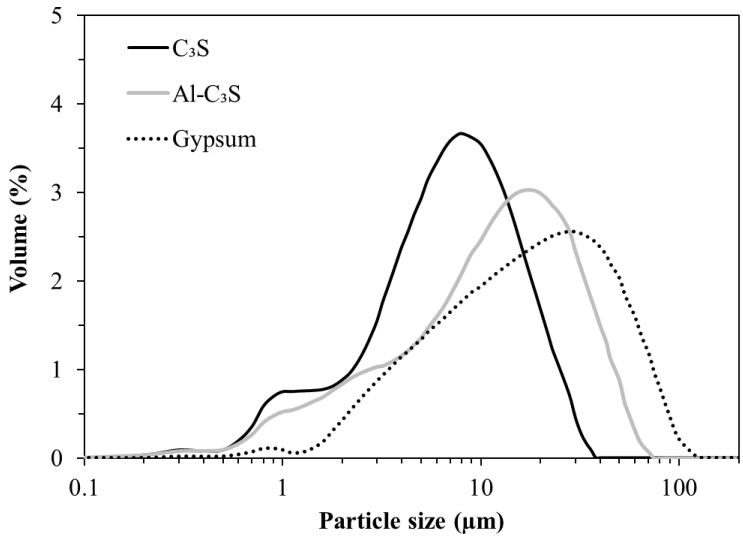

Figure 4.18 – Particle size distribution of the raw materials.

The raw materials' chemical composition was determined by X-ray fluorescence (XRF), using an ADVANT'XP+ spectrometer from Thermo Fisher Scientific (Waltham, USA). In terms of oxides, the chemical composition of C_3S, Al-C_3S, and gypsum is shown in Table 4.2.

Table 4.6 – Chemical composition, obtained by XRF, of the raw materials expressed as a weight percentage of oxides.

Constituent	C_3S	Al-C_3S	Gypsum
CaO	72.8	72.9	32.7
SiO_2	25.3	25.5	0.9
Al_2O_3	-	0.8	0.1
MgO	1.0	0.5	0.8
SO_3	-	-	44.3
*LOI	0.9	0.3	21.2

*Loss on ignition (LOI) at 1000 ºC.

4.2.2 Methods

4.2.2.1 Formulations and paste preparation

Table 4.3 shows the different formulations studied. Mixtures containing 0.00 wt.%, 2.50 wt.%, and 5.00 wt.% of gypsum (in relation to C_3S wt.%) with both tricalcium silicates were analyzed. The water/solid ratio was adjusted to 0.50. Table 4.3 also presents the tests conducted for each formulation: isothermal calorimetry (IC), thermogravimetric analysis (TGA), X-ray diffraction (XRD), and ^{27}Al and ^{29}Si nuclear magnetic resonance (^{27}Al and ^{29}Si MAS-NMR), which will be described in Section 4.2.2.2.

Table 4.7 – Formulations studied.

Mixture	C_3S (wt.%)	Gypsum (wt.%)	Test conducted
C_3S	100.00	0.00	IC, TGA, XRD, ^{29}Si NMR
C_3S_2.5%G	97.56	2.44	IC, TGA, XRD, ^{29}Si NMR
C_3S_5.0%G	95.24	4.76	IC
Al-C_3S	100.00	0.00	IC, TGA, XRD, ^{29}Si NMR, ^{27}Al NMR
Al-C_3S _2.5%G	97.56	2.44	IC, TGA, XRD, ^{29}Si NMR, ^{27}Al NMR
Al-C_3S _5.0%G	95.24	4.76	IC

The anhydrous materials (C_3S in the absence and the presence of gypsum) were manually mixed in an agate mortar for 10 minutes.

For the calorimetry analysis, 8 g of anhydrous materials were manually mixed with 4 g of distilled water for 1 min. Then, the paste was mixed in a vortex mixer for 1 extra min. Finally, ~ 6 g of paste were placed in a 20 mL glass ampoule used for the calorimetry analysis (see section 4.2.2.2).

For the TGA, XRD, and ^{27}Al and ^{29}Si MAS-NMR analysis, cylindrical specimens were molded using a hermetically closed PTFE cylindric recipient (as shown in Figure 4.3) that has eight cylinders (10 mm diameter). For this, 10 g of anhydrous materials were mixed with 5 g of distilled water in a vertical mixer (IKA model RW 20 digital). The pastes were mechanically mixed during 180 s at 800 rpm, where 30 s of stabilization time was performed. Our lab's previous results showed a good correlation between this procedure and the procedure adopted for the calorimetry analysis.

The PTFE recipient was sealed and kept rotating at 15 rpm in a benchtop roller (Wheaton) for the first 10 h to obtain homogeneous samples [24]. Then, one cylinder of each sample was demolded, and the hydration was stopped. The PTFE recipient was sealed again and kept rotating at 15 rpm for 14 h more (totaling 24 h). After this initial period, the pastes were not hard enough to demold. Thus, the device was introduced in a humidity chamber at 99% RH at 20 ± 1 °C. After each curing time (1, 3, and 7 days), one cylinder was demolded, and the hydration was stopped.

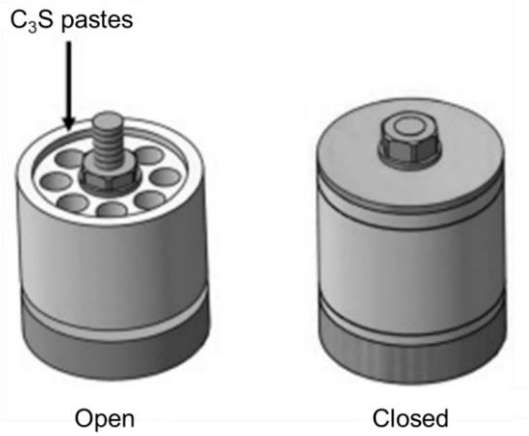

Figure 4.19 – PTFE cylinder shape recipient to prepare the C_3S pastes. Adapted from García-Maté *et al.* [24]

At 10 h, 1, 3, and 7 days, one fraction of the pastes was milled to a fine powder in an agate mortar, and the hydration was stopped by solvent exchange with isopropanol and ether according to the procedure described by García-Maté *et al.* [24]. The stopping procedure consisted of filtration in a Whatman system (90 mm diameter Whatman filter with a pore size

of 2.5 μm and Teflon support) with isopropanol (VWR Chemicals) twice and finally with diethyl ether (Prolabo S.A.). Then, thermogravimetric analysis (TGA) and X-ray diffraction (XRD) were performed in these pastes. ^{27}Al and ^{29}Si MAS-NMR of the pastes at 7 days were also assessed on them.

4.2.2.2 Tests conducted

The isothermal calorimetric study was performed in an eight-channel Thermal Activity Monitor of Tam Air, TA Instruments (New Castle, DE, USA) using glass ampoules of 20 mL. Distilled water was used as reference material. The amount of water used as reference was calculated according to Wadsö [25] to obtain the same heat capacity of the C_3S paste. The heat flow (thermal power, mW/g of solids) and the cumulative heat (integral of thermal power, J/g of solids) were collected for up to 3 days at 20 °C. Only the heat released after the first 45 minutes was considered for the cumulative heat, as the first peak has low reproducibility. These first 45 minutes were used as a stabilization period after the disturbance in calorimeter temperature after introducing the reference and the sample.

TGA measurement of C_3S pastes was done in an SDT-Q600 analyzer from TA Instruments (New Castle, DE, USA). The temperature varied from room temperature (RT) to 1000 °C at a heating rate of 10 °C/min. The samples were placed in open platinum crucibles under airflow. From the TGA results, the bound water and the portlandite content were determined. After stopping hydration, the bound water of the pastes was assigned to be the weighed loss from RT to 550°C. Due to this, the actual bounded water has to be calculated by Eq. 4.4 and the free water by Eq. 4.5 [26]:

$$\mathrm{BW} = \frac{\mathrm{BW_{ATD}} \cdot \mathrm{CM}}{100 - \mathrm{BW_{ATD}}} \tag{4.4}$$

$$\mathrm{FW} = \mathrm{TW} - \mathrm{BW} \tag{4.5}$$

Where BW corresponds to actual chemically bound water content, BW_{ATD} is the loss of mass measured up to 550 ºC from TGA curves, and CM is the cement content, and TW is the total water content added (all the numbers in weight percentage).

The portlandite content was obtained by Eq. 4.6 [27].

$$Ca(OH)_{2,\text{measured}} = WL_{Ca(OH)_2} \cdot \frac{m_{Ca(OH)_2}}{m_{H_2O}} \quad (4.6)$$

where $WL_{Ca(OH)_2}$ is the weight loss due to the decomposition of crystalline portlandite obtained by the integration of DTG peak located in the temperature range from ~450 and ~550 ºC, using the tangential method [27], the $m_{Ca(OH)_2}$ is the molecular mass of portlandite (74 g/mol) and m_{H_2O} is the molecular mass of water (18 g/mol).

For the XRD analysis, the C_3S pastes, after the hydration stoppage, were manually ground and mixed with 20 wt.% of crystalline quartz (99.5%, AlfaAesar) used as an internal standard in an agate mortar for 10 minutes. The XRD with internal standard data was collected on a D8 ADVANCE diffractometer from Bruker AXS (Massachusetts, USA) equipped with a Molybdenum X-ray tube and a Johansson Ge (111) monochromator, using strictly monochromatic Mo-Kα_1 radiation, λ = 0.7093 Å, in transmission geometry (θ/θ). The X-ray tube operated at 50 kV and 50 mA, and the data were collected between 2.5 and 35° (2θ) with a step size of 0.01° and 2.5 s/step. A spinning sample-holder (10 rpm) was used to enhance particle statistics.

The crystalline phases were identified using the X'Pert High Score software (PANalytical). Rietveld analysis was performed using GSAS II software, with the cif files of the Inorganic Crystal Structures Database (ICSD). The structural models used for the Rietveld analysis are shown in Table 4.4. The phase fractions, background coefficients, zero-shift error, and cell parameters were refined. The peak shapes were fitted by using a pseudo-Voigt function. The preferred orientation coefficient of C_3S T1, C_3S M1, and portlandite was refined by the March-Dollase ratio. Finally, the non-crystalline content (amorphous and nanocrystalline) was determined by the internal standard method [28]. The degree of hydration (DoH_{XRD}) of C_3S was calculated from the XRD results according to Eq. 4.7.

$$DoH_{C_3S\,(t)} = \frac{W_{C_3S,i} - W_{C_3S,t}}{W_{C_3S,i}} \cdot 100 \quad (4.7)$$

where $DoH_{C_3S\,(t)}$ is the degree of hydration of C_3S at a specific time (t), $W_{C_3S,i}$ is the amount of C_3S in the anhydrous mixture obtained by XRD-Rietveld, $W_{C_3S,t}$ is the amount of C_3S in the paste at a specific time (t) obtained by XRD-Rietveld.

As the total mass of solids increases with the progress of the C_3S hydration, as free water is bound into hydration products, phase contents determined by XRD-Rietveld and the portlandite content obtained by TGA need to be normalized. For this purpose, Eq. 4.8 was used to normalize the contents obtained per 100 g of paste [26]

$$W_{j,rescaled} = W_{i,measured} \cdot \frac{(100 - FW)}{100} \quad (4.8)$$

Where $W_{j,rescaled}$ is the weight of phase per 100 g of paste, $W_{i,measured}$ is the phase content obtained by TGA or XRD-Rietveld, and FW is the free water content determined by TGA according to Eq. 4.5.

Table 4.8 – Structural models used for the Rietveld analysis of C_3S and Al-C_3S pastes.

Phase	**ICSD code**	**References**
C_3S triclinic (T1)	4331	Golovastikov et al. [29]
C_3S monoclinic (M1)	-	de Noirfontaine et al. [22]
Lime	52783	Smith and Leider [30]
Gypsum	151692	De la Torre et al. [31]
Quartz	200721	Jorgensen [32]
Ettringite	155395	Goetz-Neunhoeffer and Neubauer [33]
Portlandite	15471	Petch [34]
Calcite	79673	Wartchow [35]

Solid-state single pulse ^{27}Aluminum and ^{29}Si magic angle spinning nuclear magnetic resonance spectroscopy (^{27}Al MAS-NMR and ^{29}Si MAS-NMR) of the pastes, at 7 days, were performed in an AVANCEII HD 600 spectrometer from Bruker AXS. A MAS probe of 2.5 mm was used at a spinning rate of 15 kHz. The magnetic field was 14.1 T for the ^{27}Al MAS-NMR, which corresponds to a ^{27}Al resonance frequency of 156.37 MHz. ^{27}Al MAS NMR spectra were collected with a 1 μs (corresponding to π/2 flip angle) excitation pulse with ^{1}H decoupling and summing up 200 scans. The ^{29}Si MAS-NMR spectra were recorded at 79.49 MHz and were collected with a 6 μs (corresponding to π/2 flip angle) excitation pulse with ^{1}H decoupling and summing up 800 scans.

^{29}Si MAS-NMR and ^{27}Al MAS-NMR results were normalized for 0 to 1 (0 corresponding to the minimum value and 1 the maximum value obtained), and then peak deconvolutions were computed using Excel software. The ^{29}Si MAS-NMR, distinct peaks centered in different Si sites, denoted as Q^0, Q^1, $Q^2(1Al)$, and Q^2 were fitted varying their intensity and width, assuming Gaussian line-shaped. The DoH_{NMR} of C_3S was obtained through Eq. 4.9 [36]. The mean silicate chain length (MCL)-which stands for the average polymerization degree of silicate chains in C-S-H and the fraction of tetrahedrally coordinated Al in the C-S-H phase (molar Al(IV)/Si ratio) were calculated using Eqs. 4.10 and 4.11 [36].

$$DoH_{NMR} = 1 - Q^0 \tag{4.9}$$

$$MCL = \frac{2 \cdot \left[Q^1 + Q^2 + \frac{3}{2} \cdot Q^2(1Al)\right]}{Q^1} \tag{4.10}$$

$$Al(IV)/Si = \frac{Q^2(1Al)}{2 \cdot [Q^1 + Q^2 + Q^2(1Al)]} \tag{4.11}$$

The quantitative analyses of ^{27}Al MAS-NMR are less straightforward than ^{29}Si MAS-NMR, as there are non-symmetric line shapes caused by a second-order quadrupolar broadening of the central transition for the ^{27}Al quadrupole. However, the octahedral Al sites of ettringite, monosulfoaluminates-type phases (AFm), and the so-called third aluminate hydrate (TAH) – from octahedral Al sites associated with C-(A)-S-H phase, have small ^{27}Al quadrupole coupling those results in Gaussian-like line shapes for the center band at 14.1 T. The ettringite, AFm, and TAH contents were estimated by dividing the areas of their respective gaussian peaks by the spectrum's total area.

4.2.2.3 Thermodynamic modeling

Thermodynamic modeling of C_3S and Al-C_3S pastes with different amounts of gypsum was carried out using the CemGEMS web application [37], coupled with the CEMDATA18 database [38]. For this, the chemical characterization of C_3S, Al-C_3S, and gypsum was used as input data. A four-parameter logistic (4PL) fit (Eq. 4.12) [37,39] of the Degree of Hydration (DoH) of C_3S obtained by XRD was used to describe the DoH of C_3S over time. All fits have

good correlations (with an R^2 between 0.97 and 0.98), as presented in the supplementary data (Figure B1). For the pastes with 5 wt.% of gypsum, the fits of the corresponding pastes with 2.5 wt.% of gypsum were used for the thermodynamic modeling due to the lack of the DoH obtained by XRD for these pastes. This seems plausible as the C_3S in the pastes with 5 wt.% of gypsum presents a very similar DoH of the C_3S compared to the pastes with 2.5 wt.% of gypsum, as observed by isothermal calorimetry (see Section 4.3.1). The phase assemblage (in mass, g/100g of paste), the pore solution composition (in mM), and the ionic strength (in molal) of the pore solution were analyzed by thermodynamic modeling.

$$DoH_{C_3S} = d + \frac{(a-d)}{1+\left({}^{t}/_{c}\right)^{b}} \quad (4.12)$$

where *t* is the hydration time in days, *a* is the asymptote minimum DoH value (considered here equal to 0%), *d* is the asymptote maximum DoH value (considered here equal to 97%), *b* is the maximum steepness, and *c* is the time position of the inflection point [37].

4.3 RESULTS

4.3.1 Isothermal calorimetry (IC) study

Figures 4.4 A and B show the heat flow and cumulative heat curves of C_3S and Al-C_3S pastes, respectively, without gypsum, and the systems with 2.5 wt.% and 5.0 wt.% of gypsum (in relation to C_3S wt.%) during the first 72 hours of hydration. Table 4.5 presents the main parameters obtained from the heat flow and cumulative heat curves.

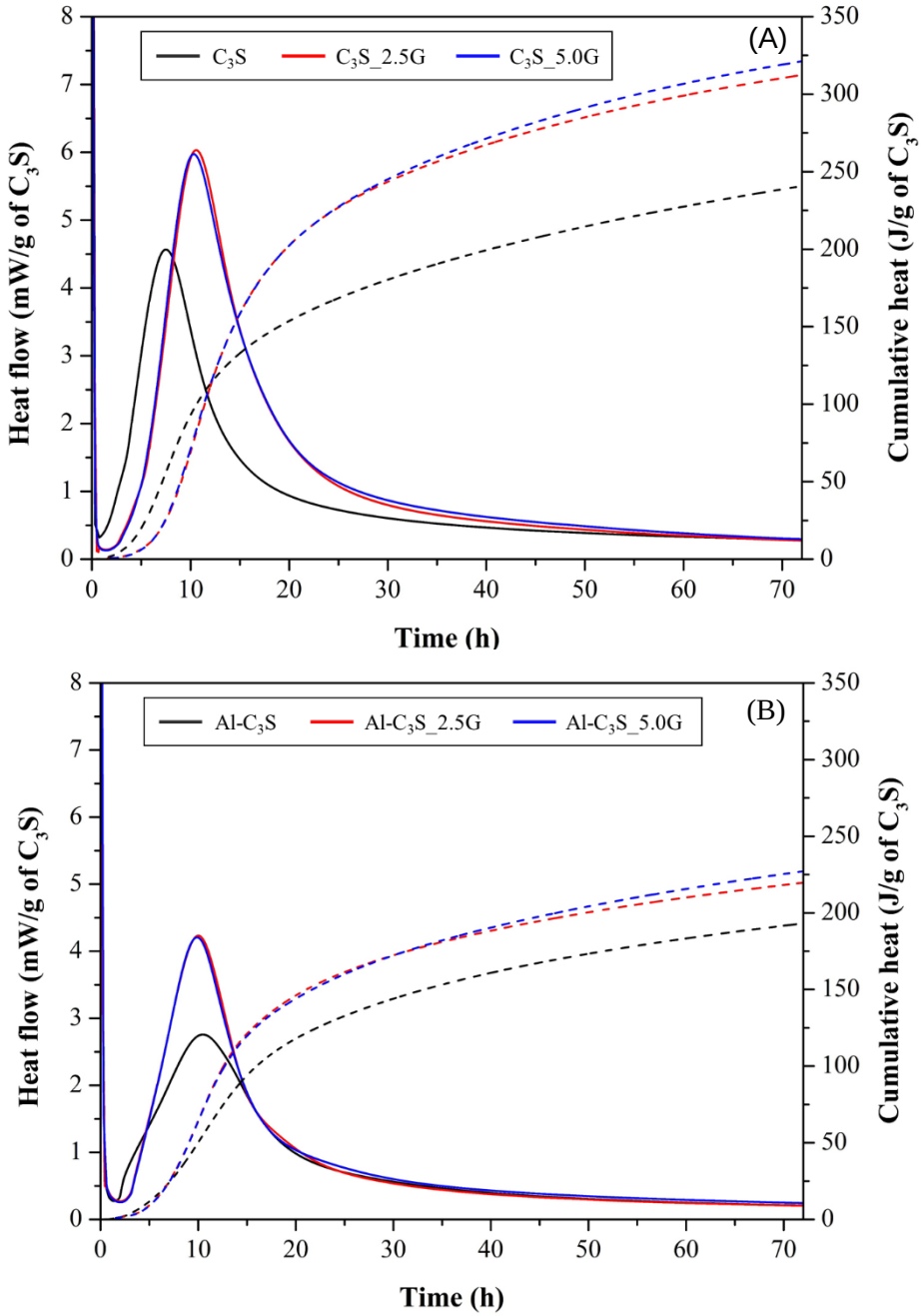

Figure 4.20 – Heat flow curves (solid lines and primary/left "y" axis) and cumulative heat curves (dashed lines and secondary/right "y" axis) of the (A) C_3S and (B) Al-C_3S pastes with different amounts of gypsum during the first 72 hours of hydration.

Table 4.9 – Parameters determined from the calorimetry results.

Parameter	C_3S	C_3S_2.5G	C_3S_5.0G	Al-C_3S	Al-C_3S_2.5G	Al-C_3S_5.0G
Induction period length (min)*	40.3	165.8	174.4	81.7	137.9	146.5
Heat flow rate at the acceleration period (mW/g of $C_3S \cdot h$)*	0.89	1.01	1.13	0.29	0.64	0.65
Maximum heat flow of the main hydration peak (mW/g of C_3S)	4.57	6.03	5.97	2.76	4.23	4.21
Heat of hydration at 24 h (J/g of C_3S)	165.77	222.90	223.16	129.79	158.77	157.21
Heat of hydration at 48 h (J/g of C_3S)	211.77	281.87	287.61	171.10	198.15	201.68
Heat of hydration at 72 h (J/g of C_3S)	240.73	312.35	321.21	193.16	219.69	227.15

* calculated as indicated in Figure B2;

Comparing both C_3S pastes without gypsum, the Al-C_3S paste presents a more extended induction period (103% longer) and a broader and lower hydration peak (40% lower), with a lower hydration rate at the acceleration period (67% lower). Besides, the cumulative heat released by the Al-C_3S paste during the first 72 hours of hydration is lower than the heat released by the C_3S paste (22%, 19%, and 20% lower at 24 h, 48 h, and 72 h, respectively). These results indicate that the Al-C_3S has a lower hydration rate when compared to the C_3S, which agrees with the results obtained by Stephan *et al.* [40], Begarin *et al.* [41], and Wagner *et al.* [42]. Moreover, these results were also expected since the particle size of Al-C_3S was coarser than the C_3S without Al doping. To decouple the role of aluminum, the heat flow and cumulative heat curves were also normalized by the specific surface area (SSA) of C_3S and Al-C_3S, as shown in the supplementary information (Figure B3). The difference between the samples reduced, but the Al-C_3S pastes still present lower hydration peak (36% lower) and lower heat release (17%, 15%, and 15% lower at 24 h, 48 h, and 72 h, respectively), and therefore still exhibits a lower hydration rate than C_3S.

The effect of gypsum on hydration was similar for both samples. The addition of 2.5 wt.% of gypsum prolonged the induction period (311% and 69% longer for the C_3S and Al-C_3S pastes, respectively) but increased the hydration rate at the acceleration period (increases of 13% and 121% for the C_3S and Al-C_3S pastes, respectively) and the main hydration peak (increases of

32% and 53% for the C_3S and Al-C_3S pastes, respectively). Thus, the cumulative heat released for the C_3S pastes without gypsum was higher than the C_3S pastes with gypsum until ~ 12 hours but lower afterward (34%, 33%, and 30% lower at 24 h, 48 h, and 72 h, respectively). The Al-C_3S pastes without gypsum presented a similar cumulative heat until ~ 7 hours, but lower after this period than the Al-C_3S pastes with gypsum (22%, 16%, and 14% lower at 24 h, 48 h, and 72 h, respectively). This indicates that gypsum retard the initial hydration of C_3S (induction period) but enhances afterward, which agrees with several previous studies [2,6,7,9,11].

The increase in the gypsum content added to 5.0 wt.% slightly prolonged the induction period (5% and 6% longer than the C_3S_2.5G and Al-C_3S_2.5G pastes, respectively) and slightly decreased the main C_3S hydration peak (decrease of 1% for the C_3S_5.0G and Al-C_3S_5.0G pastes). This indicates that further increases in the gypsum content will not increase more the C_3S hydration rate. Similar behaviors were observed in previous studies [5,9,10].

With the inclusion of gypsum on the C_3S pastes, the amount of C_3S present in the mixture decreases, and therefore, the heat released by C_3S dissolution and C-S-H and portlandite precipitation decrease. Thus, the heat flow and cumulative curves were normalized per gram of C_3S. The heat released by gypsum dissolution in the C_3S and Al-C_3S pastes with gypsum, and the heat released by ettringite formation in the Al-C_3S_2.5G and Al-C_3S_5.0G pastes, contributes to the increase in the heat release with gypsum addition. However, due to the low amount of gypsum dissolved and ettringite formed (see Sections 4.3.2 and 4.3.3 for more details), this cannot account for the great increases in the heat released observed.

4.3.2 Thermodynamic Analysis

Figure 4.5 presents the phase assemblage (in g/100g) of the C_3S and Al-C_3S pastes with different amounts of gypsum (0, 2.5, and 5.0 wt.% in relation to C_3S wt.%) obtained by thermodynamic modeling. The addition of gypsum is not expected to result in any different hydrated phases in C_3S pastes. However, in Al-C_3S, gypsum addition led to the formation of ettringite instead of monocarboaluminate (MC, CO_2-AFm) and hydrotalcite (HT, $Mg_6Al_2CO_3(OH)_{16}{\cdot}4H_2O$), as expected. For the Al-C_3S_2.5G, gypsum depletion is predicted to happen at ~ 280 hours of hydration, leading to the formation of hydrotalcite. In turn, for the Al-C_3S_5.0G, the gypsum depletion is not expected to happen up to 10000 hours of hydration. Finally, in Al-C_3S pastes, the addition of gypsum results in a decrease of portlandite (4% and 8% of reduction at 10000 hours for the pastes with 2.5 and 5.0 wt.% of gypsum, respectively).

This occurs as calcium ions are consumed for the ettringite formation. For the C_3S pastes, this does not occur as the addition of gypsum does not result in ettringite formation.

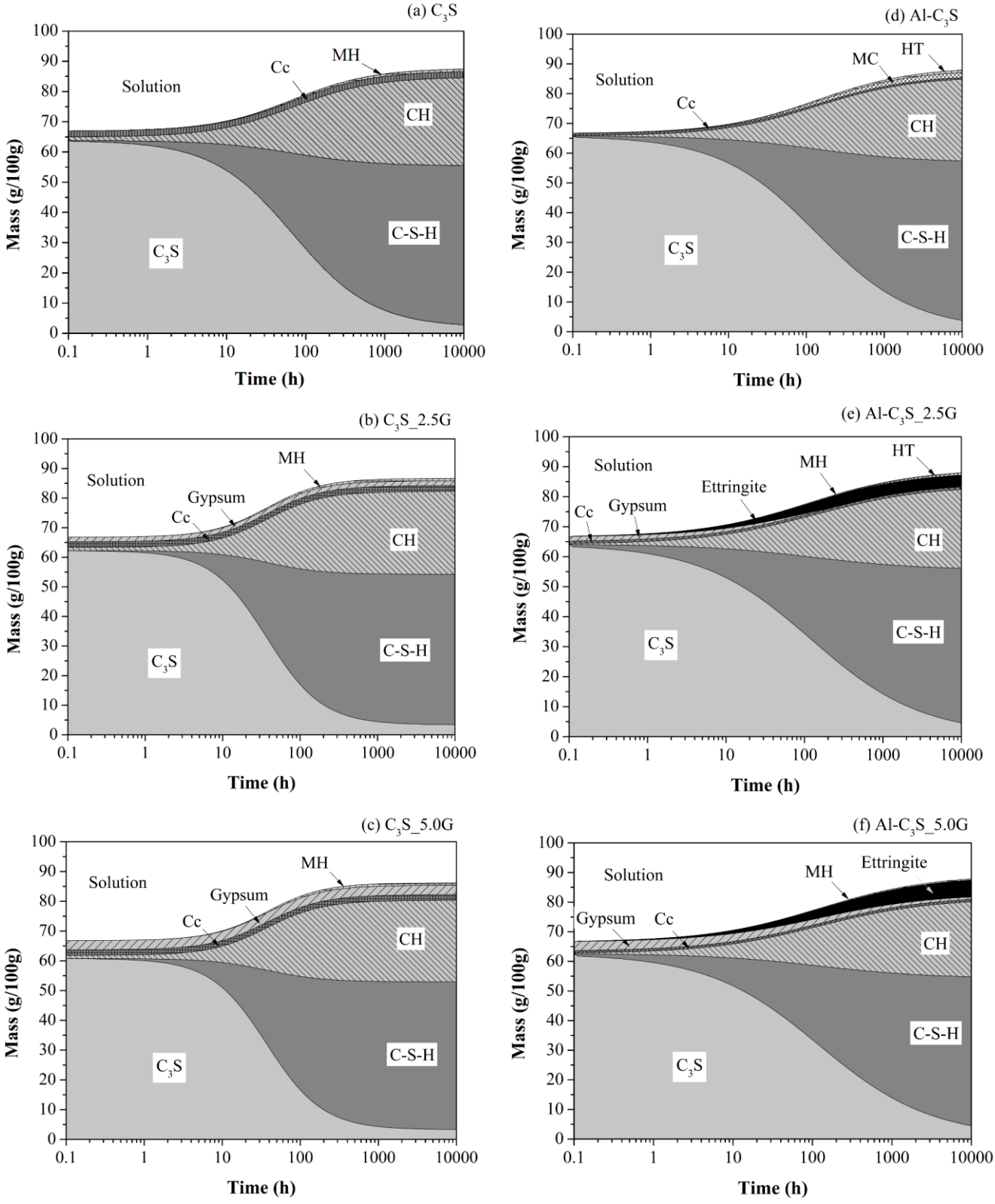

Figure 4.21 – Phase assemblage (in g/100 g of paste) of the C_3S and Al-C_3S pastes with different amounts of gypsum as predicted by cemGEMS. Where CH is Portlandite, Cc is calcium carbonate, MH is magnesium hydroxide (brucite), and HT is hydrotalcite.

The pore solution compositions of the C_3S and Al-C_3S pastes with different gypsum amounts, obtained by thermodynamic modeling, are shown in the supplementary information (Figure B4). For all pastes, the concentrations of the ions are not expected to change with the progress of the hydration, except for the Al-C_3S_2.5G, which shows a decrease in Ca (from 32.9 to 21.3 mM), S (from 12.8 to 0.4 mM), and Mg (from 0.14 μM to 0.11 μM) concentrations at ~ 280 hours (when occurs gypsum depletion), leading to the formation of hydrotalcite.

The addition of 2.5 wt.% gypsum in both C_3S and Al-C_3S resulted in an S concentration of 12.8 mM and increased the Ca concentration from 21.0 to 32.9 mM (an increase of 56.7%). Further additions of gypsum (*i.e.*, for the pastes with 5.0 wt.% of gypsum) did not result in any change of the composition of the pore solutions of the C_3S pastes in the first 10000 hours of hydration, as this further amount of gypsum is expected not to dissolve. In turn, for the Al-C_3S paste, the further addition of gypsum also did not change the initial composition of the pore solution but prevented gypsum depletion (which is expected to occur around 280 hours for the Al-C_3S_2.5G paste). Therefore, the pore solution composition of the Al-C_3S_5.0G pastes is expected to remain constant up to 10000 hours of hydration.

As shown by the thermodynamic modeling, the concentration of Al in the pore solution reduces from 0.005 mM in Al-C_3S pastes to 0 mM in Al-C_3S_2.5G and Al-C_3S_5G pastes. This result means that all the aluminum coming from the dissolution of Al-C_3S is expected to be immediately consumed by the ettringite formation in the pastes with gypsum.

The ionic strength of the pore solution of the pastes was calculated using cemGEMS. During the first 48 h, the average ionic strength of the pore solution of C_3S and Al-C_3S pastes are very similar (0.055 molal). The addition of 2.5% of gypsum is predicted to increase the ionic of both C_3S and Al-C_3S up to 0.083 molal (an increase of 51%). Further additions of gypsum are not expected to increase more the ionic strength, and the C_3S_5.0G and Al-C_3S_5.0G presented the same ionic strength as the pastes with 2.5% of gypsum (0.083 molal).

The increase in the ionic strength due to the addition of gypsum occurs due to the release of SO_4^{2-} ions into the pore solution, which is a divalent ion and greatly contributes to the increase of the ionic strength. The increase of the amount of gypsum added (from 2.5 to 5.0 wt.%) did not result in further increases, as the additional amount of gypsum is not expected to dissolve, and therefore the S concentration into the pore solution remains the same during the first days of hydration, as discussed before.

4.3.3 X-ray diffraction (XRD)

Figures 4.6 A-D present the normalized results of crystalline and non-crystalline phases quantification by the Rietveld method over time. Tables B1-B4 gives the normalized phase assemblage with time for the samples without and with 2.5 wt.% of gypsum. All Rietveld quantifications presented an R_{WP} lower than 12.0 and GOF lower than 5, indicating good refinements. Figures B5 and B6 in the supplementary information show as a representative example the Rietveld plots of C_3S_2.5G and Al-C_3S_2,5G at 1 day Figure 4.7 presents the degree of hydration of C_3S (DoH_{XRD}) over the first 7 days, determined from the XRD-Rietveld results.

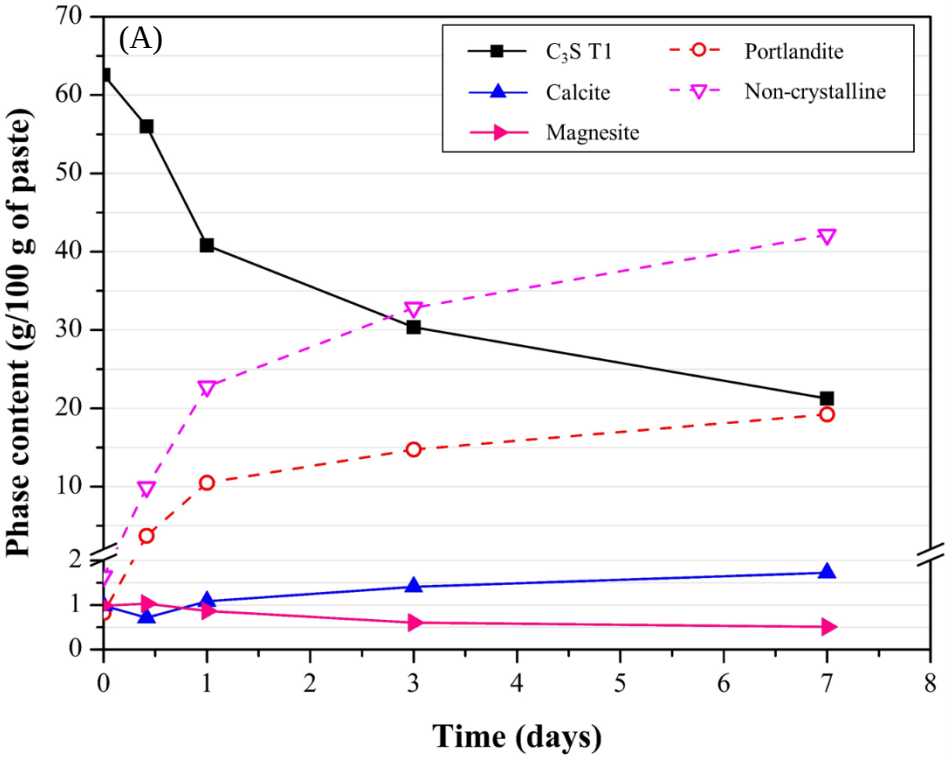
(A)
C3S T1
Portlandite
Calcite
Non-crystalline
Magnesite
Phase content (g/100 g of paste)
Time (days)

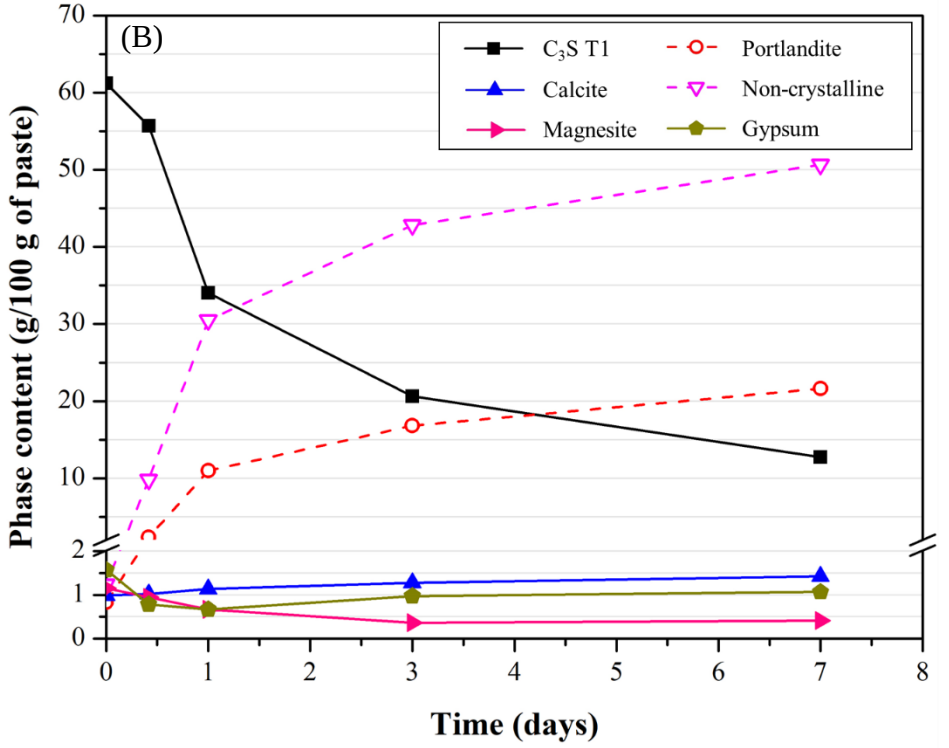
(B)
C3S T1
Portlandite
Calcite
Non-crystalline
Magnesite
Gypsum
Phase content (g/100 g of paste)
Time (days)

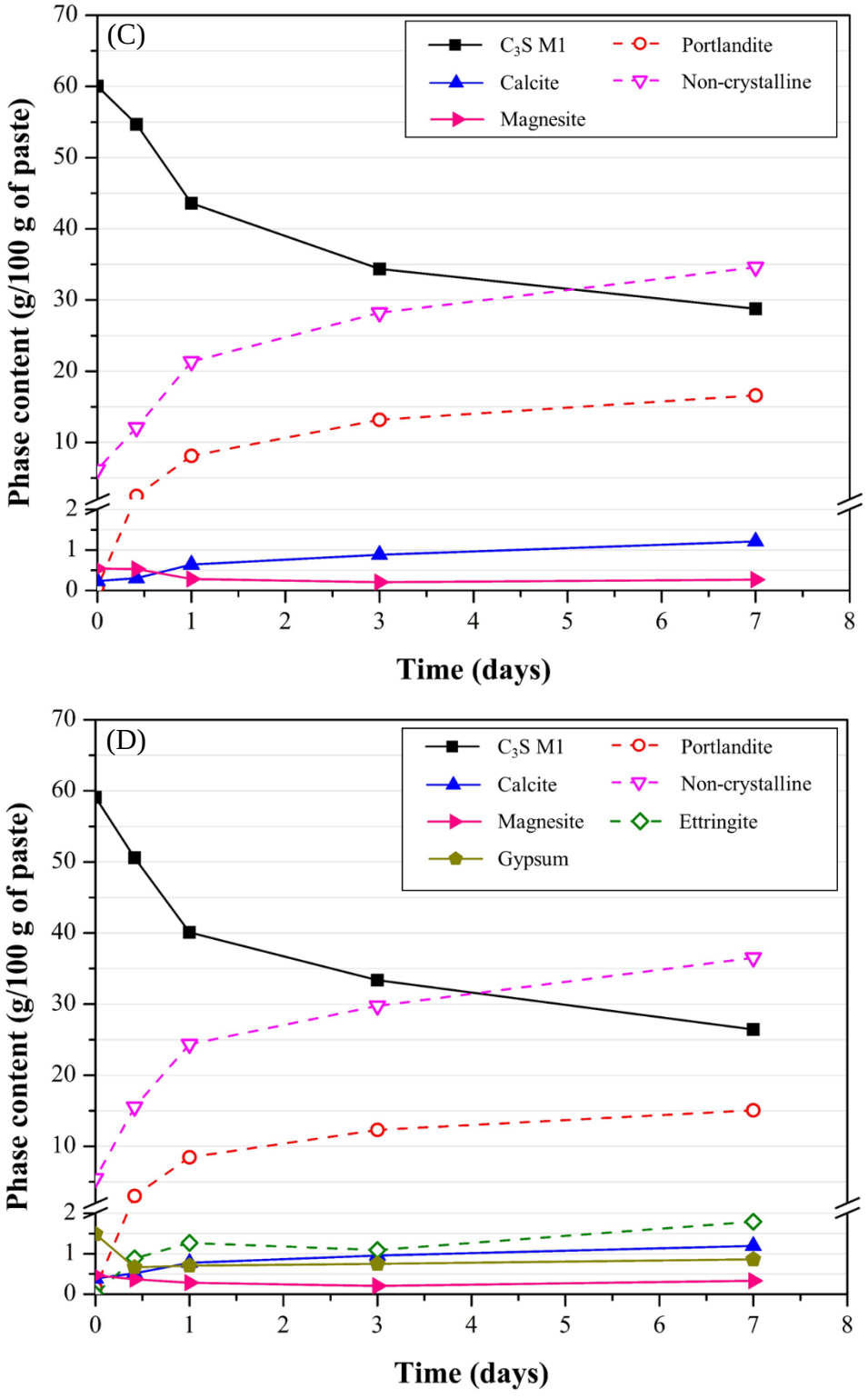

Figure 4.22 – Crystalline and non-crystalline phases content (g/100 g of paste) obtained by XRD-Rietveld: (A) C_3S; (B) C_3S_2.5%G; (C) Al-C_3S; (D) Al-C_3S_2.5%G.

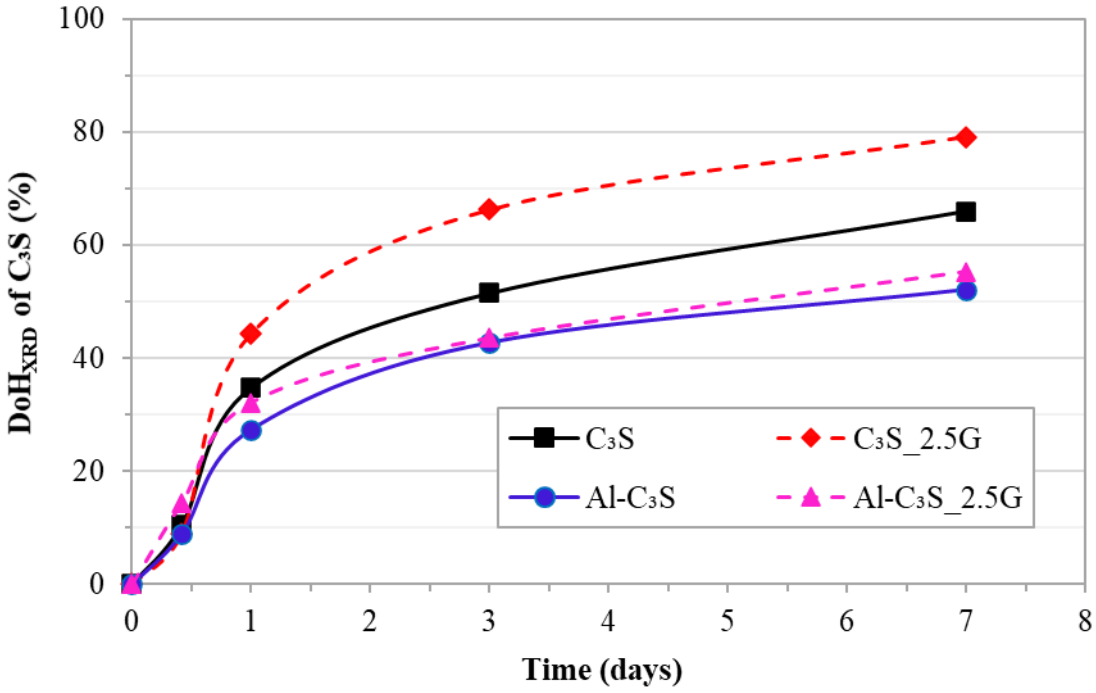

Figure 4.23 – Degree of hydration of C_3S (%) obtained by XRD-Rietveld.

As expected, the anhydrous phases (C_3S T1, C_3S M1, magnesite, and gypsum) were still remaining samples in all pastes and times of hydration. Concerning the hydration products, portlandite was identified for all pastes. In contrast, ettringite (2.3 wt.% at 7 d) was only identified for Al-C_3S_2.5%G paste, as this mixture was the only one with aluminum (from Al-C_3S) and sulfate (from gypsum). Calcite was presented for all hydrated pastes as C_3S and Al-C_3S have 1.5 wt.% and 0.4 wt.% of calcite. Calcite content increased as a function of the time for all the samples due to slight carbonation effect of samples due to reactions with the atmospheric CO_2 during sample preparation and the tests. The non-crystalline phases of all pastes are mainly related to C-S-H [43].

Comparing C_3S and Al-C_3S pastes without gypsum, the dissolution of anhydrous phases and formation of hydration products are faster in the aluminum-free paste. At 3 and 7 d, the DoH_{XRD} of C_3S is 51.5% and 66.0% for the C_3S paste and 42.7% and 52.1% for the Al-C_3S paste, respectively. The amount of portlandite formed follows the same tendency, and the C_3S pastes present 14.7 wt.% and 19.2 wt.% while the Al-C_3S shows 13.2 wt.% and 16.6 wt.% of portlandite at 3 and 7 d, respectively. This behavior is coherent with the calorimetry results, indicating that the C_3S reacts faster than the Al-C_3S.

The addition of gypsum in the C_3S (T1) pastes did not affect the crystalline hydration products coming from C_3S, but it changed the dissolution rate of anhydrous phases and the rate of formation of portlandite and non-crystalline phases. On the one hand, at 10 h, the gypsum addition slightly decreased the DoH_{XRD} of C_3S (which was 10.5% for the C_3S paste and 9.0% for the C_3S_2.5G paste) and decreased the portlandite content formed by 36.8%. On the other hand, at 1, 3, and 7 d, the presence of sulfate increased the DoH_{XRD} of C_3S by 27.6%, 28.7%, and 20.0%, and increased the portlandite content by 4.8%, 14.1%, and 12.6%, respectively. These results indicate that the addition of gypsum in the C_3S (T1) pastes retards the initial C_3S hydration (until ~ 10 h) but enhances afterward, as also observed by calorimetry.

For the Al-C_3S (M1) pastes, the delay in the dissolution of C_3S at 10 h, due to gypsum addition, was not observed. On the contrary, the DoH_{XRD} of Al-C_3S increases 61.9%, 17.5%, 1.9%, and 6.2% at 10 h, 1, 3, and 7 d, respectively. This was expected as the gypsum enhanced the Al-C_3S hydration rate after ~ 7 hours, as observed by IC. On the other hand, the portlandite content at 3 and 7 d was reduced by 6.6% and 9.2%. This agreed with thermodynamic modeling (See Section 4.3.2) and was also observed by He *et al.* [44] and is probably related to the consumption of calcium ions to ettringite formation.

4.3.4 Thermal analysis (TG/DTG)

Figures 4.8 A-D shows the DTG curves of the C_3S and Al-C_3S pastes, without and with 2.5 wt.% of gypsum, at 10 h, 1, 3, and 7 d. One peak between 400 and 500 °C, corresponding to the decomposition of portlandite [27], and one peak between 600 and 700 °C, related to the decomposition of calcium carbonates [27], were observed for all pastes, which corroborates with the XRD results. Furthermore, all samples also presented a peak of weight loss between 50 and 300 °C, which is related to the decomposition of C-S-H and C-(A)-S-H [27], and a peak between 800 and 900 °C that corresponds to the transformation of C-S-H in wollastonite ($CaSiO_3$) [27]. Finally, as also observed by XRD, the sample Al-C_3S_2.5%G was the only one that presented the signal due to the loss of water of ettringite, which is associated with a signal around 100 °C [27]. Regarding the samples with gypsum, a peak around 130°C is observed in C_3S_2.5G, while it is not observed in Al-C_3S_2.5G, indicating that gypsum dissolution is faster in the latter, which is expected due to the consumption of sulfate ions to ettringite formation.

With the increase of the hydration time, the peaks related to the hydrated phases' decomposition increased, indicating a higher amount of hydration products and a higher degree of hydration.

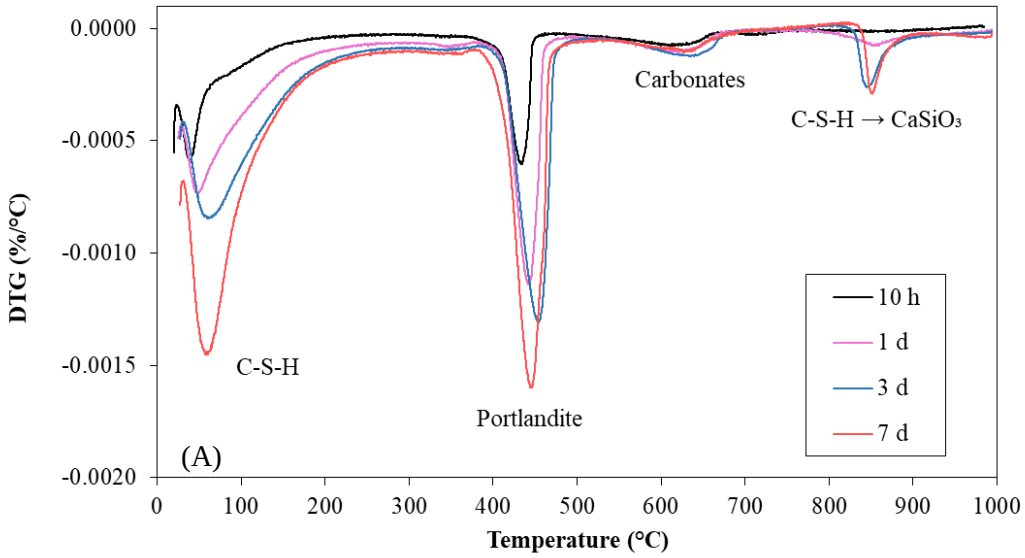
0.0000
-0.0005
-0.0010
-0.0015
-0.0020
DTG (%/°C)
Carbonates
C-S-H → CaSiO₃
C-S-H
Portlandite
(A)
10 h
1 d
3 d
7 d
0
100
200
300
400
500
600
700
800
900
1000
Temperature (°C)

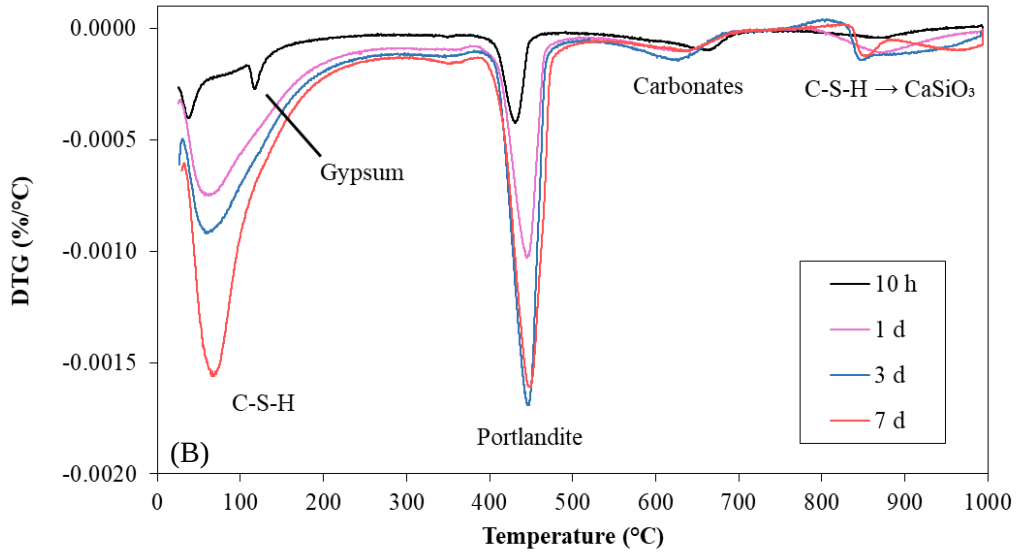
0.0000
-0.0005
-0.0010
-0.0015
-0.0020
DTG (%/°C)
Carbonates
C-S-H → CaSiO₃
Gypsum
C-S-H
Portlandite
(B)
10 h
1 d
3 d
7 d
0
100
200
300
400
500
600
700
800
900
1000
Temperature (°C)

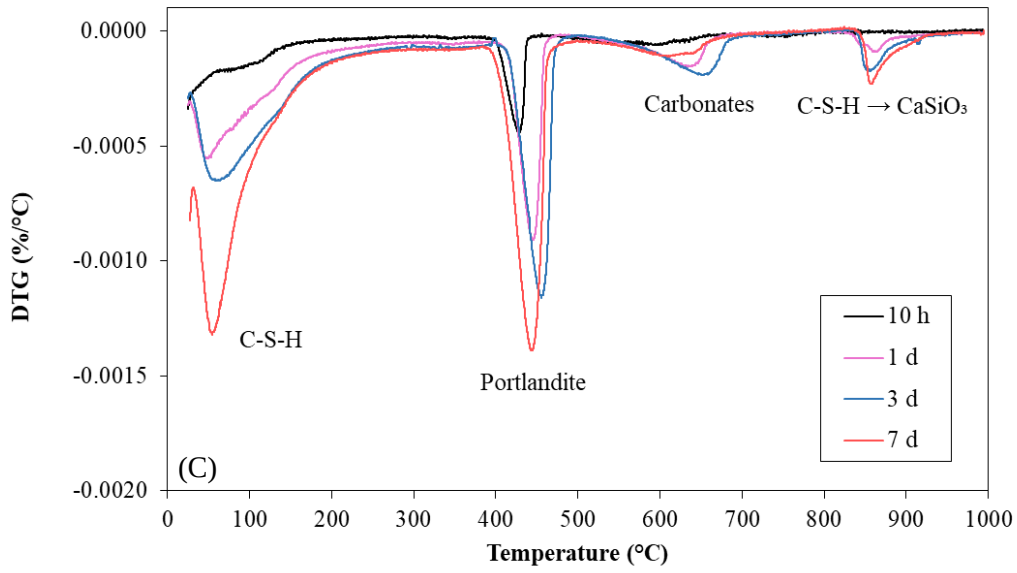
0.0000
-0.0005
-0.0010
-0.0015
-0.0020
DTG (%/°C)
Carbonates
C-S-H → CaSiO₃
C-S-H
Portlandite
(C)
10 h
1 d
3 d
7 d
0
100
200
300
400
500
600
700
800
900
1000
Temperature (°C)

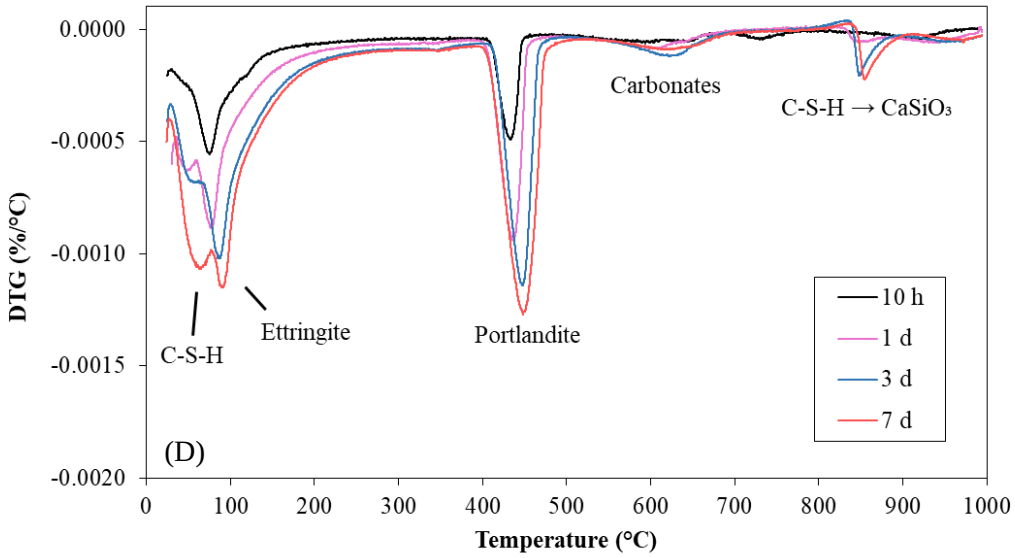

Figure 4.24 – DTG of: (A) C_3S; (B) C_3S_2.5%G; (C) Al-C_3S; (D) Al-C_3S_2.5%G pastes.

From the TGA results, the bound water content was calculated and is presented in Figure 4.9. The bound water content indicates the DoH and has an excellent linear correlation ($R^2 = 0.99$) with the IC's cumulative heat, as presented in Figure 4.10. As observed for the cumulative heat, in the gypsum-free pastes, the C_3S paste has a higher DoH when compared to the Al-C_3S one, resulting in higher bound water content for all ages evaluated. Furthermore, for both C_3S and Al-C_3S, gypsum's addition increased the bound water content, indicating higher C_3S hydration, as also observed by IC and XRD.

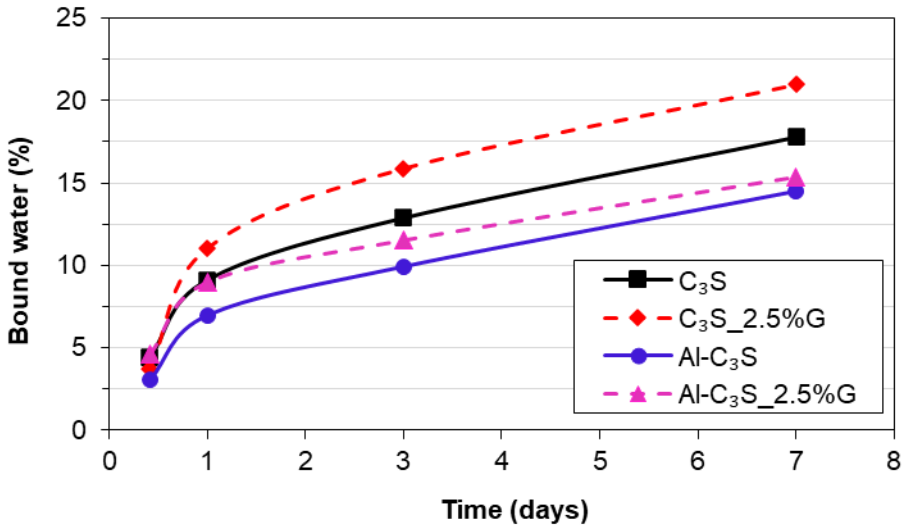

Figure 4.25 – Bound water content (wt.%) of the various pastes evaluated, obtained by TGA.

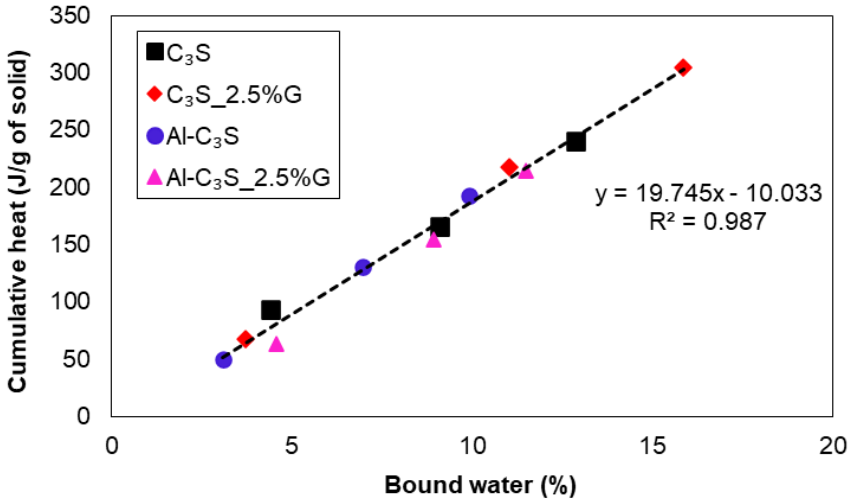

Figure 4.26 – Correlation between the cumulative heat obtained in the IC and the bond water (wt.%) determined by TGA at 10 h, 1 and 3 days.

The portlandite content was also determined from the TGA results, and the results are shown in Figure 4.11. As shown in Figure 4.12, the portlandite content determined by TGA has an excellent correlation (R^2 = 0.97) with the content obtained by XRD-Rietveld, as expected.

The C_3S pastes have a higher portlandite content for all ages tested compared to the Al-C_3S pastes. This results from the higher hydration degree, as observed by IC, XRD, and the bound water content.

The addition of gypsum in the C_3S paste decreased the portlandite content at 10 h but increased after 1 d. These data agree with the IC and XRD results, which indicate that the gypsum retards the initial C_3S hydration (until ~ 12 h) but enhances after that. On the other hand, the gypsum slightly decreased the portlandite content of the Al-C_3S paste. As mentioned before, in item 4.3.2, this results from the consumption of calcium ions during the ettringite formation.

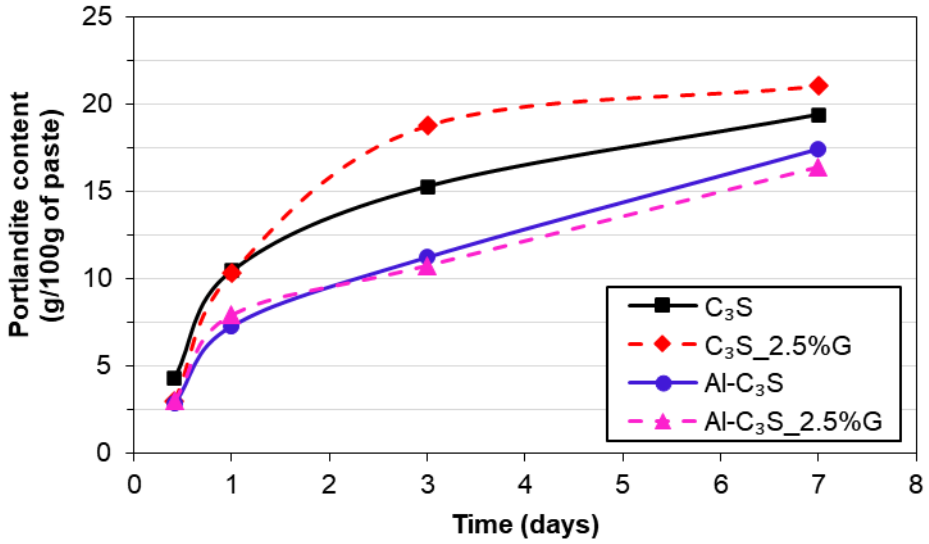

Figure 4.27 – Portlandite content (wt.%) of the various pastes evaluated, obtained by TGA.

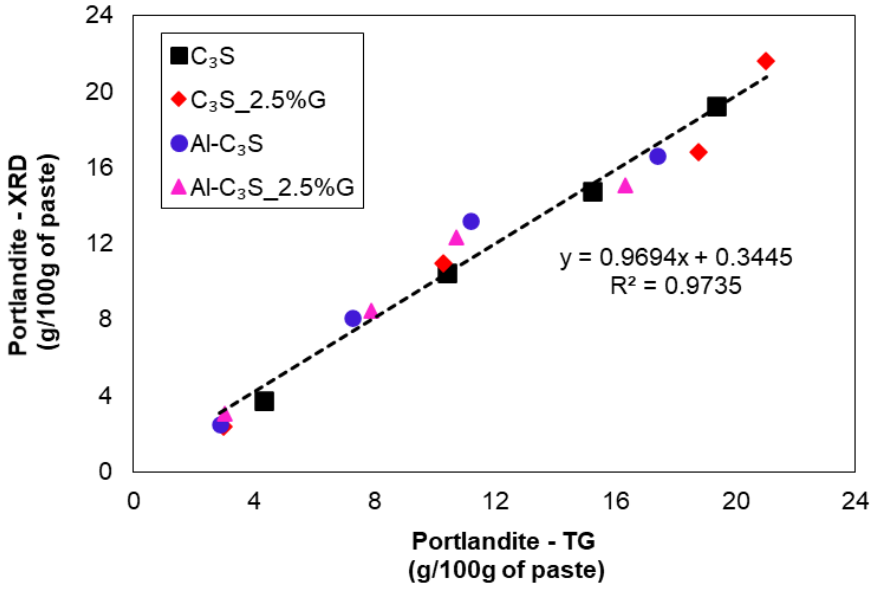

Figure 4.28 – Correlation between the portlandite content (wt.%) determined by XRD and TGA, at 10 h, 1, 3, and 7 days.

4.3.5 ^{29}Si and ^{27}Al Nuclear Magnetic Resonance (^{29}Si and ^{27}Al MAS-NMR)

Figure 4.13 presents the ^{29}Si MAS-NMR spectra of the C_3S and Al-C_3S pastes at 7 days of hydration with peak deconvolution. In the region of Q^0, five resonances at -68.4, -69.5, -71.6, -73.0, and -74.5 ppm are observed for all samples evaluated. This region corresponds to the anhydrous C_3S and Al-C_3S remaining in the first 7 d of hydration [45,46].

For all samples, two resonances at -76.9 and -79.1 ppm-in the Q^1 region-, and three resonances at -82.0, -84.1, and -85.5 ppm-in the Q^2 region- are observed. These resonances are related to the C-S-H type phases. The resonances at the Q^1 region correspond to the silica present at the end of the "dreierketten" chain of C-S-H. The resonances at the Q^2 region correspond to the silica within the "dreierketten" chain as bridging (Q^2_b)–at -82.0 ppm- and as pairing (Q^2_p)- at -84.1 and -85.5 ppm [46,47].

For the Al-C_3S and Al-C_3S_2.5G pastes, a resonance at -81.3 ppm that corresponds to the Q^2(1Al) is also observed. This is evidence of the incorporation of aluminum into C-S-H and corresponds to a pairing silica tetrahedron neighboring aluminum in the bridging position [46,47].

Table 4.6 presents the average chain length of aluminosilicate tetrahedra (MCL), the DoH_{NMR} of C_3S, and the molar ratio of tetrahedral Al incorporated in the C-(A)-S-H, obtained from the deconvolution of peaks of the ^{29}Si MAS-NMR spectra, according to the procedure described in Section 4.2.2.2.

All sample's MCL values were within the usual range of C-(A)-S-H [48]. The Al-C_3S paste presented a higher MCL than the C_3S paste, which was not expected, as the Al incorporated in C-S-H usually increases the MCL [49]. This discrepancy might be the result of the difference in C_3S polymorphism. The gypsum effect in MCL was not straightforward, as it decreased the MCL in the C_3S pastes but increased it in the Al-C_3S paste. More investigation on the impact of sulfates in the C-S-H MCL is needed.

As shown in Table 4.6, the addition of gypsum increased the DoH_{NMR} of C_3S by 12.6%, while did not significantly change the DoH_{NMR} of Al-C_3S (a slight increase of 0.4%). These results are very similar to the results of DoH_{XRD} ($R^2 = 0.96$) that showed that, at 7 d, gypsum increases the DoH_{XRD} of C_3S by 20.0%, while only increased the DoH_{XRD} of Al-C_3S by 6.2%.

The presence of gypsum decreased by 17.3% the Al(IV)/Si molar ratio, see Table 4.6. This was expected as in the Al-C_3S_2.5G paste, a part of the aluminum released with the Al-C_3S dissolution is consumed through the ettringite formation, as observed by XRD and TGA.

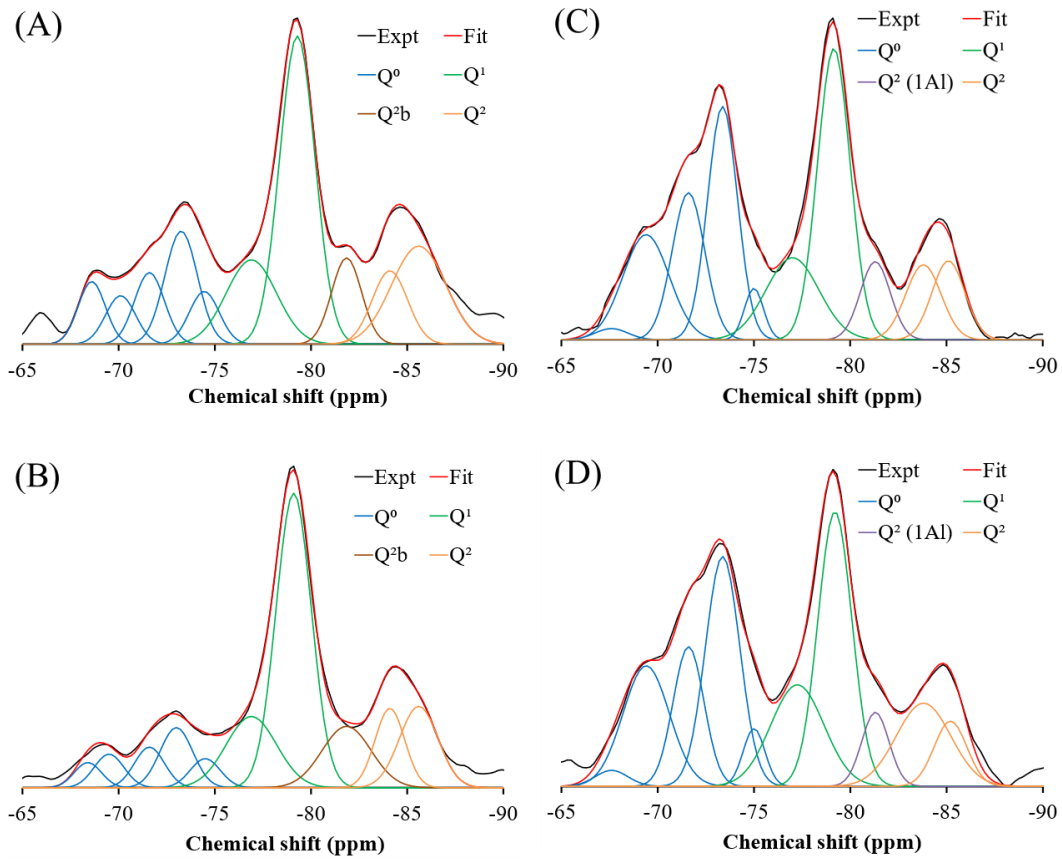

Figure 4.29 – ^{29}Si MAS-NMR spectra of the (A) C_3S, (B) C_3S_2.5G, (C) Al-C_3S, and (D) Al-C_3S_2.5G pastes at 7 days.

Figure 4.14 shows the ^{27}Al MAS-NMR spectra of the Al-C_3S and the Al-C_3S_2.5G pastes at 7 days. At the spectral region of the octahedrally coordinated aluminum Al(VI), 20 to -10 ppm, three narrow resonances centered at δ_{obs} = 5, 10, and 13 ppm are observed for the Al-C_3S_2.5G paste, which corresponds to the third aluminum hydrate (TAH)-a nanostructured amorphous aluminum hydroxide or a calcium aluminate hydrate produced in a less ordered form as a surface precipitate on the C-S-H phase [50]-, OH-AFm, and ettringite, respectively [45,46,51]. For the Al-C_3S paste, the resonance corresponding to ettringite is not observed, as this sample does not have gypsum. For both samples, a broad and low-intensity resonance are observed at the spectral region of tetrahedrally coordinated aluminum Al(IV), 80 to 50 ppm, which correspond to the aluminum incorporated in the C_3S and/or in C-S-H [45–47,51], not being possible to differentiate them with the resolution obtained in the present study.

The peaks due to OH-AFm and TAH (in both samples) are slightly broader than ettringite. This means that the degree of crystallinity of these phases is low, and consequently, they are not observed in XRD.

Table 4.6 presents the molar fractions of TAH, AFm, and ettringite phases, obtained by integrating their respectively corresponding peaks. The formation of ettringite by the addition of gypsum resulted in a decrease of 58.2% in the AFm molar fraction, as expected, and resulted in a decrease of 41.1% in the TAH molar fraction. This indicates that when gypsum is present and the ettringite is formed, less aluminum is incorporated in the C-(A)-S-H -as TAH can be considered a part of C-S-H [49]- corroborating the ^{29}Si MAS-NMR results. This result agrees with previous studies [50,52], which observed that an increase in gypsum content decreases TAH. This is due to the percentage of the Al^{3+} ions released with Al-C_3S dissolution forms ettringite when gypsum is present, decreasing the Al^{3+} ions available for the formation of AFm and TAH.

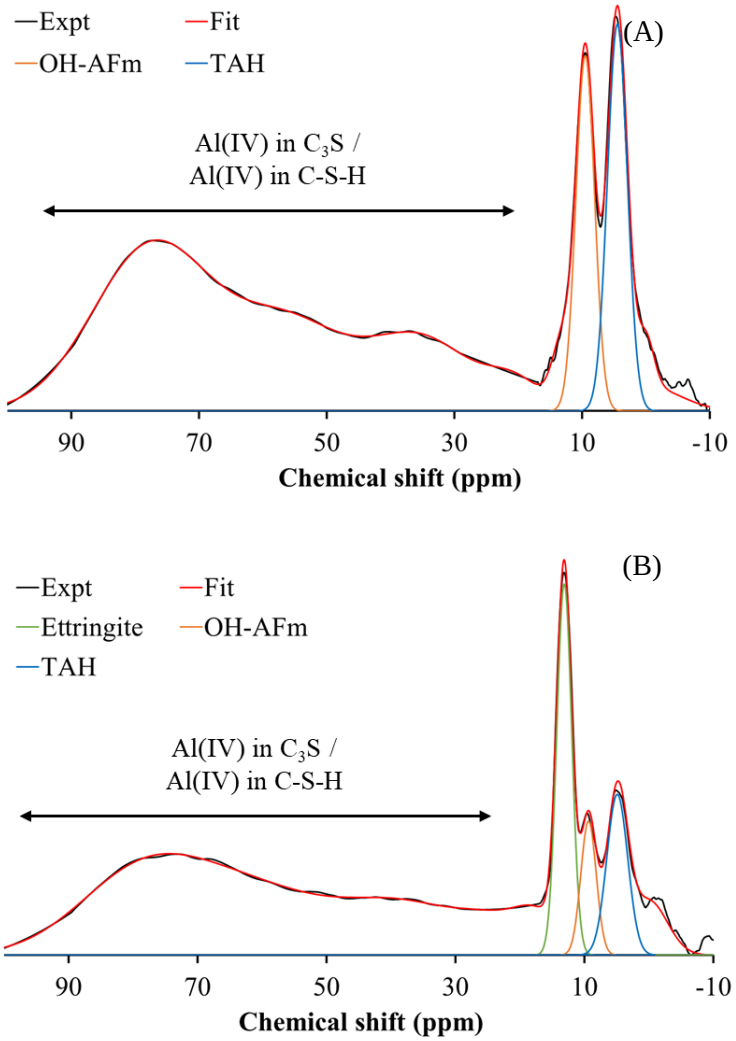

Figure 4.30 – ^{27}Al MAS-NMR spectra of the (A) Al-C_3S and (B) Al-C_3S_2.5G pastes at 7 days.

Table 4.10 – Results from spectral analysis of the ^{29}Si and ^{27}Al MAS-NMR spectra for the pastes hydrated for seven days.

Sample	^{29}Si MAS-NMR			^{27}Al MAS-NMR		
	MCL	DoH (C_3S)	Al(IV)/Si	AF_t	AF_m	TAH
C_3S	3.56	70.8%	-	-	-	-
C_3S_2.5G	3.43	79.7%	-	-	-	-
Al-C_3S	3.26	54.3%	0.052	-	12.2%	14.1%
Al-C_3S_2.5G	3.31	54.5%	0.043	13.7%	5.1%	8.3%

4.4 DISCUSSION

As observed by IC, XRD, TGA and ^{29}Si MAS-NMR, the C_3S reacts faster than the Al-C_3S, which was also seen by Quennoz and Scrivener [6], Stephan *et al.* [40], and Begarin *et al.* [41]. Several studies also showed that the C_3S has a lower hydration rate in aluminum-containing solutions [3,18,19,53]. However, the reason for that is not straight forward and some hypotheses found in the literature need to be discussed. According to Garrault *et al.* [18], Begarin *et al.* [41], and Wagner *et al*. [42], the C-(A)-S-H, formed in the Al-C_3S pastes as identified by ^{27}Al MAS-NMR (Figure 4.14), does not grow and is not as good seeding for C-S-H growth as C-S-H nuclei themselves. Therefore, the uptake of Al by C-S-H would reduce its reactive surface, leading to a lower hydration rate [42]. However, several other studies [54–56], including some in blended cements with higher Al uptake by C-S-H, show that C-(A)-S-H has a very similar morphology to C-S-H. Further research is necessary to verify if the uptake of aluminum by C-S-H indeed decreases its reactive surface or not. Another hypothesis is that the lower hydration rate of C_3S in Al-containing solution is due to the condensation of aluminum-silicate species at the C_3S surface [3,19].

Despite the initial retard on C_3S and Al-C_3S dissolution, the presence of gypsum enhanced the C_3S hydration after ~ 12 h and the Al-C_3S hydration after ~ 7 h, as observed by increases in cumulative heat (IC), in the amorphous content (XRD) and water-bound content (TG/DTG), as well as a decrease in the anhydrous content (XRD) in all the ages evaluated. Similar behaviors were observed by several authors [5–12]. However, the reason for that is not apparent yet.

IC mesurements of mixtures with 5.0 wt.% of gypsum shown similar hydration rate as those with 2.5 wt.% of gypsum. This indicates that the C_3S hydration is enhanced up to a certain gypsum content, without significant difference in higher contents, besides a slight decrease in the heat flow due to the lower amount of C_3S in the mixture, known as the dilution effect. Several authors made similar observations [5,9] with aluminum-free C_3S and are following the simulations performed by Gunay *et al.* [10], which shows that the gypsum increases the C-S-H growth rate up to plateau value at 1.0 wt.% of gypsum. As observed by IC, the Al-C_3S shows the same behavior, where the Al-C_3S_5.0G had a similar hydration rate as the Al-C_3S_2.5G, indicating that the aluminum doping of C_3S does not influence the existence of a plateau value of gypsum concerning the Al-C_3S' hydration rate.

Comparing the effect of gypsum on C_3S and Al-C_3S hydration, it is possible to note some differences. The addition of 2.5 wt.% of gypsum prolonged the induction period of C_3S hydration by 125 min (*i.e.*, an increase of 311% on the induction period length). On the other hand, the retard effect of this 2.5 wt.% of gypsum on Al-C_3S was lower, prolonging the induction period by 56 min (an increase of 69% on the induction period length). However, the enhancement effect seems to be similar, and the addition of 2.5 wt.% of gypsum resulted in increases of 1.46 mW/g of C_3S and 1.47 mW/g of Al-C_3S on the main heat flow peaks of C_3S and Al-C_3S hydration, respectively.

The thermodynamic modeling demonstrated that the presence of gypsum in the Al-C_3S pastes reduces the Al concentration of the pore solution from 0.005 to 0 mM, indicating that all the aluminum released by Al-C_3S dissolution is expected to be immediately consumed by ettringite formation. Thus, as Al^{3+} ions in the pore solution retard the C_3S hydration, resulting in longer induction periods, as previously discussed, their removal and, consequently, the absence of this species on the solution, should accelerate the C_3S hydration. This is probably the reason for the much lower retarding effect on Al-C_3S hydration due to gypsum when compared to C_3S hydration: gypsum retards both C_3S and Al-C_3S hydration, but due to the removal of Al^{3+} ions -accelerating the Al-C_3S hydration- the retard effect is lower on Al-C_3S hydration. However, contrary to Quennoz and Scrivener's [6] conclusions, the removal of Al^{3+} ions from the pore solution does not seem to influence the enhancement of C_3S hydration due to gypsum, as the enhancement effect was very similar (increases of 1.46 mW/g of C_3S and 1.47 mW/g of Al-C_3S). Furthermore, this cannot be the only or the main mechanism responsible for the enhancement of Al-C_3S hydration due to gypsum, as gypsum also enhanced the C_3S hydration.

Zunino and Scrivener [9] suggested a possible explanation for Quennoz and Scrivener [6] not observing an enhancement effect on pure C_3S: the small particle size of the used C_3S (resulting in a main heat flow peak of 11 mW/g C_3S). Thus, the enhancement effect of gypsum was probably less significant.

The enhancement of C_3S hydration due to gypsum was also previously related to the seeding effect of very fine nano-ettringite [8]. However, in C_3S pastes, which do not contain aluminum, no ettringite is formed, as observed by XRD and TGA. Therefore, none of these hypotheses can fully explain the effect of calcium sulfate on the C_3S hydration. As suggested by Zunino and Scrivener [9], the enhancement in C_3S hydration rate is probably mainly related to interactions between the calcium sulfate and the silicates (C_3S and/or C-S-H) rather than interactions that involve the aluminates.

Gunay et al. [10] reported some simulations regarding the C_3S hydration in the presence of gypsum. The authors observed an increase in C-S-H permeability with the addition of calcium sulfate. One could hypothesize that the increase of the C-S-H permeability would increase the water and ion diffusion, enhancing the C_3S hydration. However, as shown by Gallucci *et al.* [57], this "C-S-H layer" formed at the C_3S surface is very permeable. Therefore, this is NOT the reason for the enhancement in the C_3S hydration rate by gypsum.

Based on the simulations performed by Gunay *et al.* [10], the presence of gypsum increases the perpendicular and parallel C-S-H growth rate. The reason for this is still not understood. Three different hypotheses can be proposed to explain the enhancement in C_3S and Al-C_3S hydration rate by gypsum: (*i*) The sulfate ions change the C-S-H needle morphology, reducing the lateral impingement and accelerating the growth of the C-S-H needles. (*ii*) The change in the C-S-H needle morphology would provide more sites for the precipitation of hydration products. (*iii*) Sulfate ions increase the ionic strength, increasing the nucleation and growth rate of C-S-H. The first two hypotheses relate the enhancement in C_3S hydration rate by gypsum with the change of C-S-H needles' morphology. Mota *et al.* [7] showed that a negatively charged cloud of sulfate ions is physically adsorbed in the positivity charged C-S-H needles. This yields to the C-S-H needles' repulsion, leading to a more divergent needle structure instead of the convergent morphology observed in plain C_3S pastes [7].

According to the first hypothesis, this divergent needle structure would reduce the lateral impingement between the C-S-H needles, accelerating their growth and final length, as

exemplified in Figure 4.15. As suggested by Zhang et al. [58], the C-S-H needles may be described as ellipsoidal particles randomly distributed on the C_3S surface. Adjacent C-S-H needles may impinge on each other, which probably will reduce its growth rate [58,59]. Please note that we are referring to lateral impingement between adjacent C-S-H needles (from the same C_3S grain) and not to impingement between C-S-H needles from different C_3S grains, which is unlikely to occur in the first hours of hydration as discussed by Ouzia and Scrivener [60]. The convergent structure of the C-S-H needles in sulfate-free solutions probably induces more and faster lateral impingement between the adjacent C-S-H needles than the more divergent structure of C-S-H needles in solution with sulfate, which may explain the enhancement of C_3S hydration due to gypsum on the acceleration period – the moment which the nucleation and growth of C-S-H needles occur.

Furthermore, according to Ouzia and Scrivener [60] the C-S-H needles grow until a certain critical length, when the growth rate decreases abruptly, which results in the decrease of the hydration rate. The reasons for that are still unknown but increases in C-S-H needle length result in a higher hydration rate [60]. One possible reason could be the lateral impingement between C-S-H needles. If this is true, the more divergent morphology of C-S-H needles with the gypsum addition might decrease the lateral impingement, which may increase the length of C-S-H needles, as illustrated in Figure 4.15.

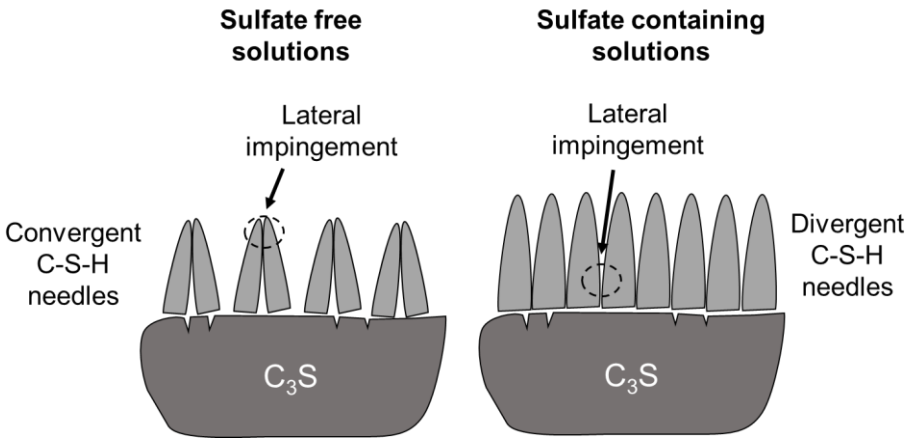

Figure 4.31 – Schematic representation of the impact of sulfate ions on C-S-H morphology (adapted from Mota et al. [7]

According to hypothesis (*ii*), the more divergent structure of the C-S-H needles would increase its surface area, resulting in more sites for the precipitation of hydration products. This hypothesis agrees with Huang and Yang's [61] results, who observed an increase in the specific surface area of the C-S-H by adding K_2SO_4 when compared to plain C_3S pastes. This might

result from the divergent morphology of C-S-H needles when adding K_2SO_4 (a similar morphology as those observed by Mota *et al.* [7] when adding gypsum). However, the surface area of the hydrating C_3S is also highly influenced by the number of C-S-H needles. In addition, the experimental errors associated with this determination should be account for as it is extremely difficult to stop the C_3S hydration quickly and precisely enough to obtained different samples at equal DoH. Therefore, further studies on this topic are necessary to verify if the more divergent structure of C-S-H needles due to sulfates addition leads to a higher surface area or not.

Finally, the enhancement in C_3S hydration rate by gypsum could be due to the increase in the ionic strength (*iii*). As observed by thermodynamic modeling (Section 4.3.2), the addition of 2.5 wt.% of gypsum increases 51% in the ionic strength (0.055 to 0.083 molal). Increases in the ionic strength favor increases in the number of C-S-H nuclei per unit surface area of C_3S/alite, increasing the nucleation rate and growth of C-S-H [62,63]. This might be the reason or one of the reasons for the enhancement of C_3S hydration. On the other hand, the further addition of gypsum (*i.e.*, the mixes with 5.0 wt.% of gypsum) did not increase the ionic strength, which might explain the plateau in the enhancement effect of gypsum on C_3S hydration.

4.5 CONCLUSIONS

- Aluminum doped C_3S has a slower hydration rate when compared to aluminum-free C_3S, which probably results from the releasing of aluminum ions into the solution with the Al-C_3S dissolution. Note that the larger particle size of Al-C_3S may also contribute to this result.

- The presence of gypsum delayed the initial hydration of C_3S and Al-C_3S, prolonging the induction period. The initial delay seems to be related to the interaction between the sulfate ions and C_3S.

- The presence of gypsum enhanced the C_3S and the Al-C_3S hydration during the nucleation and growth period (after the induction period), increasing the main hydration peak, the cumulative heat, the dissolution of C_3S and Al-C_3S, and the amount of bound water. The enhancement on the hydration due to gypsum addition was higher for the C_3S samples -increases of 20.0% and 12.6% in DoH_{XRD} and DoH_{NMR} at 7 d - compared to the Al-C_3S samples -increases of 6.2% and 0.4% in DoH_{XRD} and DoH_{NMR} at 7 d.

- As observed by thermodynamic modeling, the addition of 2.5 wt.% of gypsum increased 51% in ionic strength of the pore solution of C_3S and Al-C_3S pastes. However, further addition of gypsum (5.0 wt.%) did not result in further increases.
- For the aluminum-free C_3S pastes, the addition of gypsum increased the portlandite content due to the increase in the hydration rate. However, for the Al-C_3S, a decrease in portlandite content was observed, probably due to the consumption of calcium ions for ettringite formation despite the higher degree of hydration.
- The addition of gypsum in Al-C_3S resulted in a decrease of AFm and TAH phases and a decrease in Al incorporated in C-S-H due to the ettringite formation, which decreases Al^{3+} available in the solution.
- As observed by thermodynamic modeling, the presence of gypsum in the Al-C_3S pastes reduces the Al^{3+} concentration of the pore solution. All the aluminum released by Al-C_3S dissolution is expected to be immediately consumed by ettringite formation in the presence of 2.5 wt.% of gypsum. Thus, as Al^{3+} ions in the pore solution retards C_3S, their removal from the pore solution may contribute to the lower retarding effect of gypsum during the induction period on the Al-C_3S hydration when compared to C_3S hydration.
- As gypsum also enhanced the aluminum-free C_3S hydration, where no ettringite is formed, the formation of ettringite and the removal of Al^{3+} ions of the pore solution by the formation of ettringite is NOT the mechanism behind the enhancement of C_3S hydration by gypsum.
- The results indicate that the enhancement in C_3S and Al-C_3S hydration rate after the induction period due to gypsum is probably related to (*i, ii*) the more divergent needle-structure C-S-H morphology when sulfate is present (according to bibliography), which (*i*) may reduce the lateral impingement between adjacent C-S-H needles (from the same C_3S grain) increasing their growth rate and (*ii*) may increase the site for the precipitation of hydration products. (*iii*) The increase in ionic strength when adding gypsum.

4.6 ACKNOWLEDGEMENTS

JSAN thanks the financial support of CAPES (Coordination for the Improvement of Higher Education Personnel) [88882.439908/2019-01]. JSAN also thanks the Spanish Junta de Andalucía [UMA18-FEDERJA-095 and P18-RT-720] research projects for the research stage at the University of Málaga (Spain) and the Graduate Program in Civil Engineering: Construction and Infrastructure (PPGCI) of the Federal University of Rio Grande do Sul (UFRGS). APK was sponsored by CNPq (Brazilian National Council for Scientific and Technological Development) through the research fellowship PQ CNPq. The authors thank Alejandro Morales Cantero for the help in the calorimetry and TG tests and Márlon Augusto Longhi for helping in the MAS-NMR analysis. The authors also thank the creators and developers of cemGEMS web application, who made it available for free, as well as several tutorials on how to use it.

4.7 REFERENCES

[1] K.L. Scrivener, A. Nonat, Hydration of cementitious materials, present and future, Cement and Concrete Research. 41 (2011) 651–665. https://doi.org/10.1016/j.cemconres.2011.03.026.

[2] J. da S. Andrade Neto, A.G. de la Torre, A.P. Kirchheim, Effects of sulfates on the hydration of Portland cement – A review, Construction and Building Materials. 279 (2021). https://doi.org/10.1016/j.conbuildmat.2021.122428.

[3] L. Nicoleau, E. Schreiner, A. Nonat, Ion-specific effects influencing the dissolution of tricalcium silicate, Cement and Concrete Research. 59 (2014) 118–138. https://doi.org/10.1016/j.cemconres.2014.02.006.

[4] P. Juilland, L. Nicoleau, R.S. Arvidson, E. Gallucci, Advances in dissolution understanding and their implications for cement hydration, RILEM Technical Letters. 2 (2017) 90. https://doi.org/10.21809/rilemtechlett.2017.47.

[5] A. Bentur, Effect of Gypsum on the Hydration and Strength of C3S Pastes, Journal of the American Ceramic Society. 59 (1976) 210–213. https://doi.org/10.1111/j.1151-2916.1976.tb10935.x.

[6] A. Quennoz, K.L. Scrivener, Interactions between alite and C3A-gypsum hydrations in model cements, Cement and Concrete Research. 44 (2013) 46–54. https://doi.org/10.1016/j.cemconres.2012.10.018.

[7] B. Mota, T. Matschei, K. Scrivener, The influence of sodium salts and gypsum on alite hydration, Cement and Concrete Research. 75 (2015) 53–65. https://doi.org/10.1016/j.cemconres.2015.04.015.

[8] S.T. Bergold, F. Goetz-Neunhoeffer, J. Neubauer, Interaction of silicate and aluminate reaction in a synthetic cement system: Implications for the process of alite hydration, Cement and Concrete Research. 93 (2017) 32–44. https://doi.org/10.1016/j.cemconres.2016.12.006.

[9] F. Zunino, K. Scrivener, Factors influencing the sulfate balance in pure phase C3S/C3A systems, Cement and Concrete Research. 133 (2020) 106085. https://doi.org/10.1016/j.cemconres.2020.106085.

[10] S. Gunay, S. Garrault, a Nonat, P. Termkhajornkit, Influence of calcium sulphate on hydration and mechanical strength of tricalcium silicate, 13th International Congress on the Chemistry of Cement. (2011) 1–7.

[11] P.W. Brown, C.L. Harner, E.J. Prosen, The effect of inorganic salts on tricalcium silicate hydration, Cement and Concrete Research. 16 (1986) 17–22. https://doi.org/10.1016/0008-8846(86)90063-3.

[12] Y. Zhang, X. Zhang, Research on effect of limestone and gypsum on C3A, C3S and PC clinker system, Construction and Building Materials. 22 (2008) 1634–1642. https://doi.org/10.1016/j.conbuildmat.2007.06.013.

[13] F. Zunino, K. Scrivener, The influence of the filler effect on the sulfate requirement of blended cements, Cement and Concrete Research. 126 (2019) 105918. https://doi.org/10.1016/j.cemconres.2019.105918.

[14] H.F.W. Taylor, Cement chemistry, 2nd ed., Thomas Telford, 1997. https://doi.org/10.1680/cc.25929.

[15] K. Schraut, B. Adamczyk, C. Adam, D. Stephan, B. Meng, S. Simon, J. von Werder, Synthesis and characterisation of alites from reduced basic oxygen furnace slags, Cement and Concrete Research. 147 (2021) 106518. https://doi.org/10.1016/j.cemconres.2021.106518.

[16] K.L. Scrivener, P. Juilland, P.J.M. Monteiro, Advances in understanding hydration of Portland cement, Cement and Concrete Research. 78 (2015) 38–56. https://doi.org/10.1016/j.cemconres.2015.05.025.

[17] J. Peng, J. Zhang, J. Qu, Mechanism of the formation and transformation of ettringite, Journal Wuhan University of Technology, Materials Science Edition. 21 (2006) 158–161. https://doi.org/10.1007/BF02840908.

[18] S. Garrault, A. Nonat, Y. Sallier, L. Nicolaeau, On the Origin of the Dormant Period of Cement Hydration, in: 13th International Congress on the Chemistry of Cement., Madrid, 2011: pp. 1–7.

[19] E. Pustovgar, R.K. Mishra, M. Palacios, J.B. d'Espinose de Lacaillerie, T. Matschei, A.S. Andreev, H. Heinz, R. Verel, R.J. Flatt, Influence of aluminates on the hydration kinetics of tricalcium silicate, Cement and Concrete Research. 100 (2017) 245–262. https://doi.org/10.1016/j.cemconres.2017.06.006.

[20] D. Ménétrier, I. Jawed, J. Skalny, Effect of gypsum on C3S hydration, Cement and Concrete Research. 10 (1980) 697–701.

[21] E.M.J. Bérodier, A.C.A. Muller, K.L. Scrivener, Effect of sulfate on C-S-H at early age, Cement and Concrete Research. 138 (2020) 106248. https://doi.org/10.1016/j.cemconres.2020.106248.

[22] M.N. de Noirfontaine, M. Courtial, F. Dunstetter, G. Gasecki, M. Signes-Frehel, Tricalcium silicate Ca3SiO5 superstructure analysis: A route towards the structure of the M1 polymorph, Zeitschrift Fur Kristallographie. 227 (2012) 102–112. https://doi.org/10.1524/zkri.2012.1425.

[23] M. Palacios, H. Kazemi-Kamyab, S. Mantellato, P. Bowen, Laser diffraction and gas adsorption techniques, in: K. Scrivener, R. Snellings, B. Lothenbach (Eds.), A Practical Guide to Microstructural Analysis of Cementitious Materials, 1st ed., CRC Press, 2016: pp. 445–480.

[24] M. García-Maté, A.G. de La Torre, L. León-Reina, E.R. Losilla, M.A.G. Aranda, I. Santacruz, Effect of calcium sulfate source on the hydration of calcium sulfoaluminate eco-cement, Cement and Concrete Composites. 55 (2015) 53–61. https://doi.org/10.1016/j.cemconcomp.2014.08.003.

[25] L. Wadsö, Operational issues in isothermal calorimetry, Cement and Concrete Research. 40 (2010) 1129–1137. https://doi.org/10.1016/j.cemconres.2010.03.017.

[26] J.D. Zea-Garcia, A.G. de la Torre, M.A.G. Aranda, I. Santacruz, Processing and characterisation of standard and doped alite-belite-ye'elimite ecocement pastes and mortars, Cement and Concrete Research. 127 (2020). https://doi.org/10.1016/j.cemconres.2019.105911.

[27] B. Lothenbach, P.T. Durdziński, K. de Weerdt, Thermogravimetric analysis, in: K. Scrivener, R. Snellings, B. Lothenbach (Eds.), A Practical Guide to Microstructural Analysis of Cementitious Materials, 1st ed., CRC Press, 2016: pp. 177–212.

[28] A.G. de La Torre, S. Bruque, M.A.G. Aranda, Applied Crystallography Rietveld quantitative amorphous content analysis, J. Appl. Cryst. 34 (2001) 196–202.

[29] N.I. Golovastikov, R.G. Matveeva, N. v. Belov, Crystal structure of the tricalcium silicate 3CaO SiO2 = C3S, Soviet Physics - Crystallography. 20 (1975) 441–445.

[30] D.K. Smith, H.R. Leider, Low-temperature thermal expansion of LiH, MgO and CaO, Journal of Applied Crystallography. 1 (1968) 246–249. https://doi.org/10.1107/s0021889868005418.

[31] Á.G. de la Torre, M.-G. López-Olmo, C. Álvarez-Rua, S. García-Granda, Miguel.A.G. Aranda, Structure and microstructure of gypsum and its relevance to Rietveld quantitative phase analyses, Powder Diffraction. 19 (2004) 240–246. https://doi.org/10.1154/1.1725254.

[32] J.D. Jorgensen, Compression mechanisms in α-quartz structures - SiO2 and GeO2, Journal of Applied Physics. 49 (1978) 5473–5478. https://doi.org/10.1063/1.324517.

[33] F. Goetz-Neunhoeffer, J. Neubauer, Refined ettringite (Ca 6 Al 2 (SO 4) 3 (OH) 12 ·26H 2 O) structure for quantitative X-ray diffraction analysis , Powder Diffraction. 21 (2006) 4–11. https://doi.org/10.1154/1.2146207.

[34] H.E. Petch, The hydrogen positions in portlandite, Ca(OH)2, as indicated by the electron distribution, Acta Crystallographica. 14 (1961) 950–957. https://doi.org/10.1107/s0365110x61002771.

[35] R. Wartchow, Datensammlung nach der “learnt profile”-methode(LP) für calcit und vergleich mit der “background peak background”-methode (BPB), Zeitschrift Für Kristallographie. 186 (1989) 300–302.

[36] S. Joseph, J. Skibsted, Ö. Cizer, Hydration of polyphase Ca3SiO5-Ca3Al2O6 in the presence of gypsum and Na2SO4, Journal of the American Ceramic Society. 103 (2020) 1–30. https://doi.org/10.1111/jace.17321.

[37] D.A. Kulik, F. Winnefeld, A. Kulik, G.D. Miron, B. Lothenbach, CemGEMS – an easy-to-use web application for thermodynamic modeling of cementitious materials, RILEM Technical Letters. 6 (2021) 36–52. https://doi.org/10.21809/rilemtechlett.2021.140.

[38] B. Lothenbach, D.A. Kulik, T. Matschei, M. Balonis, L. Baquerizo, B. Dilnesa, G.D. Miron, R.J. Myers, Cemdata18: A chemical thermodynamic database for hydrated Portland cements and alkali-activated materials, Cement and Concrete Research. 115 (2019) 472–506. https://doi.org/10.1016/j.cemconres.2018.04.018.

[39] P.G. Gottschalk, J.R. Dunn, The five-parameter logistic: A characterization and comparison with the four-parameter logistic, Analytical Biochemistry. 343 (2005) 54–65. https://doi.org/10.1016/j.ab.2005.04.035.

[40] D. Stephan, S. Wistuba, Crystal structure refinement and hydration behaviour of 3CaO·SiO2 solid solutions with MgO, Al2 O3 and Fe2O3, Journal of the European Ceramic Society. 26 (2006) 141–148. https://doi.org/10.1016/j.jeurceramsoc.2004.10.031.

[41] F. Begarin, S. Garrault, A. Nonat, L. Nicoleau, Hydration of alite containing aluminium, Advances in Applied Ceramics. 110 (2011) 127–130. https://doi.org/10.1179/1743676110Y.0000000007.

[42] D. Wagner, F. Bellmann, J. Neubauer, Influence of aluminium on the hydration of triclinic C3S with addition of KOH solution, Cement and Concrete Research. 137 (2020) 106198. https://doi.org/10.1016/j.cemconres.2020.106198.

[43] R. Snellings, X-ray powder diffraction applied to cement, in: K. Scrivener, R. Snellings, B. Lothenbach (Eds.), A Practical Guide to Microstructural Analysis of Cementitious Materials, 1st ed., CRC Press, 2016: pp. 107–176.

[44] Y. He, X. Zhang, S. Liu, R.D. Hooton, T. Ji, Y. Kong, Impacts of sulphates on rheological property and hydration performance of cement paste in the function of polycarboxylate superplasticizer, Construction and Building Materials. 256 (2020) 119428. https://doi.org/10.1016/j.conbuildmat.2020.119428.

[45] B. Walkley, J.L. Provis, Solid-state nuclear magnetic resonance spectroscopy of cements, Materials Today Advances. 1 (2019) 100007. https://doi.org/10.1016/j.mtadv.2019.100007.

[46] M. Daugaard Andersen, H.J. Jakobsen, Jø. Skibsted, Incorporation of aluminum in the calcium silicate hydrate (C-S-H) of hydrated Portland cements: A high-field 27Al and 29Si MAS NMR investigation, Inorganic Chemistry. 42 (2003) 2280–2287. https://doi.org/10.1021/ic020607b.

[47] E. L’Hôpital, B. Lothenbach, D.A. Kulik, K. Scrivener, Influence of calcium to silica ratio on aluminium uptake in calcium silicate hydrate, Cement and Concrete Research. 85 (2016) 111–121. https://doi.org/10.1016/j.cemconres.2016.01.014.

[48] Y. Chiang, S.W. Chang, Bridging the gap between NMR measured mean silicate chain length and nano-scale silicate polymorphism of calcium silicate hydrates, Cement and Concrete Research. 140 (2021) 106268. https://doi.org/10.1016/j.cemconres.2020.106268.

[49] E. L’Hôpital, B. Lothenbach, G. le Saout, D. Kulik, K. Scrivener, Incorporation of aluminium in calcium-silicate-hydrates, Cement and Concrete Research. 75 (2015) 91–103. https://doi.org/10.1016/j.cemconres.2015.04.007.

[50] M.D. Andersen, H.J. Jakobsen, J. Skibsted, A new aluminium-hydrate species in hydrated Portland cements characterized by 27Al and 29Si MAS NMR spectroscopy, Cement and Concrete Research. 36 (2006) 3–17. https://doi.org/10.1016/j.cemconres.2005.04.010.

[51] A.S. Brykov, A.S. Vasil'ev, M. v. Mokeev, Hydration of portland cement in the presence of aluminum-containing setting accelerators, Russian Journal of Applied Chemistry. 86 (2013) 793–801. https://doi.org/10.1134/S1070427213060013.

[52] G. Deng, Y. He, L. Lu, S. Hu, Evolution of aluminate hydrate phases in fly ash-cement system under the sulfate conditions, Construction and Building Materials. 252 (2020) 119045. https://doi.org/10.1016/j.conbuildmat.2020.119045.

[53] T. Matschei, P. Kruspan, P. Sandberg, L. Wadso, Sulphate optimization of binders containing portland cement clinker using isothermal calorimetry, in: Proceedings of 15th International Congress on the Chemistry of Cement, Prague, 2019.

[54] F. Zunino, F. Martirena, K. Scrivener, Limestone calcined clay cements (LC3), ACI Materials Journal. 118 (2021) 49–60. https://doi.org/10.14359/51730422.

[55] F. Avet, K. Scrivener, Effect of temperature on the water content of C-A-S-H in plain Portland and blended cements, Cement and Concrete Research. 136 (2020) 106124. https://doi.org/10.1016/j.cemconres.2020.106124.

[56] F. Avet, E. Boehm-Courjault, K. Scrivener, Investigation of C-A-S-H composition, morphology and density in Limestone Calcined Clay Cement (LC3), Cement and Concrete Research. 115 (2019) 70–79. https://doi.org/10.1016/j.cemconres.2018.10.011.

[57] E. Gallucci, P. Mathur, K. Scrivener, Microstructural development of early age hydration shells around cement grains, Cement and Concrete Research. 40 (2010) 4–13. https://doi.org/10.1016/j.cemconres.2009.09.015.

[58] Z. Zhang, F. Han, P. Yan, Modelling the dissolution and precipitation process of the early hydration of C3S, Cement and Concrete Research. 136 (2020) 106174. https://doi.org/10.1016/j.cemconres.2020.106174.

[59] J.J. Thomas, A.J. Allen, H.M. Jennings, Hydration kinetics and microstructure development of normal and CaCl2-accelerated tricalcium silicate pastes, Journal of Physical Chemistry C. 113 (2009) 19836–19844. https://doi.org/10.1021/jp907078u.

[60] A. Ouzia, K. Scrivener, The needle model: A new model for the main hydration peak of alite, Cement and Concrete Research. 115 (2019) 339–360. https://doi.org/10.1016/j.cemconres.2018.08.005.

[61] L. Huang, Z. Yang, Early hydration of tricalcium silicate with potassium hydroxide and sulfate from pore solution and solid view, Construction and Building Materials. 230 (2020) 116988. https://doi.org/10.1016/j.conbuildmat.2019.116988.

[62] J. Fu, A.M. Jones, M.W. Bligh, C. Holt, L.M. Keyte, F. Moghaddam, S.J. Foster, T.D. Waite, Mechanisms of enhancement in early hydration by sodium sulfate in a slag-cement blend – Insights from pore solution chemistry, Cement and Concrete Research. 135 (2020) 106110. https://doi.org/10.1016/j.cemconres.2020.106110.

[63] A. Kumar, G. Sant, C. Patapy, C. Gianocca, K.L. Scrivener, The influence of sodium and potassium hydroxide on alite hydration: Experiments and simulations, Cement and Concrete Research. 42 (2012) 1513–1523. https://doi.org/10.1016/j.cemconres.2012.07.003.

Chapter 5

The role of sodium and sulfate sources on the rheology and hydration of C_3A polymorphs

Chapter 5 is based on the article:

José S. Andrade Neto, Paulo R. de Matos, Angeles G. De la Torre, Carlos E. M. Campos, Philippe J. P. Gleize, Paulo J. M. Monteiro, Ana Paula Kirchheim. The role of sodium and sulfate sources on the rheology and hydration of C_3A polymorphs. **Cement and Concrete Research**, v. 151, paper 106639, 2022.

5 THE ROLE OF SODIUM AND SULFATE SOURCES ON THE RHEOLOGY AND HYDRATION OF C_3A POLYMORPHS

ABSTRACT

The higher reactivity of orthorhombic C_3A (ort-C_3A) in sulfate-containing solutions, compared with cubic C_3A (cb-C_3A), was previously related to the differences in crystal structure or the sodium in the ort-C_3A pore solution. We analyzed the hydration of cb-C_3A (in water and NaOH solution) and Na-doped ort-C_3A in the presence of gypsum and hemihydrate. Calorimetry, *in-situ* XRD, TGA, and rheological tests were conducted. NaOH accelerated the hydration of cb-C_3A, but ort-C_3A still presented higher ettringite formation rate and earlier sulfate depletion. Ort-C_3A pastes showed 10-20 times higher viscosities and yield stresses. Replacing gypsum by hemihydrate increased the ettringite precipitation rate and anticipated the sulfate depletion of ort-C_3A but did not significantly influence cb-C_3A hydration. The crystallization of hemihydrate into gypsum resulted in early (<10 min) stiffing of all C_3A-hemihydrate pastes. Overall, the higher reactivity of ort-C_3A is related to differences in crystal structure rather than the sodium in the pore solution.

Keywords: cubic C_3A; orthorhombic C_3A; Calcium sulfate; Hydration; Rheology.

DOI: https://doi.org/10.1016/j.cemconres.2021.106639

5.1 INTRODUCTION

Despite its low amount in Portland cement (PC) -generally between 4 wt% and 10 wt%- the tricalcium aluminate ($Ca_3Al_2O_6$ or C_3A) greatly influences the workability, setting, and initial strength of concrete due to its high reactivity. Depending on the alkali content incorporated during clinker production (either from raw materials or fuel composition), C_3A can present different crystal structures. In the presence of sodium, Na^+ ions substitute Ca^{2+}, and another Na^+ ion occupies an otherwise vacant site in the center of $Al_6O_{18}^{18-}$ rings, resulting in solid solutions - $Na_{2x}Ca_{3-x}Al_2O_6$ [1]. The crystal structure of this solid solution depends on the amount of Na incorporated. According to Takeuchi et al. [2] and Taylor [3], cubic C_3A is stable when $0 < x < 0.10$, while cubic C_3A and orthorhombic co-exists when $0.10 < x$ 0.16. Orthorhombic is the only polymorph presented when $0.16 < x < 0.20$, while x values higher than 0.20 stabilizes the monoclinic form. However, different values are reported by other authors [4–7]. This discrepancy happens as the sodium content needed to stabilize orthorhombic C_3A depends on several parameters, such as the synthesis route, the sintering and cooling temperature, the sintering time, and the presence of other minor elements like Fe, Mg, Si, among others [4–7]. In commercial PC, cubic and orthorhombic C_3A are found alone or in combination, while the monoclinic C_3A is not observed [3,8].

Cubic C_3A (cb-C_3A) reacts almost instantly with water at room temperature, resulting in quick stiffing, making PC's most practical applications unfeasible [9,10]. Calcium sulfate (gypsum and/or anhydrite) is added to the clinker to control the C_3A hydration and allow the practical use of PC. In the presence of calcium sulfate, ettringite is formed in the first minutes, according to Eq. 5.1, and the reaction is then slowed down for some hours [11–13]. In limestone-free cements and in pure C_3A-calcium sulfate pastes, when all calcium sulfate is consumed, the ettringite becomes unstable and reacts with the remaining C_3A to form monosulfate (SO_4-AFm), according to Eq. 5.2 [11–13]. In turn, the presence of limestone stabilizes the ettringite and promote the formation of hemicarbonate and monocarbonate [14,15].

$$C_3A + 3C\bar{S}H_2 + 26H \rightarrow C_6A\bar{S}_3H_{32} \quad \text{(Eq. 5.1)}$$

$$2C_3A + C_6A\bar{S}_3H_{32} + 4H \rightarrow 3C_4A\bar{S}H_{12} \quad \text{(Eq. 5.2)}$$

Orthorhombic C_3A (ort-C_3A) reacts similarly to cb-C_3A, forming the same products in the absence and presence of calcium sulfate. However, the rate of reaction is entirely different. In the absence of calcium sulfate, ort-C_3A reacts more slowly than cb-C_3A [12,16,17]. In contrast,

the presence of calcium sulfate is ineffective in retarding the ort-C_3A reaction, and therefore it reacts faster than the cubic polymorph in the presence of calcium sulfate [10,12,16–20].

Kirchheim et al. [12] evaluated the hydration of cubic and orthorhombic C_3A alone and with different gypsum contents using calorimetry and XRD. Their results show that an increase in the gypsum contents reduces the hydration rate of cubic C_3A while increases the hydration of ort-C_3A. Similar results were observed by Myers et al. [17] when evaluating the hydration of cubic and orthorhombic C_3A in the absence and the presence of gypsum by calorimetry, XRD, and ICP-OES, and by Cheung et al. [19] and Alonso and Puertas [20] who evaluated the hydration of cubic and orthorhombic C_3A pastes with gypsum by calorimetry. Stephan and Wistuba [16] analyzing the hydration of different C_3A solutions (alone and in the presence of $CaSO_4$) by calorimetry and FTIR, found out that the sodium-doping accelerated the hydration of C_3A in the mixtures with $CaSO_4$. Kirchheim et al. [18] observed by in-situ soft X-ray and ^{27}Al NMR that the orthorhombic C_3A hydrates faster and formed larger ettringite needles than the cubic one in the presence of gypsum. Kirchheim et al. [10] also observed by SEM that orthorhombic C_3A hydration in the presence of gypsum results in larger ettringite crystals compare with cubic C_3A-gypsum pastes. These authors [10] also evaluated the rheology in a plate-plate rheometer and observed that the orthorhombic C_3A-gypsum pastes have a higher storage modulus (*i.e.*, less fluidity) than the cubic C_3A-gypsum pastes. Furthermore, as followed by Dubina et al. [21], by evaluating the pre-hydration of cubic and orthorhombic C_3A alone and with hemihydrate through water vapor sorption, the orthorhombic polymorph presents a higher probability to undergo more pronounced pre-hydration during storage. In addition, orthorhombic C_3A also has a higher likelihood of carbonate during storage [22].

Recent studies [17,23–25] suggest that the retardation of cb-C_3A hydration in the presence of calcium sulfate is due to the adsorption of SO_4^{2-} ions and/or Ca–S ion pairs in the Al-rich leached layer formed with the cb-C_3A dissolution. However, still not clear yet why the calcium sulfate is ineffective to retard the ort-C_3A hydration. This might be related to the difference in the crystalline structure or to sodium in solution with ort-C_3A dissolution. Ort-C_3A presents a higher solubility of the ring structures of $Al_6O_{18}^{18-}$ [17,26], which would impair the formation of the Al-rich leached layer on the C_3A particles and possibly affects its dissolution rate [12,17]. In turn, Stephan et al. [16] suggest that the greater reactivity of ort-C_3A is due to the presence of sodium ions, released in the dissolution of the ort-C_3A, which would destabilize the amorphous alumina layer where the Ca-S ion-pair complexes are adsorbed according to the

recent theory [23]. Another factor that can occur in ort-C_3A pastes is the formation of the U-phase at the expense of monosulfate and ettringite as final precipitate [27–29]. This corresponds to a Na-substituted AFm phase formed in highly alkaline pastes, and the ort-C_3A can provide the sodium ions required for the formation of such phase. The presence of the U-phase was previously observed in C_3A-gypsum pastes hydrating in 0.25-1.00 M [27,30,31] of NaOH solutions and in PC hydrating in 2.0-4.5 M NaOH solutions [32]. According to Li et al. [28], the U-phase formation can appear only at high alkaline concentrations, but the pH range in which this phase is stable has not been reported yet, and further studies are necessary.

As previously mentioned, gypsum ($CaSO_4 \cdot 2H_2O$) and/or natural anhydrite ($CaSO_4$) are added to the clinker to control the C_3A reaction. However, depending on the temperature of the cement mill, gypsum may dehydrate into hemihydrate ($CaSO_4 \cdot 1/2H_2O$) and/or soluble anhydrite ($CaSO_4$) [33,34], which are much more soluble than gypsum and natural anhydrite. The higher solubility of calcium sulfate will increase the available sulfate ions in the solution during the first minutes/hours and influence the C_3A hydration [35]. Pourchet et al. [35] reported that at low SO_3/C_3A ratios, the gypsum replacement by hemihydrate accelerates the cb-C_3A, forming more ettringite in the first hours and anticipating the sulfate depletion. Zunino and Scrivener [36] studied the hydration process of pure C_3S-cb-C_3A mixtures with different amounts of gypsum and hemihydrate. The authors described that the hemihydrate anticipates the sulfate depletion point. Increasing the sulfate demand of the mix - i.e., a higher wt% SO_3 is necessary to obtain optimal mechanical performance for the mixtures with hemihydrate. However, at higher SO_3/C_3A ratios, using hemihydrate as the sulfate source results in a slower hydration rate of the cb-C_3A than when gypsum is used [35]. The reason for this behavior is not known yet, and further studies are necessary.

It is vital to have a correct balance between C_3A reactivity and sulfate solubility. On the one hand, if low soluble sulfates are used in cements with higher C_3A reactivities, it may have an insufficient amount of sulfate in solution, causing flash set due to the formation of OH-AFm or SO_4-AFm [33,37,38]. On the other hand, if a high soluble calcium sulfate (e.g., hemihydrate or soluble anhydrite) is used in cements with low C_3A reactivity, a “false set” may occur due to the formation of larger gypsum crystals deriving from the re-hydration of those sulfates [33,38,39]. This reaction can negatively affect the rheology of fresh concrete and impair its proper application. Despite the importance of the compatibility between C_3A and calcium sulfate source, to the best of the author’s knowledge, there are no studies regarding the

hydration of pure ort-C_3A in the presence of hemihydrate, except for the Dubina et al. [21] study, previously mentioned, that evaluated the pre-hydration of cubic and orthorhombic C_3A in the presence of hemihydrate.

The present study aims to determine, for the first time, if either the change in the crystalline structure or the presence of sodium ions in the solutions are responsible for the higher reactivity of ort-C_3A, in comparison with cb-C_3A, in the presence of calcium sulfate. Additionally, the effect of the type of calcium sulfate source (gypsum/hemihydrate) on the hydration and rheology of cubic and orthorhombic C_3A pastes was studied. Isothermal calorimetry (IC), *in-situ* X-ray diffractometry (*in-situ* XRD), thermogravimetry analysis (TGA), scanning electron microscopy (SEM), and rheological tests were conducted.

5.2 MATERIALS AND METHODS

5.2.1 Materials

Cubic C_3A (cb-C_3A, $3CaO.Al_2O_3$) and orthorhombic C_3A (ort-C_3A, $Na_{2x}Ca_{3-x}Al_2O_6$) were purchased from Mineral Research Processing Cie (France). Both materials were synthesized in the laboratory from a stoichiometric mixture of calcium carbonate ($CaCO_3$) and alumina (Al_2O_3). Sodium carbonate ($NaCO_3$) was used to stabilize the orthorhombic polymorph. The mixtures of reagents were calcinated twice at 1350°C for 2 hours in platinum crucibles. In an intermediate step, between the calcinations, the materials were ground to a fine powder.

High purity (>96 wt%) natural gypsum ($CaSO_4 \cdot 2H_2O$) and hemihydrate ($CaSO_4 \cdot 1/2H_2O$) were used as calcium sulfate sources. Hemihydrate was prepared by heating the gypsum at 100 °C for 48 hours.

Cb-C_3A, ort-C_3A, gypsum, and hemihydrate were characterized by X-ray diffractometry (XRD) using an X´Pert MPD PRO diffractometer from PANalytical (Almelo, Netherlands) placed at Servicios Centrales de Apoyo a la Investigación (SCAI) at the University of Malaga (UMA, Spain). Monochromatic Cu-$K\alpha_1$ radiation, λ = 1.54059 Å, obtained by a Ge (111) monochromator and X'Celerator detector were used. The X-ray tube operated at 45 kV and 40 mA, and the samples were measured between 5º to 70º (2θ) with a step size of 0.0167° 2θ, using a spinning sample-holder (16 rpm) to enhance particle statistics. The crystalline phases of the raw materials were identified using the X'Pert Highscore software (PANalytical) and quantified by the Rietveld method using the GSAS II software. The fitting process was adjusted to obtain

an R_{WP} lower than 15% and a goodness-of-fit ($GOF = R_{WP}/R_{exp}$) lower than 4. Figures 5.1 and 5.2 present the XRD patterns, and Table 5.1 shows the XRD-Rietveld results of both C_3A samples and the sulfate sources.

Table 5.11 – ICSD collection codes and XRD-Rietveld results (in weight percentages) of the raw materials.

Phase	**Chemical composition**	**ICSD**	**cb-C_3A**	**ort-C_3A**	**Gypsum**	**Hemihydrate**
Cubic C_3A	$Ca_3Al_2O_6$	1841	96.9	5.6	-	-
Orthorhombic C_3A	$Na_{2x}Ca_{3-x}Al_2O_6$	1880	-	94.4	-	-
Mayenite	$Ca_{12}Al_{14}O_{33}$	261589	2.0	-	-	-
Lime	CaO	75786	1.1	-	-	-
Gypsum	$CaSO_4 \cdot 2H_2O$	151692	-	-	96.1	-
Hemihydrate	$CaSO_4 \cdot 1/2H_2O$	69060	-	-	-	97.2
Dolomite	$CaMg(CO_3)_2$	66333	-	-	3.4	2.4
Quartz	SiO_2	200721	-		0.5	0.4
	R_{WP} /%		13.3	14.7	11.7	11.3
	GOF		3.1	4.1	3.1	2.7

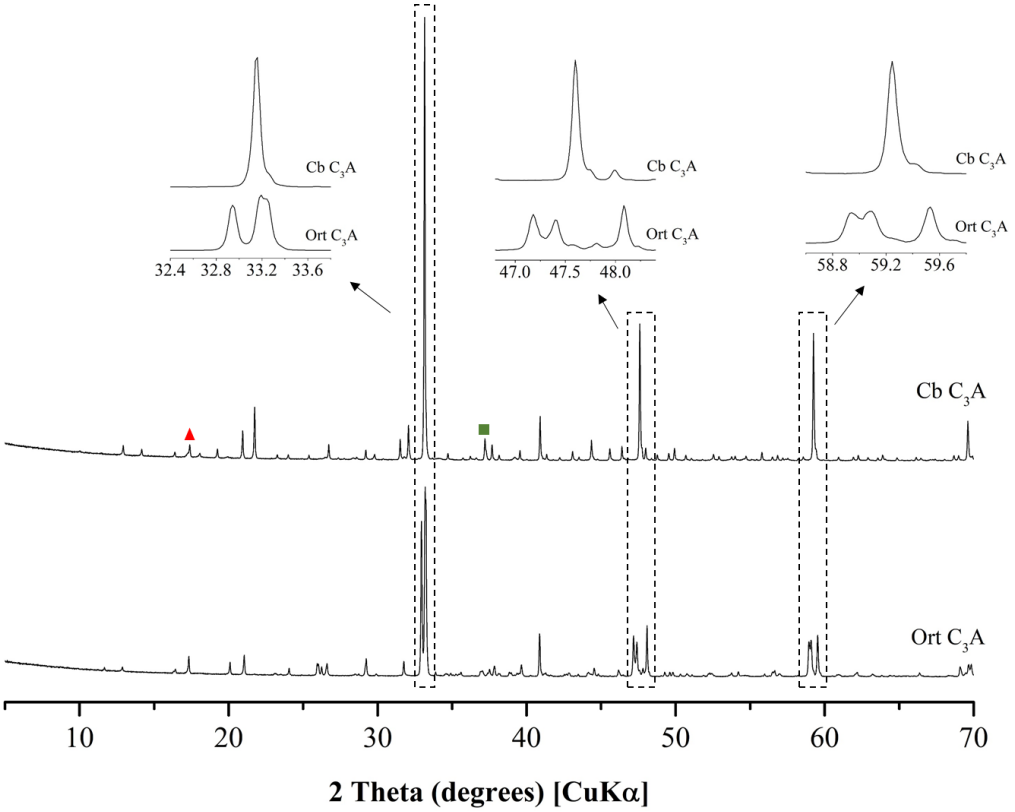

Figure 5.32 – XRD patterns for the cubic and orthorhombic C_3A. The non-labeled peaks correspond to C_3A reflections, while symbols indicate the main reflections of the minor phases. Triangle: Mayenite; Square: Lime. Note that in some cases, the peaks overlap with the peak of the main phases.

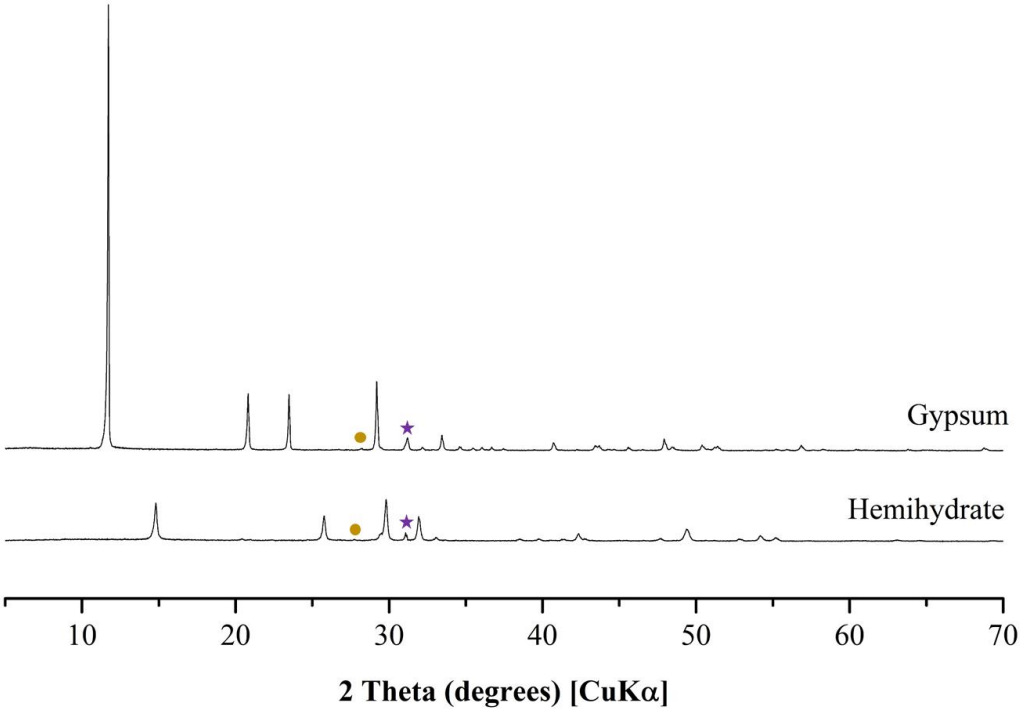

Figure 5.33 – XRD patterns for gypsum and hemihydrate. The non-labeled peaks correspond to gypsum or bassanite (crystalline hemihydrate) reflections, while symbols indicate the main reflections of the minor phases. Circle: Quartz; Star: Dolomite. Note that in some cases, the peaks overlap with the peak of the main phases.

The BET surface area of the raw materials was determined using ASAP 2420 equipment from Micromeritics (Georgia, USA), according to the guidelines presented by Palacios et al. [40]. The density was determined in an AccuPyc II 1340 pycnometer from Micromeritics (Georgia, USA), both equipment placed at SCAI at UMA. The particle size distribution was determined through laser diffraction, using PSA 1090 equipment from Anton Paar (Graz, Austria), with isopropanol as the dispersant, and considering Mie theory [40]. Table 5.2 presents the results of the physical characterization of the raw materials, and Figure 5.3 shows their particle size distribution. Both C_3As presented similar physical characteristics, with an equivalent median diameter and comparable BET surface area (difference of only 0.29 m^2/g, which maybe within the error of the method). Gypsum and hemihydrate presented similar particle size distribution and BET surface area as expected.

Table 5.12 – Physical characterization of the raw materials.

Property	**cb-C_3A**	**ort-C_3A**	**Gypsum**	**Hemihydrate**
BET surface area (m^2/g)	1.42	1.13	1.33	1.38
D_v 90 (μm)	30.8	28.7	51.8	40.8
D_v 50 (μm)	7.5	7.6	16.9	14.8
D_v 10 (μm)	1.6	1.8	3.6	3.5
Density (kg/m^3)	2940	2990	2350	--

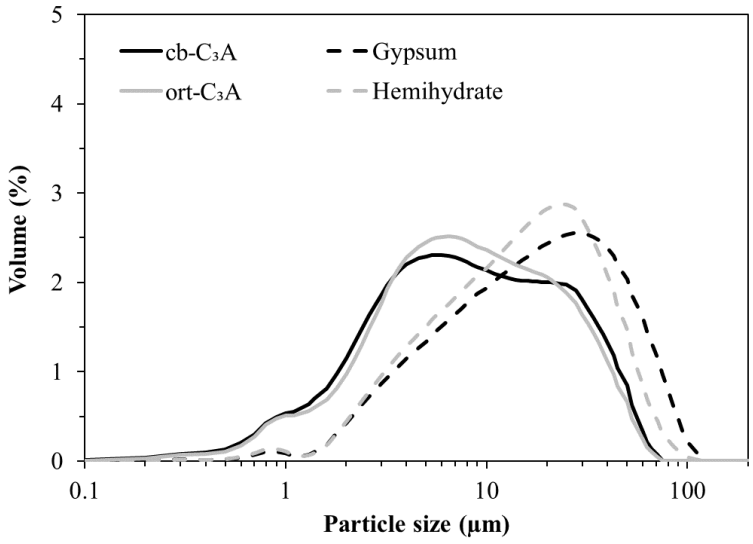

Figure 5.34 – Particle size distribution of the raw materials.

Table 5.3 presents the chemical composition of cb-C_3A, ort-C_3A, and gypsum, obtained by X-ray fluorescence (XRF), using an ADVANT'XP+ spectrometer from Thermo Fisher Scientific (Waltham, USA), placed at SCAI at UMA. For this test, the samples using fusion to form fused beads, providing a homogeneous representation of the sample. Cb-C_3A and ort-C_3A presented LOI of 2.76% and 2.20%, respectively, which probably is due to the absorption of water on their surface and slightly pre-hydration during grinding and storage as discussed by Dubina et al. [21].

Table 5.13 – Chemical composition, obtained by XRF, of the raw materials, expressed as the weight percentage of oxides. Loss on ignition (LOI) is also included.

Constituent	**cb-C_3A**	**ort-C_3A**	**Gypsum**
CaO	60.89	56.58	34.04
Al_2O_3	35.52	36.70	0.09
Na_2O	0.03	3.98	-
SiO_2	0.43	0.18	0.95
Fe_2O_3	0.08	0.06	0.16
MgO	0.11	0.09	0.81
SO_3	0.02	0.03	46.05
LOI	2.76	2.20	17.53

The amount of Na^+ released in ort-C_3A dissolution was quantified by inductively coupled plasma atomic emission spectroscopy (ICP-OES), using an Optima 7300DV spectrometry from Perkin Elmer (Massachusetts, USA). A release of 3.5 wt% of Na^+ (or 4.7 wt% of Na_2O) was observed with the dissolution of ort-C_3A in water, and this information was used for mix design (Section 5.2.2.1). This value is slightly higher than the value obtained by XRF (3.98 wt%), and this can be attributed to the inherent deviations on XRF tests.

5.2.2 Methods

5.2.2.1 Formulations and sample preparation

Table 5.4 shows the different formulations studied. Mixes with cb-C_3A, cb-C_3A + NaOH, and ort-C_3A were produced with gypsum or hemihydrate. For the mixes with cb-C_3A and ort-C_3A, distilled water was used, while for those with Na-cb-C_3A, a 0.99 M NaOH solution was used. The molarity of NaOH solution was chosen to maintain the amount of Na^+ released with the

dissolution of ort-C_3A, as obtained by ICP-OES (3.5 wt% of Na^+). Furthermore, as the sodium is progressively liberated with the dissolution of ort-C_3A, while it is fully available from the beginning on the Na-cb-C_3A, it is interesting to study the impact of different NaOH molarities on cb-C_3A hydration. Thus, in addition to the 0.99 M, the hydration of cb-C_3A_GYP pastes at 0.24 M and 0.48 M of NaOH solutions was also evaluated (only by calorimetry). These correspond to 25% and 50% of the Na^+ released with the total dissolution of ort-C_3A.

A fixed SO_3/C_3A ratio of 0.293 by weight was used for all mixtures, resulting in a gypsum/C_3A ratio of 0.64 and a hemihydrate/C_3A ratio of 0.58. This ratio falls within the range of SO_3/C_3A ratio usually found in PC (considering a C_3A content of 8 wt% and an SO_3 content of 2.3 wt.%), and similar ratios were used in several studies with C_3A-gypsum pastes [10–12,41]. The water/solid ratio was fixed at 1.00 by weight since it is the most common ratio used for C_3A pastes in literature [11,13,25,41], being enough to fully hydrate the C_3A and promote adequate workability. The w/s ratio used here does not consider the chemical bound water present in gypsum and hemihydrate, as it will not be available during mixing and the beginning of the reaction.

Table 5.14 – Formulations studied.

Mixture	C_3A (wt%)	Gypsum (wt%)	Hemihydrate (wt%)	Solution	SO_3/C_3A	w/s
cb-C_3A_GYP	61.08	38.92	-	Distilled water	0.29	1.0
Na-cb-C_3A_GYP	61.08	38.92	-	0.99 M NaOH		
ort-C_3A_GYP	61.08	38.92	-	Distilled water		
cb-C_3A_HEM	64.22	-	35.78	Distilled water		
Na-cb-C_3A_HEM	64.22	-	35.78	0.99 M NaOH		
ort-C_3A_HEM	64.22	-	35.78	Distilled water		

The anhydrous materials (C_3A and gypsum/hemihydrate) were manually mixed for 10 minutes in an agate mortar. At room temperature, the 0.99 M NaOH solution was prepared by dissolving NaOH in distilled water by magnetic stirring for 30 minutes. As the NaOH dissolution is exothermic, the solutions were prepared at least 24 hours before mixing the C_3A pastes to prevent the heat release in its dissolution from interfering with the C_3A hydration and the isothermal calorimetry results.

For the preparation of the C_3A pastes, 2 g of pre-mixed anhydrous materials (cb-C_3A/ort-C_3A and gypsum/hemihydrate) were placed in a 20 mL vessel. Then, the deionized water or the Na^+ water solutions was added, and the materials were mixed for 2 minutes using a rotational mixer at 350 rpm.

For the calorimetry analysis, the mixing procedure was conducted inside the 20 mL glass ampoule used for the isothermal calorimetry tests (see section 5.2.2.2), and the plastic rod was left inside the glass ampoule to minimize the loss of material during mixing. The mixing procedure and insertion of glass ampoule in the calorimetry were done in less than 3 minutes after the initial contact between water and C_3A. For the TGA, in-situ XRD, SEM, and rheological tests, the mixes were prepared in plastic vessels and then hermetically closed. For the TGA and SEM analysis, the paste remained inside the closed vessels until the hydration stoppage.

For the SEM analysis, the hydration of C_3A pastes was stopped at 30 and 120 minutes for the gypsum containing and at 10 minutes for the hemihydrate-containing samples. The hydration was stopped at 1 hour, 1, 2, and 3 days for the TGA analysis. About 1 g of each paste was mixed with 50 ml of isopropanol for 30 minutes while stirring; due to the soft consistency of the pastes for up to 3 days, no grinding process was required. Then, the sample was filtered at a low vacuum through a nylon filter with a 15 µm opening for 10 minutes and dried in an oven at 40 °C for another 10 minutes. Finally, the sample was stored in a desiccator with silica gel and low vacuum until testing.

5.2.2.2 Isothermal calorimetry (IC)

For IC analyses, an eight-channel Thermal Activity Monitor of Tam Air, TA Instruments (New Castle, DE, USA) was used. The pastes were mixed ex-situ, but inside the glass ampoule, as described in item 2.2.1. Distilled water was used as reference material, and the amount of water used as reference was calculated according to Wadsö [42] to obtain the same heat capacity as the C_3A paste. The heat flow (thermal power, mW/g of solids) and the cumulative heat (integral of thermal power, J/g of solids) were recorded for up to 3 days at 20°C.

5.2.2.3 In-situ X-ray diffraction (In-situ XRD)

In-situ XRD was conducted up to 48 hours in an X`Pert Pro (PANalytical) diffractometer equipped with Soller and anti-scattering slits, 1/2^o fixed divergent slit set up, and X´Celerator

detector. The diffractometer operated at 45 kV and 40 mA with CuKα radiation given a wavelength of 1.5418Å. The scanning range, step size, and counting time were respectively 7-55° 2θ, 0.0167° 2θ, and 24.765 sec/step, and the sample was rotated at 2 sec/rev to improve the statistics of data collection. Immediately after mixing, the fresh paste was placed on the sample holder and covered with a Kapton film to prevent water loss and carbonation. The measurements started 40 minutes after the first contact between the water and the dry materials; each scan took about 10 minutes, and three samples were tested alternatively, placed at X-ray beam automatically by a robotic arm, providing an XRD pattern for each sample every 30 minutes, totalizing about 90 measurements for each sample.

For XRD data analysis, TOPAS v.5 software was used. The U-phase was found in most pastes (discussed later in Section 5.3.2), which corresponds to a sodium-substituted AFm phase formed in highly alkaline cement pastes [27,29]. According to Ectors [43], the layered nature of AFm-type structures often results in stacking disorder and anisotropic peak broadening in XRD, making the crystal structure determination difficult. The lack of a well-defined crystal structure for this phase would make Rietveld quantitative phase analysis inaccurate. Thus, a semi-quantitative phase analysis (SQPA) was conducted as detailed next. The crystallographic information files used for phase identification are detailed in Table 5.5.

Table 5.15 – Crystallographic information files used for phase identification.

Phase	Reference code	Reference
C_3A cubic	1841*	Mondal and Jeffery [7]
C_3A orthorhombic	1880*	Nishi and Takeuchi [1]
Ettringite	155395*	Goetz-Neunhoeffer and Neubauer [44]
Gypsum	151692*	de la Torre et al. [45]
Hemihydrate	69060*	Bezou et al. [46]
U-phase	00-044-0272**	Post and Pollmann [47]

*ICSD code; **ICDD code.

5.2.2.3.1 Kapton film and free water fitting

In order to systematically account for the background contributions caused by the Kapton film and free water while avoiding manual background fitting (which highly depends on the operator), those were fitted using hkl phases. The Kapton film was first measured over

a silicon single crystal, and the data were fitted with a Pawley range using the structural parameters proposed by Scherb et al. [48]: P4/mmm space group and lattice parameter a = 9.72 Å; c = 26.53 Å. The crystallite size (Lorentzian function) and hkl intensities were refined in this step. Subsequently, a corundum (α-Al_2O_3) sample covered with Kapton was measured, and the lattice parameters of the Kapton hkl phase were refined. This allowed placing the hkl phase along the 2θ axis correctly. For the free water model creation, corundum:water paste (in 50:50 wt%) covered with Kapton was measured. The lattice parameters, the crystallite size (Lorentzian function), and scale factor of corundum, the scale factor of the Kapton hkl phase, and the background (n=0 order Chebyshev) were refined in the pure corundum sample above-mentioned and fixed for the corundum:water sample (except for the scale factor of the corundum phase which was allowed to be refined). The diffuse scattering caused by the water was then fitter with a Pawley range using the space group P4/mmm. The lattice parameters, the crystallite size (Lorentzian function), and the hkl intensities of the free water model were refined and fixed. Figure 5.4 shows an example of a fitted *in-situ* diffractogram accounting for the contribution of both Kapton film and free water, in addition to the crystalline phases.

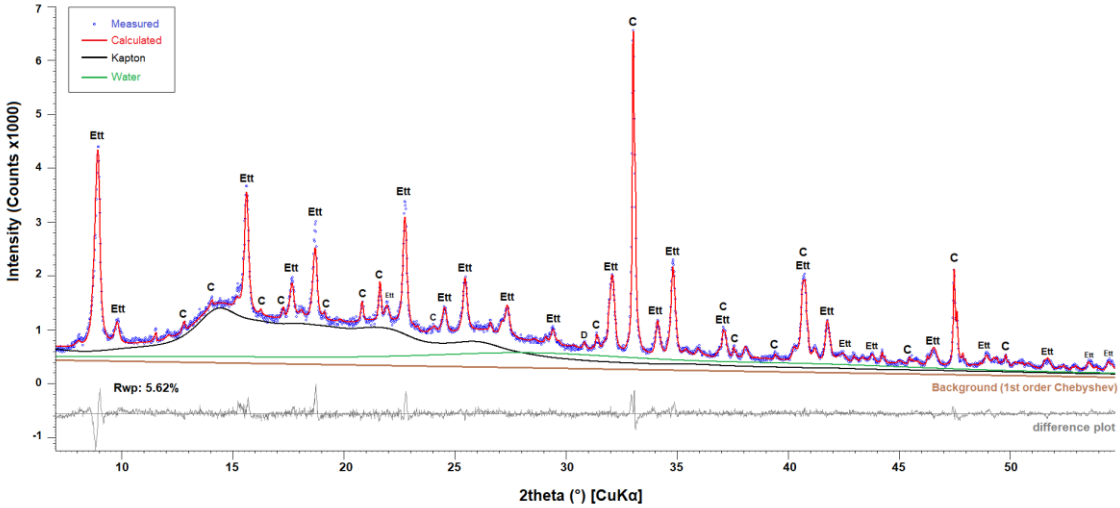

Figure 5.35 – Example of fitted XRD pattern of in-situ measurement for cb-C_3A_GYP paste at 48 hours of hydration. Ett: ettringite; C: C_3A (cubic); D: dolomite.

5.2.2.3.2 Semi-quantitative phase analysis (SQPA)

SQPA was conducted by determining the scale factor of each crystalline phase over time relative to its highest scale factor measured. Different qualitative or SQPA approaches based on peak intensities of XRD patterns were used to evaluate the cement paste hydration. Guo et al. [49], Gardner et al. [50], and Shunman et al. [51] analyzed absolute intensity values at given 2θ positions to assess the formation of hydrated phases (e.g., portlandite) in powder XRD. More

elaborately, Quennoz and Scrivener [11,52] evaluated the area of a single representative peak for each phase over time for in situ XRD measurements, manually subtracting the background. However, relying on a single peak may provide misleading results since preferred orientation can occur, while the scale factor of the phases accounts for the whole XRD pattern. It is stressed that the weight fraction of a given crystalline phase is linearly proportional to its scale factor [53].

The global parameters refined were sample displacement (to account for height variations caused by paste expansion/shrinkage over time) and background (1st order Chebyshev polynomial). After including the Kapton and free water hkl phases (detailed in Section 5.2.3.3.1) in the refinement, the crystalline phases were included one by one. For the U-phase, a hkl phase was created using the space group, lattice parameters, and relative intensities of the ICDD 00-044-0272 file, detailed in the Supplementary Material (Table C1 and C2, Figure C1). The lattice parameters and peak shape (Thompson-Cox-Hastings pseudo-Voigt profile function [54]) of the anhydrous phases (i.e., C_3A, gypsum, and bassanite) were previously refined in dry samples and fixed for hydrating samples. The lattice parameters and peak shape of the hydrated phases (i.e., ettringite and U-phase) were refined for each mix using the XRD pattern that had the highest content of the respective phase and then were fixed for the other patterns. Pseudo-Voigt peak shape fitting instead of the fundamental parameters approach was chosen because it led to more stable refinements over time. The preferred orientation of gypsum (020), ettringite (010), and U-phase (003) were refined using the March-Dollase function [55] for accounting for crystal orientation on the surface of the Kapton film.

5.2.2.4 Thermogravimetry analysis (TGA)

TGA was performed in a TGA 2 analyzer from Mettler Toledo (Columbus, Ohio, USA). The samples (≈10 mg) were placed in open platinum crucibles under airflow. The temperature ranged between room temperature (RT) and 1000 °C with a heating rate of 10 °C/min. From the TGA results, the bound water content was determined. After stopping hydration, the bound water content of the pastes was assigned to the weight loss from RT to 550°C. The actual bounded water can be calculated by Eq. 5.3 [56]:

$$BW = \frac{BW_{ATD} \cdot CM}{100 - BW_{ATD}} \quad \text{(Eq. 5.3)}$$

BW corresponds to actual chemically bound water content, BW_{ATD} is the mass loss measured up to 550ºC from TGA curves, and CM is the solid, i.e., C_3A-sulfate source content (all the numbers in weight percentages).

5.2.2.5 Scanning electron microscopy (SEM)

SEM images of the hydrated samples in dry powder form (detailed in Section 5.2.2.1) were recorded using a VEGA3 (TESCAN) microscope operating at 15 kV. A small portion of powder was placed over a carbon adhesive tape and coated with gold. Images were acquired at the ×5000-40000 range.

5.2.2.6 Rheological tests

The rheological tests were conducted on a Haake MARS III (Thermo Scientific) rheometer using a parallel plate geometry with 20 mm diameter and serrated surface. The axial gap was 1.000 mm, and the temperature was kept at 23.0 ± 0.1°C. The measurements started 10 minutes after the first contact between the water and the dry materials, and a shear cycle was recorded every 10 minutes until 120 minutes of hydration. An insulation hood was used to prevent water evaporation.

Firstly, the sample was pre-sheared at 100 s^{-1} for 30 seconds, followed by a 30-second rest. Subsequently, the shear rate was increased from 0.1 to 100 s^{-1} in 10 steps and then decreased back to 0.1 s^{-1} in the same steps. Each step took 10 seconds (which was confirmed to be enough to reach a steady-state flow) and the last 3 seconds were recorded. The decreasing portion of the flow curves was used to obtain the rheological properties of the paste. The yield stress was determined using the Casson model [57] (Eq. 5.4), as also used in several studies with cement pastes [58–60].

$$\sqrt{\tau} = \sqrt{\tau_0} + \sqrt{\mu_\infty} \cdot \sqrt{\dot{\gamma}} \qquad \text{(Eq, 5.4)}$$

Where τ is the shear stress (in Pa), $\dot{\gamma}$ is the shear rate (in s^{-1}), τ_0 is the yield stress (in Pa), and μ_∞ is the viscosity (in Pa.s).

This model provided the best overall fit for the data, while the Herschel-Bulkley model (conventionally used to describe the pseudoplastic flow of cement pastes) provided unrealistic values, i.e., negative yield stress values or visible misfits. The Casson model only provides the

viscosity at an infinite shear rate, and this has no practical meaning for cement-based materials, so it was used here only for comparison between the samples.

5.3 RESULTS

5.3.1 Isothermal Calorimetry

Figure 5.5 presents the heat flow, and cumulative heat curves of C_3A pastes with gypsum up to 90 hours. All pastes evaluated presented the typical heat flow curve profile of C_3A hydration, divided into three periods. In the first ~30 minutes of hydration, a great exothermic peak of heat release is observed, followed by a sharp reduction in the heat flow. According to Quennoz and Scrivener [11], this first heat release is related to the initial dissolution of C_3A and gypsum and the formation of the first ettringite and OH-AFm crystals. After the end of this great heat release, a low heat releasing period begins. Several hypotheses were proposed to explain the mechanism responsible for the occurrence of this period of low heat release, which is not observed in the C_3A hydration without calcium sulfate. The most accepted theory nowadays is that SO_4^{2-} ions and/or Ca–S ion-pair complexes are adsorbed on an Al-rich leached layer formed at the partially dissolved C_3A surface [17,23,61,62]. During the period of low heat release, the sulfates are being consumed due to ettringite formation. Finally, when all sulfate from the solution is consumed – known as sulfate depletion– a new exothermic peak is observed due to a new fast dissolution of C_3A and formation of AFm phases, as confirmed by XRD (see Section 5.3.2) and previously observed by Quennoz and Scrivener [11] and Kirchheim *et al*. [12].

As shown in Figures 5.5 and C2, the length of the period of low heat release and the intensity of the main heat flow peak were greatly influenced by the presence of sodium. The cb-C_3A_GYP sample exhibited a low (~ 6.5 mW/g of C_3A) and a broad main peak of heat release -between 25 and 70 h. The external addition of sodium in solution (i.e., incorporation of NaOH) anticipated and increased the main peak of heat release -which now occurred between 15 and 35 hours with a maximum value of ~ 27 mW/g of C_3A. As observed in Figure C2, the amount of external sodium added (*i.e.*, varying the NaOH molarity) did not influence the beginning of the second peak, indicating that the amount of NaOH does not influence the moment of sulfate depletion occurrence. However, the greater the amount of sodium added (*i.e.*, the higher the NaOH molarity), the higher is the second peak: the sample hydrating at the 0.24 M presented a maximum of the second peak of ~ 12 mW/g of C_3A while the sample hydrating at 0.99 M of NaOH presented a maximum of ~ 27 mW/g of C_3A.

Finally, the reaction of ort-C_3A, which has Na^+ in its crystalline structure, was even faster, with most of the reaction occurring within the first 24 hours. Furthermore, ort-C_3A presented two peaks in the first 24 hours: the first peak is related to very fast ettringite precipitation and gypsum consumption, while the second is related to a new C_3A dissolution and AFm precipitation, as observed in the XRD results and discussed in Section 5.3.2. These results corroborate with previous studies [12,17,20], which observed a higher heat-releasing of ort-C_3A-GYP compared with cb-C_3A-GYP in the first hours of hydration.

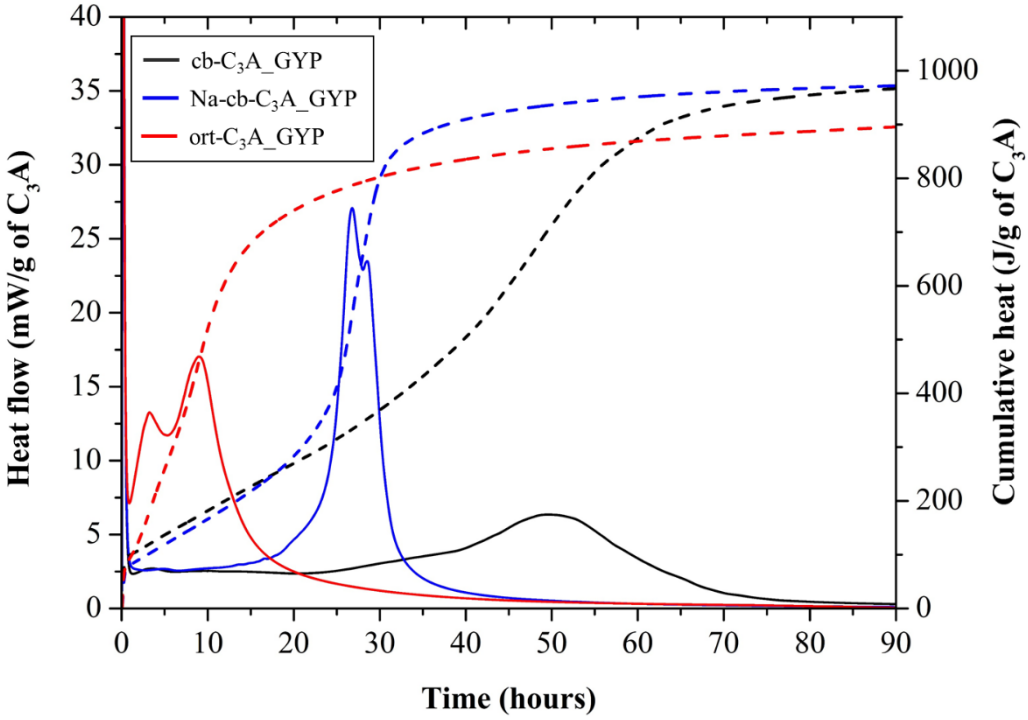

Figure 5.36 – Heat flow curves (solid lines and primary/left "y" axis) and cumulative heat curves (dashed lines and secondary/right "y" axis) of the C_3A pastes with gypsum during the first 90 hours of hydration.

Figure 5.6 presents the heat flow and cumulative heat curves of cb-C_3A, Na-cb-C_3A, and ort-C_3A with gypsum and hemihydrate. The replacement of gypsum with hemihydrate had different impacts on the hydration of C_3A polymorphs: it increased the heat released in the first hours in the ort-C_3A, retarded the second heat flow peak of the Na-cb-C_3A, while did not influence the heat flow and cumulative heat curves of the cb-C_3A.

Regarding the cb-C_3A (Figure 5.6a), the paste with hemihydrate presented a slightly broader and smaller peak – between 20 and 80 hours with a maximum value of ~ 4.7 mW/g of C_3A. Therefore, the calcium sulfate source did not have a great influence on the cb-C_3A hydration.

In turn, the use of hemihydrate in Na-cb-C_3A (Figure 5.6b) delayed the main heat flow peak (by about 11 hours) but increased by approximately 30% compared to the gypsum samples. Pourchet et al. [35] observed that the replacement of gypsum with hemihydrate delayed the cb-C_3A reaction when more than 15wt.% of equivalent gypsum (related to the C_3A wt.%) was used, which corroborates with the behavior observed for the Na-cb-C_3A, but not for the cb-C_3A (this is later discussed in Section 5.4.2).

As for the ort-C_3A, the replacement of gypsum with hemihydrate increased the intensity of the heat flow peak, increasing the heat release within the first day (Figure 5.6c). Ort-C_3A_HEM hydration showed three heat release peaks between 30 minutes and 24 hours. These peaks are respectively related to hemihydrate conversion into gypsum, very fast ettringite precipitation, C_3A and gypsum dissolutions, and AFm precipitation, as further discussed in Section 5.3.2.

It is worth noting that all the mixes with hemihydrate presented a higher heat release within the first hour when compared with the respective mixes containing gypsum. This probably results from hemihydrate hydration and recrystallization in gypsum, which is exothermic and generally occurs in the first hour (as confirmed by XRD and SEM; see Sections 5.3.2 and 5.3.4). This hypothesis agrees with thermodynamic modeling (see Supplementary Materials, Figure C3), which showed that the use of hemihydrate instead of gypsum in the cb-C_3A paste is expected to increase the cumulative heat by 83 J/g of C_3A. This value is very close to the increase of 79.7 J/g of C_3A in the cumulative heat obtained by calorimetry at 90 hours when hemihydrate is used instead of gypsum.

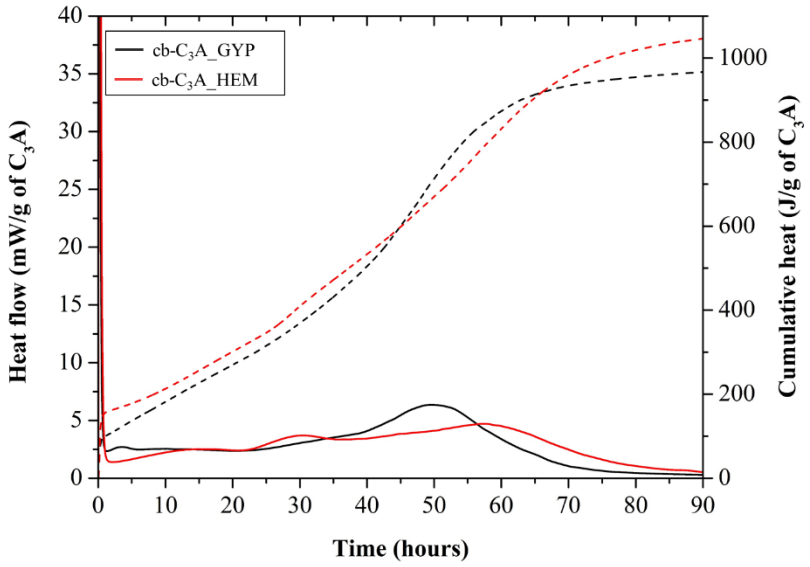

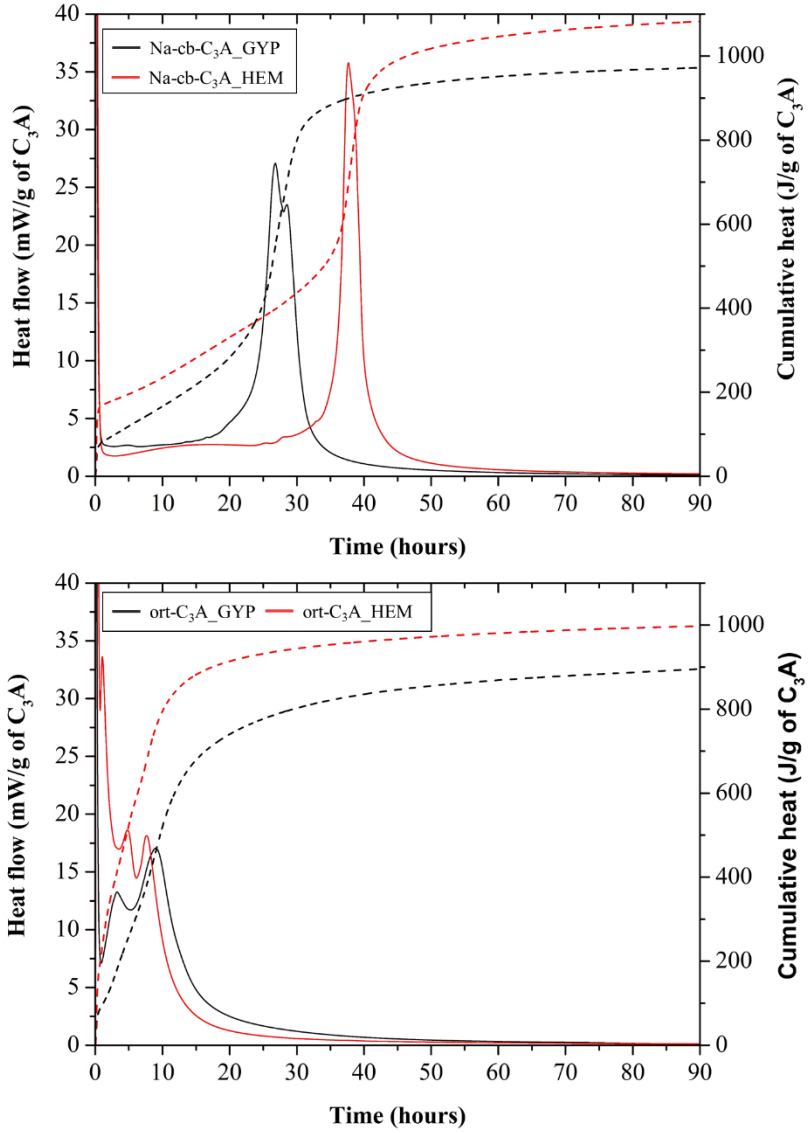

Figure 5.37 – Heat flow curves (solid lines and primary/left "y" axis) and cumulative heat curves (dashed lines and secondary/right "y" axis) of the (A) cb-C_3A, (B) Na-cb-C_3A, and (C) ort-C_3A pastes with gypsum and hemihydrate during the first 90 hours of hydration.

5.3.2 In-situ X-ray diffraction (XRD)

The set of XRD patterns of the pastes over time up to 48 hours is presented in Figure C4. Figure 5.7 presents some key XRD patterns. Figure 5.8 shows the relative scale factor of the crystalline phases over time. No bassanite (crystalline hemihydrate) was found in the pastes with hemihydrate addition (Figure 5.7c-d and Figure 5.8d-f), indicating that it converted into gypsum before the first XRD measurement (i.e., within the first 40 minutes of hydration). This is in line with that reported by Jakob et al. [4] and García-Maté et al. [63], which observed this phenomenon before 10-20 minutes of hydration.

For the cb-C_3A_GYP and Na-cb-C_3A_GYP samples (Figure 5.7a and b, respectively), the diffuse scattering promoted by the free water prevented the clear identification of the crystalline phases up to about 8 hours of hydration, as seen in the first two patterns of Figure 5.7a and Figures C4 (a,b). This issue was also reported by Scherb et al. [48] for pastes with high w/s ratios. In general, the beginning of AFm formation was identified simultaneously with the beginning of ettringite consumption as expected. The Na-cb-C_3A and ort-cb-C_3A mixes with both gypsum and hemihydrate incorporation formed U-phase as AFm, resulting from the presence of sodium either from the C_3A composition (for ort- C_3A) or from external addition (for Na-cb-C_3A), exemplified in Figures 5.7 (b,c,d). The presence of U-phase in these pastes agrees with previous studies [27,30,31], which observed U-phase in C_3A-gypsum pastes hydrating at 0.25-1.0 M of NaOH (note that Na-cb-C_3A is hydrating at a 0.99 M of NaOH solution).

The U-phase ($4CaO \cdot 0.9Al_2O_3 \cdot 1.1SO_3 \cdot 0.5Na_2O \cdot 16H_2O$) belongs to the group of hexagonal or pseudo-hexagonal layered structures (AFm), being similar to monosulfate but with Na between the layers and has a higher interlayer distance [28,29,64]. The U-phase is formed in the presence of SO_4^{2-} and Na^+ ions and a high alkaline medium [64]. The actual pH range that leads to U-phase formation is still not clear.

The U-phase formation occurred similarly to that usually observed for monosulfate, i. e., after the sulfate depletion, leading to a consumption of ettringite [11,33]. This ettringite consumption is expected from equilibrium conditions at the sulfate depletion since the U-phase also contains SO_4^{2-} content in its composition, but a lower content compared with ettringite.

In contrast, no AFm formation was identified in the cb-C_3A_GYP and cb-C_3A_HEM samples for up to 48 hours (see Figure 5.7a and Figure C4a,d). Although the gypsum depletion was identified at about 32-36 hours for these mixes (Figures 5.8a and 5.8d), the maximum ettringite content (and subsequent conversion into AFm) generally occurred a few hours after the sulfate depletion for the other mixes (Figure 5.8b,c,e,f). This is in line with the results reported by Jansen et al. [8], who showed that ettringite formation depends on the coupled availability of sulfur and aluminum (the latter, from C_3A dissolution). In fact, a relatively low reduction in the scale factor of C_3A was observed within the first two days of hydration in the cb-C_3A mixes with both gypsum and hemihydrate, suggesting the low consumption of C_3A and justifying the lack of AFm formation during this period. The continuous ettringite formation after gypsum

depletion happened even after the gypsum depletion (observed by XRD), suggesting the presence of sulfate ions in the solution as observed by Jansen et al. [65].

Regarding the rate of hydration, the XRD results are in agreement with the calorimetry results. For the samples with gypsum, the ort-C_3A presented the earlier gypsum depletion occurring at 7.8 hours and the maximum of ettringite and beginning of U-phase formation at 11.2 hours. The Na-cb-C_3A_GYP presented gypsum depletion at 15 hours and U-phase formation at 35 hours. The cb-C_3A_GYP presented the later gypsum depletion at ~36 hours, and no AFm formation was detectable up to 48 hours.

As for the replacement of gypsum with hemihydrate, the XRD results also corroborate with the calorimetry data. This replacement led to a later start of sulfate depletion, and gypsum was still present in the cb-C_3A_HEM paste after 48 hours of hydration. The use of hemihydrate in the Na-cb-C_3A_HEM sample delayed the gypsum depletion by 17 hours and the U-phase formation by 8.9 hours compared to the Na-cb-C_3A-GYP sample. Finally, the use of hemihydrate instead of gypsum in the ort-C_3A paste led to a higher ettringite formation rate and anticipated gypsum depletion by 0.4 hours and U-phase formation by 2.2 hours.

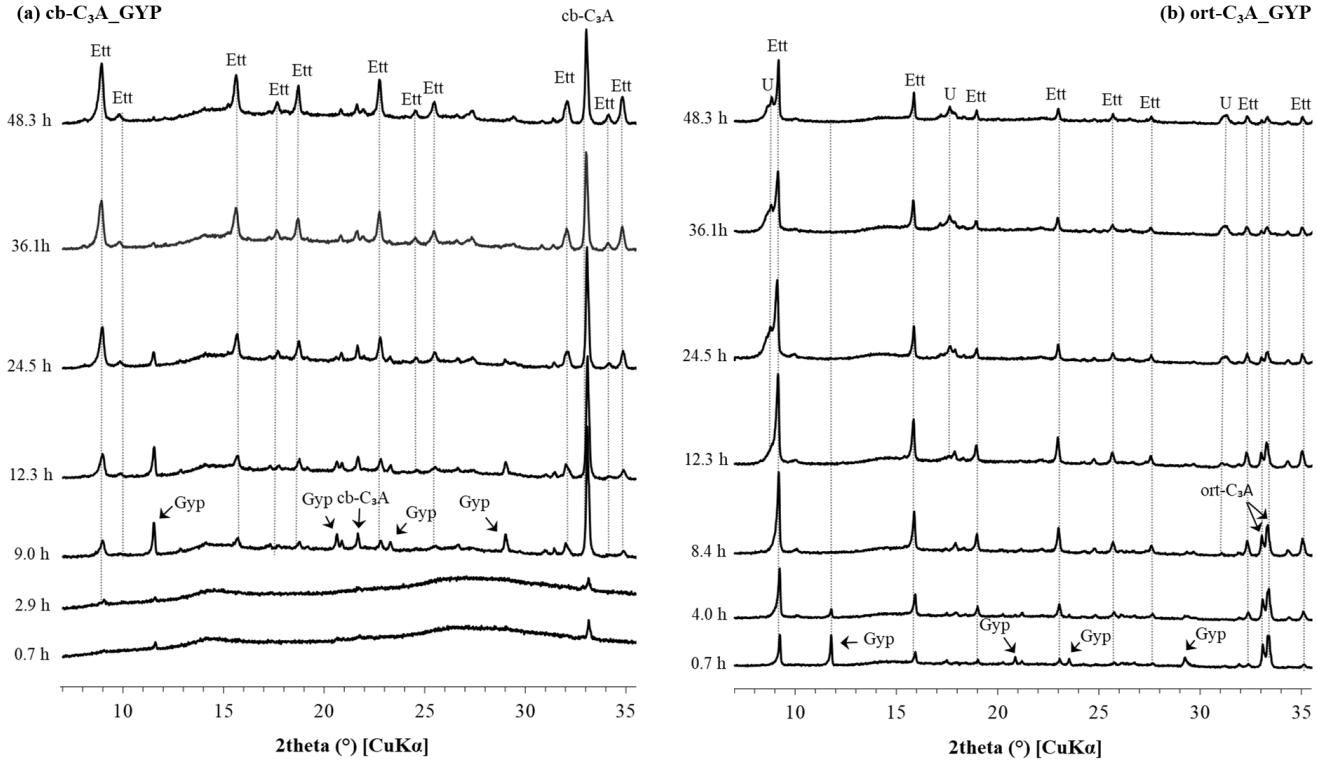

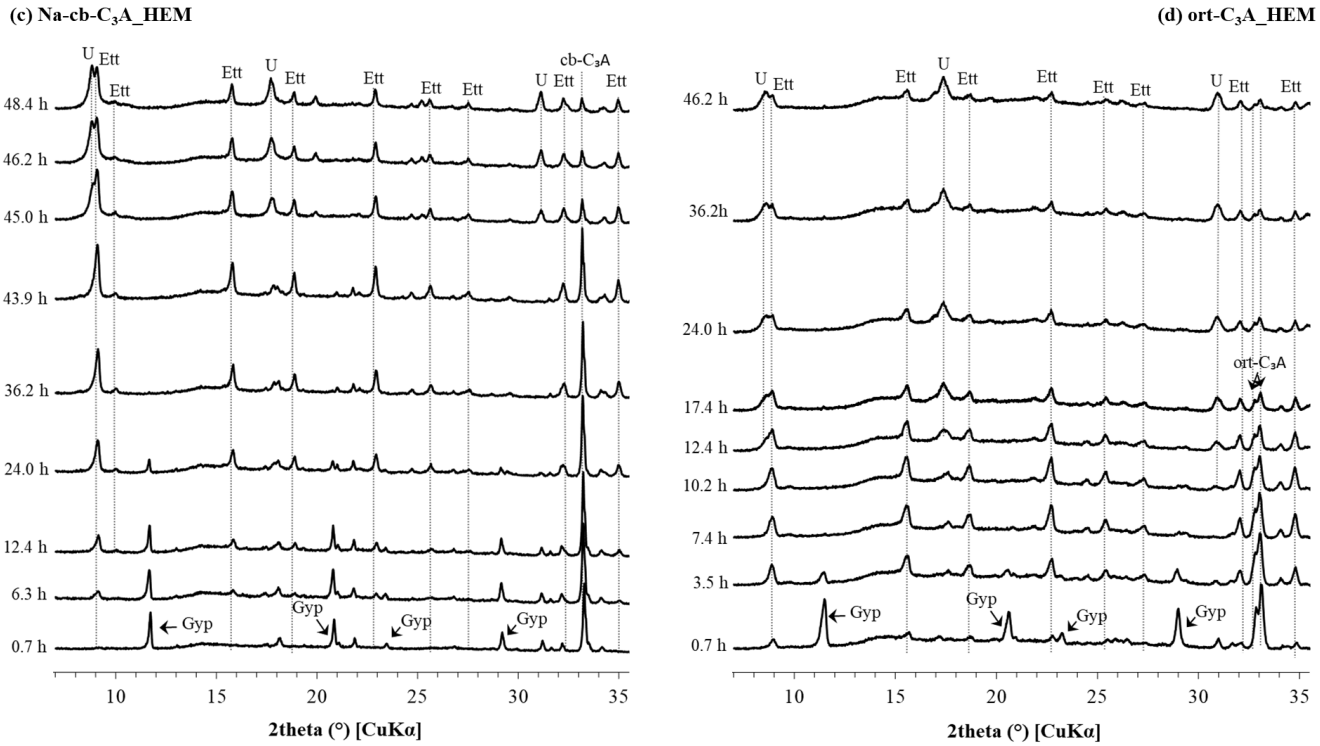

Figure 5.38 – Key XRD patterns of in-situ measurement for the different C_3A pastes with gypsum and hemihydrate. Ett: ettringite, U: U-phase, Gyp: Gypsum, cb-C_3A: cubic C_3A, ort-C_3A: orthorhombic C_3A.

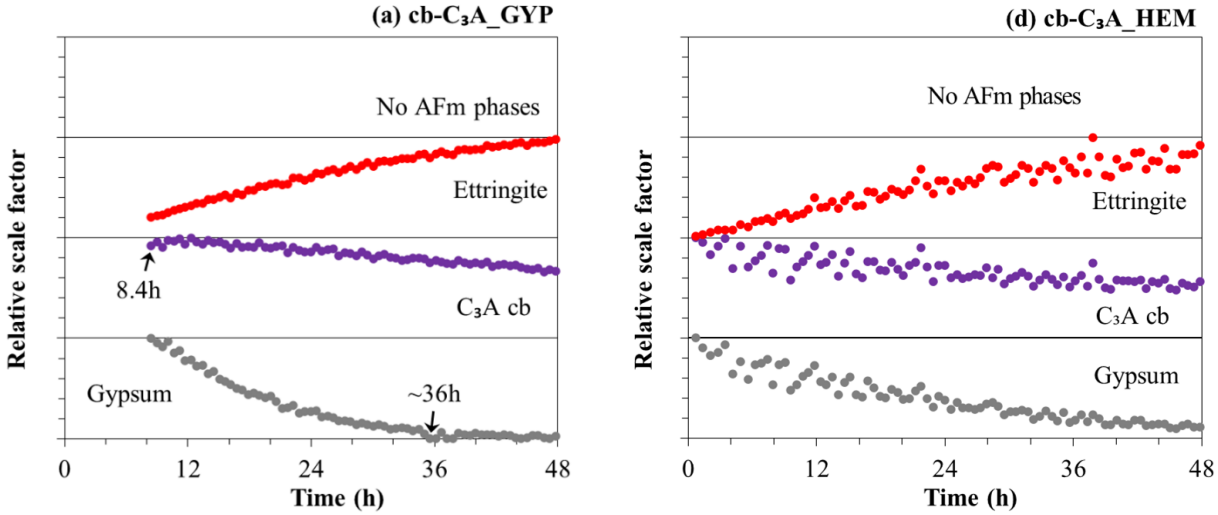

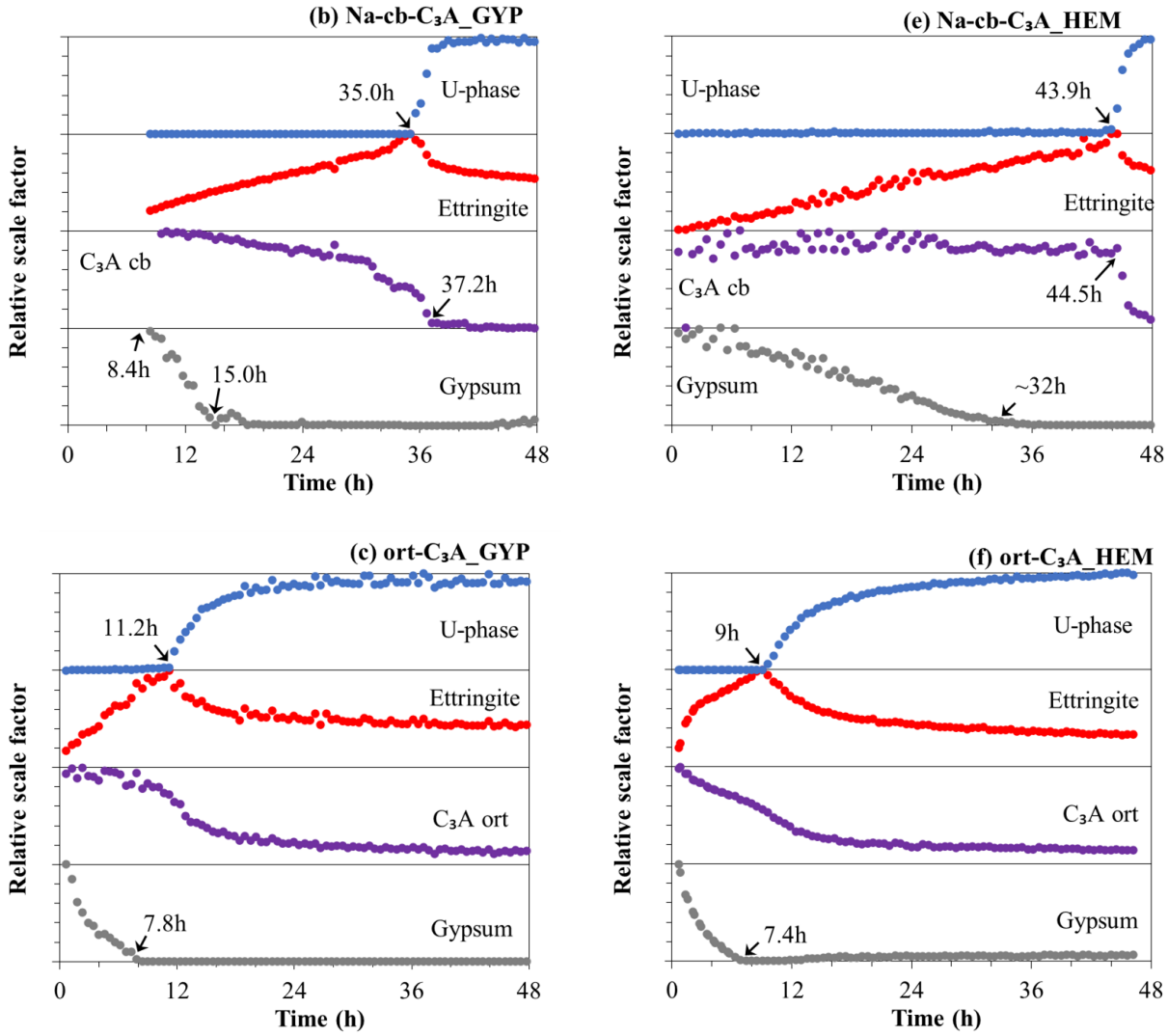

Figure 5.39 – Relative scale factor evolution of the crystalline phases monitored by in-situ XRD: (A) cb-C_3A-GYP, (B) Na-cb-C_3A_GYP, (C) ort-C_3A_GYP pastes, (D) cb-C_3A-HEM, (E) Na-cb-C_3A_HEM, and (F) ort-C_3A_HEM pastes during the first 48 hours of hydration. The lack of data for (a) and (b) within the first hours is explained in the text.

5.3.3 Thermogravimetric analysis (TGA)

Figure 5.9 presents the DTG curves of C_3A pastes with gypsum and hemihydrate at 1 h, 1, 2, and 3 d of hydration. Peaks related to the decomposition of ettringite (80–105 °C), gypsum (120-160 °C), AFm phases (160–190 °C and 270–300 °C), and carbonates (600–750°C) are observed [66]. Figure 5.10 shows the bound water content (in g/100g of paste) up to 3 days of hydration.

At 1 hour, a peak between 240-260 °C was observed for all samples but was not present at 1, 2, and 3 days. This peak corresponds to the thermal decomposition of $Al(OH)_3$ and was also

observed by Myers *et al*. [17] in cb-C_3A, and ort-C_3A pastes with gypsum at 8 minutes of hydration. This phase was not detectable by XRD, which agrees with previous studies [17] that reported that this phase is poorly crystalline.

Following the trends observed in calorimetry and *in-situ* XRD, the ort-C_3A pastes reacted much faster than the cb-C_3A, and Na-cb-C_3A pastes. At 1 hour, the ort-C_3A pastes presented a higher ettringite peak, a lower gypsum peak, and a higher bound water content than the cb-C_3A pastes, indicating its higher reactivity. Furthermore, at 1 day, it is already possible to identify AFm peaks in ort-C_3A. The ort-C_3A reaction is almost complete at this age since no significant changes were observed in TGA curves from 1 to 2 and 3 days, following the calorimetry and XRD results.

NaOH also accelerated the C_3A hydration, but only after 1 day (see Figure 5.10). At 48 hours, the peak of gypsum dehydration is no longer present in the Na-cb-C_3A pastes, and AFm peaks appeared, which agrees with the calorimetry and XRD results. In cb-C_3A pastes, the gypsum peak is still present at 48 hours, which is also consistent with XRD results (see Figure 5.8). In the cb-C_3A_GYP sample, small AFm decomposition peaks are observed at 48 hours, although no AFm was observed in XRD. This discrepancy might result from the low amount of AFm phase at 48 hours in the cb-C_3A samples and of the difficulty in identifying the AFm phases in XRD due to their layered and poorly crystalline nature [43].

Regarding the replacement of gypsum with hemihydrate, the TGA results corroborate with the calorimetry and XRD results. The initial hydration of cb-C_3A and Na-cb-C_3A with gypsum and hemihydrate was very similar. However, after the first day, hemihydrate retarded the cb-C_3A and Na-cb-C_3A hydration compared to gypsum (see Figure 5.10). In turn, the replacement of gypsum with hemihydrate accelerated the ort-C_3A hydration within the first day and was similar afterward.

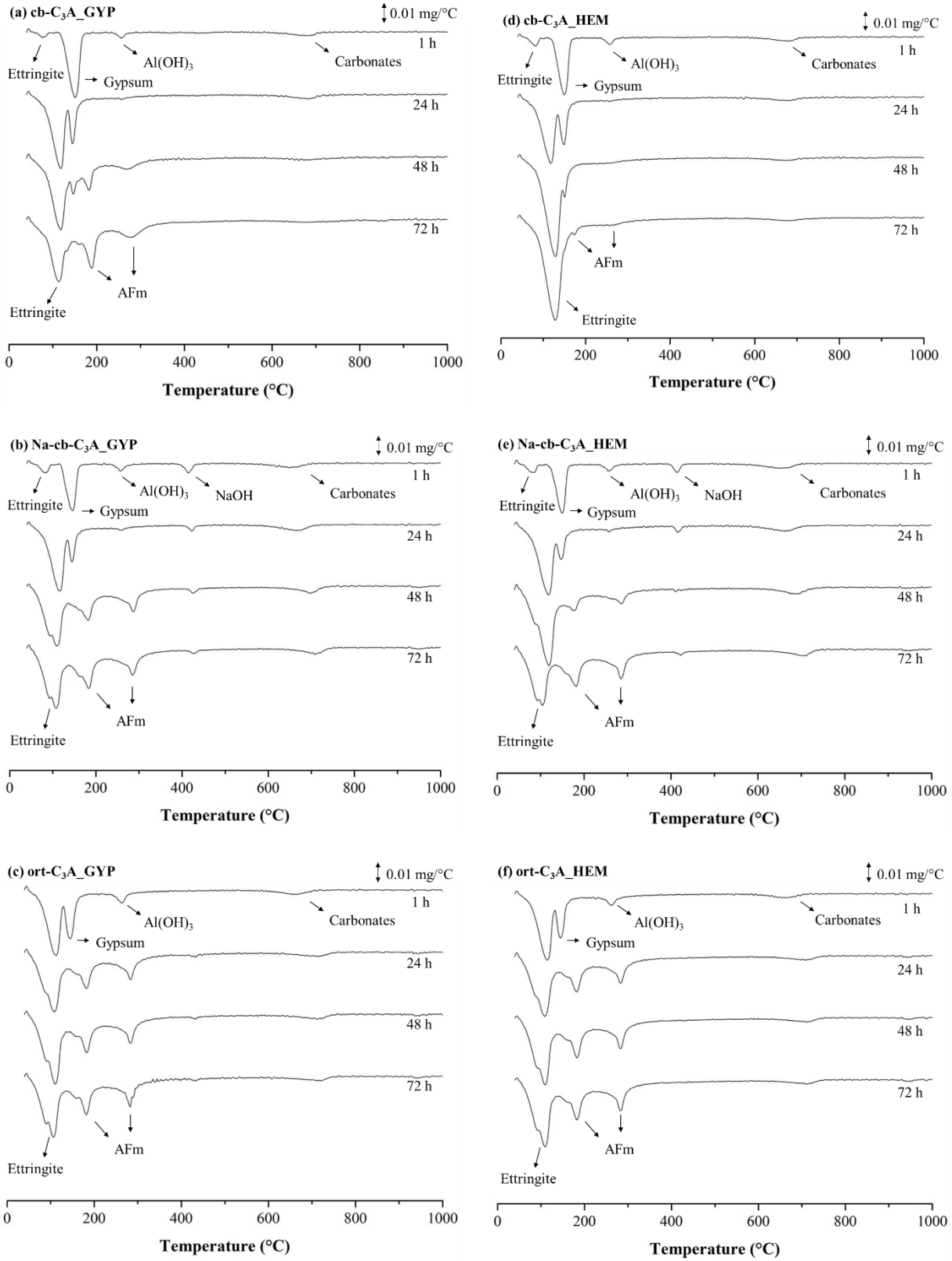

Figure 5.40 – DTG curves of: (A) cb-C_3A-GYP, (B) Na-cb-C_3A_GYP, (C) ort-C_3A_GYP pastes, (D) cb-C_3A-HEM, (E) Na-cb-C_3A_HEM, and (F) ort-C_3A_HEM pastes at 1 h, 24 h, 48 h, and 72 hours of hydration.

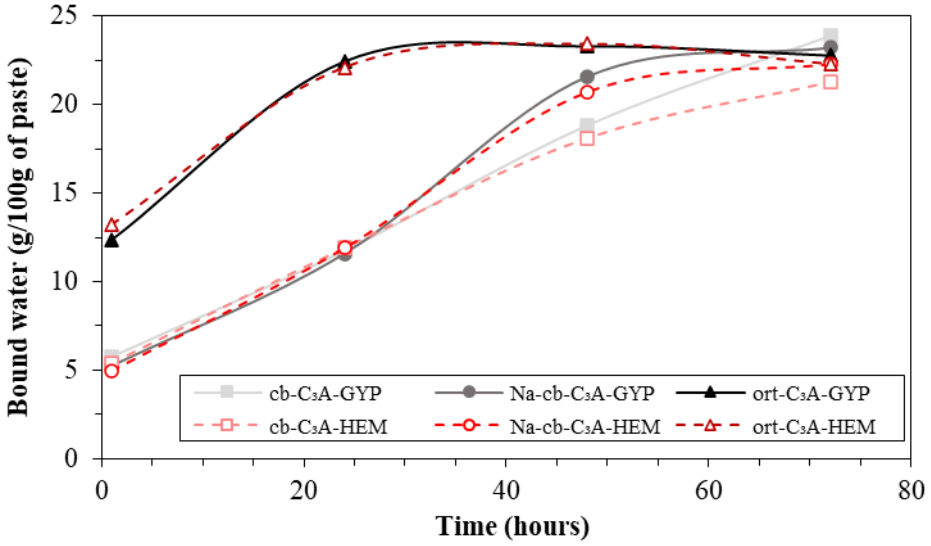

Figure 5.41 – Bound water content (g/100g of paste) of C_3A pastes with gypsum and hemihydrate up to 72 hours of hydration.

5.3.4 Rheometry

Figure 5.11 shows the rheological properties of the C_3A pastes produced with gypsum, and Figure 5.12 shows fresh pastes during the rheological tests. After 120 minutes, both mixes cb-C_3A_GYP and Na-cb-C_3A_GYP remained flowable (Figure 5.11a), while the ort-C_3A_GYP sample was flowable only until 70 minutes. After that, the shearing cycles could not be performed since the sample was already stiff (Figure 5.11b). In turn, the hemihydrate-containing samples lost their workability within the first 10 minutes of hydration when the first shearing cycle was applied (Figure 5.11c); therefore, the rheological evaluation of these mixes was not able to be performed. This is due to the hydration of hemihydrate and consequent precipitation of gypsum -also observed in XRD results and SEM images (Figure C8)-, resulting in the so-called “false set” [33,67].

For all the gypsum-containing mix, the yield stress and viscosity increased exponentially over time (correlations with R^2 of 0.92-0.98). This is consistent with that reported by Jakob et al. [68], which attributed this phenomenon mainly to the change in the solid fraction with water consumption and ettringite formation over time. In addition, the needle-like shape of ettringite can increase the interparticle friction and hinder the flow, increasing the yield stress and the viscosity [69,70].

For the cubic C_3A pastes, this increase was relatively low up to 70 minutes due to the lower ettringite formation within this period, as seen in the SEM images of Figure C5(a,b) and Figure

C6(a,b). At 30 minutes of hydration, only a few ettringite crystals with tenths of a micrometer were found. In turn, at 120 minutes of hydration, more ettringite crystals were found (Figure C5(c,d) and Figure C6(c,d)), corroborating with the hypothesis of Jakob et al. [68]. The presence of NaOH further increased the yield stress and viscosity of paste from 70 to 120 minutes, which can be explained by the higher reaction rate in the presence of such hydroxide (discussed in Sections 5.3.1–5.3.3).

As for the ort-C_3A_GYP paste, a significant amount of ettringite crystals can be found already at 30 minutes of hydration (Figure C7(a,b)) due to the faster ettringite formation of orthorhombic C_3A in the presence of gypsum compared with cubic C_3A, as observed by calorimetry, XRD, and TGA, and as reported by previous studies [12,17,20]. This can explain the several times greater yield stress and viscosity of the mix containing orthorhombic C_3A than those produced with cubic C_3A even at 10 minutes of hydration. These results agree with the results observed by Kirchheim et al. [10], who observed that the ort-C_3A-GYP pastes presented storage modulus (G') three times higher (*i. e.*, lower fluidity) than the cb-C_3A-GYP pastes.

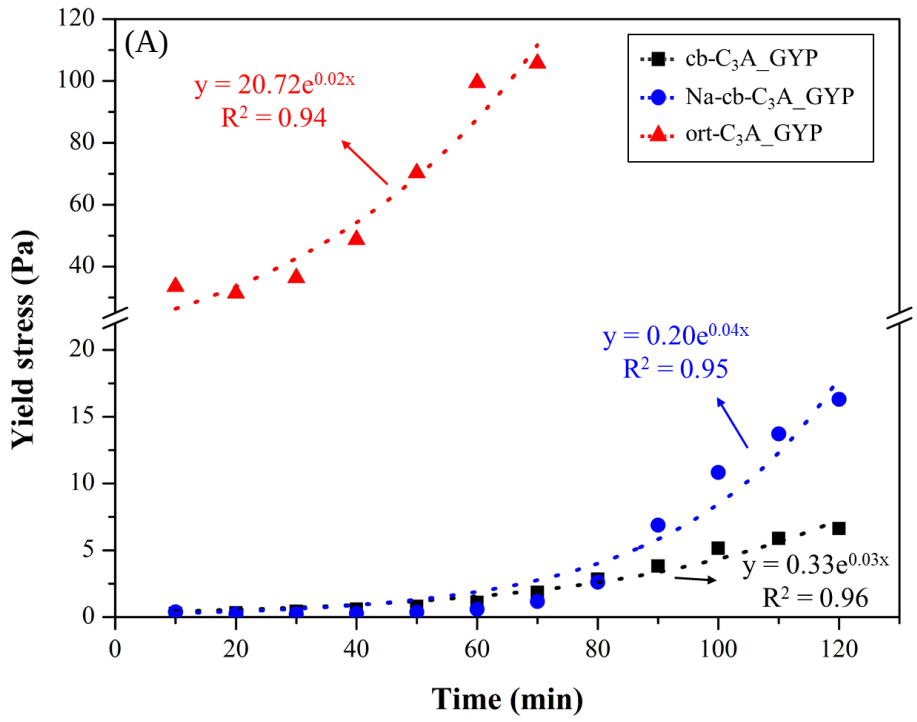

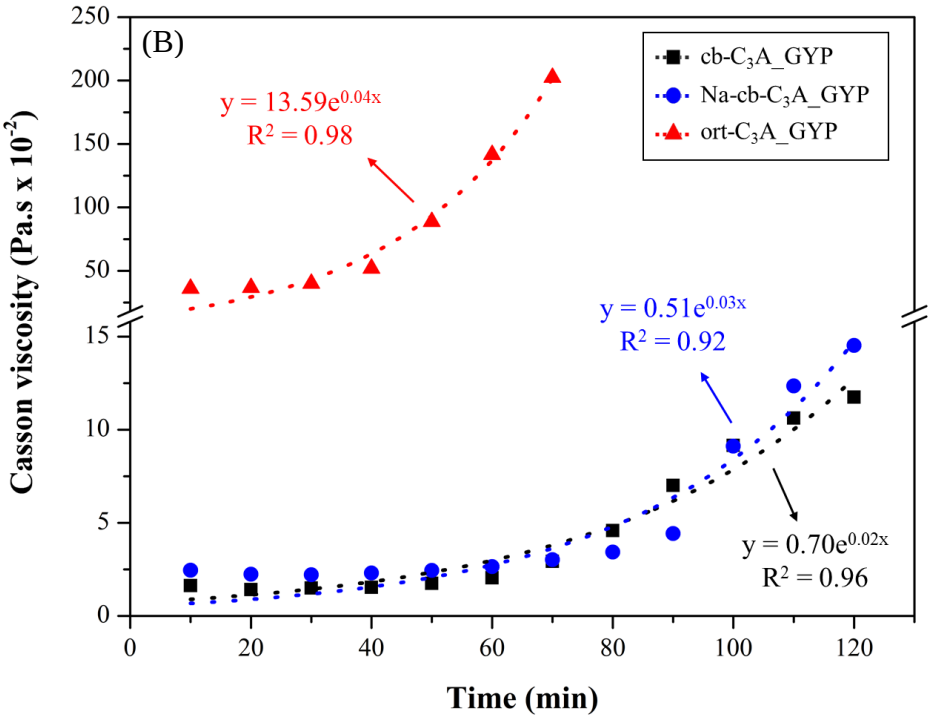

Figure 5.11 – (A) yield stress and (B) Casson viscosity of C_3A-gypsum pastes up to 120 min of hydration.

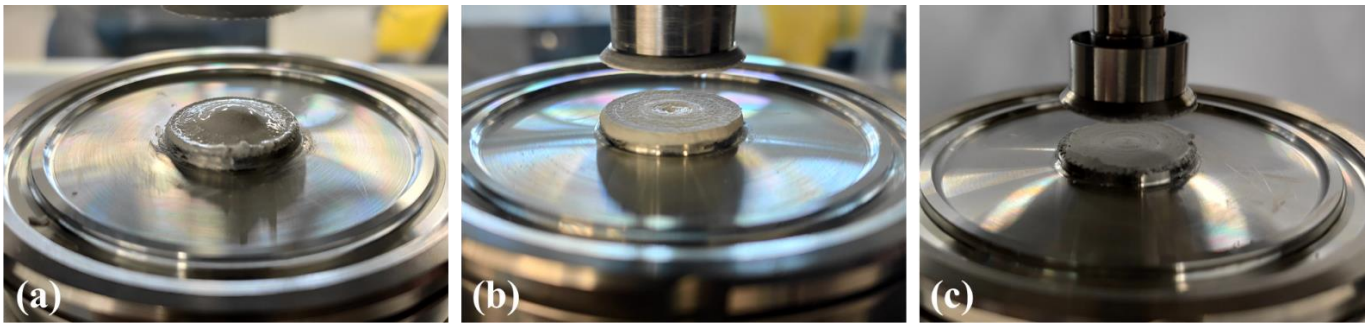

Figure 5.12 – Fresh pastes during the rheological tests. (a) cb-C_3A_GYP after 120 minutes; (b) ort-C_3A_GYP after 120 minutes; (c) cb-C_3A_HEM after 10 minutes.

5.4 DISCUSSION

5.4.1 The role of sodium on the hydration of C_3A

As observed in this study and by several authors [12,17,20], pure ort-C_3A reacts much faster than cb-C_3A in the presence of calcium sulfates. The reason for that is not apparent yet. However, two main hypotheses exist to explain this behavior: (*i*) the dissolution of ort-C_3A releases sodium into the solution, increasing its alkalinity, which would destabilize the

amorphous alumina layer preventing the adsorption of SO_4^{2-} and/or Ca–S ion-pair [16]; and (*ii*) sodium-doping increases the solubility of the ring structures of $Al_6O_{18}^{18-}$, which would impair the formation of the Al-rich leached layer on the C_3A particles, inhibiting the adsorption of SO_4^{2-} and/or Ca–S ion-pair [12,17]. The first hypothesis relates this behavior to the presence of sodium in the solution, while the second relates it to the differences in the crystal structure.

As revealed by our calorimetry, *in-situ* XRD, and TGA, the external sodium incorporation (i.e., the addition of NaOH) did not significantly affect cb-C_3A hydration in the first hours (up to 20-24 hours) but enhanced it after that. In turn, the Na-doped C_3A crystals (i.e., ort-C_3A) had a much higher hydration rate from the beginning, with almost all the C_3A reacted within the first day. From our results, hypothesis (*i*) looks unlikely since, in the Na-cb-C_3A systems, all the sodium was already dissolved in the solution, while the sodium of ort-C_3A was gradually released with its dissolution. Therefore, hypothesis (*i*) predicted that Na-cb-C_3A to react faster than ort-C_3A, which was not validated experimentally. In turn, the predictions of hypothesis (*ii*) agree well with our results: the much higher ort-C_3A reactivity in sulfate-containing solution is related to the difference in crystal structure rather than the presence of sodium in the solution.

The external addition of NaOH anticipated the onset of the second peak and increased the second peak intensity. As observed in Figure C2, the NaOH amount did not impact the moment of the onset, and all samples with NaOH presented the onset of the main hydration peak around 15 hours (*i.e.*, ≈ 10 hours earlier than the cb-C_3A-GYP paste). However, the greater is the NaOH amount (*i.e.*, the higher the NaOH molarity), the higher is the main heat flow peak.

The anticipation of the onset of the second peak due to the NaOH is probably related to the higher solubility of gypsum in NaOH highly alkaline solutions [71]. As observed by Ghorab and Abou El Fetouh [71], gypsum dissolution increases with the increase of NaOH molarity up to 0.05 M of NaOH and remains constant afterward. The higher solubility of gypsum in the NaOH solution anticipates the gypsum depletion -as observed by XRD-, and therefore anticipates the onset of the main heat flow peak -as observed by calorimetry. In addition, as all solutions evaluated here had NaOH molarities higher than 0.05 M (0.24, 0.48, and 0.99 M), gypsum solubility should be similar among these solutions according to the Ghorab and Abou El Fetouh [71] results, which explains why the NaOH molarity did not impact the moment of the onset of the main heat flow peak.

In turn, the increase of the main heat flow peak intensity with the increase of NaOH molarity indicates an increase in the AFm precipitation rate [11]. This is probably related to the amount of Na^+ available for the formation of the U-phase (the only AFm observed in the Na-containing samples). This would increase the rate of U-phase formation, as observed by the higher heat flow peak in Figure C2, but probably did not alter the amount of U-phase formed by the end of the 90 hours, as the cumulative heat was similar. The amount of U-phase formed is depended on the relation between gypsum and C_3A, and as was the same for all the samples, it did not change. Further studies on this topic are encouraged to additional conclusions.

In both Na-cb-C_3A and ort-C_3A pastes, U-phase was formed instead of monosulfate after sulfate depletion. This occurred because sodium was incorporated into the interlayer space of AFm. The U-phase formation led to a decrease in the ettringite content, similar to what is observed during the formation of monosulfate, and this was expected since the U-phase ($4CaO \cdot 0.9Al_2O_3 \cdot 1.1SO_3 \cdot 0.5Na_2O \cdot 16H_2O$) contains sulfate in its composition. Since there is no more sulfate available in the solution, a portion of ettringite decomposed, releasing the sulfate ions required for U-phase formation.

5.4.2 The effect of hemihydrate on the hydration of C_3A polymorphs

The replacement of gypsum with hemihydrate did not have a great impact on the cb-C_3A but delayed the sulfate depletion and the AFm phase formation of the Na-cb-C_3A paste. In turn, for the ort-C_3A, the use of hemihydrate resulted in faster ettringite precipitation and earlier sulfate depletion and U-phase formation when compared to the pastes with gypsum, as shown by calorimetry, XRD, and TGA.

Porchet et al. [35] observed an acceleration in cb-C_3A hydration when replaced gypsum with hemihydrate (when using less than 15 wt% equivalents of gypsum by wt% of C_3A amount). In turn, they observed a delay in cb-C_3A hydration when using higher amounts of calcium sulfate (more than 15 wt% equivalents of gypsum by wt% of C_3A). The reasons for that are still not clear.

Pourchet *et al*. [35] have observed that the use of hemihydrate instead of gypsum in cb-C_3A pastes increases the concentration of Ca and SO_4 in the pore solution, leading to higher super saturation degrees with regarding to the ettringite. As pointed out by the authors, according to the classical nucleation theory, the frequency of nucleation increases with the increase of the

supersaturation degree. Therefore, the higher solubility of hemihydrate may contribute to the increase of ettringite nucleation, with a greater quantity of nuclei, accelerating the ettringite formation and, thus, the sulfate consumption. However, the reason for this only accelerated the sulfate depletion on ort-C_3A and not on cb-C_3A (at least at the gypsum/C_3A ratio used here) is not clear yet. Thus, further studies on this topic are necessary to fully understand the influence of the sulfate source solubility on cb-C_3A and ort-C_3A hydration.

Finally, for all pastes, the use of hemihydrate resulted in early stiffing (the so-called false setting) due to the formation of larger gypsum crystals in the first minutes, as observed by XRD and SEM and also reported in previous studies. This might have important implications for fresh PC concrete, as discussed in the next section.

5.4.3 Implications for fresh PC concrete

The much higher reactivity of ort-C_3A in sulfate-containing solution, compared with cb-C_3A may lead to setting and/or rheology problems in fresh PC concrete. Furthermore, the higher rate of ettringite formation and sulfate depletion may result in sulfate balance issues, leading to undersulfated mixtures, negatively impacting the rheology and early strength of PC concrete.

However, note that there are essential differences between the pure phases -as those studied here- and the phases present in commercial PC, such as the type of alkalis incorporated (in commercial cements, K_2O is usually incorporated in the C_3A structure, while Na_2O is generally used for the synthesis of orthorhombic C_3A in the laboratory); the incorporation of other ions (such as Fe); different particle size distribution and surface area; and mainly the interactions with other clinker phases needs to be kept in mind. Thus, although it is easier to isolate the actuation mechanisms in pure phase systems, further studies with industrial clinkers with different C_3A polymorphs evaluating the sulfate balance, rheology, hydration, and strength are necessary to understand the impact of ort-C_3A on PC concrete fully.

Finally, the use of hemihydrate as the sulfate source may lead to early stiffing (i.e., false set) due to its crystallization into gypsum, as observed in previous studies [67,72] and in the current work, which impairs concrete application and performance. Therefore, the cement industry must control the grinding process to avoid the transformation of gypsum into hemihydrate. Furthermore, since hemihydrate intensifies ort-C_3A reaction, it can also intensify the application issues of ort-C_3A previously discussed.

5.5 CONCLUSIONS

This study has spread light to:

- The orthorhombic C_3A presented faster ettringite precipitation in the first hours and a much earlier sulfate depletion and AFm precipitation compared with cubic C_3A. This is probably related to the differences in crystal structure rather than the release of sodium and the increase of solution alkalinity. The external addition of sodium (i.e., NaOH incorporation) in cubic C_3A paste anticipated the sulfate depletion and the new fast C_3A dissolution. However, it did not significantly influence the cubic C_3A hydration in the first 20-24 hours, while the orthorhombic C_3A had almost entirely reacted by then.

- In pastes with cubic C_3A + NaOH or orthorhombic C_3A, U-phase was formed instead of monosulfate after sulfate depletion, leading to a decrease in ettringite content.

- Orthorhombic C_3A paste produced with gypsum presented viscosity and yield stress values 10-20 times higher than those containing cubic C_3A with and without NaOH, as a result of its much higher reactivity and quick formation of larger ettringite crystals in the first minutes.

- The replacement of gypsum with hemihydrate (in an SO_3/C_3A ratio of 0.29) did not significantly influence cb-C_3A hydration. However, the use of hemihydrate instead of gypsum retarded Na-cb C_3A hydration, delaying the sulfate depletion and AFm formation. In contrast, it had an opposite effect on the hydration of orthorhombic C_3A, increasing the ettringite formation rate and anticipating the sulfate depletion and AFm formation.

- The use of hemihydrate in pastes with either cubic or orthorhombic C_3A resulted in early stiffing (the so-called false set) within the first 10 minutes due to the hydration of hemihydrate and precipitation of larger gypsum crystals, making it lose workability.

Future studies comparing the pore solution composition and pH of the orthorhombic C_3A and cubic C_3A hydrating at NaOH solutions are encouraged to fully understand the main mechanism responsible for the higher ettringite precipitation and early sulfate depletion of orthorhombic C_3A. In addition, future studies with industrial clinkers should address the implications of the difference of C_3A polymorphism on the PC properties (sulfate balance, rheology, hydration,

and strength). The impact of the solubility of the calcium sulfate on cubic and orthorhombic C_3A needs more studies to clarify its mechanisms. Finally, more studies regarding the U-phase are necessary.

5.6 ACKNOWLEDGEMENTS

JSAN, PEM, and PJPG thanks the financial support of CAPES (Coordination for the Improvement of Higher Education Personnel) [88882.439908/2019-01]. JSAN thanks the University of Malaga (Spain), where the experiments for the characterization of the raw materials were performed. JSAN and AGdT also thank the Spanish Junta de Andalucía [P18-RT-720] research project for the research stage at the University of Málaga (Spain) and the Graduate Program in Civil Engineering: Construction and Infrastructure (PPGCI) of the Federal University of Rio Grande do Sul (UFRGS). PRM and PJPG thank the Brazilian funding agency FAPESC. The participation APK and CEMC were sponsored by CNPq (Brazilian National Council for Scientific and Technological Development) through the research fellowships PQ2017 305530/2017- 8 and PQ2019 304756/2019-9. The in-situ XRD data collection was carried out by PRM and CEMC at Laboratório de Difração de Raios-X (LDRX-UFSC). Ms. Patrícia Prates from Laboratório de Materiais (LabMAT-UFSC) is kindly acknowledged for the assistance in the SEM analysis.

5.7 REFERENCES

[1] F. Nishi, Y. Takeuchi, The A16018 Rings of Tetrahedra in the Structure of Cas.sNaA16O18, Acta Crystallographica Section B Structural Crystallography and Crystal Chemistry. 31 (1975) 1169–1173.

[2] Y. Takeuchi, F. Nishi, I. Maki, Structural aspects of the C3A-Na20 solid solutions, in: Proc. 7th International Congress on the Chemistry of Cement, Paris, 1980.

[3] H.F.W. Taylor, Cement chemistry, 2nd ed., Thomas Telford, 1997. https://doi.org/10.1680/cc.25929.

[4] Y. Takéuchi, F. Nishi, Crystal-chemical characterization of the 3 CaO.Al2O3 solid-solution series, Zeitschrift Für Kristallographie. 152 (1980) 259–307.

[5] K. Fukuda, S. Inoue, H. Yoshida, Cationic substitution in tricalcium aluminate, Cement and Concrete Research. 33 (2003) 1771–1775. https://doi.org/10.1016/S0008-8846(03)00172-8.

[6] A.I. Boikova, A.I. Domansky, V.A. Paramonova, THE INFLUENCE OF Na20 ON THE STRUCTURE AND PROPERTIES OF 3CaO.Al203, 7 (1977) 483–491.

[7] P. Mondal, J.W. Jeffery, The Crystal Structure of Triealeium Aluminate, Ca3Al2O6, Acta Crystallographica. (1975) 689.

[8] A.P. Kirchheim, D.C. Dal Molin, P. Fischer, A.H. Emwas, J.L. Provis, P.J.M. Monteiro, Real-time high-resolution X-ray imaging and nuclear magnetic resonance study of the hydration of pure and Na-doped C3A in the presence of sulfates, Inorganic Chemistry. 50 (2011) 1203–1212. https://doi.org/10.1021/ic101460z.

[9] K.L. Scrivener, A. Nonat, Hydration of cementitious materials, present and future, Cement and Concrete Research. 41 (2011) 651–665. https://doi.org/10.1016/j.cemconres.2011.03.026.

[10] A.P. Kirchheim, V. Fernàndez-Altable, P.J.M. Monteiro, D.C.C. Dal Molin, I. Casanova, Analysis of cubic and orthorhombic C3A hydration in presence of gypsum and lime, Journal of Materials Science. 44 (2009) 2038–2045. https://doi.org/10.1007/s10853-009-3292-3.

[11] A. Quennoz, K.L. Scrivener, Hydration of C 3A-gypsum systems, Cement and Concrete Research. 42 (2012) 1032–1041. https://doi.org/10.1016/j.cemconres.2012.04.005.

[12] A.P. Kirchheim, E.D. Rodríguez, R.J. Myers, L.A. Gobbo, P.J.M. Monteiro, D.C.C. Dal Molin, R.B. de Souza, M.A. Cincotto, Effect of gypsum on the early hydration of cubic and Na-doped orthorhombic tricalcium aluminate, Materials. 11 (2018) 1–16. https://doi.org/10.3390/ma11040568.

[13] S. Joseph, J. Skibsted, Ö. Cizer, A quantitative study of the C3A hydration, Cement and Concrete Research. 115 (2019) 145–159. https://doi.org/10.1016/j.cemconres.2018.10.017.

[14] T. Matschei, B. Lothenbach, F.P. Glasser, The role of calcium carbonate in cement hydration, Cement and Concrete Research. 37 (2007) 551–558. https://doi.org/10.1016/j.cemconres.2006.10.013.

[15] T. Matschei, B. Lothenbach, F.P. Glasser, The AFm phase in Portland cement, Cement and Concrete Research. 37 (2007) 118–130. https://doi.org/10.1016/j.cemconres.2006.10.010.

[16] D. Stephan, S. Wistuba, Crystal structure refinement and hydration behaviour of doped tricalcium aluminate, Cement and Concrete Research. 36 (2006) 2011–2020. https://doi.org/10.1016/j.cemconres.2006.06.001.

[17] R.J. Myers, G. Geng, E.D. Rodriguez, P. da Rosa, A.P. Kirchheim, P.J.M. Monteiro, Solution chemistry of cubic and orthorhombic tricalcium aluminate hydration, Cement and Concrete Research. 100 (2017) 176–185. https://doi.org/10.1016/j.cemconres.2017.06.008.

[18] A.P. Kirchheim, D.C. Dal Molin, P. Fischer, A.H. Emwas, J.L. Provis, P.J.M. Monteiro, Real-time high-resolution X-ray imaging and nuclear magnetic resonance study of the hydration of pure and Na-doped C3A in the presence of sulfates, Inorganic Chemistry. 50 (2011) 1203–1212. https://doi.org/10.1021/ic101460z.

[19] J. Cheung, A. Jeknavorian, L. Roberts, D. Silva, Impact of admixtures on the hydration kinetics of Portland cement, Cement and Concrete Research. 41 (2011) 1289–1309. https://doi.org/10.1016/j.cemconres.2011.03.005.

[20] M.M. Alonso, F. Puertas, Adsorption of PCE and PNS superplasticisers on cubic and orthorhombic C3A. Effect of sulfate, Construction and Building Materials. 78 (2015) 324–332. https://doi.org/10.1016/j.conbuildmat.2014.12.050.

[21] E. Dubina, J. Plank, L. Black, L. Wadsö, Impact of environmental moisture on C3A polymorphs in the absence and presencemof CaSO4 .0.5H2O, Advance and Cement Research. 26 (2014) 29–40.

[22] E. Dubina, J. Plank, L. Black, Impact of water vapour and carbon dioxide on surface composition of C3A polymorphs studied by X-ray photoelectron spectroscopy, Cement and Concrete Research. 73 (2015) 36–41. https://doi.org/10.1016/j.cemconres.2015.02.026.

[23] R.J. Myers, G. Geng, J. Li, E.D. Rodríguez, J. Ha, P. Kidkhunthod, G. Sposito, L.N. Lammers, A.P. Kirchheim, P.J.M. Monteiro, Role of adsorption phenomena in cubic tricalcium aluminate dissolution, Langmuir. 33 (2016) 45–55. https://doi.org/10.1021/acs.langmuir.6b03474.

[24] G. Geng, R.J. Myers, Y.-S. Yu, D.A. Shapiro, R. Winarski, P.E. Levitz, D.A.L. Kilcoyne, P.J.M. Monteiro, Synchrotron X-ray nanotomographic and spectromicroscopic study of the tricalcium aluminate hydration in the presence of gypsum, Cement and Concrete Research. 111 (2018) 130–137. https://doi.org/10.1016/j.cemconres.2018.06.002.

[25] X. Liu, P. Feng, C. Lyu, S. Ye, The role of sulfate ions in tricalcium aluminate hydration: New insights, Cement and Concrete Research. 130 (2020) 105973. https://doi.org/10.1016/j.cemconres.2020.105973.

[26] F.P. Glasser, M.B. Marinho, Early stages of the hydration of tricalcium aluminate and its sodium-cotaining solid solutions, Proceedings of the British Ceramic Society. 35 (1984) 221–236.

[27] Y. Shimada, J.F. Young, Thermal stability of ettringite in alkaline solutions at 80 j C, 34 (2004) 2261–2268. https://doi.org/10.1016/j.cemconres.2004.04.008.

[28] G. Li, P. le Bescop, M. Moranville, The U phase formation in cement-based systems containing high amounts of Na2SO4, Cement and Concrete Research. 26 (1996) 27–33. https://doi.org/https://doi.org/10.1016/0008-8846(95)00189-1.

[29] G. Li, P. le Bescop, M. Moranville-Regourd, Synthesis of the U phase (4CaO . 0.9Al2O3 . 1.1SO3. 0.5Na2O . 16H2O), Cement and Concrete Research. 27 (1997) 7–13. https://doi.org/10.1016/S0008-8846(96)00194-9.

[30] B.A. Clark, P.W. Brown, Formation of ettringite from monosubstituted calcium sulfoaluminate hydrate and gypsum, Journal of the American Ceramic Society. 82 (1999) 2900–2905. https://doi.org/10.1111/j.1151-2916.1999.tb02174.x.

[31] B.A. Clark, P.W. Brown, Formation of calcium sulfoaluminate hydrate compounds. Part II, Cement and Concrete Research. 30 (2000) 233–240. https://doi.org/10.1016/S0008-8846(99)00234-3.

[32] S.J. Way, A. Shayan, Early hydration of a portland cement in water and sodium hydroxide solutions: Composition of solutions and nature of solid phases, Cement and Concrete Research. 19 (1989) 759–769. https://doi.org/10.1016/0008-8846(89)90046-X.

[33] J. da S. Andrade Neto, A.G. de la Torre, A.P. Kirchheim, Effects of sulfates on the hydration of Portland cement – A review, Construction and Building Materials. 279 (2021). https://doi.org/10.1016/j.conbuildmat.2021.122428.

[34] V.H. Dodson, T.D. Hayden, Another look at the Portland cement/chemical admixture incompatibility problem, Cement, Concrete and Aggregates. 11 (1989) 52–56. https://doi.org/10.1520/cca10102j.

[35] S. Pourchet, L. Regnaud, J.P. Perez, A. Nonat, Early C3A hydration in the presence of different kinds of calcium sulfate, Cement and Concrete Research. 39 (2009) 989–996. https://doi.org/10.1016/j.cemconres.2009.07.019.

[36] F. Zunino, K. Scrivener, Factors influencing the sulfate balance in pure phase C3S/C3A systems, Cement and Concrete Research. 133 (2020) 106085. https://doi.org/10.1016/j.cemconres.2020.106085.

[37] P.J. Sandberg, L.R. Roberts, Cement-Admixture Interactions Related to Aluminate Control, 2 (2005) 1–14.

[38] P.K. Mehta, P.J.M. Monteiro, Concrete: Microstructure, Properties, and Materials, 4th ed., McGraw-Hill Professional Publishing, 2014.

[39] P.J. Sandberg, L.R. Roberts, Cement-admixture interactions related to aluminate control, Journal of ASTM International. 2 (2005) 219–232. https://doi.org/10.1520/jai12296.

[40] M. Palacios, H. Kazemi-Kamyab, S. Mantellato, P. Bowen, Laser diffraction and gas adsorption techniques, in: K. Scrivener, R. Snellings, B. Lothenbach (Eds.), A Practical Guide to Microstructural Analysis of Cementitious Materials, 1st ed., CRC Press, 2016: pp. 445–480.

[41] L. Black, C. Breen, J. Yarwood, C.-S. Deng, J. Phipps, G. Maitland, Hydration of tricalcium aluminate (C A) in the presence and absence of gypsum—studied by Raman spectroscopy and X-ray diffraction, Journal of Materials Chemistry. (2006) 1–21. https://doi.org/https://doi.org/10.1039/B509904H.

[42] L. Wadsö, Operational issues in isothermal calorimetry, Cement and Concrete Research. 40 (2010) 1129–1137. https://doi.org/10.1016/j.cemconres.2010.03.017.

[43] D. Ectors, Advances in the analysis of cementitious reactions and hydrate phases, 2016.

[44] F. Goetz-Neunhoeffer, J. Neubauer, Refined ettringite (Ca 6 Al 2 (SO 4) 3 (OH) 12 ·26H 2 O) structure for quantitative X-ray diffraction analysis , Powder Diffraction. 21 (2006) 4–11. https://doi.org/10.1154/1.2146207.

[45] Á.G. de la Torre, M.-G. López-Olmo, C. Álvarez-Rua, S. García-Granda, Miguel.A.G. Aranda, Structure and microstructure of gypsum and its relevance to Rietveld quantitative phase analyses, Powder Diffraction. 19 (2004) 240–246. https://doi.org/10.1154/1.1725254.

[46] C. Bezou, A. Nonat, J.C. Mutin, A. Nørlund Christensen, M.S. Lehmann, Investigation of the crystal structure of γ-CaSO4, CaSO4 · 0.5 H2O, and CaSO4 · 0.6 H2O by powder diffraction methods, Journal of Solid State Chemistry. 117 (1995) 165–176. https://doi.org/10.1006/jssc.1995.1260.

[47] K. Post, H. Pollmann, PDF 00-044-0272, ICDD Grant-in-Aid, Friedrich-Alexander-Universität. (1992).

[48] S. Scherb, N. Beuntner, K.C. Thienel, J. Neubauer, Quantitative X-ray diffraction of free, not chemically bound water with the PONKCS method, Journal of Applied Crystallography. 51 (2018) 1535–1543. https://doi.org/10.1107/S1600576718012888.

[49] C. Guo, E. Wang, X. Hou, J. Chen, W. Zhang, J. Ye, Characterization and mechanism of early hydration of calcium aluminate cement with anatase-TiO 2 nanospheres additive, Construction and Building Materials. 261 (2020) 119922. https://doi.org/10.1016/j.conbuildmat.2020.119922.

[50] L.J. Gardner, S.A. Walling, C.L. Corkhill, S.A. Bernal, V. Lejeune, M.C. Stennett, J.L. Provis, N.C. Hyatt, Cement and Concrete Research Temperature transformation of blended magnesium potassium phosphate cement binders, Cement and Concrete Research. 141 (2021) 106332. https://doi.org/10.1016/j.cemconres.2020.106332.

[51] C. Shunman, A. Wu, W. Yiming, W. Wei, Coupled effects of curing stress and curing temperature on mechanical and physical properties of cemented paste backfill, Construction and Building Materials. 273 (2021) 121746. https://doi.org/10.1016/j.conbuildmat.2020.121746.

[52] A. Quennoz, K.L. Scrivener, Interactions between alite and C3A-gypsum hydrations in model cements, Cement and Concrete Research. 44 (2013) 46–54. https://doi.org/10.1016/j.cemconres.2012.10.018.

[53] R.J. Hill, C.J. Howard, Quantitative phase analysis from neutron powder diffraction data using the Rietveld method, Journal of Applied Crystallography. 20 (1987) 467–474. https://doi.org/10.1107/S0021889887086199.

[54] P. Thompson, D.E. Cox, J.B. Hastings, Rietveld Refinement of Debye-Scherrer Synchrotron X-ray Data from Al203, Journal of Applied Crystallography. 20 (1987) 79–83.

[55] W.A. Dollase, Correction of Intensities for Preferred Orientation in Powder Diffractometry: Application of the March Model, Journal of Applied Crystallography. 19 (1986) 267–272.

[56] J.D. Zea-Garcia, A.G. de la Torre, M.A.G. Aranda, I. Santacruz, Processing and characterisation of standard and doped alite-belite-ye'elimite ecocement pastes and mortars, Cement and Concrete Research. 127 (2020). https://doi.org/10.1016/j.cemconres.2019.105911.

[57] N. Casson, A Flow Equation for Pigment-Oil Suspensions of the Printing Ink Type, in: C.C. Mill (Ed.), Rheology of Disperse Systems, Pergamon Press, Oxford, 1959: pp. 84–104.

[58] H. Li, S. Ding, L. Zhang, J. Ouyang, B. Han, Rheological behaviors of cement pastes with multi-layer graphene, Construction and Building Materials. 269 (2021) 121327. https://doi.org/10.1016/j.conbuildmat.2020.121327.

[59] X. Zhang, J. Han, The effect of ultra-fine admixture on the rheological property of cement paste, Cement and Concrete Research. 30 (2000) 827–830. https://doi.org/10.1016/S0008-8846(00)00236-2.

[60] M. Nehdi, M.A. Rahman, Estimating rheological properties of cement pastes using various rheological models for different test geometry, gap and surface friction, Cement and Concrete Research. 34 (2004) 1993–2007. https://doi.org/10.1016/j.cemconres.2004.02.020.

[61] H. Minard, S. Garrault, L. Regnaud, A. Nonat, Mechanisms and parameters controlling the tricalcium aluminate reactivity in the presence of gypsum, Cement and Concrete Research. 37 (2007) 1418–1426. https://doi.org/10.1016/j.cemconres.2007.06.001.

[62] A.S. Brand, S.B. Feldman, P.E. Stutzman, A. v. Ievlev, M. Lorenz, D.C. Pagan, S. Nair, J.M. Gorham, J.W. Bullard, Dissolution and initial hydration behavior of tricalcium aluminate in low activity sulfate solutions, Cement and Concrete Research. 130 (2020) 105989. https://doi.org/10.1016/j.cemconres.2020.105989.

[63] M. García-Maté, A.G. de La Torre, L. León-Reina, E.R. Losilla, M.A.G. Aranda, I. Santacruz, Effect of calcium sulfate source on the hydration of calcium sulfoaluminate eco-cement, Cement and Concrete Composites. 55 (2015) 53–61. https://doi.org/10.1016/j.cemconcomp.2014.08.003.

[64] M.J. Sánchez-Herrero, A. Fernández-Jiménez, A. Palomo, C4A3Š hydration in different alkaline media, Cement and Concrete Research. 46 (2013) 41–49. https://doi.org/10.1016/j.cemconres.2013.01.008.

[65] D. Jansen, Ch. Naber, D. Ectors, Z. Lu, X.-M. Kong, F. Goetz-Neunhoeffer, J. Neubauer, The early hydration of OPC investigated by in-situ XRD, heat flow calorimetry, pore water analysis and 1H NMR: Learning about adsorbed ions from a complete mass balance approach, Cement and Concrete Research. 109 (2018) 230–242. https://doi.org/10.1016/j.cemconres.2018.04.017.

[66] B. Lothenbach, P.T. Durdziński, K. de Weerdt, Thermogravimetric analysis, in: K. Scrivener, R. Snellings, B. Lothenbach (Eds.), A Practical Guide to Microstructural Analysis of Cementitious Materials, 1st ed., CRC Press, 2016: pp. 177–212.

[67] C.W. Chung, P. Suraneni, J.S. Popovics, L.J. Struble, Using ultrasonic wave reflection to monitor false set of cement paste, Cement and Concrete Composites. 84 (2017) 10–18. https://doi.org/10.1016/j.cemconcomp.2017.08.010.

[68] C. Jakob, D. Jansen, N. Ukrainczyk, E. Koenders, U. Pott, D. Stephan, J. Neubauer, Relating ettringite formation and rheological changes during the initial cement hydration: A comparative study applying XRD analysis, rheological measurements and modeling, Materials. 12 (2019). https://doi.org/10.3390/ma12182957.

[69] R. Talero, C. Pedrajas, M. González, C. Aramburo, A. Blázquez, V. Rahhal, Role of the filler on Portland cement hydration at very early ages: Rheological behaviour of their fresh cement pastes, Construction and Building Materials. 151 (2017) 939–949. https://doi.org/10.1016/j.conbuildmat.2017.06.006.

[70] P.R. de Matos, L.R. Prudêncio, R. Pilar, P.J.P. Gleize, F. Pelisser, Use of recycled water from mixer truck wash in concrete: Effect on the hydration, fresh and hardened properties, Construction and Building Materials. 230 (2020) 116981. https://doi.org/10.1016/j.conbuildmat.2019.116981.

[71] H.Y. Ghorab, S.H. Abou el Fetou, Factors Affecting the Solubility of Gypsum: II. Effect of Sodium Hydroxide under Various Conditions, Journal of Chemical Technology and Biotechnology. 35 A (1985) 36–40. https://doi.org/10.1002/jctb.5040350107.

[72] R.M. Mota, A.S. Silva, V.H.S. Ramos, J.C.T. Rezende, E. de Jesus, Effects of storage temperature and time on false setting behavior of CPI-S Portland cement, Ceramica. 66 (2020) 321–329. https://doi.org/10.1590/0366-69132020663792842.

Chapter 6

Hydration and interactions between C_3S and C_3A polymorphs in the presence of different calcium sulfates

Chapter 6 is based on the article:

José S. Andrade Neto, Paulo R. de Matos, Angeles G. de la Torre, Carlos E. M. Campos, Sandro M. Torres, Paulo J. M. Monteiro, Ana Paula Kirchheim. Hydration and interactions between C_3S and C_3A polymorphs in the presence of different calcium sulfates. Submitted to **Cement and Concrete Research**.

6 HYDRATION AND INTERACTIONS BETWEEN C_3S AND C_3A POLYMORPHS IN THE PRESENCE OF DIFFERENT CALCIUM SULFATES

ABSTRACT

This research studied the hydration of C_3S-C_3A-calcium sulfate systems made of combinations of two C_3S (triclinic pure C_3S and monoclinic Al-doped C_3S), two C_3A polymorphs (cubic and orthorhombic), and two calcium sulfates (gypsum and hemihydrate). For each system, the hydration of four different SO_3 contents (0.25-2.0 wt%) was assessed by calorimetry. The optimum SO_3 content was fixed from calorimetry results, and the mixtures were evaluated by *in-situ* XRD and TGA. The type of C_3S was the factor that most affected the sulfate balance of the systems. The mixes with Al-C_3S produced a higher amount of ettringite in the first hours, resulting in much earlier sulfate depletions when compared to the mixes with C_3S. The mixes with ort-C_3A also showed faster sulfate depletion due to its higher reactivity compared with cb-C_3A. Finally, the replacement of gypsum by hemihydrate resulted in faster sulfate depletion caused by the higher hemihydrate solubility.

Keywords: C_3S; C_3A; Calcium sulfate; Polymorphism; Hydration.

6.1 INTRODUCTION

Calcium sulfate, such as gypsum and/or anhydrite, is added to the Portland clinker to control the C_3A hydration and prevent flash set [1]. In addition, the amount of calcium sulfate added needs to be enough to delay the renewed hydration of C_3A until after the main C_3S hydration peak. Otherwise, the C_3S hydration is hindered, negatively affecting the early strength of Portland cement (PC) concrete [1]. However, if an excess of sulfate is used, the mechanical strength decreases [1–4], and durability problems with delayed ettringite formation (DEF) in pastes cured at high temperatures may occur [5,6]. Thus, there is an optimum sulfate content in which the mixture presents the lowest shrinkage and highest compressive strength without causing problems of quick setting and DEF. In a properly sulfated cement, the calcium sulfate depletion and the renewed hydration of C_3A occur after the main C_3S hydration. Therefore, factors interfering in sulfate's supply or consumption will affect the optimum sulfate content [1,7]. Sulfate ions are mainly supplied by calcium and alkaline sulfates dissolution and consumed by the ettringite formation and C-S-H adsorption [1].

Zunino and Scrivener [7] showed that increasing C_3S and C_3A fineness – and consequently their reactivities – increases the C-S-H and ettringite formation and increases the optimum amount of calcium sulfate. In addition to their fineness, the polymorphism and ion doping of C_3S and C_3A also change their reactivities [1,8–14]. However, to the best of the authors' knowledge, no systematic study regarding the C_3S and C_3A polymorphism on the optimum sulfate content was reported. The correct understanding of the influence of polymorphism or ion doping on the optimization of sulfates is essential to ensure that the cements meet performance requirements.

The incorporation of aluminum in C_3S decreases its reactivity [8–11]. With aluminum-doped C_3S (Al-C_3S) dissolution, the aluminum ions are released in the solution, which is known to retard C_3S hydration [10,15–17]. The reason for that is not clear, but it may be related to the formation of C-A-S-H, which according to some authors [10,16] is not a good substrate for the C-S-H growth as the C-S-H nuclei itself, or it may be related to the condensation of aluminum-silicate species at C_3S surface [15,17]. Either way, the delay in the C_3S hydration decreases the amount of C-S-H formed in the first days and tends to reduce the amount of sulfate consumption due to adsorption by C-S-H. However, the aluminum coming from Al-C_3S dissolution may contribute to ettringite formation. Although, as pointed out by Jansen et al. [18], it is not yet clear if the aluminum coming from the alite/Al-C_3S plays a role in the sulfate demand or not.

Therefore, the incorporation of aluminum in C_3S may change the optimum sulfate content of cement, but which phenomenon is predominant (i.e., lower sulfate adsorption by C-S-H or higher sulfate consumption by ettringite formation) is still not known.

Regarding the aluminates, the polymorphism of C_3A depends on the sulfate/alkali balance during clinker production, and therefore the alkali content incorporated in the C_3A structure. In industrial Portland clinkers, the C_3A may be present as cubic (cb-C_3A) and/or orthorhombic (ort-C_3A) polymorphs [19,20], depending on the raw materials and fuel used. Despite forming the same hydration products (ettringite and AFm phases), ort-C_3A reacts much faster than cb-C_3A in the presence of calcium sulfate [12–14]. This will probably influence the sulfate balance in the PC hydration, but no study regarding this has been published to date, and there is a gap on this topic.

Finally, during cement milling, gypsum ($CaSO_4 \cdot 2H_2O$) may dehydrate into hemihydrate ($CaSO_4 \cdot 1/2H_2O$) and/or soluble anhydrite ($CaSO_4$), which are much more soluble than gypsum or natural anhydrite [21,22]. As shown by previous studies, gypsum delays the initial hydration of C_3S, prolonging the induction period, but enhances afterward, resulting in higher main heat flow peaks. However, no studies regarding the effect of hemihydrate on C_3S have been conducted yet. In relation to C_3A, as showed by Andrade Neto et al. [14], the replacement of gypsum with hemihydrate did not significantly influence cb-C_3A but accelerated ort-C_3A reaction. The authors used only one sulfate/C_3A ratio, and the effect of different gypsum/hemihydrate content on the cb- and ort-C_3A hydration need further studies to understand better their impact on the sulfate balance of Portland cements.

Zunino and Scrivener [7] studied the T1-C_3S/cb-C_3A systems and reported that the use of hemihydrate instead of gypsum resulted in higher ettringite precipitation until the renewed hydration of C_3A. This occurs due to the faster dissolution rate of hemihydrate than gypsum, resulting in more sulfate ions in the pore solutions [7]. The higher ettringite precipitation leads to an earlier sulfate depletion, increasing the sulfate demand of the mixtures. However, how this change in sulfate source will influence the sulfate balance of systems with Al-C_3S or with ort-C_3A, which have quite different reactivities than C_3S and cb-C_3A, is an important question to answer.

The objective of the present study is to evaluate the influence of the aluminum doping C_3S, the C_3A polymorph, and the calcium sulfate type on the hydration and sulfate demand of the system

and their interactions. Additionally, it is studied the effect of calcium sulfate composition (gypsum/hemihydrate) on the C_3S and Al-C_3S hydration and the effect of different gypsum/hemihydrate contents on the cb-C_3A and ort-C_3A hydrations. First, the hydration of the C_3S and C_3A polymorphs (alone and in the presence of gypsum or hemihydrate) was evaluated separately through isothermal calorimetry. Then, mixtures of both types of C_3S and C_3A in a constant C_3S/C_3A ratio of 92/8 were produced with four different contents of gypsum or hemihydrate and were also evaluated by calorimetry. An optimum SO_3 content was fixed from these results, and the hydration of the mixes was evaluated by *in-situ* XRD and TGA.

6.2 MATERIALS AND METHODS

6.2.1 Materials

Powder samples of C_3S, aluminum-doped C_3S (Al-C_3S), cubic C_3A (cb-C_3A), and orthorhombic C_3A (ort-C_3A) were acquired from Mineral Research Processing Cie (MRPC, France). The C_3S and Al-C_3S were synthesized at MRPC by heating a stoichiometric mixture of reagent grade $CaCO_3$ and SiO_2 at around 1450°C. Cb-C_3A and ort-C_3A were synthesized by heating twice at 1350°C, a stoichiometric mixture of calcium carbonate ($CaCO_3$) and alumina (Al_2O_3). For the ort-C_3A, sodium carbonate ($NaCO_3$) was also used. High purity (>96 wt%) natural gypsum ($CaSO_4 \cdot 2H_2O$) and hemihydrate ($CaSO_4 \cdot 1/2H_2O$) were used as calcium sulfate sources. Hemihydrate was prepared by heating the gypsum at 100 °C for 48 hours. Details about elemental composition and mineralogy have been reported elsewhere [11,14] and are presented in the Supplementary Materials (Tables D1 and D2). The C_3S is mainly consisted of triclinic (T1) C_3S (95.7 wt%), while the Al-C_3S has 98.7 wt% of monoclinic (M1) C_3S. The C_3S does not have aluminum in its composition, while Al-C_3S has 0.8 wt.%. Cub-C_3A has 96.9% of cubic C_3A, while ort-C_3A has 94.4 wt.% of orthorhombic C_3A and 5.6 wt.% of cubic C_3A. Finally, the gypsum and the hemihydrate are 96.1 wt.% and 97.2 wt.% pure.

Figure 6.42 shows the particle size distribution with details of BET surface area, Dv_{10}, Dv_{50} and Dv_{90} as an inset. The particle size distribution was determined by laser diffraction, using a PSA 1090 equipment from Anton Paar (Graz, Austria), using isopropanol as the dispersant, and considering Mie theory [24]. The BET surface area was determined using an ASAP 2420 equipment from Micromeritics (Georgia, USA).

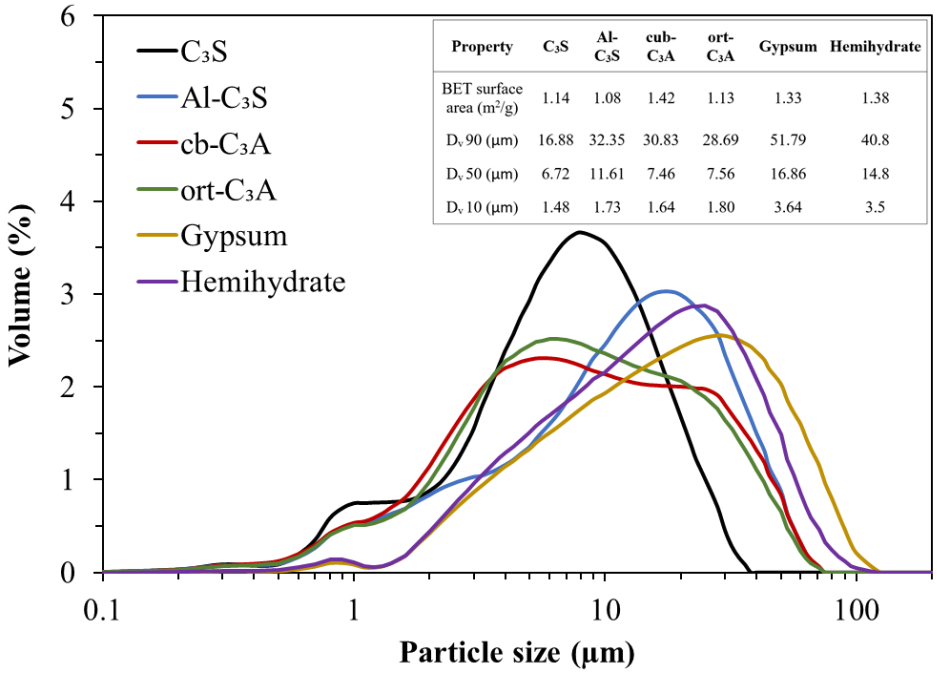

Property	C_3S	Al-C_3S	cub-C_3A	ort-C_3A	Gypsum	Hemihydrate
BET surface area (m^2/g)	1.14	1.08	1.42	1.13	1.33	1.38
D_v90 (µm)	16.88	32.35	30.83	28.69	51.79	40.8
D_v50 (µm)	6.72	11.61	7.46	7.56	16.86	14.8
D_v10 (µm)	1.48	1.73	1.64	1.80	3.64	3.5

Figure 6.42 – Particle size distribution of the raw materials.

6.2.2 Methods

6.2.2.1 Mixture proportions and sample preparation

Firstly, the hydration of C_3S and Al-C_3S alone and in the presence of gypsum or hemihydrate were evaluated by isothermal calorimetry (see section 6.2.2.2). For this purpose, a water-to-solid ratio of 0.50 by mass was used. In the mixes with gypsum or hemihydrate, the C_3S was replaced with the amount of calcium sulfate to result in an SO_3 content of 1.5 wt% (≈ 3.22 wt% of gypsum or ≈ 2.81 wt% of hemihydrate). This SO_3 content was chosen as the one that resulted in properly sulfated C_3S/C_3A mixes (see Section 6.3.1.2) and used to analyze the three-phase systems.

The hydration of cb-C_3A and ort-C_3A, alone and in the presence of gypsum or hemihydrate, were also assessed by calorimetry. A water-to-solid ratio of 1.0 by mass was used for these mixes because it is enough to hydrate the C_3A fully and provide good workability. Different amounts of calcium sulfate were used, resulting in mixtures with SO_3-to-C_3A ratios of 0, 0.03, 0.06 and 0.12 by weight (≈ 0, 5.9, 11.6, and 21.4 wt% of gypsum or ≈ 0, 5.2, 10.3, 19.2 wt% of hemihydrate). These values were chosen as corresponds to the SO_3-to-C_3A ratios of the binary mixes with 0.25%, 0.50% and 1.00% of SO_3.

Mixtures of C_3S (C_3S or Al-C_3S) with C_3A (cb-C_3A or ort-C_3A) and different amounts of gypsum or hemihydrate were evaluated. The C_3S/C_3A ratio was fixed at 92/8 by weight, which is the same ratio used by Zunino and Scrivener [7] and Quennoz and Scrivener [27] and is similar to the ratio usually found in Portland cement clinkers. The water/solid ratio of all mixtures was kept at 0.50 by weight. Firstly, the hydration of C_3S/C_3A systems with four different contents of calcium sulfate (gypsum or hemihydrate), totalizing 32 mixtures, was evaluated by isothermal calorimetry. From these results, a 1.5 wt% SO_3 content was fixed for all the mixtures for the other analysis, i.e., *in situ* XRD and TGA (see sections 6.2.2.3 and 6.2.2.4, respectively). This content was chosen since none of the C_3S/C_3A systems was undersulfated on this level of sulfates (for more details, see section 6.3.1.3).

For the preparation of the pastes, 2 g of anhydrous materials (C_3S, C_3A, and calcium sulfate) were previously manually mixed in an agate mortar for 10 minutes, subsequently mixed with distilled water at 350 rpm for 2 minutes using a rotational mixer. For the calorimetry analysis, the mixing procedure was conducted in the glass ampoule used in the test. The plastic rod was left inside the glass ampoule to minimize the loss of material during mixing. The mixing procedure and insertion of glass ampoule in the calorimetry took less than 3 minutes after the initial contact with the water. For the TGA and *in-situ* XRD tests, the mixes were prepared in plastic vessels. For the TGA analysis, the paste remained inside the hermetically closed vessels until the hydration stoppage.

The hydration of the pastes was stopped at 8 hours, 1, 3, and 7 days for the TGA. The pastes were first ground to a fine powder using an agate mortar. Then, ~0.5 g of each paste was mixed with 25 ml of isopropanol for 30 minutes while stirring. In the sequence, the sample was filtered at a low vacuum through a nylon filter with a 15 µm opening for 10 minutes and dried in an oven at 40°C for another 10 minutes.

6.2.2.2 Isothermal calorimetry (IC)

For the IC analyses, an eight-channel Thermal Activity Monitor of Tam Air, TA Instruments (New Castle, DE, USA) was used. The pastes were mixed *ex-situ* but inside the glass ampoule, as described in item 2.2.1. A glass ampoule with distilled water was used as the reference. The amount of distilled water was defined according to Wadsö [28] to obtain a similar heat capacity of C_3S/C_3A pastes. The heat flow (thermal power, in mW/g of solids) and the cumulative heat

(integral of thermal power, in J/g of solids) were recorded up to 48 hours at 22 °C for all the pastes.

6.2.2.3 Thermogravimetry analysis (TGA)

The TGA of the pastes at 8 hours, 1, 3, and 7 days were performed in a TGA 2 analyzer from Mettler Toledo (Columbus, Ohio, USA). The samples were placed in open platinum crucibles under airflow, and the temperature varied between room temperature (RT) and 1000°C with a heating rate of 10 °C/min.

From TGA results, the bound water and the portlandite contents were determined. After stopping the hydration, the bound water of the pastes after stopping hydration content was assigned to the weighed loss from RT to 550°C. Eq. 6.1 calculates the actual bounded water and Eq. 6.2 determines the amount of free water [29].

$$\mathrm{BW} = \frac{\mathrm{BW_{ATD}} \cdot \mathrm{CM}}{100 - \mathrm{BW_{ATD}}} \tag{6.1}$$

$$\mathrm{FW} = \mathrm{TW} - \mathrm{BW} \tag{6.2}$$

Where BW corresponds to actual chemically bound water content; BW_{ATD} is the mass loss measured between RT and 550ºC from TGA curves; CM is the cement (C_3S + C_3A + calcium sulfate) content; TW is the total water content added (all the numbers in weight percentages).

Also, the portlandite content was determined by Eq. 6.3 [30].

$$Ca(\mathrm{OH})_{2,\mathrm{measured}} = \mathrm{WL_{Ca(OH)_2}} \cdot \frac{\mathrm{m_{Ca(OH)_2}}}{\mathrm{m_{H_2O}}} \tag{6.3}$$

Where $WL_{Ca(OH)_2}$ is the weight loss due to the evaporation of water, obtained by the integration of DTG peak located in the temperature range from ~400 to ~500 ºC using the tangential method [30]; $m_{Ca(OH)_2}$ is the molecular mass of portlandite (74 g/mol); and m_{H_2O} is the molecular mass of water (18 g/mol).

The total mass of solids increases with C_3S/C_3A hydration progress, as free water is bound into hydration products. Therefore, the portlandite content obtained by TGA was normalized per 100 g of paste according to Eq. 6.4.

$$Ca(OH)_{2,\text{rescaled}} = Ca(OH)_{2,\text{measured}} \cdot \frac{(100 - \text{FW})}{100} \quad (6.4)$$

Where $Ca(OH)_{2,\text{rescaled}}$ is the portlandite content in g/100 g of paste; $Ca(OH)_{2,\text{measured}}$ is the portlandite content obtained by TGA; and FW is the free water content determined by TGA according to Eq. 6.2.

6.2.2.4 In-situ X-ray diffraction (In-situ XRD)

In-situ XRD was conducted using an X'Pert Pro (PANalytical) diffractometer operating at 45 kV and 40 mA, equipped with an X'Celerator detector with an active length of 2.122°. The following experimental setup was used: Bragg–Brentano θ-2θ geometry with a 240 mm radius goniometer; CuKα radiation with a wavelength of 1.5418 Å; a 0.04 rad Soller slit, a 10 mm beam mask, a 1° fixed anti-scatter slit, and a 1/2° fixed divergence slit on the incident beam; a 5.0 mm fixed anti-scatter slit, a 0.04 rad Soller slit, and a 0.020 mm Ni filter on the diffracted beam; and knife-edge at the first division.

For this analysis, scans were recorded at the range from 7 to 55° 2θ with a counting time of 24.76 seconds per step, totaling about 10 minutes per scan. The fresh sample was placed on the sample holder and immediately covered with a Kapton film to prevent water loss and carbonation. The measurements started 30 minutes after the first contact between the water and the dry materials and were recorded for up to 48 hours. Three samples were tested alternatively, placed at an X-ray beam automatically by a robotic arm, providing an XRD pattern for each sample every 30 minutes. Immediately before each 48-hour measurement set, a corundum (α-Al_2O_3) sample covered with Kapton was measured in the same testing conditions to be used as an external standard.

Rietveld quantitative phase analysis (QPA) was conducted using TOPAS v.5 software [31], and the crystallographic information files used are detailed in Table 6.1. All the XRD patterns of each mix were refined together, and the same refinement steps were applied for each group of patterns (i.e., for each mix). The refinement of *in-situ* XRD data is somehow delicate since it deals with simultaneous amorphous contributions (e.g., C-S-H, free water and Kapton film), besides analyzing several files and phases simultaneously. Thus, using an adequate refinement strategy is essential due to two main reasons: (i) a good strategy improves the robustness of the analysis and reduces the chances of drifting; and (ii) a well-defined script improves the consistency of the analysis for different operators or for a sequence of patterns related to the

same starting material (e.g., a time-dependent series) [32]. The steps used for C-S-H, free water, and Kapton film phase model creation and the refinement strategy conducted in this work are detailed in the Supplementary Material, while Figure 6.43 and Figure D1 illustrate fitted *in-situ* XRD patterns.

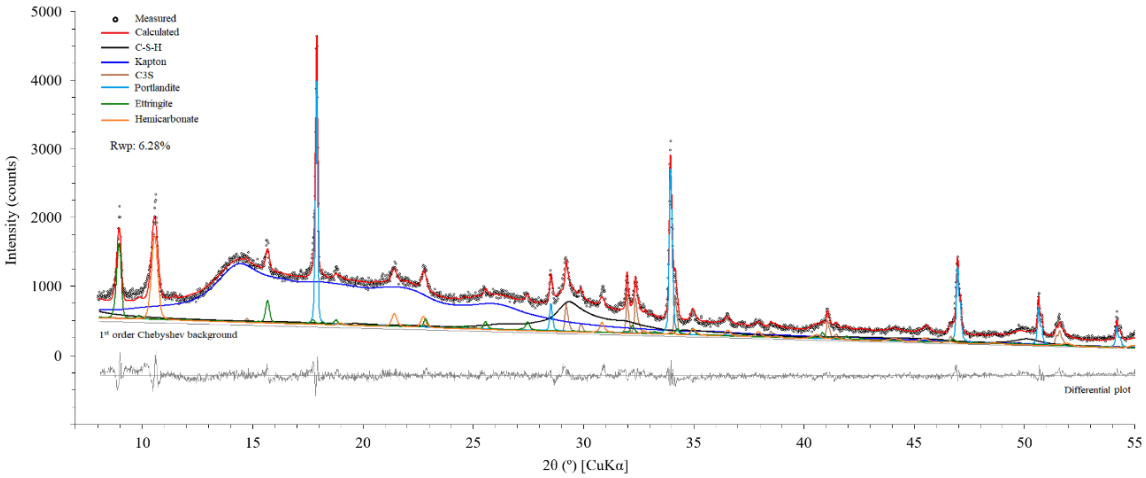

Figure 6.43 – Example of fitted *in-situ* XRD pattern (for Al-C_3S_cb-C_3A_GYP at 48 hours of hydration).

The absolute weight fraction of each crystalline phase was determined by the external standard method [33] using the G-factor approach (Eqs. 6.5-6.6) [34]. The corundum sample covered with Kapton was used as an external standard for this purpose. The mass absorption coefficient (MAC) of the paste was calculated from the chemical composition of the powder fraction and the water MAC.

$$W_i = S_i \frac{\rho_i V_i^2}{G} \mu^* \tag{6.5}$$

$$G = S_s \frac{\rho_s V_s^2 \mu_s}{W_s} \tag{6.6}$$

where W is the weight fraction of the phase (i) or the standard (s), in wt%; S is the refined scale factor of the phase (i) or the standard (s); ρ is the density of the phase (i) or the standard (s), V is the unit cell volume of the phase (i) or the standard (s) in Å^3; and μ is the MAC of the sample (*) or the standard (s), in cm^2/g. The density and unit cell volume of each phase are presented in Table 6.1, and the MAC of the raw materials and pastes are presented in the Supplementary Materials (Tables D1 and D3).

The weight fraction of C-S-H was calculated using the mass balance given by Eq. (6.7) [37,38] together with the factor F given by Eq. (6.8) [35], where C = CaO; S = SiO_2; and H = H_2O. Firstly, the expected amount of C-S-H formed after 48 hours was calculated from the amount of alite consumed at this age (i.e., the difference between the initial amount added and that determined by XRD after 48 hours) using Eq. (6.7). Then, factor F was determined using Eq. (6.5); by setting *Wi* equal to the C-S-H content yielded by the stoichiometric calculation and knowing the G and μ^* terms, the only unknown part of Eq. (6.5) is $\rho \cdot V^2$, i.e., the factor F. The calibration of factor F with the last measurement of each *in-situ* sample resulted in an F = $1.11 \pm 0.03 \times 10^{-45}$ g·cm³ (average ±standard deviation). It is stressed that the stoichiometry of C-S-H is not well defined, but since alite is the only silicate in the system, it seems reasonable to assume the mass balance of Eq. (6.7). The stoichiometry of C-S-H was considered as $C_{1.8}SH_{4.0}$, which is the average composition of C-S-H formed by the C_3S hydration according to Cuesta et al. [37,38].

$$C_3S + 5.2\ H \rightarrow C_{1.8}SH_{4.0} + 1.2\ CH \quad (6.7)$$

$$F = \rho . V^2 \quad (6.8)$$

Table 6.16 – Crystallographic information files (CIFs) used for Rietveld QPA.

Phase	ICSD code	Unit cell volume (Å³)	Density (g/cm³)	Reference
C_3S T1	4331	2167.64	3.148	Golovastikov et al. [39]
C_3S M1	---	2175.02	3.138	de Noirfontaine et al. [23]
C_3A cubic	1841	3557.89	3.027	Mondal and Jeffery [40]
C_3A orthorhombic	1880	1790.35	3.018	Nishi and Takeuchi [41]
Portlandite	15471	54.49	2.260	Petch [42]
Ettringite	155395	2345.34	1.780	Goetz-Neunhoeffer and Neubauer [43]
Gypsum	151692	496.25	2.304	de la Torre et al. [44]
Bassanite (Hemihydrate)	69060	1060.51	2.727	Bezou et al. [45]
Hemicarbonate	263124	1410.15	1.900	Runčevski et al. [46]

Note.: The unit cell volume and density values for both C_3S and C_3A polymorphs, gypsum and bassanite were refined in dry samples, while those for portlandite, ettringite and hemicarbonate correspond to the theoretical values from the CIF files.

6.3 RESULTS

6.3.1 Isothermal calorimetry

6.3.1.1 Effect of the calcium sulfate source on C_3S and Al-C_3S hydration

Figure 6.44a and b show the heat flow and cumulative heat curves of the C_3S and Al-C_3S pastes, respectively, without calcium sulfate and with gypsum and hemihydrate (1.5 wt% SO_3), within the first 48 hours of hydration. Comparing the mixtures without calcium sulfate, C_3S hydrated much faster than the Al-C_3S, generating a higher heat flow peak and higher cumulative heat at 48 hours. These results agree well with previous studies [8–10] and are probably due to the effect of aluminum ions in solution leading to a delay and suppression of C_3S hydration. In addition, the greater particle size of Al-C_3S (see Figure 6.1) probably contributed to the lower reactivity of this phase.

The addition of gypsum had similar effects in both C_3S and Al-C_3S hydration: a slight initial delay, prolonging the induction period, but an enhancement afterward, increasing the main heat flow peak. This agrees with previous studies which evaluated the hydration of C_3S in the presence of gypsum. The initial delay is probably related to the adsorption of sulfate ions in the C_3S surface, delaying its dissolution [17,47]. In turn, the enhancement in the main hydration peak is a result of a change in the C-S-H morphology and of the increase in the ionic strength of the pore solution [11].

The hemihydrate had a very similar effect to gypsum on both C_3S and Al-C_3S. Therefore, it is observed, for the first time, that the solubility of the calcium sulfate does not seem to impact the effect of calcium sulfate on C_3S hydration. Despite the gypsum- and hemihydrate-containing mixes presenting similar heat flow and cumulative heat curves, the latter had a small heat release peak between 30 minutes and 2 hours. This peak is related to the hydration of hemihydrate and the precipitation of gypsum crystals, confirmed later by the *in-situ* XRD results, which showed gypsum in the hemihydrate-containing mixes already at 30 minutes of hydration (see Section 6.3.2). Consequently, the cumulative heat curves of the mixtures with hemihydrate were slightly higher than those with gypsum.

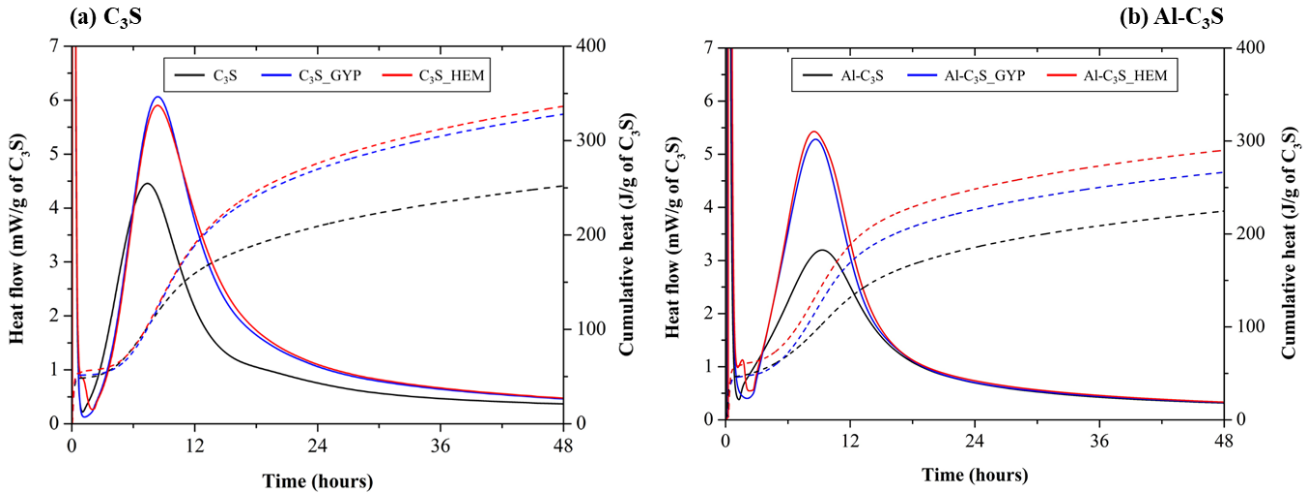

Figure 6.44 – Heat flow curves (solid lines) and cumulative heat curves (dashed lines) of the (A) C_3S and (B) Al-C_3S pastes during the first 48 hours of hydration.

6.3.1.2 Effect of the calcium sulfate source on cb-C_3A and ort-C_3A hydration

Figure 6.45a and b show the heat flow and cumulative heat curves of cub-C_3A and ort-C_3A, respectively, without calcium sulfate and with different levels of gypsum and hemihydrate (SO_3/C_3A ratios of 0.03, 0.06, and 0.12) during the first 90 hours of hydration. Without calcium sulfate, cb-C_3A reacted much faster than ort-C_3A, presenting a higher heat released in the first 48 hours. This behavior was also observed in previous studies [12,13,49].

The addition of calcium sulfate (as gypsum or as hemihydrate) delayed both cb- and ort-C_3A initial hydration. However, this retard effect was much stronger on cb-C_3A. The cb-C_3A mixes with 0.03, 0.06 and 0.12 presented induction periods of 4.2, 5.0, and 11.0 h, when gypsum was used, and of 6.0, 6.4, and 14.8 h, when hemihydrate was used. In turn, despite calcium sulfate retarding the initial ort-C_3A hydration, as can be observed by the lower heat release in the first hours, all mixtures with gypsum or hemihydrate presented higher cumulative heats than the reference sample after 8.5 hours of hydration. Similar behaviors were observed by several authors [12–14,25]. The lower retarding effect of calcium sulfate in ort-C_3A hydration compared with the cb-C_3A hydration happens because the sodium-doping of ort-C_3A increases the solubility of $Al_6O_{18}^{18-}$, preventing the formation of the Al-rich leached layer on the C_3A particles, inhibiting the adsorption of S^{2-} and/or Ca–S ion-pair that are responsible for the delay in cb-C_3A hydration [13,14].

Interestingly, the hemihydrate seems to be more effective in retarding the ort-C_3A hydration in the SO_3/C_3A ratios tested. This is contrary to what was observed by Andrade Neto et al. [14],

in which the replacement of gypsum by hemihydrate led to an acceleration in the ort-C_3A hydration when using a much higher SO_3/C_3A ratio (0.29). The reasons for that are not clear yet and further studies are necessary.

Figure 6.45 – Heat flow curves (solid lines) and cumulative heat curves (dashed lines) of the (a) cb-C_3A_GYP, (b) cb_C_3A-HEM, (c) ort-C_3A_GYP and (D) ort-C_3A_HEM pastes during the first 48 hours of hydration.

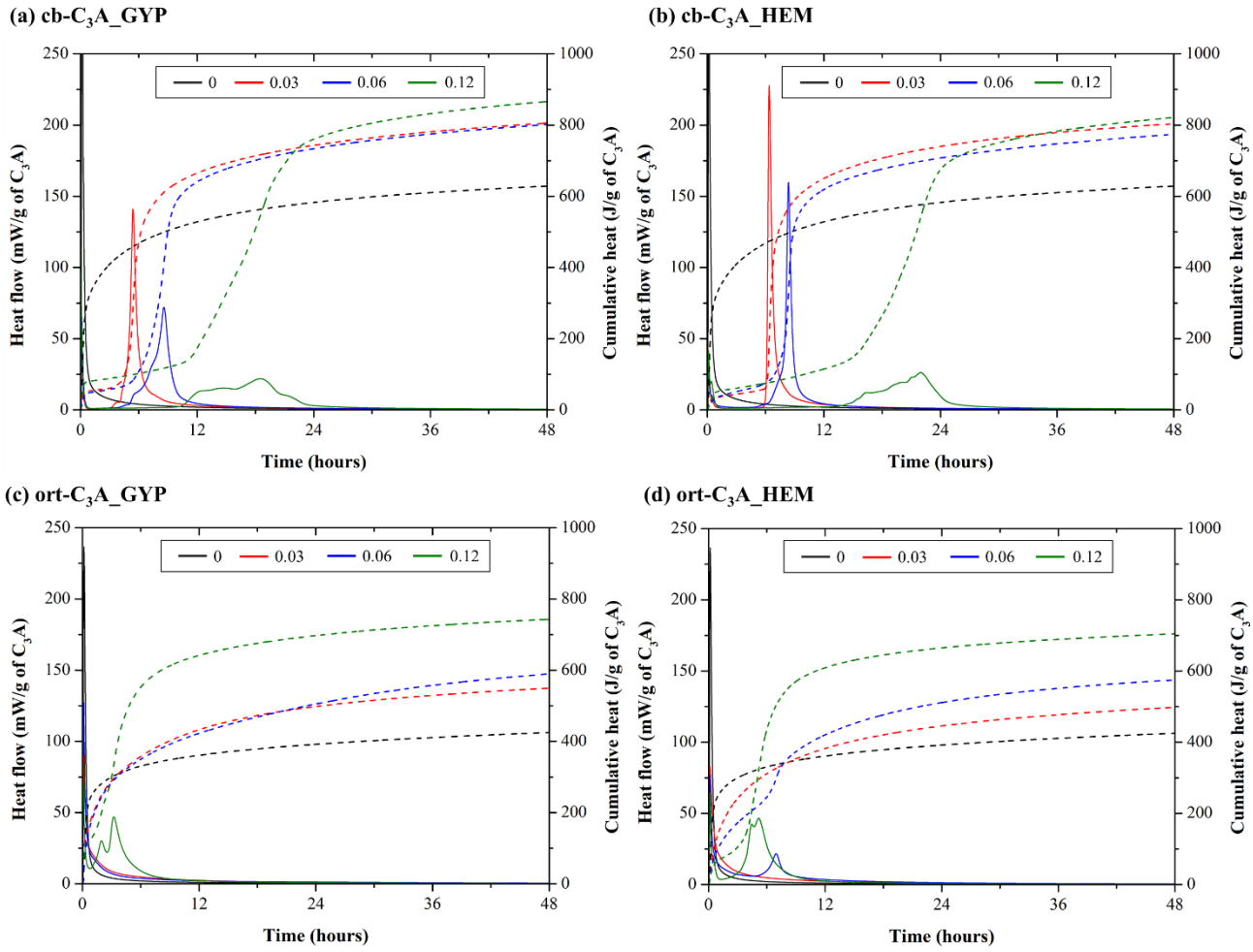

6.3.1.3 Effect of the SO_3 content on C_3S/C_3A systems

The heat flow curves of the C_3S/C_3A pastes with different contents of gypsum or hemihydrate are presented in Figure 6.46. The silicate, aluminate, and hemihydrate hydration heat flow peaks are indicated.

By comparing the hydration of the C_3S/C_3A/calcium sulfate systems (Figure 6.46) with the C_3S/calcium sulfate systems (Figure 6.44), it is possible to see that in undersulfated mixes (i.e.,

when the sulfate depletion and the renewed hydration of C_3A occur earlier than the main C_3S hydration peak), the hydration of both C_3S and Al-C_3S was retarded and suppressed. This agrees with previous results [7,27,48], and probably occurs due to the earlier C_3A dissolution, releasing a significant amount of aluminum into the solution. As discussed in Section 6.3.1.1, aluminum retards and suppresses the C_3S hydration – whether due to the formation of alumino-silicate species on the C_3S surface, hindering its dissolution, or due to the C-A-S-H formation. In turn, in the proper sulfated mixes (i.e., when the sulfate depletion and the renewed hydration of C_3A happens after the main C_3S hydration peak), the C_3S and Al-C_3S hydration occurred as in the C_3S/calcium sulfate mixtures, with the maximum heat flow peak happening around 8 hours. In the proper sulfated mixes (> 0.50% SO_3 for the C_3S mixes and 2.0% SO_3 for the Al-C_3S mixes), the C_3A polymorphism does not seem to significantly influence the C_3S or Al-C_3S hydration rate. For these mixtures, regardless of the C_3A type, the induction period length and the silicate peak are very similar, indicating very similar C_3S hydration rates.

As for C_3A, the time for the renewed hydration of cb-C_3A occurred much earlier in the three-phase systems with the Al-C_3S (Figure 6.5) than in the C_3A pastes (Figure 6.4) even for the same SO_3/C_3A ratios. One can note the time of occurrence of the aluminate peak (indicated as Ap) in Figure 6.5(c,d) is around 4-5 hours for the mixes with 0.5 wt%SO_3 and around 8-10 hours for the mixes with 1.0 wt%SO_3. In turn, for the cb-C_3A_(GYP, HEM) pastes (see Figure 6.4), the time for the aluminate peak is around 7-8 hours and around 12-14 hours for the mixes with the SO_3/C_3A ratios of 0.06 and 0.12 (which corresponds to the same SO_3/C_3A ratios of the three-phase systems with 0.5 wt% and 1.0 wt% of SO_3). This happens in the mixes with Al-C_3S as the higher aluminum content in the solution (released from Al-C_3S dissolution) increases ettringite formation and, consequently, accelerates the sulfate depletion (as confirmed by *in-situ* XRD, see Section 6.3.2). Interestingly, the ort-C_3A presented slower hydration in C_3S/C_3A/calcium sulfates when compared to the ort-C_3A/calcium sulfates pastes. The ort-C_3A hydration is significantly influenced by the bulk composition of the pore solution [13], and the presence of C_3S seems to retard its reaction. Further analyses on this topic are necessary.

The type of C_3S was the major fact influencing the sulfate balance of the system. For the mixes with C_3S (Figure 6.46a-d), 0.5 wt%SO_3 was already enough to result in properly sulfated mixtures, i.e., that the renewed C_3A hydration occurred after the main C_3S hydration peak. In turn, for the mixes with Al-C_3S (Figure 6.46e-h), 1.5-2.0 wt%SO_3 was required to reach the proper sulfate content. This happens because a higher concentration of aluminum into the pore

solution is expected in the mixes with Al-C_3S, resulting in higher ettringite formation and sulfate consumption (as confirmed by *in-situ* XRD, see Section 6.3.2).

The C_3A polymorphism also influenced the sulfate balance of the system but to a less extent. Also, the effect of C_3A polymorph on sulfate balance depends on the wt% SO_3 content. On the one hand, for the mixes with 0.25 and 0.5 wt%SO_3, the mixes with cub-C_3A presented sulfate depletion and renewed hydration of C_3A earlier than those with ort-C_3A, increasing the sulfate demand of the system. On the other hand, for the mixes with 1.0 wt%SO_3 or more, the opposite behavior was observed, i.e., the mixes with ort-C_3A present earlier sulfate depletion and renewed hydration of C_3A. This apparent discrepancy might be due to the differences in cb-C_3A and ort-C_3A hydration, which depends on the sulfate level, as observed and discussed in Section 6.3.1.2. For sulfate-free solutions, cb-C_3A hydrates faster than the ort-C_3A. However, the addition of calcium (gypsum or hemihydrate) retards the C_3A hydration much more efficiently than the ort-C_3A hydration (see Figure 6.4). Therefore, for the three-phase mixes with 0.25 and 0.50 wt%SO_3 (SO_3/C_3A ratio of 0.03 and 0.06, respectively), the very low sulfate content was not enough to retard the cb-C_3A hydration and make it slower than the ort-C_3A hydration. Finally, 1.0 wt%SO_3 (SO_3/C_3A ratio of 0.13) seems to be enough to make the cb-C_3A reaction slower than the ort-C_3A reaction.

Regarding the calcium sulfate source, the mixes with hemihydrate presented earlier sulfate depletion and renewed hydration of C_3A than the mixes with gypsum, which agrees with previous results [7]. This was expected since hemihydrate is more soluble than gypsum [21,22], resulting in higher sulfate concentrations in the pore solution, which lead to higher ettringite formation (as confirmed by *in-situ* XRD, see Section 6.3.2) and anticipating the sulfate depletion. The calcium sulfate composition did not influence the C_3S and the Al-C_3S hydration in the proper sulfated mixes, which corroborates with the C_3S pastes results (Section 6.3.1.1) that showed that gypsum and hemihydrate led to very similar effects on C_3S and Al-C_3S hydrations.

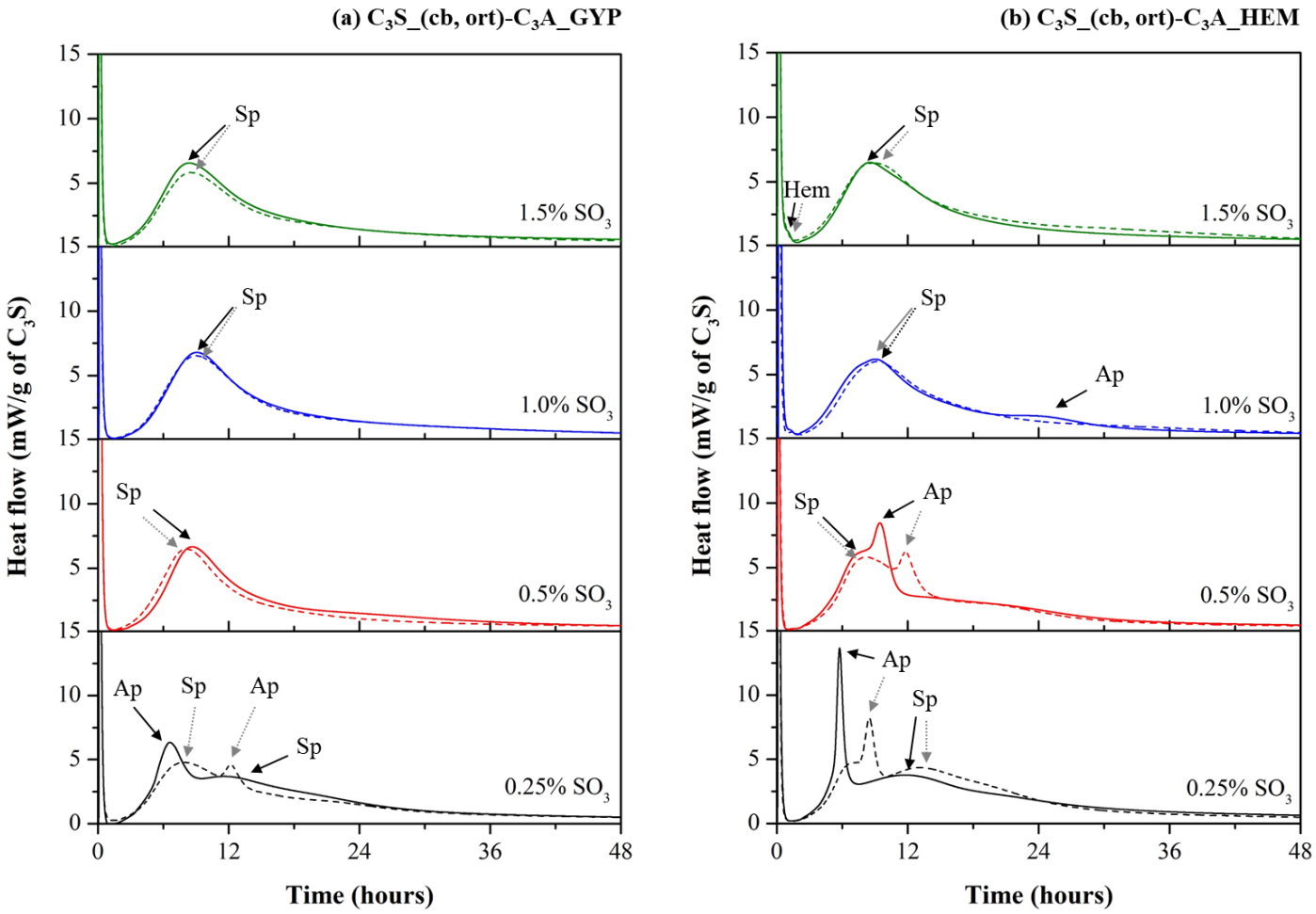
(a) C3S_(cb, ort)-C3A_GYP
(b) C3S_(cb, ort)-C3A_HEM
Heat flow (mW/g of C3S)
Time (hours)
Sp
Ap
Hem
1.5% SO3
1.0% SO3
0.5% SO3
0.25% SO3
0
5
10
15
0
12
24
36
48

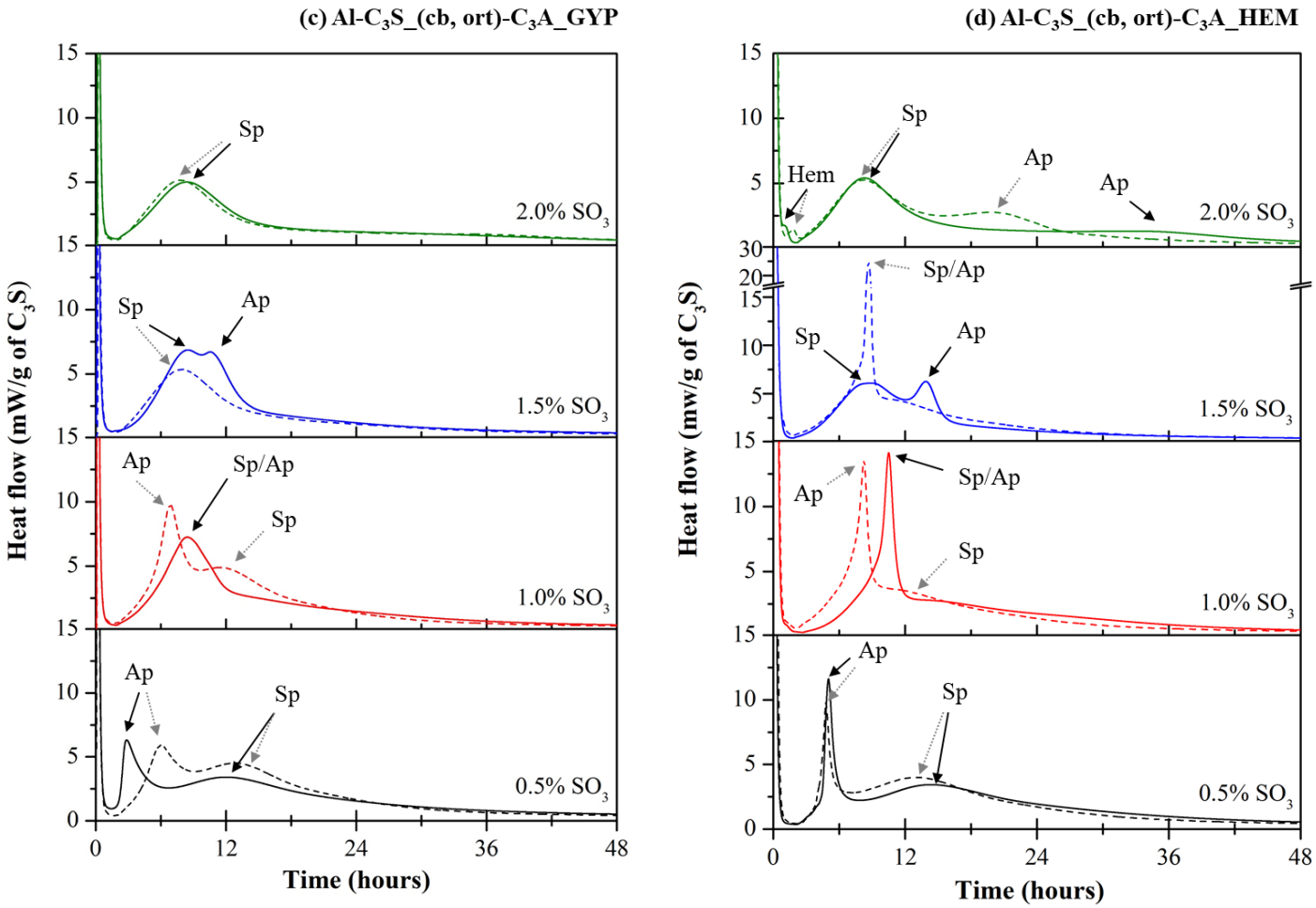

Figure 6.46 – Heat flow curves of the pastes with different gypsum and hemihydrate contents during the first 48 hours of hydration. The solid lines indicate the mixes with cb-C_3A and the dashed lines represent the mixes with ort-C_3A. The moment of the occurrence of the Aluminate peak (Ap), Silicate peak (Sp), and the peak related to the hydration of hemihydrate into gypsum (Hem) are indicated.

6.3.2 *In-situ* X-ray diffraction (XRD)

Figure 6.47 shows the XRD patterns of each mix at 0.5 and 48 hours of hydration. All the mixes had 1.5 wt% SO_3 as according to the calorimetry results at this sulfate content, none of the mixes was undersulfated (except for the Al-C_3S_ort-C_3A_HEM it was slightly undersulfated). No bassanite (i.e., crystalline hemihydrate) was found in hydrated pastes, indicating that it quickly converted into gypsum before the first XRD measurement, before 30 minutes. This is in line with that reported by Jakob et al. [52], Jansen et al. [53], and García-Maté et al. [54], which observed this phenomenon before 10-20 minutes of hydration in Portland cement pastes and also supported by Andrade Neto et al. [14] who observed the hydration of hemihydrate into gypsum in the first 30 minutes in C_3A pastes.

The mixes with Al-C_3S (i.e., 3, 4, 7, and 8) showed ettringite peaks at 0.5 hours, especially at 9.1° 2θ. In addition, the Al-C_3S_(cb,ort)-C_3A_GYP mixes (i.e., 3 and 4) had virtually no gypsum traces at the first measurement, while the C_3S_(cb,ort)-C_3A_GYP mixes (i.e., 1 and 2) showed gypsum peak at 11.6° 2θ.

Regarding the hydration of the aluminates, the mixes with C_3S (i.e., 1, 2, 5, and 6) showed evident C_3A peaks after 48 hours of hydration (at around 33° 2θ). Those mixes produced with cubic C_3A (i.e., 1 and 5) had practically no change on the relative intensity of such C_3A peak, indicating the low consumption of this phase along the first two days of hydration.

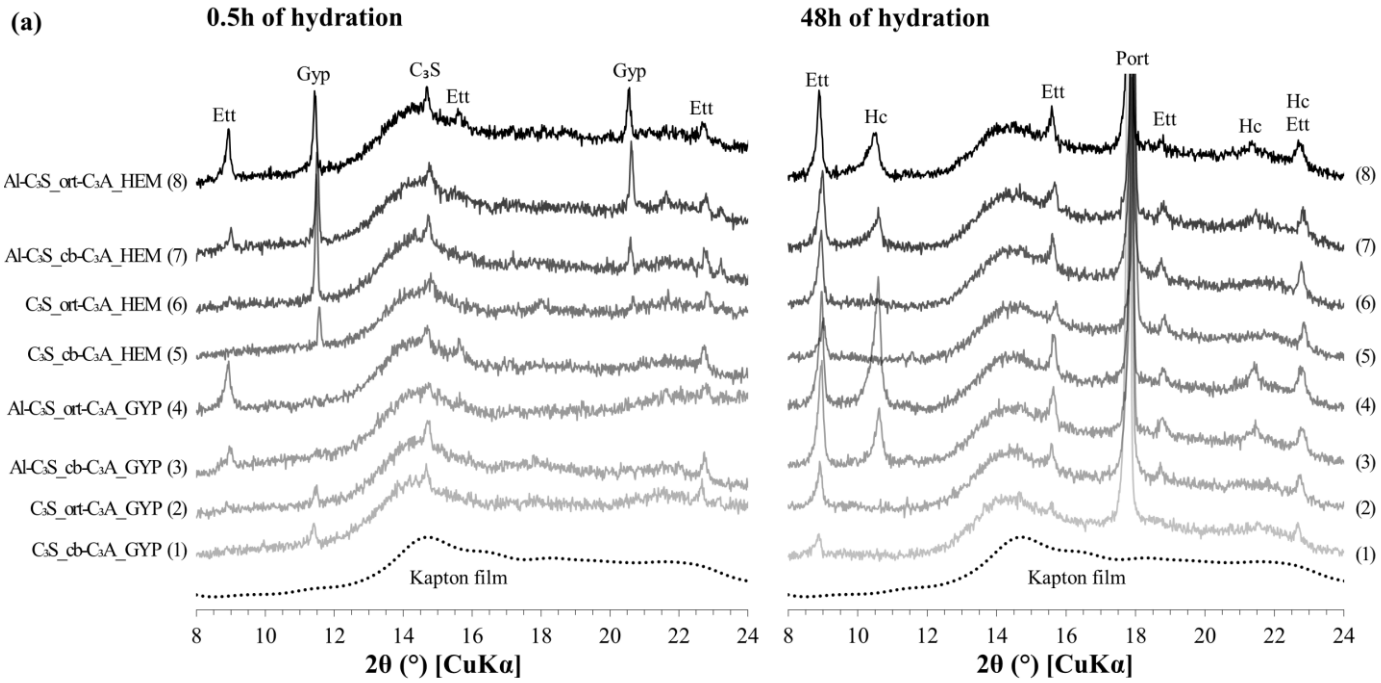

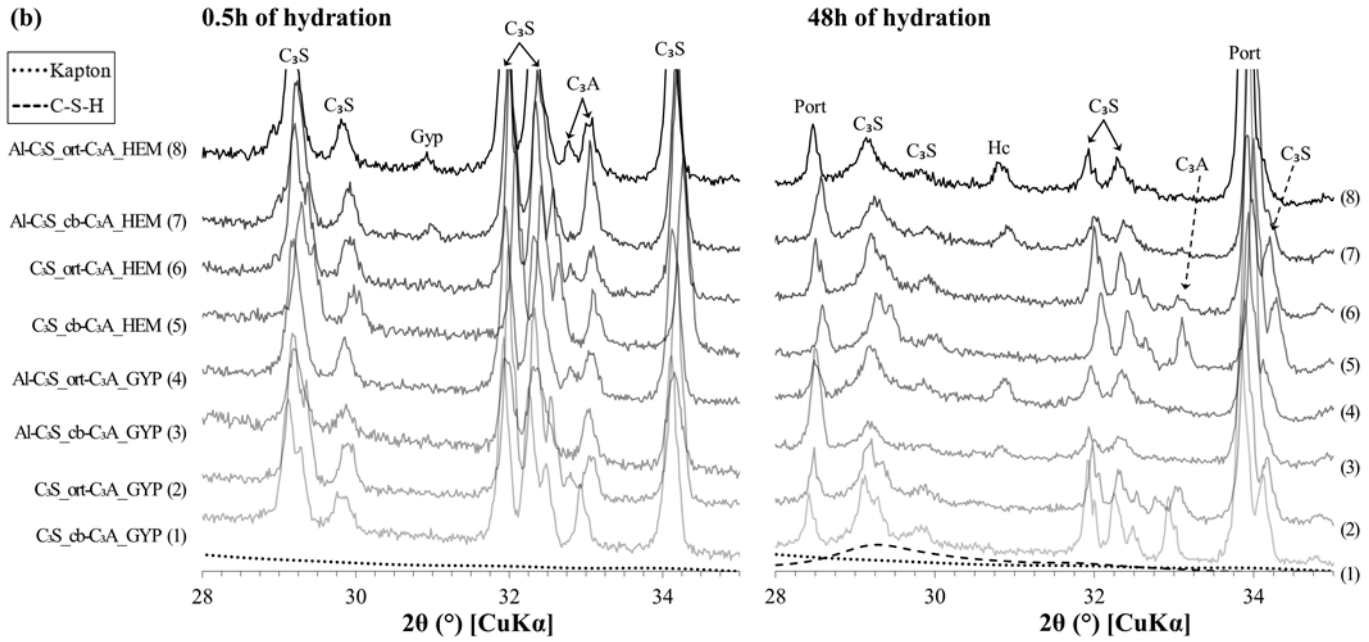

Figure 6.47 – Selected ranges of the XRD patterns of the mixes at 0.5 and 48 hours of hydration. (a) 8-24° 2θ range; (b) 28-35° 2θ range. Ett: ettringite; Gyp: gypsum; Port: portlandite; Hc: hemicarbonate. Note: the patterns were vertically shifted for visualization, but the relative intensities (in linear scale) were not changed. The Kapton and C-S-H models are also shown as dotted and dashed lines, respectively.

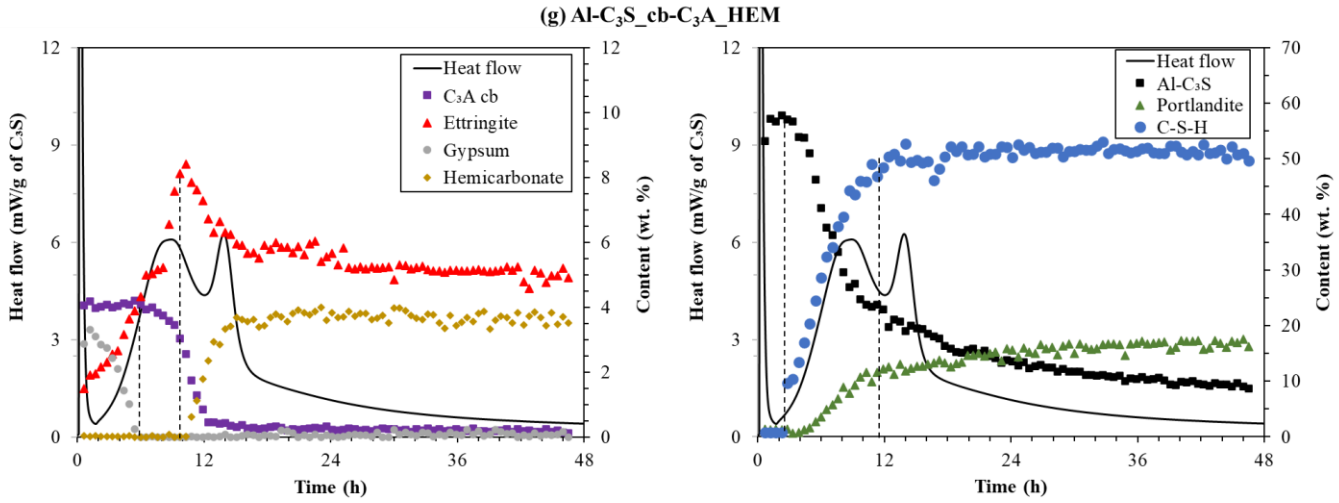

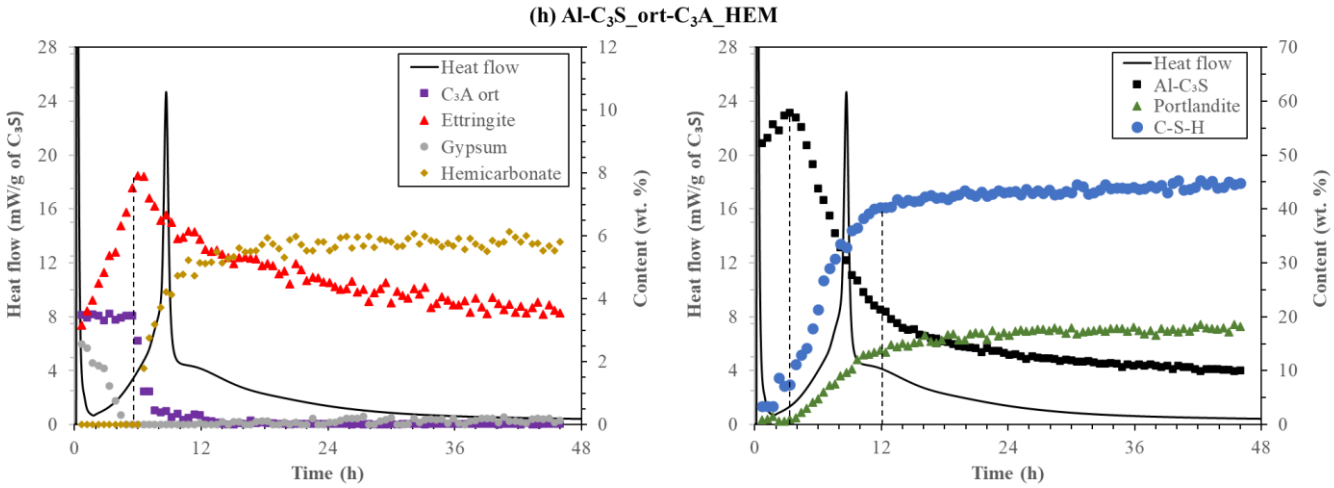

Figure 6.48(a-h) presents the phase content over time determined by XRD-Rietveld QPA and the heat flow within the first 48 hours of hydration. Regarding the silicates, all the mixtures showed very similar behavior. The C_3S content was approximately constant (considering the intrinsic deviations in Rietveld quantification) during the first ≈ 4 hours, up to the end of the induction period. At the beginning of the acceleration period, the C_3S contents start to reduce, indicating its dissolution, while C-S-H and portlandite begin to form, which agrees with previous studies [52,53]. The C_3S dissolution and the C-S-H and portlandite formation initially presented faster rates but slowed down after the main heat flow peak. The lower C_3S dissolution rate can explain the decrease in the rate of heat release in IC curves.

As for the aluminates, for all the mixes, it was observed an extremely fast initial C_3A dissolution (with approximately 50% of the C_3A dissolving within the first 30 minutes – before the first XRD measurement) and then its content remains virtually constant. Ettringite was formed in the first minutes (already detected in the first XRD scan), and its content kept increasing in the first hours, associated with gypsum dissolution. After 6-16 hours (varying from mix to mix), gypsum depletion is observed. From this point on, the mixes with Al-C_3S presented very different behaviors when compared with the mixes with C_3S. In the mixes with Al-C_3S, a few

hours after gypsum depletion, the C_3A started to dissolve again very quickly (

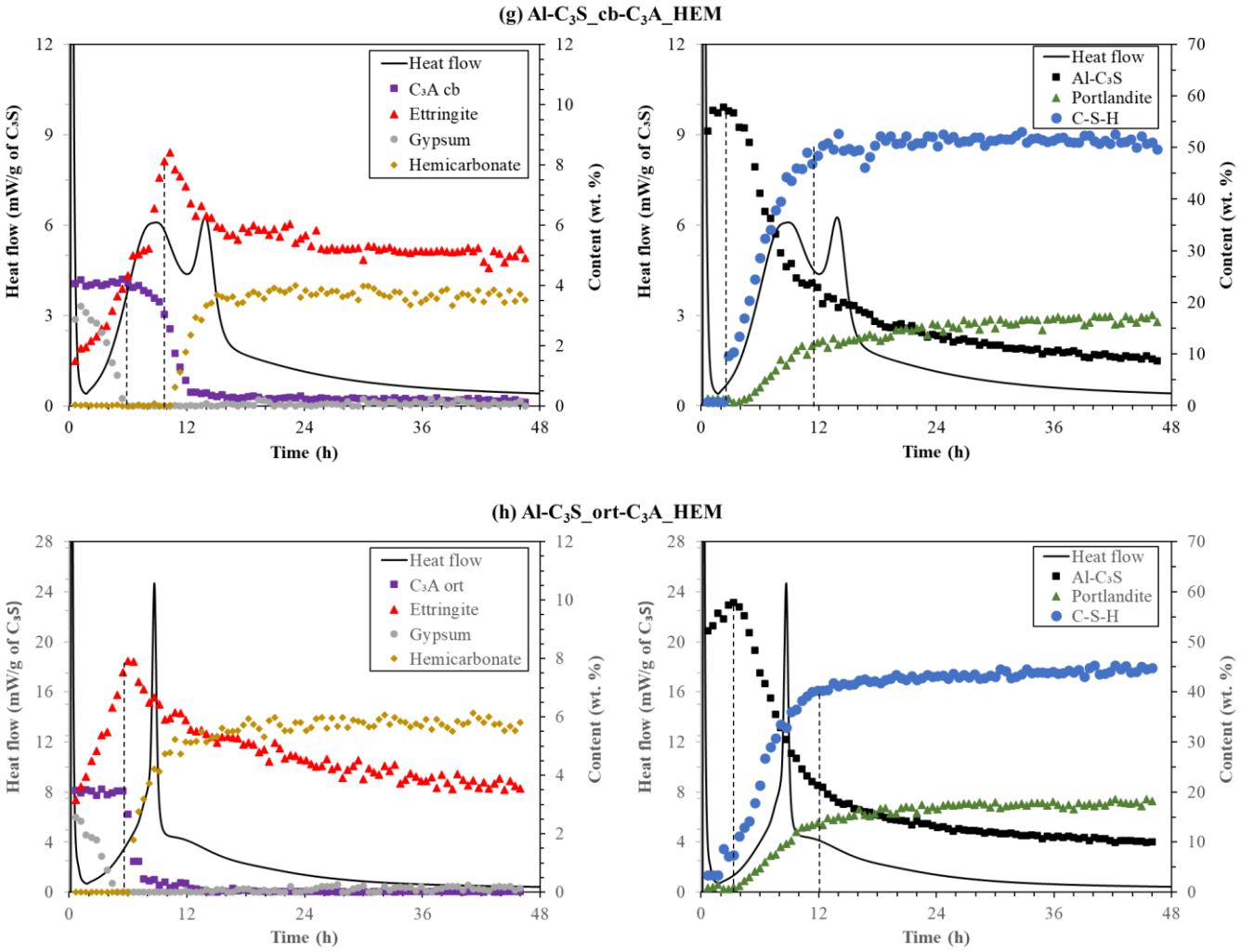

Figure 6.48c,d,g,h). For those mixes, the ettringite content initially increased fast up to a limit and then started to dissolve synchronously with the start of hemicarbonate formation. In turn, for the C_3S mixes, the C_3A also starts to dissolve again after the sulfate depletion, but much slower than the mixtures with Al-C_3S. As a result, no AFm was detected in the C_3S-containing mixes up to 48 hours, as observed in Figure 6.47a (see mixes 1, 2, 5, and 6) where the only reflection observed up to 12 ° 2θ was that from ettringite.

The formation of hemicarboaluminate instead of monosulfate on Al-C_3S mixes occurred due to the presence of calcite (0.5 wt%) and magnesite (0.9 wt%) on the Al-C_3S composition (see Section 6.2.1). In turn, for the C_3S mixes, no ettringite dissolution and hemicarbonate or monosulfate formations were observed in the first 48 hours of hydration. Interestingly, the mixes with ort-C_3A also formed hemicarbonate instead of U-phase ($4CaO \cdot 0.9Al_2O_3 \cdot 1.1SO_3 \cdot 0.5Na_2O \cdot 16H_2O$), which also belongs to the group of hexagonal or pseudo-hexagonal layered structures (AFm) and were observed in pure ort-C_3A pastes [14]. The U-phase is formed in the

presence of SO_4^{2-} and Na^+ ions in a highly alkaline medium [55]. However, since the C_3S/C_3A mixes had much lower ort-C_3A amounts than pure C_3A pastes, the amount of Na^+ ions released was probably not enough to ensure the sufficiently high pH for the U-phase formation.

For better visualization, Figure 6.49 presents only the ettringite content during the first 48 hours. It is possible to notice that the C_3S type had the greatest influence on ettringite formation, and the Al-C_3S mixes presented higher ettringite contents in the first hours. This is probably a result of the higher aluminum content in the solution due to the Al-C_3S dissolution.

The C_3A type also influenced the amount of ettringite formed in the first hours. The mixes with ort-C_3A generally presented higher ettringite contents when compared with cb-C_3A mixes. This result was expected due to the higher reactivity of ort-C_3A, as observed and discussed in section 6.3.1.2. As a result of the higher ettringite formation and the faster sulfate consumption, the Al-C_3S_ort-C_3A_GYP paste presented earlier hemicarboaluminate formation (≈ 9 hours) compared to the Al-C_3S_cb-C_3A_GYP paste (≈ 16 hours).

The calcium sulfate type also influenced the ettringite formation rates. The mixes with hemihydrate (Figure 6.49b) showed faster ettringite formation in the first hours, which agrees with Zunino and Scrivener's [7] results. This was expected since the hemihydrate presents a higher solubility when compared with gypsum [21,22], resulting in higher sulfate concentration in pore solution, leading to a faster ettringite formation. Finally, the replacement of gypsum with hemihydrate also influenced the beginning of hemicarbonate formation, anticipating it in 6 hours for the Al-C_3S_cb-C_3A pastes (from 16 hours for the mix with GYP to 10 hours for the mix with HEM) and in 3 hours for the Al-C_3S_ort-C_3A pastes (from 9 hours for the mix with GYP to 6 hours for the mix with HEM).

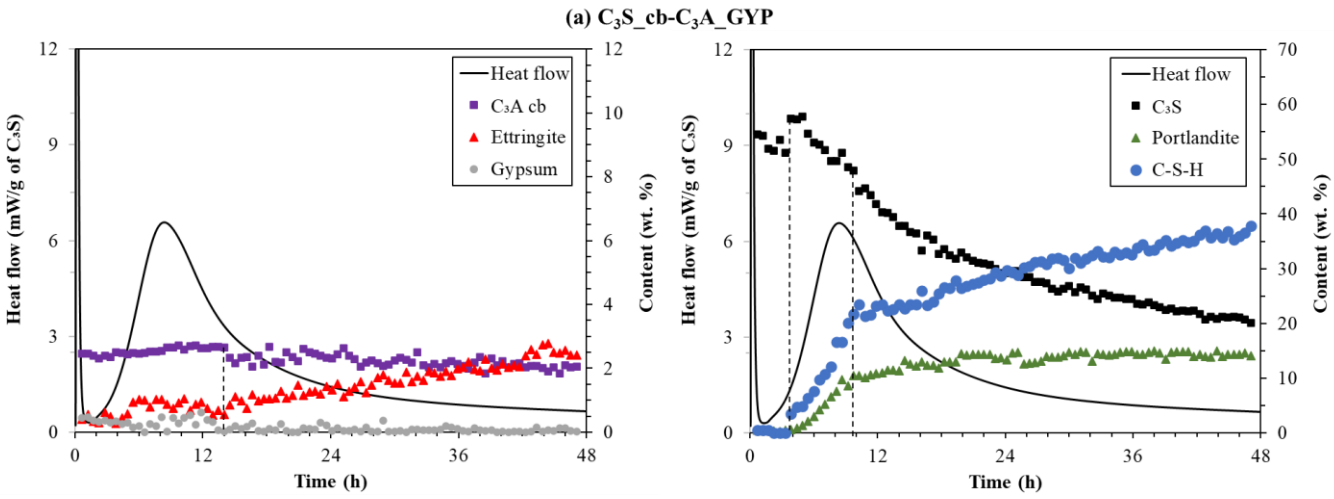

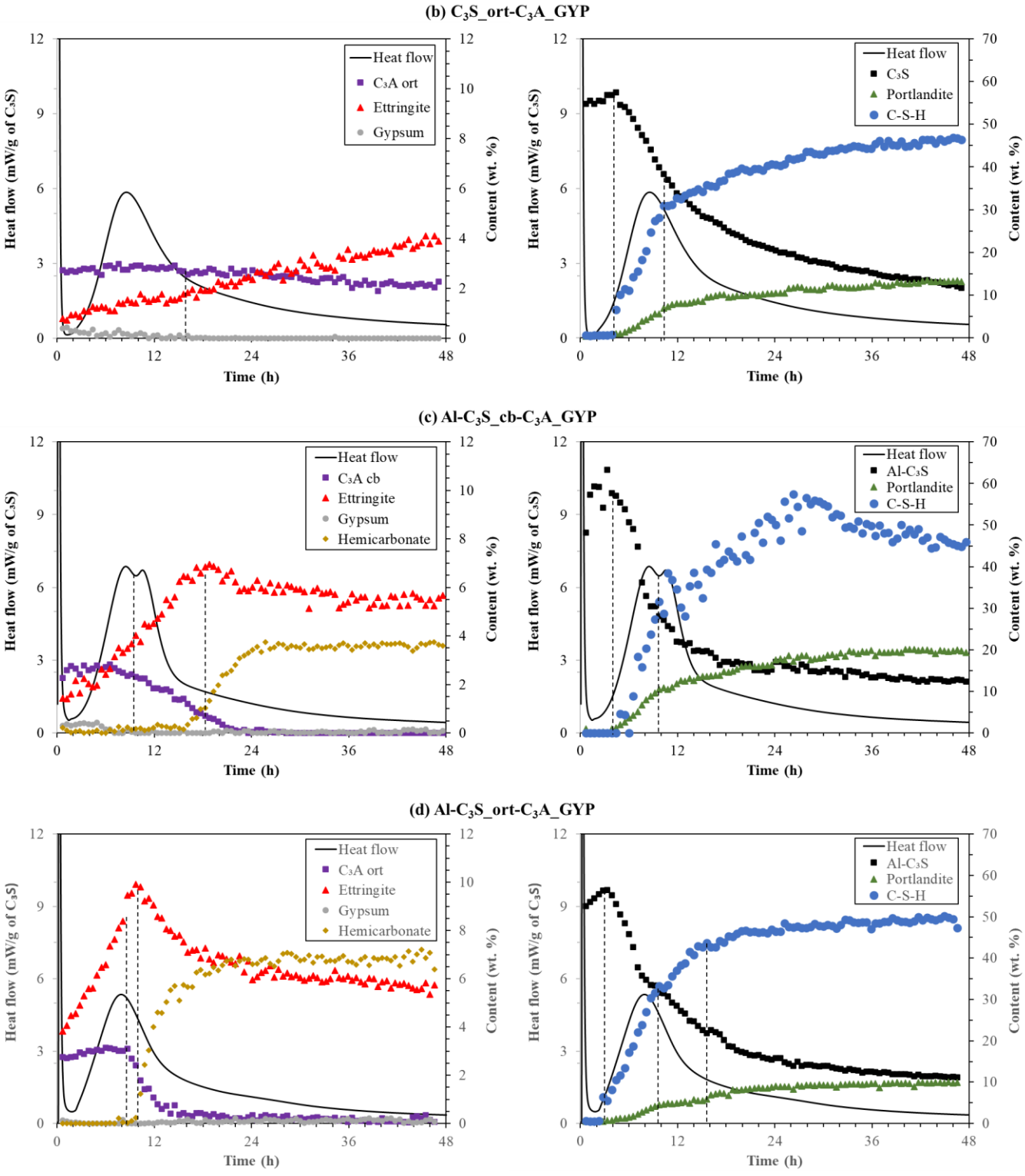
(b) C3S_ort-C3A_GYP
Heat flow
C3A ort
Ettringite
Gypsum
C3S
Portlandite
C-S-H
(c) Al-C3S_cb-C3A_GYP
C3A cb
Hemicarbonate
Al-C3S
(d) Al-C3S_ort-C3A_GYP
Heat flow (mW/g of C3S)
Content (wt. %)
Time (h)

(e) C_3S_cb-C_3A_HEM

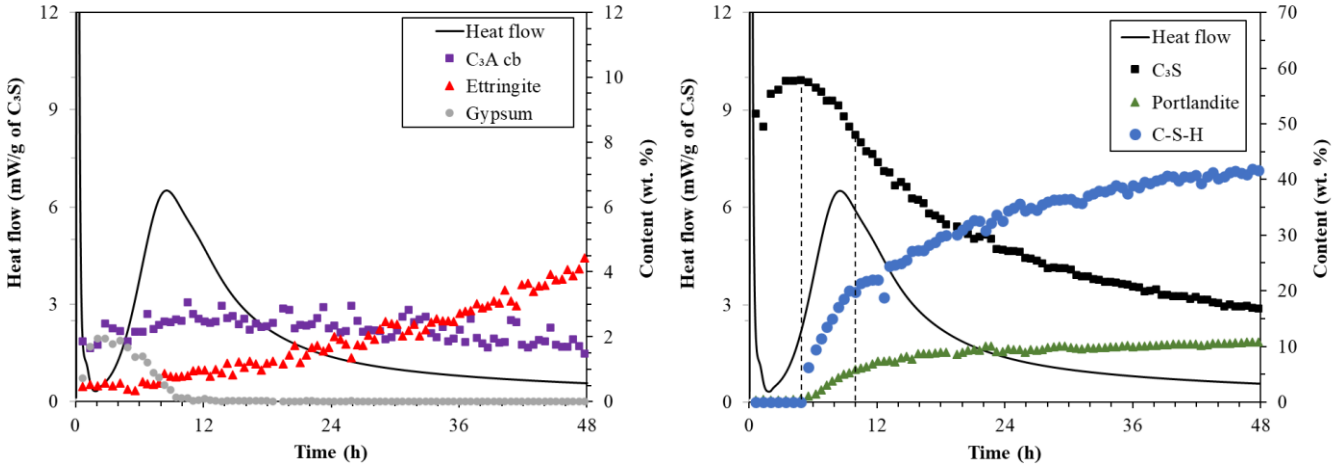

(f) C_3S_ort-C_3A_HEM

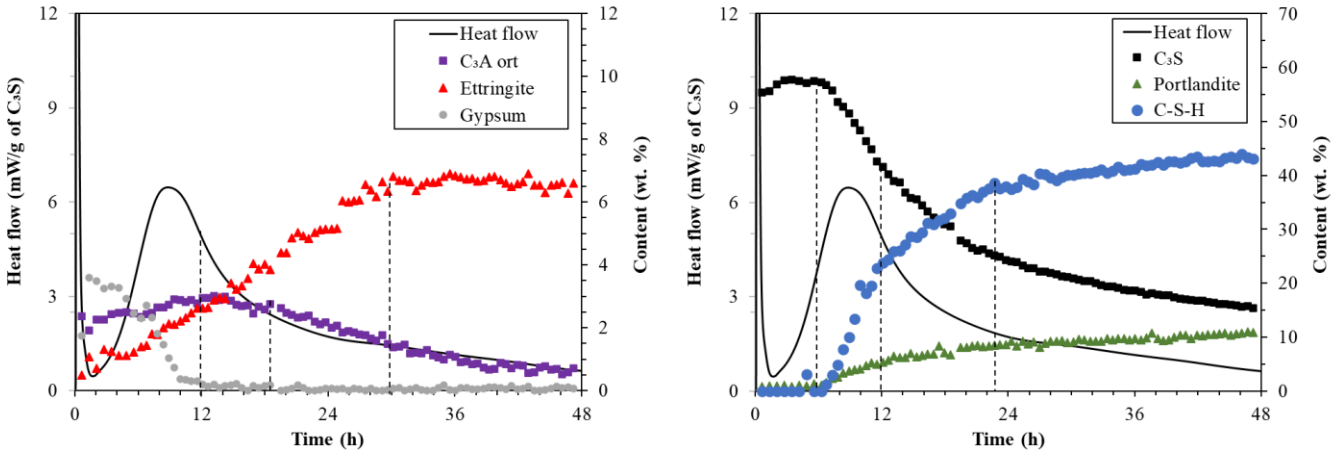

(g) Al-C_3S_cb-C_3A_HEM

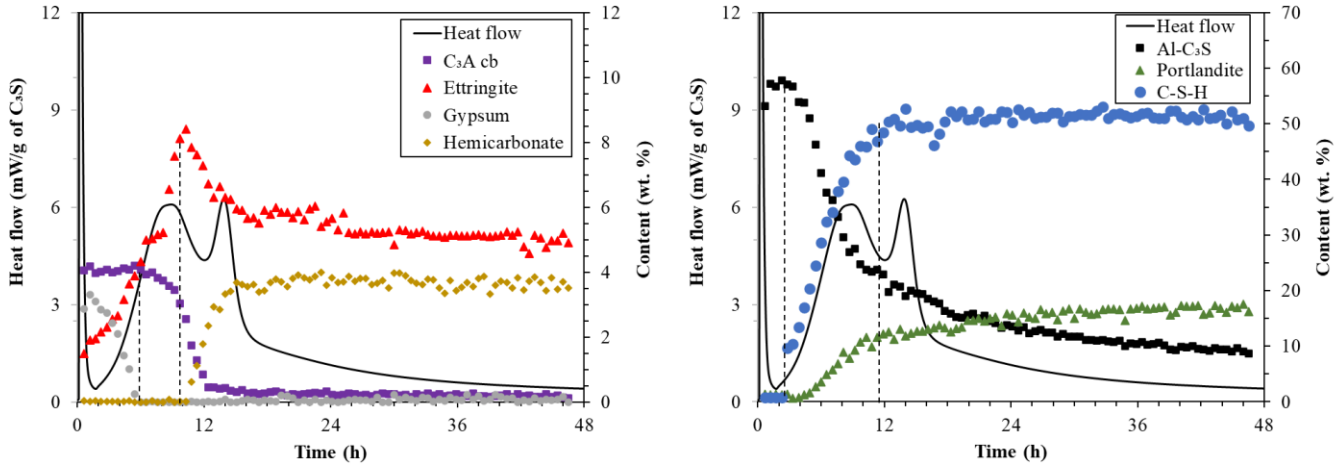

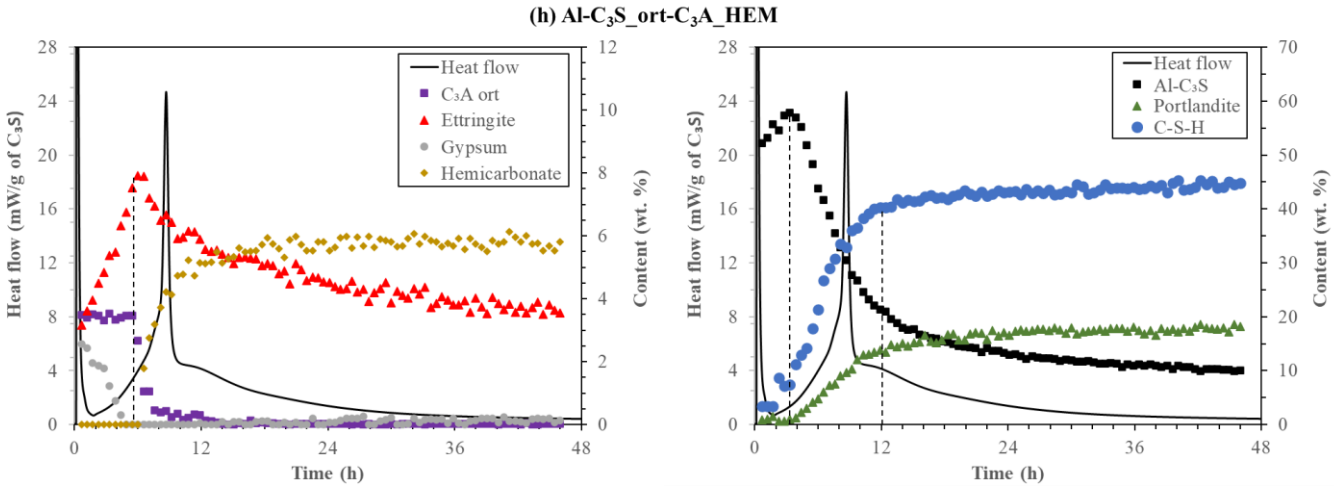

Figure 6.48 – Heat flow curves and phase content (wt%) over the first 48 hours of hydration.

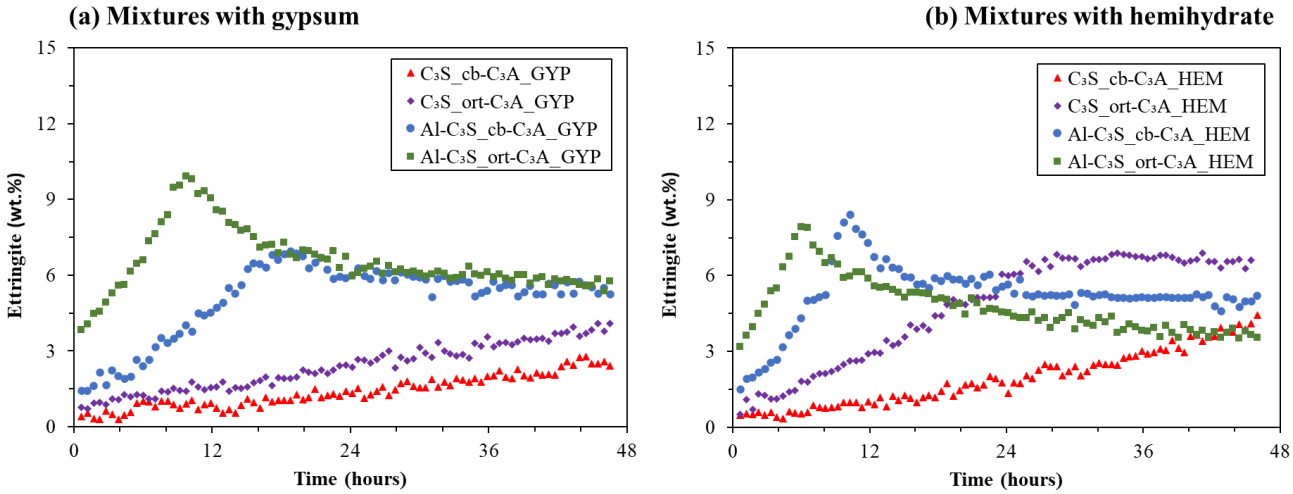

Figure 6.49 – Ettringite content (wt%) in the C_3S/C_3A pastes with (a) gypsum and (b) hemihydrate over the first 48 hours.

6.3.3 Thermogravimetric analysis (TGA)

Figure 6.50 shows the DTG curves of the C_3S/C_3A pastes with 1.5 wt% SO_3 (with gypsum or hemihydrate) at 8 hours, 1, 3, and 7 days of hydration. Peaks related to C-S-H (between 50 and 300°C), ettringite (≈ 100°C), gypsum (≈ 140°C), AFm phases (≈ 155°C), portlandite (between 400 and 500°C), and carbonates (between 600 and 700°C) were observed [30]. As expected, the peaks related to the hydrated phases' decomposition increased with the increase of the hydration time, indicating higher amounts of hydrated phases and a higher degree of hydration. In turn, the gypsum peaks were only presented in the mixtures with C_3S at 8 hours, which agrees

with XRD-Rietveld results, showing that the sulfate depletion occurred after 10 hours of hydration for those samples, while occurred up to 6 hours for the mixes with Al-C_3S.

The C_3S type had a great influence on the moment of AFm formation. While the Al-C_3S pastes already presented the peaks related to AFm phases' decomposition at 8 hours or 1 day, no AFm phases peaks are observed in the C_3S mixes up to 7 days. This result also corroborates the XRD-Rietveld results, in which no AFm phases were observed in the first 48 hours for the C_3S mixes while starting to form between 6 to 16 hours for the Al-C_3S pastes.

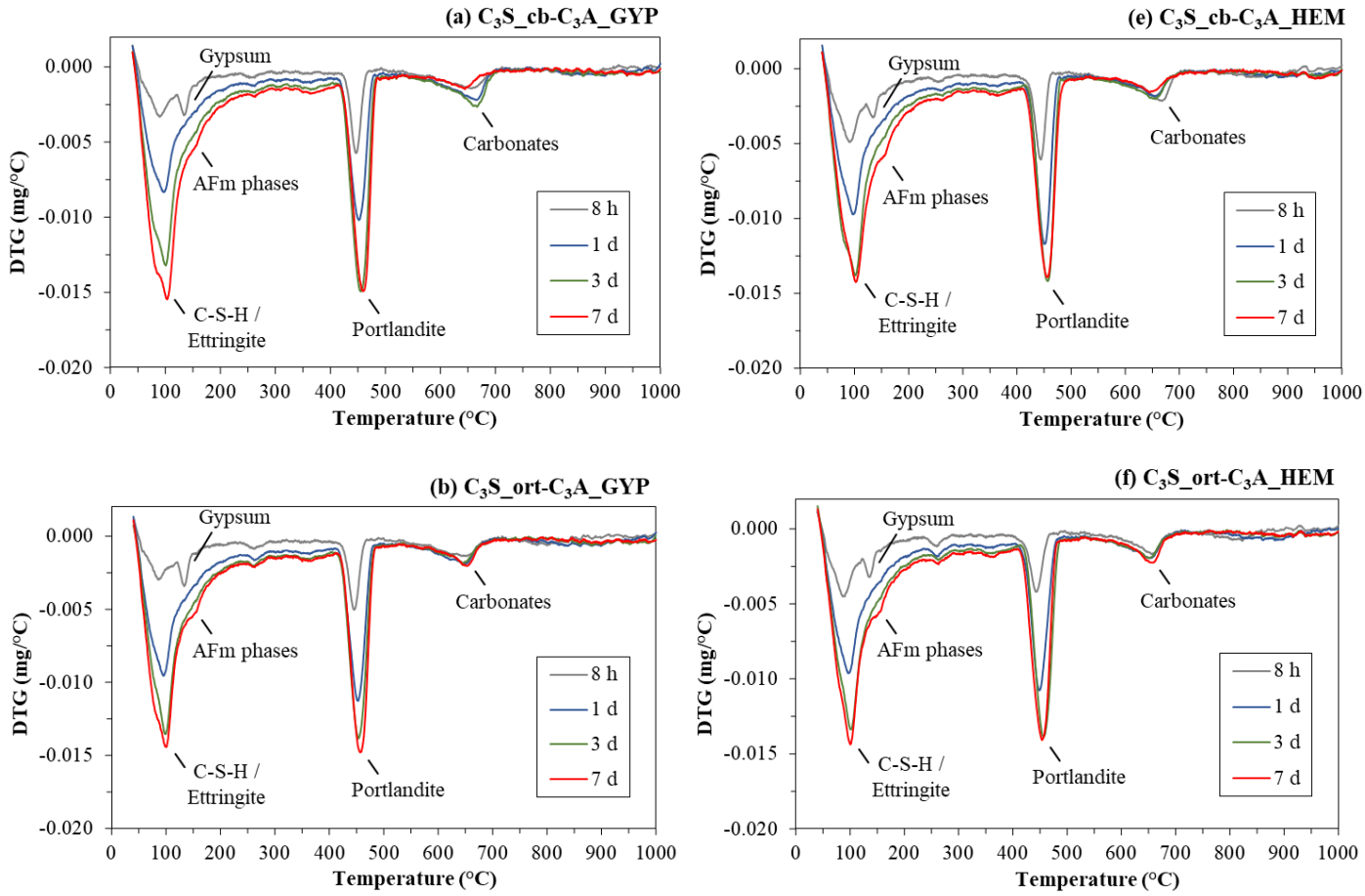

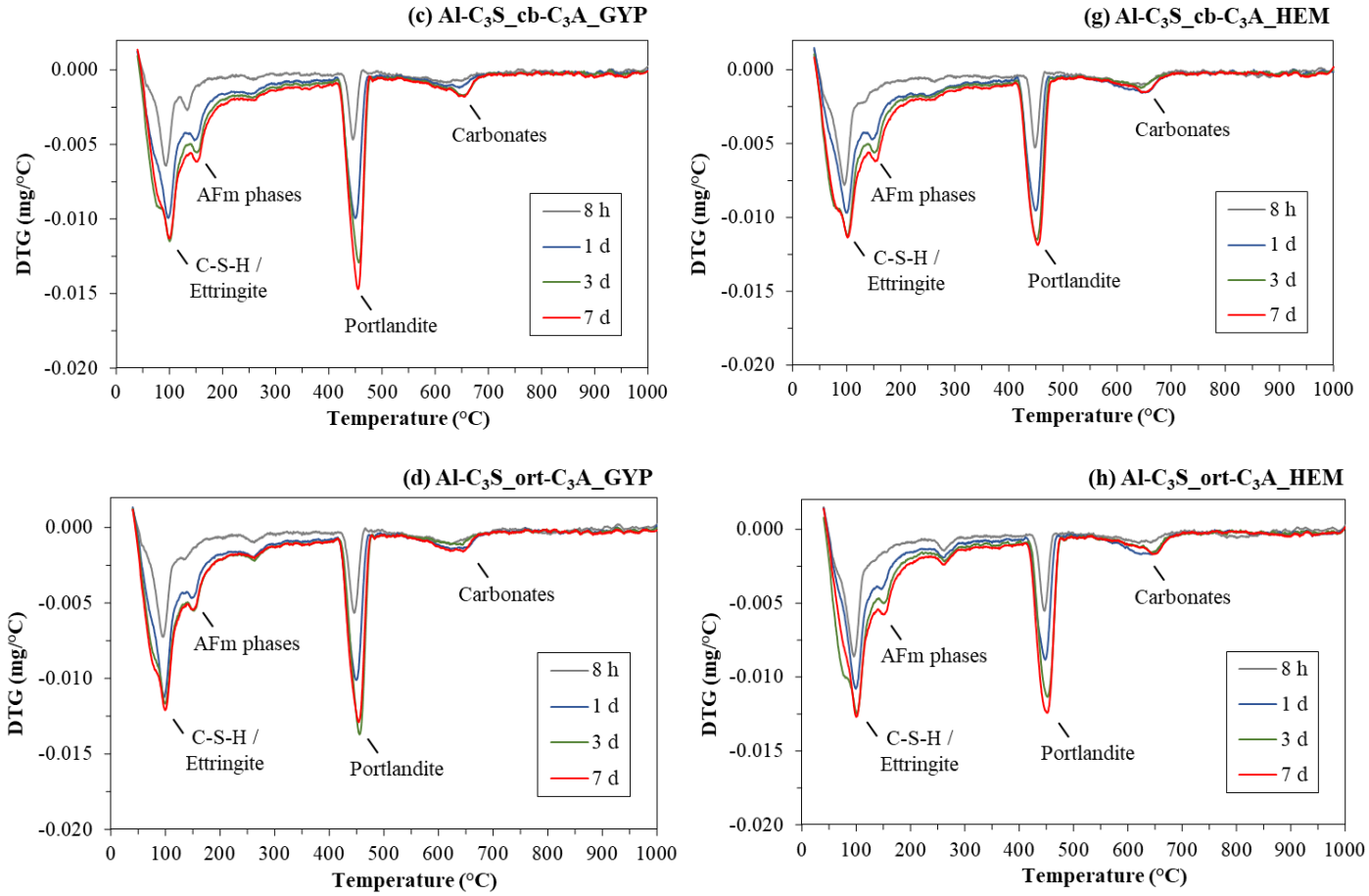

Figure 6.50 – DTG curves of the C_3S/C_3A pastes with gypsum and hemihydrate at 8 h, 1, 3, and 7 d of hydration.

From the TGA results, the bound water content was calculated and is presented in Figure 6.51. The mixes with C_3S presented higher bound water content than those with Al-C_3S. The bound water is related to the degree of hydration (DoH) of C_3S. As observed by isothermal calorimetry (see Section 6.3.1.1), the C_3S is much more reactive than Al-C_3S, which explains the higher bound water content of the mixtures with C_3S. In turn, the C_3A and calcium sulfate types did not significantly influence the bound water content of the mixes, which may be explained by their much lower content compared with C_3S.

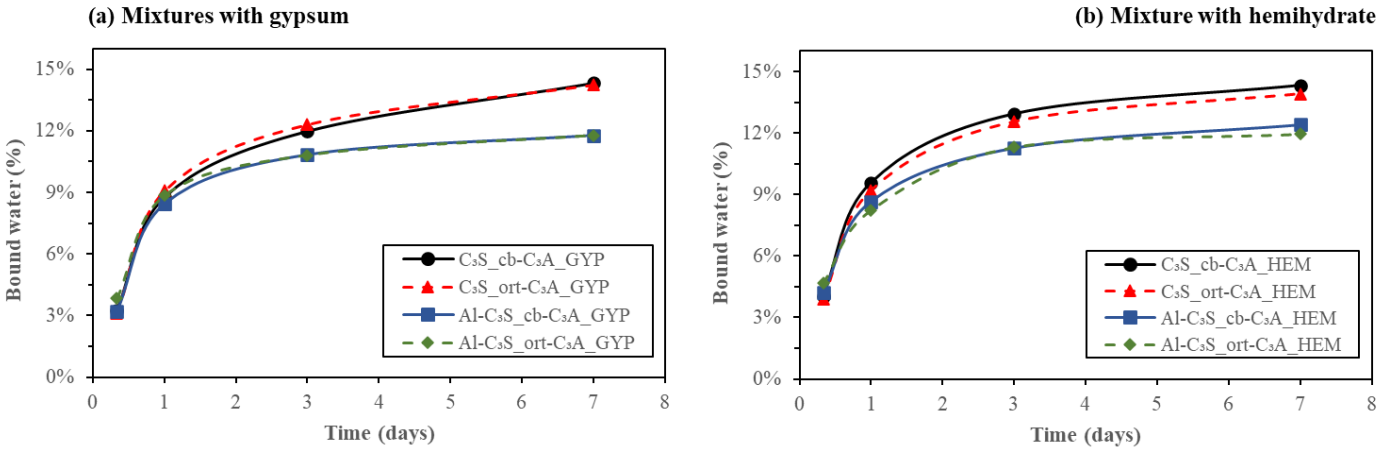

Figure 6.51 – Bound water (%) of the C_3S/C_3A pastes with (a) gypsum and (b) hemihydrate over the first 7 days of hydration.

Figure 6.52 presents the portlandite content (in g/100g of paste) of the C_3S/C_3A pastes with gypsum in (a) and hemihydrate in (b), during the first 7 days of hydration. The portlandite content showed the same trend observed for the bound water content: the C_3S type was the only factor that significantly influenced the portlandite content, where the mixes with C_3S presented higher portlandite content than the mixes with Al-C_3S, which was expected since C_3S is more reactivity than Al-C_3S.

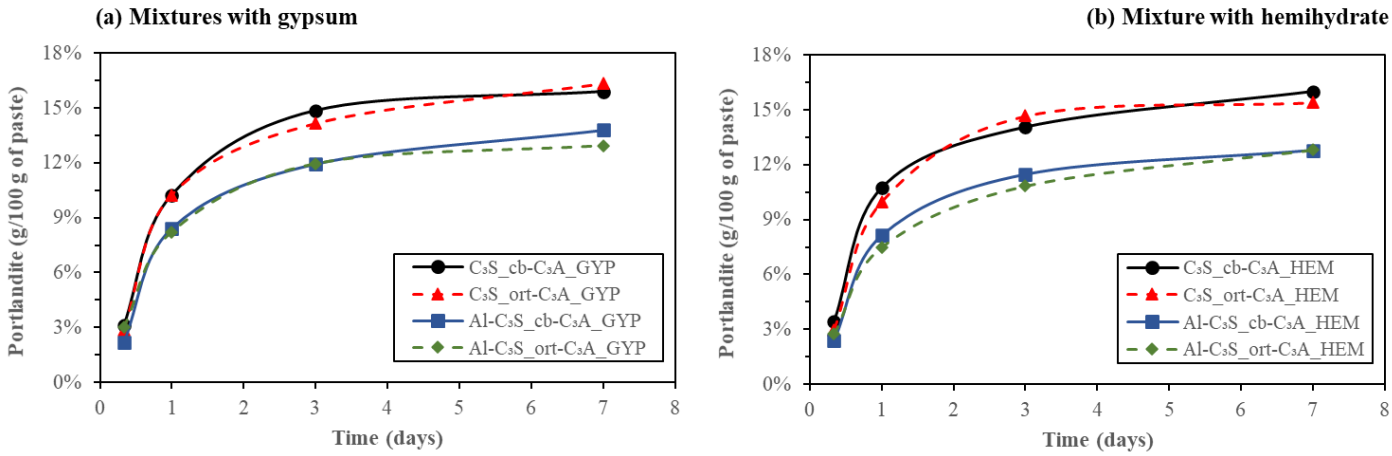

Figure 6.52 – Portlandite content (g/100 of paste), determined by TGA, of the C_3S/C_3A pastes with (a) gypsum and (b) hemihydrate over the first 7 days of hydration.

6.4 DISCUSSION

6.4.1 The impact of aluminum doping of C_3S on sulfate demand

Among the factors analyzed, the aluminum doping of C_3S had the most pronounced influence on the sulfate demand of the systems. The beginning of ettringite decomposition and hemicarbonate formation occurred between 6 and 16 hours (depending on C_3A polymorph and calcium sulfate type used) in the mixes with Al-C_3S (as observed by *in-situ* XRD and confirmed by TGA), while only occurred between 3 and 7 days of hydration for the mixes with C_3S (as seen by TGA).

Zunino and Scrivener [7] studied C_3S T1/cb-C_3A/gypsum systems varying the C_3S fineness and concluded that the higher the C_3S fineness, the earlier is the sulfate depletion and the higher is the sulfate demand of the system. This occurs because the increase of the fineness of C_3S increases its reactivity and, consequently, increases the rate of C-S-H formation [7]. As mentioned early, the sulfates are physically adsorbed by the C-S-H due to charge affinity [56], consuming the sulfates from the solution. Therefore, the higher the amount of C-S-H formed in the first hours, the higher the amount of sulfates adsorbed on the C-S-H surface, and the earlier will be the sulfate depletion of the system.

Interestingly, the opposite behavior was observed here: the systems with Al-C_3S, which presented lower reactivity when compared with C_3S (see Section 6.3.1), presented higher sulfate demand. For instance, the mixes with Al-C_3S required 1.5-2.0 wt% SO_3 to be properly sulfated, while the mixes with C_3S only required 0.5 wt% SO_3. This happens because of the impact of aluminum on sulfate consumption – the higher the aluminum content available in the pore solution, the higher the ettringite formation (observed here by *in-situ* XRD) and the faster will be the sulfate depletion.

Note that Zunino and Scrivener [7] used the same C_3S used here (T1, without aluminum) but with different fineness. Therefore, we can propose that not only the C_3S reactivity will influence the sulfate balance of the system (as observed by [7]) but also the aluminum content in the C_3S. In addition, the latter factor seems to have a greater impact on the sulfate demand than the former, since the mixes with the less reactive Al-C_3S (with 0.8 wt% Al_2O_3) presented a much higher sulfate demand than the mixes with the more reactive C_3S (without aluminum).

6.4.2 The impact of C_3A polymorphism on sulfate demand

The C_3A polymorphism also influenced the sulfate demand of the mixes, but to a less extent than the aluminum doping of C_3S. Furthermore, the influence of the C_3A polymorphism on the sulfate demand depended on the wt% SO_3 used. For the mixes with low SO_3 contents (0.25 and 0.50 wt%SO_3), the systems with cb-C_3A presented earlier sulfate depletion and renewed hydration of C_3A than those mixes with ort-C_3A. However, for the mixes with 1.00 wt% SO_3 or more, the opposite behavior was observed, i.e., the mixes with ort-C_3A presented earlier sulfate depletion.

This behavior is probably due to the different impacts of calcium sulfates on cb-C_3A and ort-C_3A hydration. Without calcium sulfates, cb-C_3A hydrates faster than the orthorhombic one. Besides, the addition of calcium sulfates is much more efficient in delaying the cb-C_3A hydration than the ort-C_3A hydration (for the reasons for this, see Section 6.3.1.2 and other papers [12,13,51]). Therefore, when low amounts of calcium sulfate are used, the cb-C_3A hydration is not sufficiently retarded to be slower than the ort-C_3A hydration.

6.4.3 The impact of calcium sulfate type on C_3S and C_3A hydration and sulfate demand

The addition of calcium sulfate slightly prolonged the induction period of both C_3S and Al-C_3S but enhanced their hydration afterward, resulting in higher heat flow peaks and higher cumulative heat in the first 48 hours. The initial delay probably occurred due to the adsorption of sulfate ions on the C_3S surface [7,17,47], while the enhancement thereafter seems to be related to either the change in the C-S-H morphology due to the sulfate's adsorption or due to the increase in the ionic strength of the solution with the addition of calcium sulfate [11].

However, the calcium sulfate type did not significantly influence the C_3S hydration. The C_3S-gypsum and the C_3S-hemihydrate pastes (with a 1.5 wt% SO_3) presented very similar heat flow curves in the first 48 hours, except for a small heat flow peak between 30 minutes and 2 hours associated with the hydration of hemihydrate and formation of gypsum crystals.

As for the C_3A, the presence of gypsum or hemihydrate retarded both cb-C_3A hydration and ort-C_3A reaction, but the retard effect was much less efficient for the latter. This occurs due to the higher solubility of $Al_6O_{18}^{18-}$ rings on the ort-C_3A, inhibiting the adsorption of S^{2-} and/or Ca–S ion-pair that are responsible for the delay in cb-C_3A hydration [13,14]. The replacement of gypsum with hemihydrate leads to a strong delay on both cb-C_3A and ort-C_3A. The higher

solubility of hemihydrate, releasing more sulfate ions into the pore solution in the first hours might explain this, but more studies on this are necessary to fully understand its mechanism.

The analysis of the effect of calcium sulfate type on the hydration of C_3S/C_3A/calcium sulfate systems showed that the use of hemihydrate resulted in earlier sulfate depletion and hemicarbonate formation (as observed by calorimetry and *in-situ* XRD), consequently presenting a higher sulfate demand to obtain properly sulfated systems, which agrees with Zunino and Scrivener results [7]. This occurs due to the higher solubility of hemihydrate compared with gypsum, resulting in higher sulfite concentrations in the pore solution in the first hours, increasing ettringite's formation (observed here by *in-situ* XRD).

6.4.4 Implications for PC production and PC concrete properties

As observed, the aluminum content in C_3S greatly impacts the sulfate balance of C_3S/C_3A/calcium sulfate systems, which usually correspond to about 70 wt% of ordinary Portland cement. Therefore, Portland clinkers with higher aluminum content (including the aluminum incorporated in the C_3S structure) will present higher sulfate demand, i.e., a higher amount of calcium sulfate will be required to obtain optimal fresh and mechanical properties.

The C_3A polymorph also affected the sulfate balance of the systems studied. For the mixes with 1.0 wt% SO_3 or more, the ort-C_3A reacted faster than the cb-C_3A, leading to faster sulfate depletion (note that commercial PCs usually need 2.5-4.5 wt% SO_3 to be properly sulfated). Therefore, clinkers with ort-C_3A are likely to require more sulfate to reach optimum properties.

Finally, the presence of hemihydrate (which might occur in commercial PCs due to gypsum's dehydration during milling) also increased the sulfate demand of the mixes. Therefore, a higher sulfate content will be needed to optimize the properties of concrete produced with PC containing this type of sulfate source. Furthermore, the crystallization of gypsum and the higher ettringite formation in the presence of hemihydrate tends to decrease PC concrete workability and may result in a false setting [1,57,58].

The understanding of how these parameters influence the sulfate demand of PC will help the cement industry controls the amount and type of calcium sulfate that should be used. However, it stresses the need for further studies on this topic with commercial clinkers since pure phases have inherent differences compared with those present in the clinkers produced by the industry.

6.5 CONCLUSIONS

From our results, we can conclude that:

- Both gypsum and hemihydrate delayed the initial hydration of C_3S and Al-C_3S, prolonging the induction period but accelerating the reaction thereafter. The C_3S-gypsum and C_3S-hemihydrate pastes presented very similar behaviors for the same SO_3 content (1.5 wt% SO_3).

- Aluminum doping of C_3S greatly influenced the sulfate balance of C_3S/C_3A/calcium sulfate mixes. The mixes with Al-C_3S presented faster and higher ettringite formation in the first hours, anticipating the sulfate depletion, the renewed hydration of C_3A, and the hemicarbonate formation.

- The impact of C_3A polymorphism on the sulfate demand varied with the SO_3 content used. For the systems with 0.25 and 0.50 wt% SO_3, the mixes with cb-C_3A presented earlier sulfate depletion and renewed hydration of C_3A. However, for the systems with 1.0 wt% SO_3 or more, those with ort-C_3A presented earlier sulfate depletion and renewed dissolution of C_3A. Therefore, in commercial PCs, which usually need higher sulfate contents to be properly sulfated (usually 2.5- 4.5 wt% SO_3), those clinkers with ort-C_3A will probably require more sulfate to reach optimal fresh and mechanical properties. In proper sulfated mixes, the C_3A polymorphism does not seem to significantly influence the C_3S or Al-C_3S hydration rate

- The replacement of gypsum with hemihydrate in the C_3S/C_3A/calcium sulfate mixes resulted in faster ettringite formation, anticipating the sulfate depletion and renewed hydration of C_3A. This happens due to the higher solubility of hemihydrate when compared with gypsum. In addition, hemihydrate incorporation led to higher sulfate demand, which may require greater sulfate contents in commercial clinkers when this type of sulfate source is used.

6.6 Acknowledgments

JSAN and PRM thank the financial support of (Coordination for the Improvement of Higher Education Personnel) [88882.439908/2019-01]. JSAN thanks the University of Malaga (Spain), where the experiments for the characterization of the raw materials were performed. JSAN also

thanks the Spanish Junta de Andalucía [UMA18-FEDERJA-095] research project for the research stage at the University of Málaga (Spain) and the Graduate Program in Civil Engineering: Construction and Infrastructure (PPGCI) of the Federal University of Rio Grande do Sul (UFRGS), Brazil. The participation APK was sponsored by CNPq (Brazilian National Council for Scientific and Technological Development) through the research fellowships PQ2017 305530/2017- 8. The staff of Laboratório de Difração de Raios-X (LDRX-UFSC) is acknowledged for the *in-situ* XRD data collection.

6.7 References

[1] J. da S. Andrade Neto, A.G. de la Torre, A.P. Kirchheim, Effects of sulfates on the hydration of Portland cement – A review, Construction and Building Materials. 279 (2021). https://doi.org/10.1016/j.conbuildmat.2021.122428.

[2] S. Adu-Amankwah, L. Black, J. Skocek, M. ben Haha, M. Zajac, Effect of sulfate additions on hydration and performance of ternary slag-limestone composite cements, Construction and Building Materials. 164 (2018) 451–462. https://doi.org/10.1016/j.conbuildmat.2017.12.165.

[3] S. Mohammed, O. Safiullah, Optimization of the SO3 content of an Algerian Portland cement: Study on the effect of various amounts of gypsum on cement properties, Construction and Building Materials. 164 (2018) 362–370. https://doi.org/10.1016/j.conbuildmat.2017.12.218.

[4] M. Zajac, J. Skocek, A. Müller, M. ben Haha, Effect of sulfate content on the porosity distribution and resulting performance of composite cements, Construction and Building Materials. 186 (2018) 912–919. https://doi.org/10.1016/j.conbuildmat.2018.07.247.

[5] K. Tosun, Effect of SO3 content and fineness on the rate of delayed ettringite formation in heat cured Portland cement mortars, Cement and Concrete Composites. 28 (2006) 761–772. https://doi.org/10.1016/j.cemconcomp.2006.06.003.

[6] A. Pavoine, X. Brunetaud, L. Divet, The impact of cement parameters on Delayed Ettringite Formation, Cement and Concrete Composites. 34 (2012) 521–528. https://doi.org/10.1016/j.cemconcomp.2011.11.012.

[7] F. Zunino, K. Scrivener, Factors influencing the sulfate balance in pure phase C3S/C3A systems, Cement and Concrete Research. 133 (2020) 106085. https://doi.org/10.1016/j.cemconres.2020.106085.

[8] D. Wagner, F. Bellmann, J. Neubauer, Influence of aluminium on the hydration of triclinic C3S with addition of KOH solution, Cement and Concrete Research. 137 (2020) 106198. https://doi.org/10.1016/j.cemconres.2020.106198.

[9] D. Stephan, S. Wistuba, Crystal structure refinement and hydration behaviour of 3CaO·SiO2 solid solutions with MgO, Al2 O3 and Fe2O3, Journal of the European Ceramic Society. 26 (2006) 141–148. https://doi.org/10.1016/j.jeurceramsoc.2004.10.031.

[10] F. Begarin, S. Garrault, A. Nonat, L. Nicoleau, Hydration of alite containing aluminium, Advances in Applied Ceramics. 110 (2011) 127–130. https://doi.org/10.1179/1743676110Y.0000000007.

[11] J.S. Andrade Neto, E.D. Rodríguez, P.J.M. Monteiro, A.G. de la Torre, A.P. Kirchheim, Hydration of C3S and Al-doped C3S in the presence of gypsum, Cement and Concrete Research. Submitted (2021).

[12] A.P. Kirchheim, E.D. Rodríguez, R.J. Myers, L.A. Gobbo, P.J.M. Monteiro, D.C.C. Dal Molin, R.B. de Souza, M.A. Cincotto, Effect of gypsum on the early hydration of cubic and Na-doped orthorhombic tricalcium aluminate, Materials. 11 (2018) 1–16. https://doi.org/10.3390/ma11040568.

[13] R.J. Myers, G. Geng, E.D. Rodriguez, P. da Rosa, A.P. Kirchheim, P.J.M. Monteiro, Solution chemistry of cubic and orthorhombic tricalcium aluminate hydration, Cement and Concrete Research. 100 (2017) 176–185. https://doi.org/10.1016/j.cemconres.2017.06.008.

[14] J.S. Andrade Neto, P.R. Matos, A.G. de la Torre, C.E.M. Campos, P.J.P. Gleize, P.J.M. Monteiro, A.P. Kirchheim, The role of sodium and sulfate sources on the rheology and hydration of C3A polymorphs, Cement and Concrete Research. 151 (2022) 106639. https://doi.org/10.1016/j.cemconres.2021.106639.

[15] E. Pustovgar, R.K. Mishra, M. Palacios, J.B. d'Espinose de Lacaillerie, T. Matschei, A.S. Andreev, H. Heinz, R. Verel, R.J. Flatt, Influence of aluminates on the hydration kinetics of tricalcium silicate, Cement and Concrete Research. 100 (2017) 245–262. https://doi.org/10.1016/j.cemconres.2017.06.006.

[16] S. Garrault, A. Nonat, Y. Sallier, L. Nicolaeau, On the Origin of the Dormant Period of Cement Hydration, in: 13th International Congress on the Chemistry of Cement., Madrid, 2011: pp. 1–7.

[17] L. Nicoleau, E. Schreiner, A. Nonat, Ion-specific effects influencing the dissolution of tricalcium silicate, Cement and Concrete Research. 59 (2014) 118–138. https://doi.org/10.1016/j.cemconres.2014.02.006.

[18] D. Jansen, Ch. Naber, D. Ectors, Z. Lu, X.-M. Kong, F. Goetz-Neunhoeffer, J. Neubauer, The early hydration of OPC investigated by in-situ XRD, heat flow calorimetry, pore water analysis and 1H NMR: Learning about adsorbed ions from a complete mass balance approach, Cement and Concrete Research. 109 (2018) 230–242. https://doi.org/10.1016/j.cemconres.2018.04.017.

[19] K. Fukuda, S. Inoue, H. Yoshida, Cationic substitution in tricalcium aluminate, Cement and Concrete Research. 33 (2003) 1771–1775. https://doi.org/10.1016/S0008-8846(03)00172-8.

[20] L. Gobbo, L. Sant'Agostino, L. Garcez, C3A polymorphs related to industrial clinker alkalies content, Cement and Concrete Research. 34 (2004) 657–664. https://doi.org/10.1016/j.cemconres.2003.10.020.

[21] V.H. Dodson, T.D. Hayden, Another look at the Portland cement/chemical admixture incompatibility problem, Cement, Concrete and Aggregates. 11 (1989) 52–56. https://doi.org/10.1520/cca10102j.

[22] S. Pourchet, L. Regnaud, J.P. Perez, A. Nonat, Early C3A hydration in the presence of different kinds of calcium sulfate, Cement and Concrete Research. 39 (2009) 989–996. https://doi.org/10.1016/j.cemconres.2009.07.019.

[23] M.N. de Noirfontaine, M. Courtial, F. Dunstetter, G. Gasecki, M. Signes-Frehel, Tricalcium silicate Ca3SiO5 superstructure analysis: A route towards the structure of the M1 polymorph, Zeitschrift Fur Kristallographie. 227 (2012) 102–112. https://doi.org/10.1524/zkri.2012.1425.

[24] M. Palacios, H. Kazemi-Kamyab, S. Mantellato, P. Bowen, Laser diffraction and gas adsorption techniques, in: K. Scrivener, R. Snellings, B. Lothenbach (Eds.), A Practical Guide to Microstructural Analysis of Cementitious Materials, 1st ed., CRC Press, 2016: pp. 445–480.

[25] A.P. Kirchheim, V. Fernàndez-Altable, P.J.M. Monteiro, D.C.C. Dal Molin, I. Casanova, Analysis of cubic and orthorhombic C3A hydration in presence of gypsum and lime, Journal of Materials Science. 44 (2009) 2038–2045. https://doi.org/10.1007/s10853-009-3292-3.

[26] A. Quennoz, K.L. Scrivener, Hydration of C 3A-gypsum systems, Cement and Concrete Research. 42 (2012) 1032–1041. https://doi.org/10.1016/j.cemconres.2012.04.005.

[27] A. Quennoz, K.L. Scrivener, Interactions between alite and C3A-gypsum hydrations in model cements, Cement and Concrete Research. 44 (2013) 46–54. https://doi.org/10.1016/j.cemconres.2012.10.018.

[28] L. Wadsö, Operational issues in isothermal calorimetry, Cement and Concrete Research. 40 (2010) 1129–1137. https://doi.org/10.1016/j.cemconres.2010.03.017.

[29] J.D. Zea-Garcia, A.G. de la Torre, M.A.G. Aranda, I. Santacruz, Processing and characterisation of standard and doped alite-belite-ye'elimite ecocement pastes and mortars, Cement and Concrete Research. 127 (2020). https://doi.org/10.1016/j.cemconres.2019.105911.

[30] B. Lothenbach, P.T. Durdziński, K. de Weerdt, Thermogravimetric analysis, in: K. Scrivener, R. Snellings, B. Lothenbach (Eds.), A Practical Guide to Microstructural Analysis of Cementitious Materials, 1st ed., CRC Press, 2016: pp. 177–212.

[31] A.A. Coelho, TOPAS and TOPAS-Academic: An optimization program integrating computer algebra and crystallographic objects written in C++: An, Journal of Applied Crystallography. 51 (2018) 210–218. https://doi.org/10.1107/S1600576718000183.

[32] R. Snellings, X-ray powder diffraction applied to cement, in: K. Scrivener, R. Snellings, B. Lothenbach (Eds.), A Practical Guide to Microstructural Analysis of Cementitious Materials, 1st ed., CRC Press, 2016: pp. 107–176.

[33] B.H. O'Connor, M.D. Raven, Application of the Rietveld Refinement Procedure in Assaying Powdered Mixtures, Powder Diffraction. 3 (1988) 2–6. https://doi.org/10.1017/S0885715600013026.

[34] D. Jansen, F. Goetz-Neunhoeffer, C. Stabler, J. Neubauer, A remastered external standard method applied to the quantification of early OPC hydration, Cement and Concrete Research. 41 (2011) 602–608. https://doi.org/10.1016/j.cemconres.2011.03.004.

[35] S.T. Bergold, F. Goetz-Neunhoeffer, J. Neubauer, Quantitative analysis of C-S-H in hydrating alite pastes by in-situ XRD, Cement and Concrete Research. 53 (2013) 119–126. https://doi.org/10.1016/j.cemconres.2013.06.001.

[36] S. Dittrich, J. Neubauer, F. Goetz-Neunhoeffer, The influence of fly ash on the hydration of OPC within the first 44 h - A quantitative in situ XRD and heat flow calorimetry study, Cement and Concrete Research. 56 (2014) 129–138. https://doi.org/10.1016/j.cemconres.2013.11.013.

[37] A. Cuesta, J.D. Zea-Garcia, D. Londono-Zuluaga, A.G. de La Torre, I. Santacruz, O. Vallcorba, M. Dapiaggi, S.G. Sanfélix, M.A.G. Aranda, Multiscale understanding of tricalcium silicate hydration reactions, Scientific Reports. 8 (2018) 1–11. https://doi.org/10.1038/s41598-018-26943-y.

[38] A. Cuesta, Á.G. de La Torre, I. Santacruz, A. Diaz, P. Trtik, M. Holler, B. Lothenbach, M.A.G. Aranda, Quantitative disentanglement of nanocrystalline phases in cement pastes by synchrotron ptychographic X-ray tomography, IUCrJ. 6 (2019) 473–491. https://doi.org/10.1107/S2052252519003774.

[39] N.I. Golovastikov, R.G. Matveeva, N. v. Belov, Crystal structure of the tricalcium silicate 3CaO SiO2 = C3S, Soviet Physics - Crystallography. 20 (1975) 441–445.

[40] P. Mondal, J.W. Jeffery, The Crystal Structure of Triealeium Aluminate, Ca3Al2O6, Acta Crystallographica. (1975) 689.

[41] F. Nishi, Y. Takeuchi, The A16018 Rings of Tetrahedra in the Structure of Cas.sNaA16O18, Acta Crystallographica Section B Structural Crystallography and Crystal Chemistry. 31 (1975) 1169–1173.

[42] H.E. Petch, The hydrogen positions in portlandite, Ca(OH)2, as indicated by the electron distribution, Acta Crystallographica. 14 (1961) 950–957. https://doi.org/10.1107/s0365110x61002771.

[43] F. Goetz-Neunhoeffer, J. Neubauer, Refined ettringite (Ca 6 Al 2 (SO 4) 3 (OH) 12 ·26H 2 O) structure for quantitative X-ray diffraction analysis , Powder Diffraction. 21 (2006) 4–11. https://doi.org/10.1154/1.2146207.

[44] Á.G. de la Torre, M.-G. López-Olmo, C. Álvarez-Rua, S. García-Granda, Miguel.A.G. Aranda, Structure and microstructure of gypsum and its relevance to Rietveld quantitative phase analyses, Powder Diffraction. 19 (2004) 240–246. https://doi.org/10.1154/1.1725254.

[45] C. Bezou, A. Nonat, J.C. Mutin, A. Nørlund Christensen, M.S. Lehmann, Investigation of the crystal structure of γ-CaSO4, CaSO4 · 0.5 H2O, and CaSO4 · 0.6 H2O by powder diffraction methods, Journal of Solid State Chemistry. 117 (1995) 165–176. https://doi.org/10.1006/jssc.1995.1260.

[46] T. Runčevski, R.E. Dinnebier, O. v. Magdysyuk, H. Pöllmann, Crystal structures of calcium hemicarboaluminate and carbonated calcium hemicarboaluminate from synchrotron powder diffraction data, Acta Crystallographica Section B: Structural Science. 68 (2012) 493–500. https://doi.org/10.1107/S010876811203042X.

[47] P. Juilland, L. Nicoleau, R.S. Arvidson, E. Gallucci, Advances in dissolution understanding and their implications for cement hydration, RILEM Technical Letters. 2 (2017) 90. https://doi.org/10.21809/rilemtechlett.2017.47.

[48] S.T. Bergold, F. Goetz-Neunhoeffer, J. Neubauer, Interaction of silicate and aluminate reaction in a synthetic cement system: Implications for the process of alite hydration, Cement and Concrete Research. 93 (2017) 32–44. https://doi.org/10.1016/j.cemconres.2016.12.006.

[49] F.P. Glasser, M.B. Marinho, Early stages of the hydration of tricalcium aluminate and its sodium-cotaining solid solutions, Proceedings of the British Ceramic Society. 35 (1984) 221–236.

[50] J.S. Andrade Neto, P.R. Matos, A.G. de la Torre, C.E.M. Campos, P.J.P. Gleize, P.J.M. Monteiro, A.P. Kirchheim, The role of sodium and sulfate sources on the rheology and hydration of C3A polymorphs, Cement and Concrete Research. Submitted (2021).

[51] M.M. Alonso, F. Puertas, Adsorption of PCE and PNS superplasticisers on cubic and orthorhombic C3A. Effect of sulfate, Construction and Building Materials. 78 (2015) 324–332. https://doi.org/10.1016/j.conbuildmat.2014.12.050.

[52] C. Jakob, D. Jansen, N. Ukrainczyk, E. Koenders, U. Pott, D. Stephan, J. Neubauer, Relating ettringite formation and rheological changes during the initial cement hydration: A comparative study applying XRD analysis, rheological measurements and modeling, Materials. 12 (2019). https://doi.org/10.3390/ma12182957.

[53] D. Jansen, J. Neubauer, F. Goetz-Neunhoeffer, R. Haerzschel, W.D. Hergeth, Change in reaction kinetics of a Portland cement caused by a superplasticizer - Calculation of heat flow curves from XRD data, Cement and Concrete Research. 42 (2012) 327–332. https://doi.org/10.1016/j.cemconres.2011.10.005.

[54] M. García-Maté, A.G. de La Torre, L. León-Reina, E.R. Losilla, M.A.G. Aranda, I. Santacruz, Effect of calcium sulfate source on the hydration of calcium sulfoaluminate eco-cement, Cement and Concrete Composites. 55 (2015) 53–61. https://doi.org/10.1016/j.cemconcomp.2014.08.003.

[55] M.J. Sánchez-Herrero, A. Fernández-Jiménez, A. Palomo, C4A3Š hydration in different alkaline media, Cement and Concrete Research. 46 (2013) 41–49. https://doi.org/10.1016/j.cemconres.2013.01.008.

[56] B. Mota, T. Matschei, K. Scrivener, The influence of sodium salts and gypsum on alite hydration, Cement and Concrete Research. 75 (2015) 53–65. https://doi.org/10.1016/j.cemconres.2015.04.015.

[57] C.W. Chung, P. Suraneni, J.S. Popovics, L.J. Struble, Using ultrasonic wave reflection to monitor false set of cement paste, Cement and Concrete Composites. 84 (2017) 10–18. https://doi.org/10.1016/j.cemconcomp.2017.08.010.

[58] R.M. Mota, A.S. Silva, V.H.S. Ramos, J.C.T. Rezende, E. de Jesus, Effects of storage temperature and time on false setting behavior of CPI-S Portland cement, Ceramica. 66 (2020) 321–329. https://doi.org/10.1590/0366-69132020663792842.

Chapter 7

Final considerations

7 FINAL CONSIDERATIONS

As idealized in the structuring of this dissertation, the document was divided into specific chapters, which were written in the form of articles, in which the state of the art, the materials, and the experimental method used, as well as the results, discussions and main conclusions of each chapter are presented in each one. In this way, the main conclusions of the work are pointed out here.

In the review article (chapter 3), the most important findings on the effects of sulfates on cement properties were summarized. The effects of sulfates on C_3A, C_3S, and PC hydration and on concrete properties were discussed. The main factors which influence the sulfate balance and the methods most used to determine the optimum sulfate content were presented. Finally, recommendations for future research were also discussed. In light of this, different studies were planned to better understand the effects and mechanisms of different calcium sulfate types on the C_3S and C_3A polymorphs hydration.

In chapter 4, it was presented the study regarding the hydration of C_3S and Al-doped C_3S in the presence of gypsum. It was observed that the presence of gypsum delayed the initial hydration of C_3S and Al-C_3S, prolonging the induction period, which seems to be related to the interaction between the sulfate ions and C_3S. However, the presence of gypsum accelerated the C_3S and the Al-C_3S hydration during the nucleation and growth period (after the induction period). This acceleration is probably related to (i) the more divergent needle-structure C-S-H morphology when sulfate is present (according to bibliography), which increases the site for the precipitation of hydration products. (ii) the increase in ionic strength when adding gypsum. Further investigations on this subject are needed to confirm these hypotheses.

In the sequence, in chapter 5, the role of sodium and calcium sulfate type on the hydration and rheology of C_3A polymorphs were studied. It was showed that the higher reactivity of orthorhombic C_3A in sulfate-containing solution, compared with cubic C_3A is related to the differences in crystal structure rather than the release of sodium and the increase of solution alkalinity. The external addition of sodium (i.e., NaOH incorporation) in cubic C_3A paste indeed accelerated its hydration rate, but not reached the very high reaction rate of orthorhombic C_3A. Orthorhombic C_3A paste produced with gypsum presented viscosity and yield stress values 10-20 times higher than those containing cubic C_3A with and without NaOH, as a result

of its much higher reactivity. The replacement of gypsum with hemihydrate (in a SO_3/C_3A ratio of 0.29) retarded cubic C_3A hydration but accelerated the orthorhombic C_3A hydration. Finally, it was shown that the use of hemihydrate in pastes with either cubic or orthorhombic C_3A resulted in early stiffing (the so-called false set) within the first 10 minutes due to the hydration of hemihydrate and precipitation of larger gypsum crystals, making it lose workability.

In the last study presented in chapter 6, the hydration of three-phase systems (C_3S-C_3A-calcium sulfate) was analyzed. It was showed that aluminum doping of C_3S greatly influenced the sulfate balance of C_3S/C_3A/calcium sulfate mixes. The mixes with Al-C_3S presented faster and higher ettringite formation in the first hours, anticipating, the sulfate depletion, the renewed hydration of C_3A, and the hemicarbonate formation. It was also observed that the impact of C_3A polymorphism on the sulfate demand varied with the SO_3 content used. For the systems with 0.50 wt.% SO_3, the mixes with cb-C_3A presented earlier sulfate depletion and renewed hydration of C_3A. However, for the systems with 1.0 wt.% SO_3 or more, those with ort-C_3A presented earlier sulfate depletion and renewed dissolution of C_3A. Therefore, in commercial PCs which usually need higher sulfate contents to be properly sulfated (usually 2.5- 4.5 wt.% SO_3), those clinkers with ort-C_3A will probably require more sulfate to reach optimal fresh and mechanical properties. Finally, the replacement of gypsum with hemihydrate in the C_3S/C_3A/calcium sulfate mixes resulted in faster ettringite formation, which anticipated the sulfate depletion and renewed hydration of C_3A. This happens due to the higher solubility of hemihydrate when compared with gypsum. Hemihydrate incorporation led to higher sulfate demand, which may require greater sulfate contents in commercial clinkers when this type of sulfate source is presented (which might be due the high temperature acquired during the milling process).

Overall, this dissertation spread light to the effect of aluminum-doping on C_3S and sodium-doping on C_3A in their hydration and in the sulfate balance of three-phase systems. It was also showed the impact of the calcium sulfate type on the sulfate demand of these mixtures. As highlighted through the discussion of each chapter, the results presented here contributed to the understanding of the mechanism and factors that influence the hydration of these phases and showed some possible implications for cement production and PC concrete properties. It is stressed out the needing to confirm these findings on studies with commercial clinkers, as the pure clinker phases studied here present some differences from the phases of commercial clinker, as previously discussed.

7.1 Suggestions for future studies

- To evaluate the role of aluminum from SCMs on the sulfate demand of Portland clinkers.
- To investigate the reason for the high sulfate demand on Portland cements with plasticizers.
- To analyze the impact of C_3S and C_3A polymorphs on the properties and on the sulfate demand of commercial cements.
- To evaluate the effect of the calcium sulfate type on the sulfate demand of commercial cements.

ANNEX A

Other activities developed during the Master's

8 OTHER ACTIVITIES DEVELOPED DURING THE MASTER'S

Articles that support this Master dissertation

[1] José S. Andrade Neto, Angeles G. de la Torre, Ana Paula Kirchheim. Effects of sulfates on the hydration of Portland cement – A review. **Construction and Building Materials**, v. 279, paper 122428, 2021. https://doi.org/10.1016/j.conbuildmat.2021.122428

[2] José S. Andrade Neto, Erich D. Rodríguez, Paulo J. M. Monteiro, Angeles G. de la Torre, Ana Paula Kirchheim. Hydration of C_3S and Al-doped C_3S in the presence of gypsum. Accepted for publication in **Cement and Concrete Research**.

[3] José S. Andrade Neto, Paulo R. de Matos, Angeles G. de la Torre, Carlos E. M. Campos, Philippe J. P. Gleize, Paulo J. M. Monteiro, Ana Paula Kirchheim. The role of sodium and sulfate sources on the rheology and hydration of C_3A polymorphs. Accepted for publication in **Cement and Concrete Research**.

[4] José S. Andrade Neto, Paulo R. de Matos, Angeles G. de la Torre, Carlos E. M. Campos, Sandro M. Torres, Paulo J. M. Monteiro, Ana Paula Kirchheim. Hydration and interactions between C_3S and C_3A polymorphs in the presence of different calcium sulfates. To be submitted to **Cement and Concrete Research**.

Other publications during the period of the Master's (March 2019 – May 2021)

[1] Raphael D. Mariano, **José S. Andrade Neto**, Márcio R. Morelli, Daniel V. Ribeiro. Retarding effect of grinding dust and its influence on the physical-mechanical and rheological properties of cementitious matrices. **Revista IBRACON de estruturas e materiais**, v. 12, p. 486-508, 2019.

[2] Bruna B. Mariani, **José S. Andrade Neto**, Nilson S. Amorim Júnior, Daniel V. Ribeiro. Efeito da incorporação de resíduo de TiO2 (MNR) na formação das fases mineralógicas de clínquer Portland. **Ambiente Construído**, v. 19, p. 57-71, 2019.

[3] Diana D. M. Albuquerque, **José S. Andrade Neto**, Nilson S. Amorim Júnior, Daniel V. Ribeiro. Propriedades das argamassas de revestimento contendo resíduo proveniente da produção do TiO_2 (MNR). **Cerâmica**, v. 65, p. 340-350, 2019.

[4] André G. Gomes, Tiago A. Santos, **José S. Andrade Neto**, Daniel V. Ribeiro. Mineralogical analysis of Portland clinker produced from the incorporation of granitic rock fines (GRF). **Key Engineering Materials,** v. 803, p. 309-313, 2019.

[5] **José S. Andrade Neto**, Diana D. M. Albuquerque, Nilson S. Amorim Júnior, Daniel V. Ribeiro. Effect of the Addition of Unreacted Ilmenite (UOW) on the Hydration of White Portland Cement - Hydrated Lime Pastes. **Key Engineering Materials**, v. 803, p. 289-293, 2019.

[6] **José S. Andrade Neto,** Bruna B. Mariani, Nilson S. Amorim Júnior, Daniel V. Ribeiro. Characterization of Cements Produced from Clinker Co-Processed with TiO_2 Waste (UOW). **Key Engineering Materials**, v. 803, p. 278-283, 2019.

[7] **José S. Andrade Neto,** Tiago A. Santos, Raphael D. Mariano, Márcio R. Morelli, Daniel V. Ribeiro. Influence of Clutch Disc Waste (Grinding Dust) on Portland Cement Hydration. **Key Engineering Materials**, v. 803, p. 284-288, 2019.

[8] Adriana Nicolini, Vinícius G. Maciel, **José S. Andrade Neto**, Saulo R. Bragança, Marly M. Jacobi. Rheological behavior of fresh latex polymeric mortar by squeeze-flow technique. **Construction and Building Materials**, v. 267, p. 121175, 2020.

[9] Thaís, P. L. Siqueira, **José S. Andrade Net**o, Cléber M. R. Dias, Daniel V. Ribeiro. Adição de finos de rocha granítica e seus efeitos nas propriedades de argamassas autoadensáveis. **Ambiente Construído**, v. 20, p. 451-466, 2020.

[10] Henrique A. Santana, **José S. Andrade Neto**, Nilson S. Amorim Júnior, Daniel V. Ribeiro, Marcelo S. Cilla, Cleber M. R. Dias. Self-compacting geopolymer mix (SCGM): dosing based on statistical design of mixtures and multiple optimization. **Construction and Building Materials**, v. 249, p. 1-11, 2020.

[11] Paulo R. de Matos, **José S. Andrade Neto**, Carlos E. M. Campos, Is the R index accurate to assess the preferred orientation of portlandite in cement pastes? **Construction and Building Materials**, v. 292, p. 123471, 2021.

[12] Nilson S. Amorim Júnior, **José S. Andrade Neto**, Henrique A. Santana, Marcelo S. Cilla, Daniel V. Ribeiro. Durability and service life analysis of metakaolin-based geopolymer concretes with respect to chloride penetration using chloride migration test and corrosion potential. **Construction and Building Materials**, v. 287, p. 122970, 2021.

[13] **José S. Andrade Neto**, Tiago A. Santos, Silas A. Pinto, Cleber M. R. Dias, Daniel V. Ribeiro. Effect of the combined use of carbon nanotubes (CNT) and metakaolin on the properties of cementitious matrices. **Construction and Building Materials**, v. 271, p. 121903, 2021.

[14] **José S. Andrade Neto**, Mavisson J. S. França, Nilson S. Amorim Júnior, Daniel V. Ribeiro. Effects of adding sugarcane bagasse ash on the properties and durability of concrete. **Construction and Building Materials,** v. 266, p. 1-13, 2021.

[15] **José S. Andrade Neto**, Jéssica D. Bersch, Thaís S. M. Silva, Erich D. Rodríguez, Seiiti Suzuki, Ana Paula Kirchheim. Influence of phosphogypsum purification with lime on the properties of cementitious matrices with and without plasticizer. **Construction and Building Materials**, v. 299, paper 123935, 2021.

[16] Daniel V. Ribeiro, Silas A. Pinto, Nilson S. Amorim Júnior, **José S. Andrade Neto**, Mavisson J. S. França. Effects of binders characteristics and concrete dosing parameters on the chloride diffusion coefficient. **Cement & Concrete Composites**, v. 122, paper 104114, 2021.

[17] Nagilla Azevedo, **José S. Andrade Neto**, Paulo de Matos, Andrea Betioli, Maciej Szelag, Philippe Gleize. Utilization of Thermally Treated SiC Nanowhiskers and Superplasticizer for Cementitious Composite Production. **Materials**, v. 14, paper 4062, 2021.

[18] Henrique A. Santana, **José S. Andrade Neto**, Daniel V. Ribeiro, Marcelo S. Cilla, Cleber M. R. Dias. Accelerated alkaline attack of 3D printing polymers to assess their durability in geopolymer-based matrices. **Journal of Materials in Civil Engineering**, In press, 2021.

[19] Daniel V. Ribeiro, Nilson S. Amorim Júnior, **José S. Andrade Neto**, Diana D. M. de Albuquerque, Barbara Mazzilli. Performance and radiological implications of using a residue from the TiO_2 production as a component of coating mortar. **Construction and Building Materials**, In press, 2021.

[20] Tiago A. Santos, **José S. Andrade Neto**, Marcelo S. Cilla, Daniel V. Ribeiro. Influence of the content of alkalis (Na_2O and K_2O), MgO and SO_3 present in the granite rock fine (GRF) in the production of Portland clinker. **Journal of Materials in Civil Engineering**, In press, 2021.

Book chapters (March 2019 – May 2021)

[1] Tiago A. Santos, **José S. Andrade Neto**, Daniel V. Ribeiro. Processo de produção e tipos de cimento. In: Daniel Véras Ribeiro. (Org.). Princípios da ciência dos materiais cimentícios: Produção, reações, aplicações e avanços tecnológicos. 1ed.Curitiba: Appris, 2021, v. 1, p. 29-66.

[2] **José S. Andrade Neto**, Tiago A. Santos, Daniel V. Ribeiro. Hidratação do cimento Portland. In: Daniel Véras Ribeiro. (Org.). Princípios da ciência dos materiais cimentícios: Produção, reações, aplicações e avanços tecnológicos. 1ed.Curitiba: Appris, 2021, v. 1, p. 67-94.

[3] Nilson S. Amorim Júnior, Henrique A. Santana, Tiago A. Santos, **José S. Andrade Neto**, Marcelo S. Cilla, Daniel V. Ribeiro. Ligantes alternativos. In: Daniel Véras Ribeiro.

(Org.). Princípios da ciência dos materiais cimentícios: Produção, reações, aplicações e avanços tecnológicos. 1ed.Curitiba: Appris, 2021, v. 1, p. 131-184.

[4] Thaís P. L. Siqueira, **José S. Andrade Net**o, Cléber M. R. Dias, Daniel V. Ribeiro. Reologia das matrizes cimentícias. In: Daniel Véras Ribeiro. (Org.). Princípios da ciência dos materiais cimentícios: Produção, reações, aplicações e avanços tecnológicos. 1ed.Curitiba: Appris, 2021, v. 1, p. 269-306.

[5] Tiago A. Santos, **José S. Andrade Neto**, Daniel V. Ribeiro. Técnicas de caracterização de matrizes cimentícias. In: Daniel Véras Ribeiro. (Org.). Princípios da ciência dos materiais cimentícios: Produção, reações, aplicações e avanços tecnológicos. 1ed.Curitiba: Appris, 2021, v. 1, p. 185-268.

Publication in conferences (March 2019 – May 2021)

[1] Nilson S. Amorim Júnior, Felipe R. Azevedo, **José S. Andrade Neto**, Daniel V. Ribeiro. Desempenho de compósitos de poliéster reforçados com fibra de vidro utilizados em postes de distribuição elétrica submetidos ao envelhecimento artificial acelerado por exposição à radiação ultravioleta (UVA). In: 61° Congresso Brasileiro do Concreto, 2019, Fortaleza. Anais do 61° Congresso Brasileiro do Concreto, 2019. p. 1-11.

[2] Nilson S. Amorim Júnior, Mavisson J. S. França, **José S. Andrade Neto**, Marcelo S. Cilla, Daniel V. Ribeiro. Avaliação da durabilidade de concretos geopoliméricos em comparação aos concretos convencionais. In: 61° Congresso Brasileiro do Concreto, 2019, Fortaleza. Anais do 61° Congresso Brasileiro do Concreto, 2019. p. 1-16.

[3] Henrique A. Santana, **José S. Andrade Neto**, Nilson S. Amorim Júnior, Daniel V. Ribeiro, Marcelo S. Cilla, Cleber M. R. Dias. Argamassa geopolimérica autoadensável: Dosagem por meio de projeto estatístico de mistura. In: 61° Congresso Brasileiro do Concreto, 2019, Fortaleza. Anais do 61° Congresso Brasileiro do Concreto, 2019. p. 1-13.

[4] Thaís P. L. Siqueira, **José S. Andrade Net**o, Cléber M. R. Dias, Daniel V. Ribeiro. Influência da adição de finos de rocha granítica nas propriedades reológicas e mecânicas de argamassas autoadensáveis. In: XIII Simpósio Brasileiro de Tecnologia das Argamassas (SBTA), 2019, Goiânia. Anais do XIII Simpósio Brasileiro de Tecnologia das Argamassas (SBTA), 2019. p. 127-135.

[5] **José S. Andrade Neto**, Silas A. Pinto, Tiago A. Santos, Cleber M. R. Dias, Daniel V. Ribeiro. Comportamento reológico, físico e mecânico de misturas cimentícias com nanotubos de carbono (NTC). In: XIII Simpósio Brasileiro de Tecnologia das Argamassas (SBTA), 2019, Goiânia. Anais do XIII Simpósio Brasileiro de Tecnologia das Argamassas (SBTA), 2019. p. 251-259.

[6] Nilson S. Amorim Júnior, **José S. Andrade Neto**, Henrique A. Santana, Marcelo S. Cilla, Daniel V. Ribeiro. Durabilidade de concretos geopoliméricos em relação à penetração de cloretos quanto ao potencial de corrosão e migração de cloretos. In: 3 Seminário Baiano de Durabilidade e Desempenho das Construções (BADUCON), 2020, Salvador. Anais do 3 Seminário Baiano de Durabilidade e Desempenho das Construções, 2020. v. 1. p. 173-189.

[7] Kaline G. Calazans, Thaís P. L. Siqueira, **José S. Andrade Net**o, Paulo R. L. Lima. Revisão sobre o processo de carbonatação no concreto armado e compósitos de fibrocimento e os principais fatores que o influenciam. In: 3 Seminário Baiano de Durabilidade e Desempenho das Construções (BADUCON), 2020, Salvador. Anais do 3 Seminário Baiano de Durabilidade e Desempenho das Construções, 2020. p. 217-230.

Conferences (March 2019 – May 2021)

[1] “Comportamento reológico, físico e mecânico de misturas cimentícias com nanotubos de carbono (NTC)” presented at XIII Simpósio Brasileiro de Tecnologia das Argamassas (SBTA), 2019, Goiânia, Brazil.

[2] 15th International Congress on the Chemistry of Cement (ICCC), 2019, Prague, Czech Republic.

Courses (March 2019 – May 2021)

[1] "Argamassas: Importância e Caracterização dos Momentos Reológicos". (Duration: 4h). Associação Nacional de Tecnologia do Ambiente Construído, ANTAC. Goiânia, Brazil.

[2] "Supplementary Cementitious Materials". (Duration: 5h). 15th International Congress on the Chemistry of Cement (ICCC), 2019, Prague, Czech Republic.

[3] "Hydration of Cementitious Materials". (Duration: 5h). 15th International Congress on the Chemistry of Cement (ICCC), 2019, Prague, Czech Republic

[4] LC^3 doctoral school: Characterization methods of blended cements. (Duration: 24h). Ecole Polytechnique Fédérale de Lausanne, EPFL, 2020. Lausanne, Switzerland.

Lectures for undergraduation and graduation students (march 2019 – may 2021)

[1] Otimização de sulfatos no cimento Portland (Duration: 2h). In: Cimento Portland e alternativos: produção, produtos formados na hidratação e técnicas de análise microestrutural, (PPGCI/UFRGS, graduation). August, 2020

[2] Argamassas (Duration: 3h). In: Técnicas de Edificação A (Architecture/UFRGS, undergraduation). April, 2021.

[3] Otimização de sulfatos no cimento Portland (Duration: 1h). In: Reunião do grupo do Laboratório de Inovação em Cimentos Ecoeficientes (LINCE).

[4] Discussion regarding the article "The early hydration of OPC investigated by in-situ XRD, heat flow calorimetry, pore water analysis and ^{1}H NMR (Duration: 1h). In: Reunião do grupo do Laboratório de Inovação em Cimentos Ecoeficientes (LINCE).

[5] Hidratação de diferentes polimorfos do C_3S na presença de gipsita (Duration: 1h). In: Reunião do grupo do Laboratório de Inovação em Cimentos Ecoeficientes (LINCE).

[6] Revisão sistemática de literatura: Menor relação água/cimento para a completa hidratação do cimento Portland (Duration: 1h). In: Reunião do grupo do Laboratório de Inovação em Cimentos Ecoeficientes (LINCE).

[7] Práticas recomendadas – calorimetria isotérmica (Duration: 1h). In: Reunião do grupo do Laboratório de Inovação em Cimentos Ecoeficientes (LINCE).

Lectures for the cement industry (March 2019 – May 2021)

[1] Otimização de sulfatos no cimento Portland (Duration: 2h). August, 2020.

[2] Fosfogesso – Compatibilidade com aditivos plastificantes (Duration: 3h). August, 2020.

Supervision (October 2019 – February 2021)

[1] Isadora Lemes de Oliveira. Efeito do fíler calcário no teor ótimo de sulfatos no cimento Portland. Iniciação científica.

ANNEX B

Supplementary Material for chapter 4:
Hydration of C_3S and Al-doped C_3S in the presence of gypsum

---

9 SUPPLEMENTARY MATERIAL FOR CHAPTER 4

Table B17 – Phase quantification (g/100g of paste) obtained by XRD-Rietveld of C_3S paste.

Phase	Hydration time				
	Anhydrous	**10 h**	**1 d**	**3 d**	**7 d**
C_3S T1	62.6	56.0	40.8	30.4	21.3
Magnesite	1.0	1.0	0.9	0.6	0.5
Calcite	1.0	0.7	1.1	1.4	1.7
Portlandite	0.8	3.7	10.5	14.7	19.2
Non-crystalline	1.6	9.9	22.8	32.8	42.1
R_{wp}	10.8	10.8	10.9	10.9	11.4
GOF	3.8	3.8	3.9	3.9	4.2

Table B18 – Phase quantification (g/100g of paste) obtained by XRD-Rietveld of C_3S_2.5G paste.

Phase	Hydration time				
	Anhydrous	**10 h**	**1 d**	**3 d**	**7 d**
C_3S T1	61.2	55.7	34.1	20.7	12.7
Magnesite	1.2	0.9	0.7	0.4	0.4
Calcite	1.0	1.0	1.1	1.3	1.4
Gypsum	1.6	0.8	0.7	1.0	1.1
Portlandite	0.8	2.4	11.0	16.8	21.6
Non-crystalline	1.2	9.8	30.5	42.8	50.7
R_{wp}	11.4	11.1	10.9	11.0	11.9
GOF	4.1	3.9	4.0	4.0	4.4

Table.B19 – Phase quantification (g/100g of paste) obtained by XRD-Rietveld of Al-C_3S paste.

Phase	Hydration time				
	Anhydrous	**10 h**	**1 d**	**3 d**	**7 d**
C_3S M1	60.0	54.7	43.6	34.4	28.8
Magnesite	0.5	0.5	0.3	0.2	0.3
Calcite	0.2	0.3	0.6	0.9	1.2
Portlandite	0.1	2.5	8.1	13.2	16.6
Non-crystalline	6.2	12.1	21.3	28.2	34.6
Rwp	11.3	10.5	10.3	10.5	10.6
GOF	4.0	3.7	3.6	3.8	3.8

Table.B20 – Phase quantification (g/100g of paste) obtained by XRD-Rietveld of Al-C_3S_2.5G paste.

Phase	**Hydration time**				
	Anhydrous	**10 h**	**1 d**	**3 d**	**7 d**
C_3S M1	59.1	50.6	40.1	33.4	26.4
Magnesite	0.5	0.4	0.3	0.2	0.3
Calcite	0.4	0.5	0.8	1.0	1.2
Gypsum	1.5	0.7	0.7	0.8	0.9
Ettringite	0.0	0.9	1.3	1.1	1.8
Portlandite	0.2	3.0	8.5	12.3	15.1
Non-crystalline	5.5	15.5	24.4	29.7	36.5
Rwp	11.0	10.3	10.1	10.1	10.4
GOF	3.9	3.7	3.6	3.6	3.6

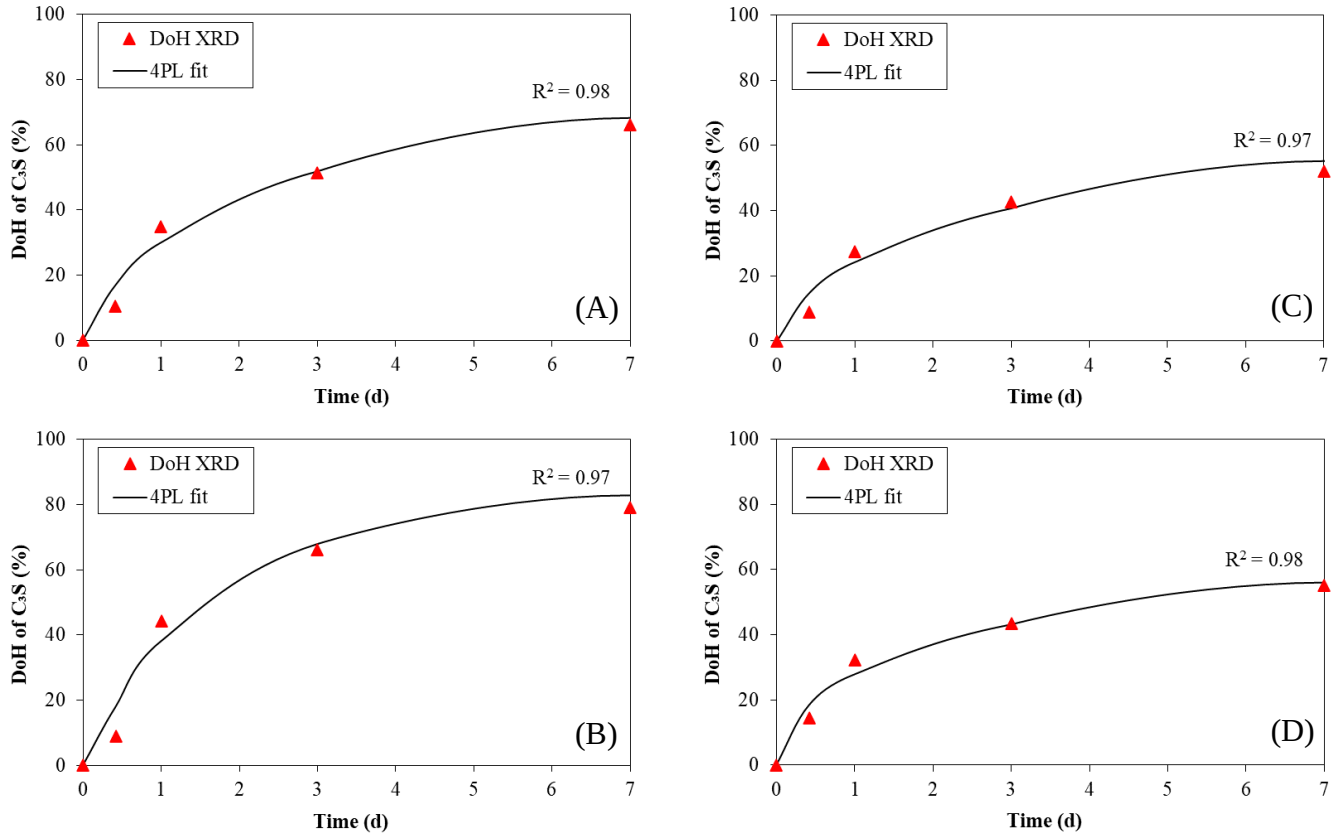

Figure B1 – Degree of Hydration (DoH) of C_3S in (A) C_3S, (B) C_3S_2.5G, (C) Al-C_3S, and (D) Al-C_3S_2.5G pastes obtained by XRD and by the 4PL model used for GEMS analysis.

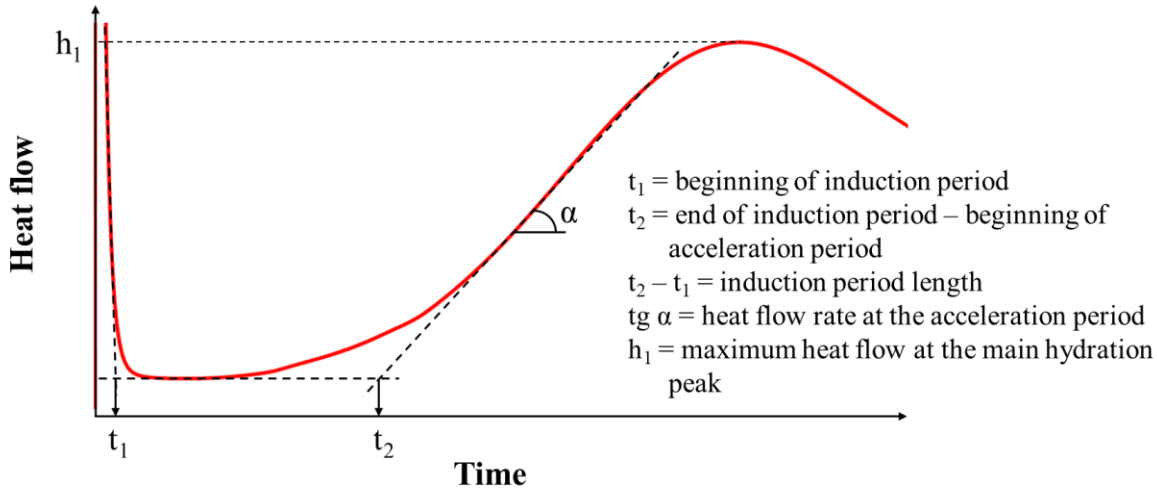

Figure B2 – Illustration of heat flow as a function of time and the parameters obtained to determine the induction period length and the heat flow rate at the acceleration period.

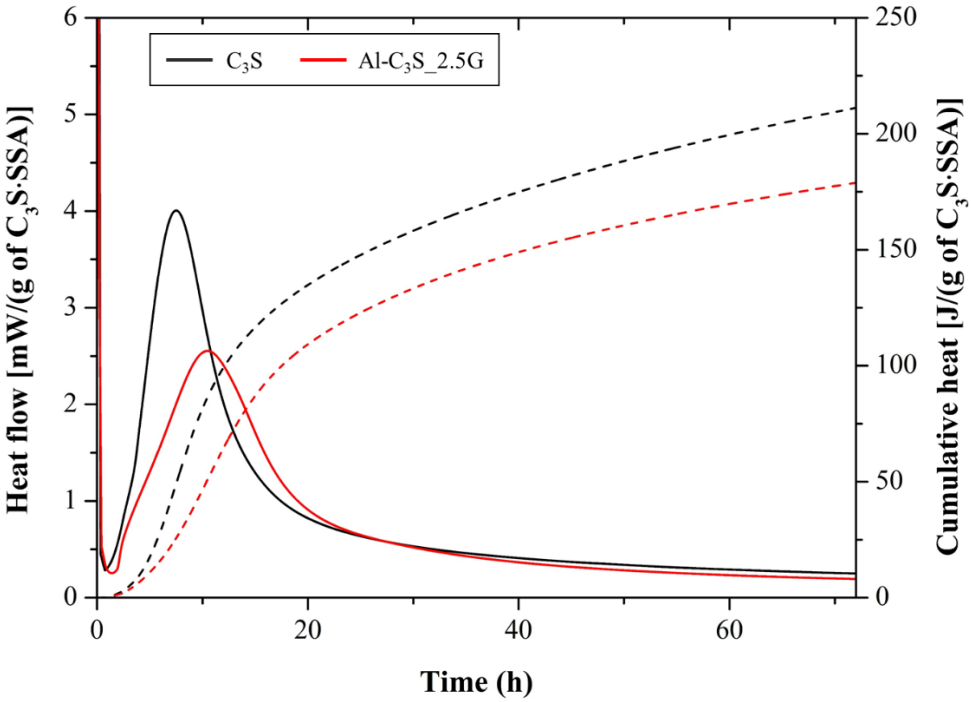

Figure B3 – Heat flow curves (solid lines and primary/left "y" axis) and cumulative heat curves (dashed lines and secondary/right "y" axis) of the C_3S and Al-C_3S pastes, normalized by the SSA of C_3S and Al-C_3S, during the first 72 hours of hydration.

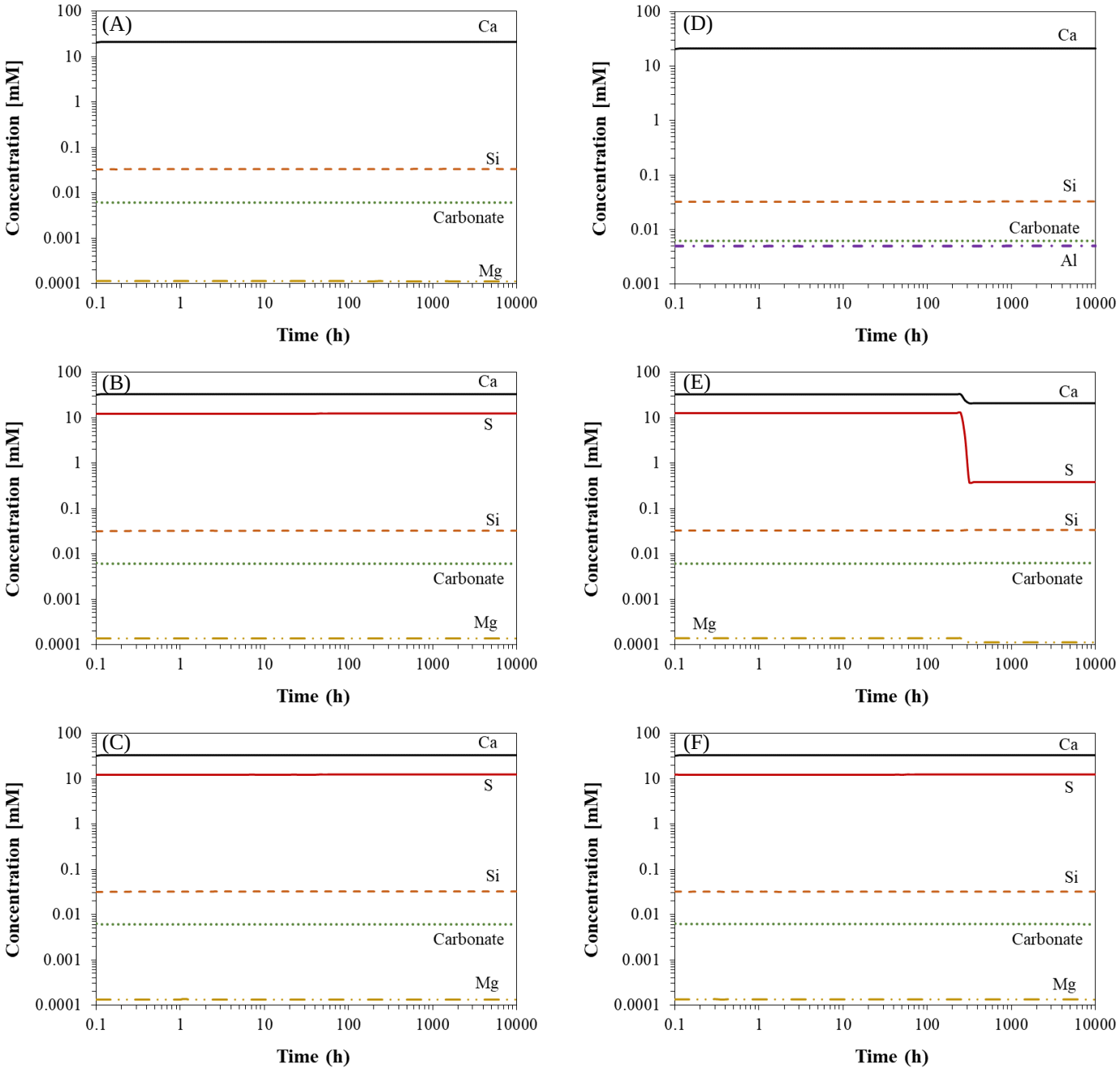

Figure B4 – Ca, S, Si, Al, Carbonate, and Mg concentration in the pore solution of (A) C_3S, (B) C_3S_2.5G, (C) C_3S_5.0G, (D) Al-C_3S, (E) Al-C_3S_2.5G, and (F) Al-C_3S_5.0G calculated by GEMS.

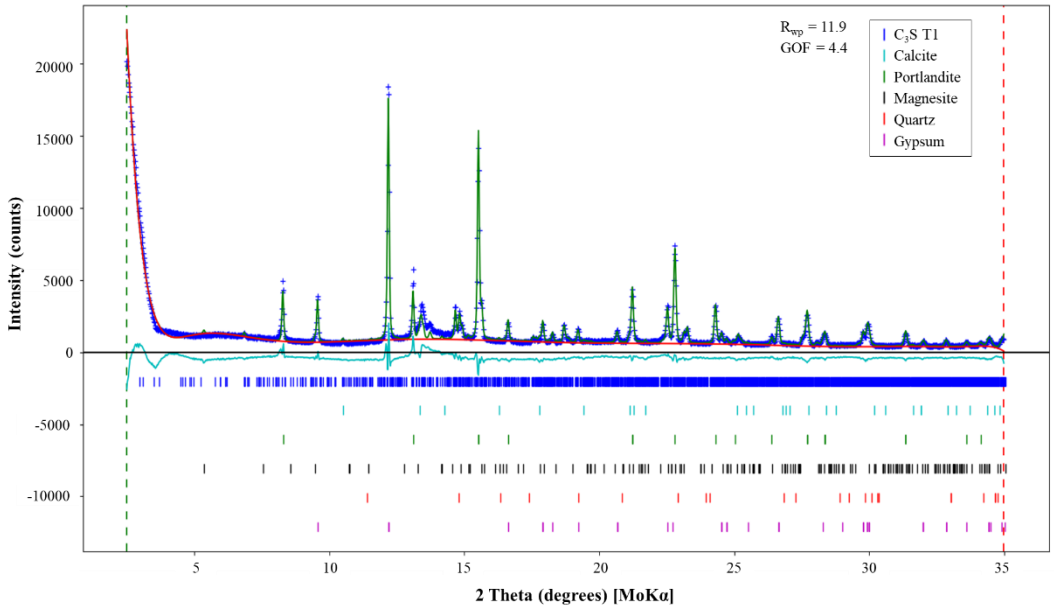

Figure B5– Example of fitted XRD patterns: C_3S_2.5G paste at 7 d.

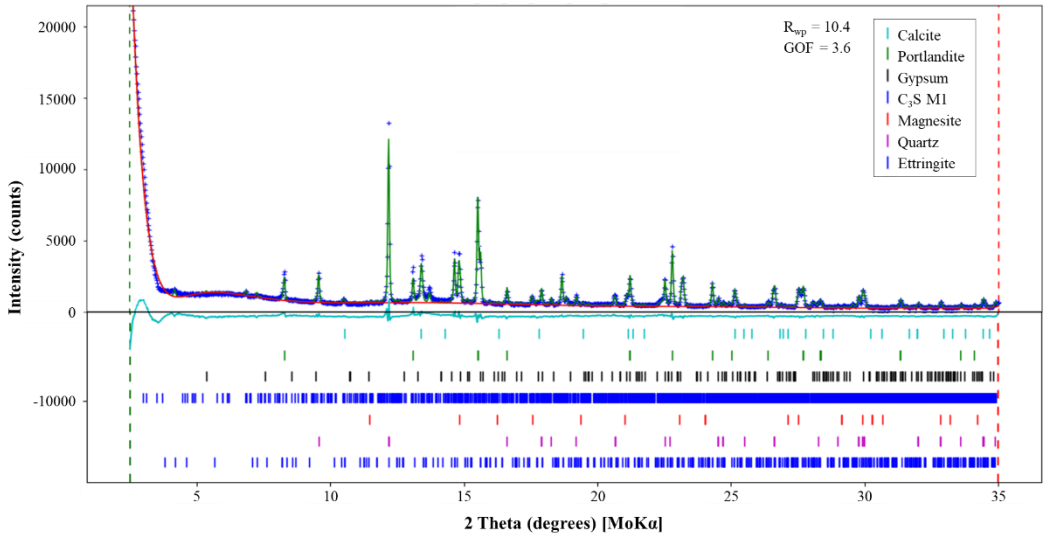

Figure B6 – Example of fitted XRD patterns: Al-C_3S_2.5G paste at 7 d.

ANNEX C

Supplementary Material for Chapter 5:
The role of sodium and sulfate sources on the rheology and hydration of C_3A polymorphs

---

10 SUPPLEMENTARY MATERIAL FOR CHAPTER 5

10.1 Methodology applied for the thermodynamic modeling

In order to verify the theoretical contribution of the hemihydrate crystallization into gypsum on the total heat release by the C_3A pastes hydration, thermodynamic modelling of the total heat release during the hydration of cb-C_3A-GYP and cb-C_3A-HEM pastes were done. Due to the lack of thermodynamic data of ort-C_3A and U-phase (the AFm phase formed in the sodium containg C_3A pastes), the thermodynamic modelling of Na-cb-C_3A and ort-C_3A pastes were not done.

Thermodynamic modeling of cb-C_3A-GYP and cb-C_3A-HEM pastes was carried out using the CemGEMS web application [1], coupled with the CEMDATA18 database [2]. For this, the chemical and physical characterization of cb-C_3A, gypsum and hemihydrate were used as input data. The reaction of cb-C_3A was modelled by the mP&K model, as presented by Kulik et al. [1], The total heat released during the first 10,000 hours of hydration of these pastes were analyzed and are presented in Figure S2.

Table C21 – Information of the reference pattern used for U-phase refinement.

References	Primary reference:	Post, K., Pollmann, H., Friedrich-Alexander Univ., Erlangen-Nurnberg, Erlangen, Germany., *ICDD Grant-in-Aid*, (1992)
	ICDD Reference code:	00-044-0272
Name and formula	Compound name:	Sodium Calcium Aluminum Sulfate Hydrate
	PDF index name:	Sodium Calcium Aluminum Sulfate Hydrate
	Empirical formula:	$Al_2Ca_4H_{30}NaO_{27}S_{1.5}$
	Chemical formula:	$NaCa_4Al_2O_6(SO_4)_{1.5}\cdot 15H_2O$
	Second chemical formula:	$3CaO\cdot Al_2O_3\cdot CaSO_4\cdot 0.5Na_2SO_4\cdot 15H_2O$
Crystallographic parameters	Crystal system:	Trigonal
	Space group:	P-3
	Space group number:	147
	a (Å):	5.7450
	b (Å):	5.7450
	c (Å):	30.0700
	Alpha (°):	90.0000
	Beta (°):	90.0000
	Gamma (°):	120.0000
	Calculated density (g/cm^3):	2.130
	Volume of cell (10^6 pm^3):	859.50
	Z:	1.50
	Reference intensity ratio (RIR):	0.50

Table C22 – Peak list of the reference pattern PDF 00-044-0272 (ICDD) [47] used for U-phase refinement.

Peak No.	Intensity [%]	d-spacing [Å]	2Theta (CuKα) [°]	HKL
1	53.0	10.02693	9	0 0 3
2	100.0	5.01193	18	0 0 6
3	9.0	4.45338	20	1 0 3
4	14.0	3.52951	25	1 0 6
5	9.0	3.34095	27	0 0 9
6	18.0	2.87136	31	1 1 0
7	9.0	2.77319	32	1 0 9
8	7.0	2.76150	32	1 1 3
9	9.0	2.50520	36	0 0 12
10	25.0	2.49262	36	1 1 6
11	17.0	2.41438	37	2 0 3
12	1.0	2.36047	38	2 0 4
13	23.0	2.23703	40	1 0 12
14	12.0	2.17872	41	1 1 9
15	12.0	1.99464	45	2 0 9
16	10.0	1.88778	48	1 1 12
17	9.0	1.85949	49	1 0 15
18	7.0	1.84754	49	2 1 3
19	11.0	1.76533	52	2 0 12
20	5.0	1.76058	52	2 1 6
21	10.0	1.65813	55	3 0 0
22	9.0	1.63578	56	3 0 3
23	3.0	1.58361	58	1 0 18
24	7.0	1.57417	59	3 0 6
25	3.0	1.56112	59	2 0 15
26	6.0	1.50381	62	2 1 12
27	4.0	1.49968	62	2 0 16
28	3.0	1.44391	64	1 1 18
29	5.0	1.43593	65	2 2 0
30	2.0	1.43179	65	0 0 21
31	3.0	1.42148	66	2 2 3
32	1.0	1.41742	66	3 0 11
33	2.0	1.38683	67	2 0 18
34	4.0	1.37994	68	3 1 0
35	5.0	1.37600	68	1 0 21
36	3.0	1.37139	68	2 1 15
37	2.0	1.36704	69	3 1 3
38	1.0	1.32933	71	2 1 16
39	1.0	1.31895	71	2 2 9
40	2.0	1.27542	74	3 1 9

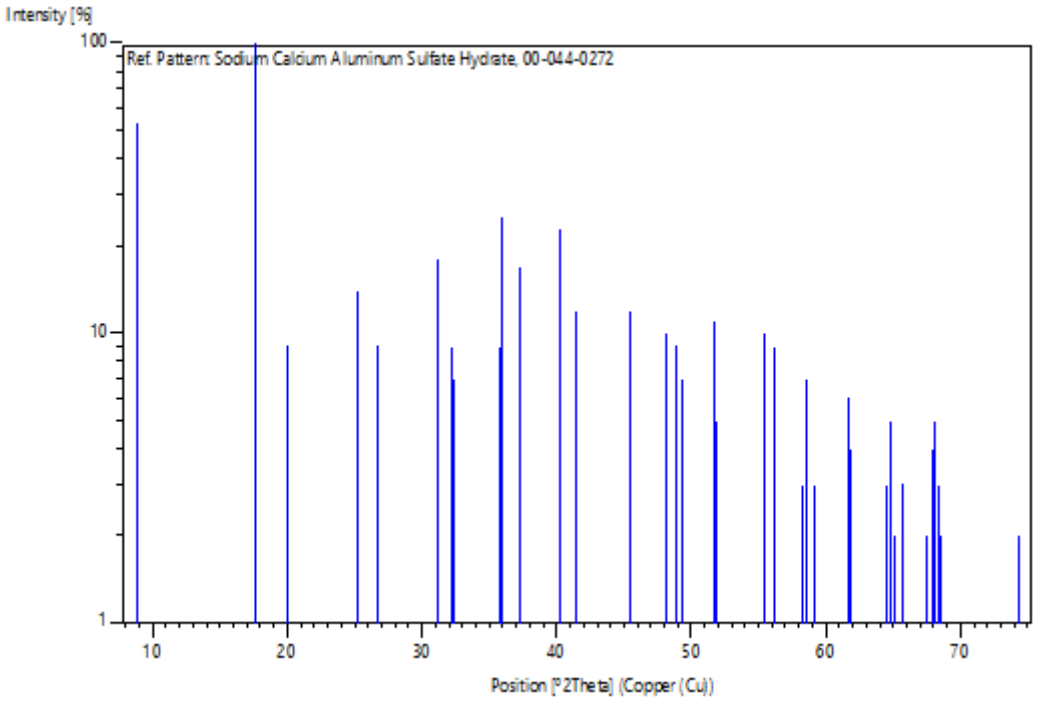

Figure C1 – Theoretical XRD pattern of the U-phase PDF 00-044-0272 (ICDD) [3]

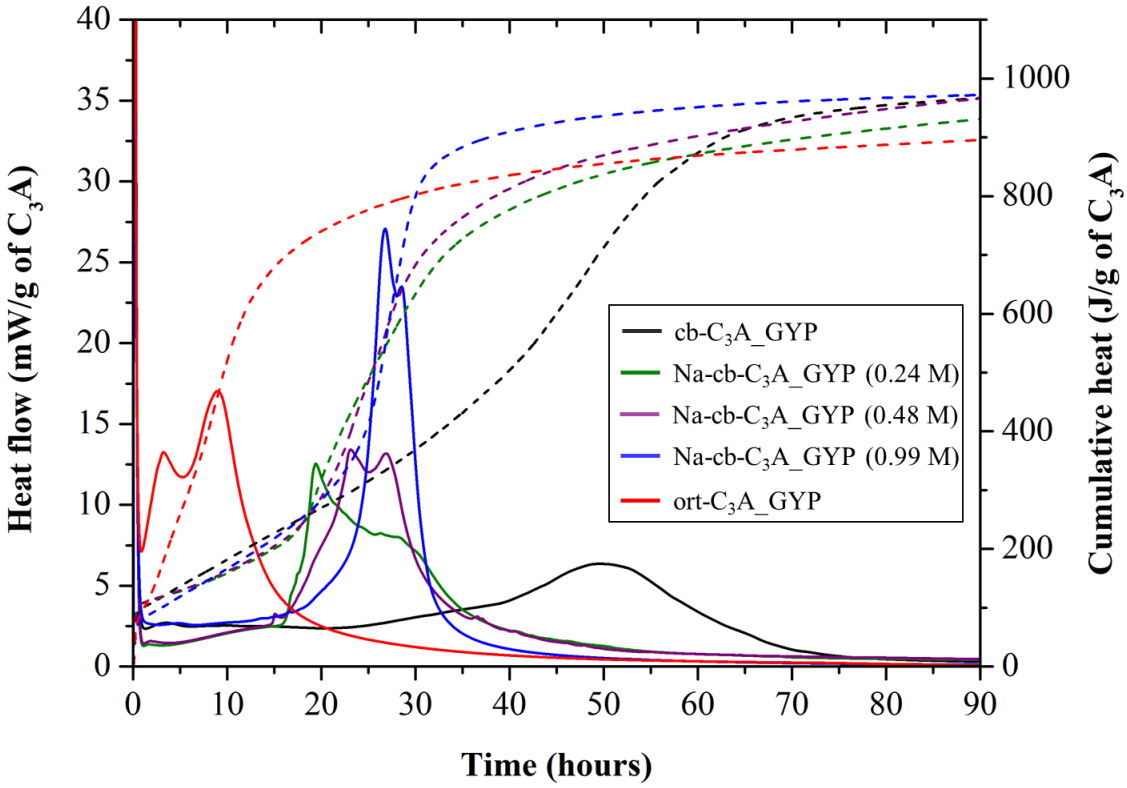

Figure C2 – Heat flow curves (solid lines and primary/left "y" axis) and cumulative heat curves (dashed lines and secondary/right "y" axis) of the cb-C_3A-gypsum pastes hydrating at different NaOH solutions and the ort-C_3A paste during the first 90 hours of hydration.

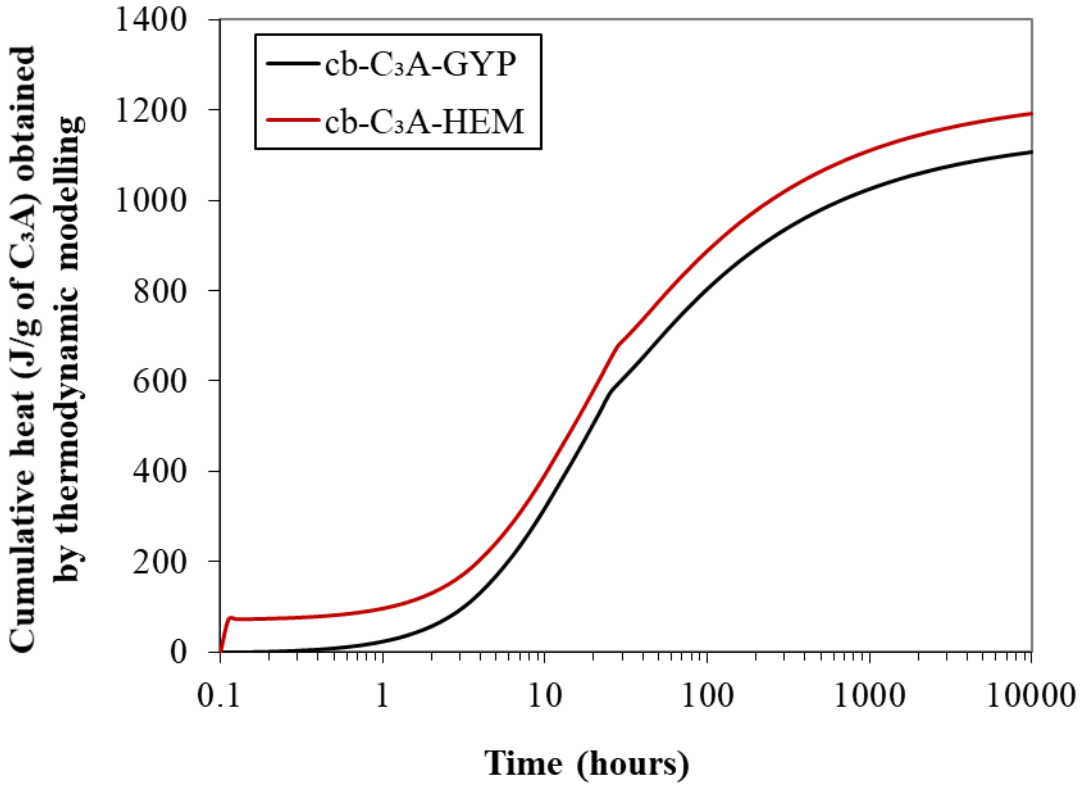

Figure C3 – Cumulative heat of cb-C_3A pastes with gypsum and hemihydrate during the first 10000 hours of hydration. Obtained by thermodynamic modelling.

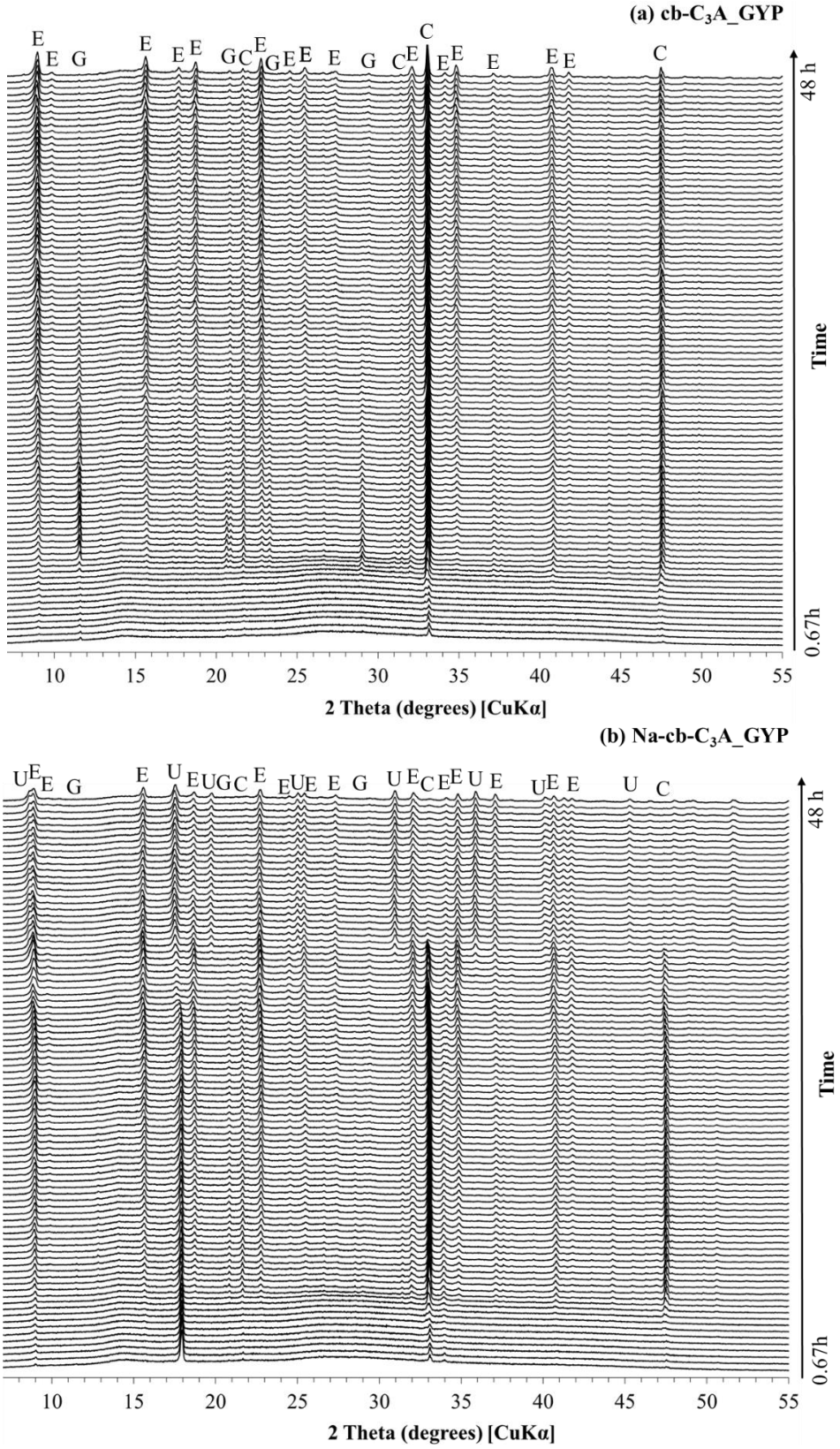
(a) cb-C3A_GYP
E
E G
E
E E
E
G C
E
G E
E
E
G
C E
C
E E
E
E
E E
C
48 h
Time
0.67h
10
15
20
25
30
35
40
45
50
55
2 Theta (degrees) [CuKα]
(b) Na-cb-C3A_GYP
U E
E G
E
U
E U G C
E
E U E
E
G
U
E C E E
U
E
U E
E
U
C
48 h
Time
0.67h
10
15
20
25
30
35
40
45
50
55
2 Theta (degrees) [CuKα]

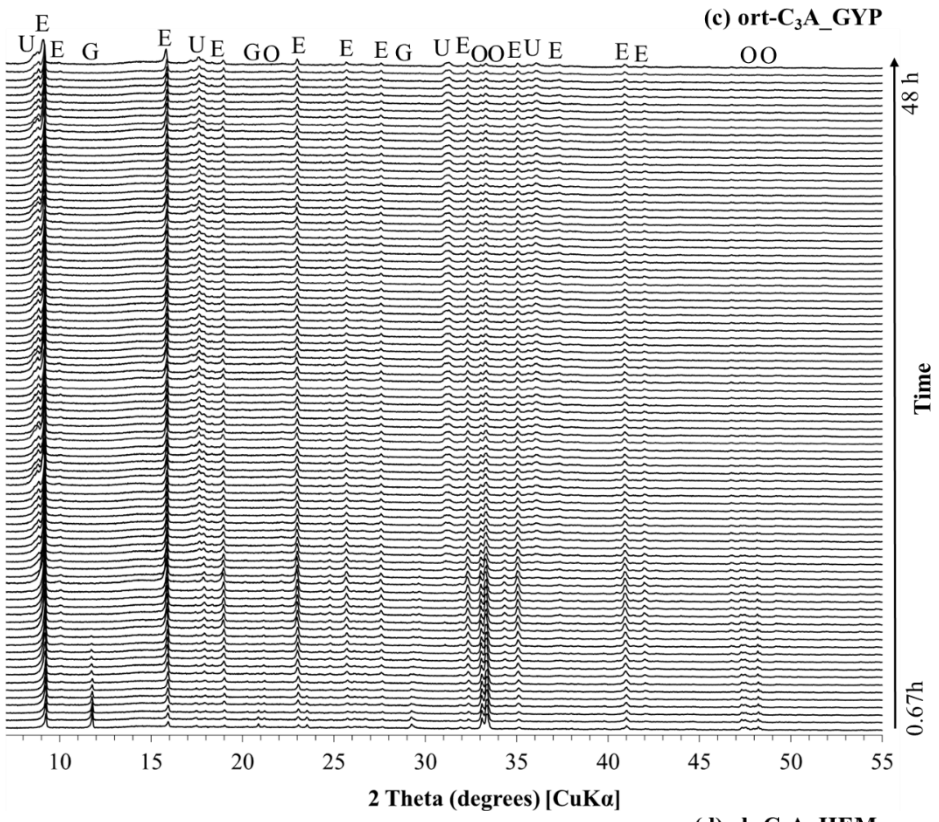
(c) ort-C3A_GYP
E
U E G E U E GO E E E G U E OO E U E E E O O
48 h
Time
0.67h
10 15 20 25 30 35 40 45 50 55
2 Theta (degrees) [CuKα]

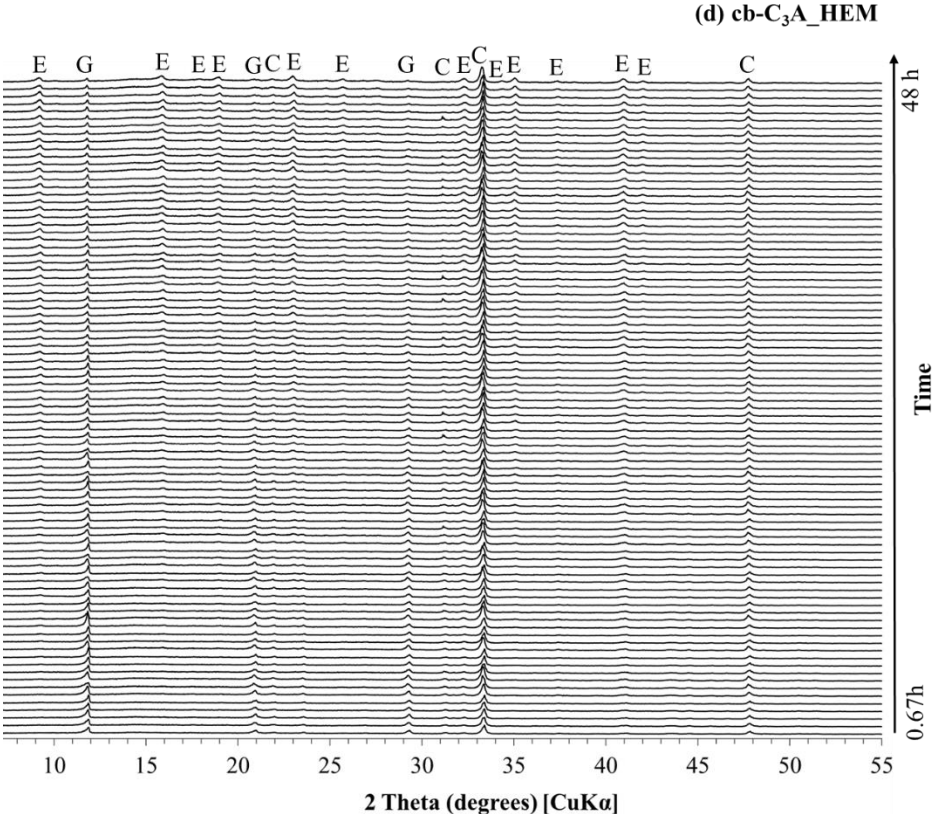
(d) cb-C3A_HEM
E G E E E G C E E G C E C E E E E E C
48 h
Time
0.67h
10 15 20 25 30 35 40 45 50 55
2 Theta (degrees) [CuKα]

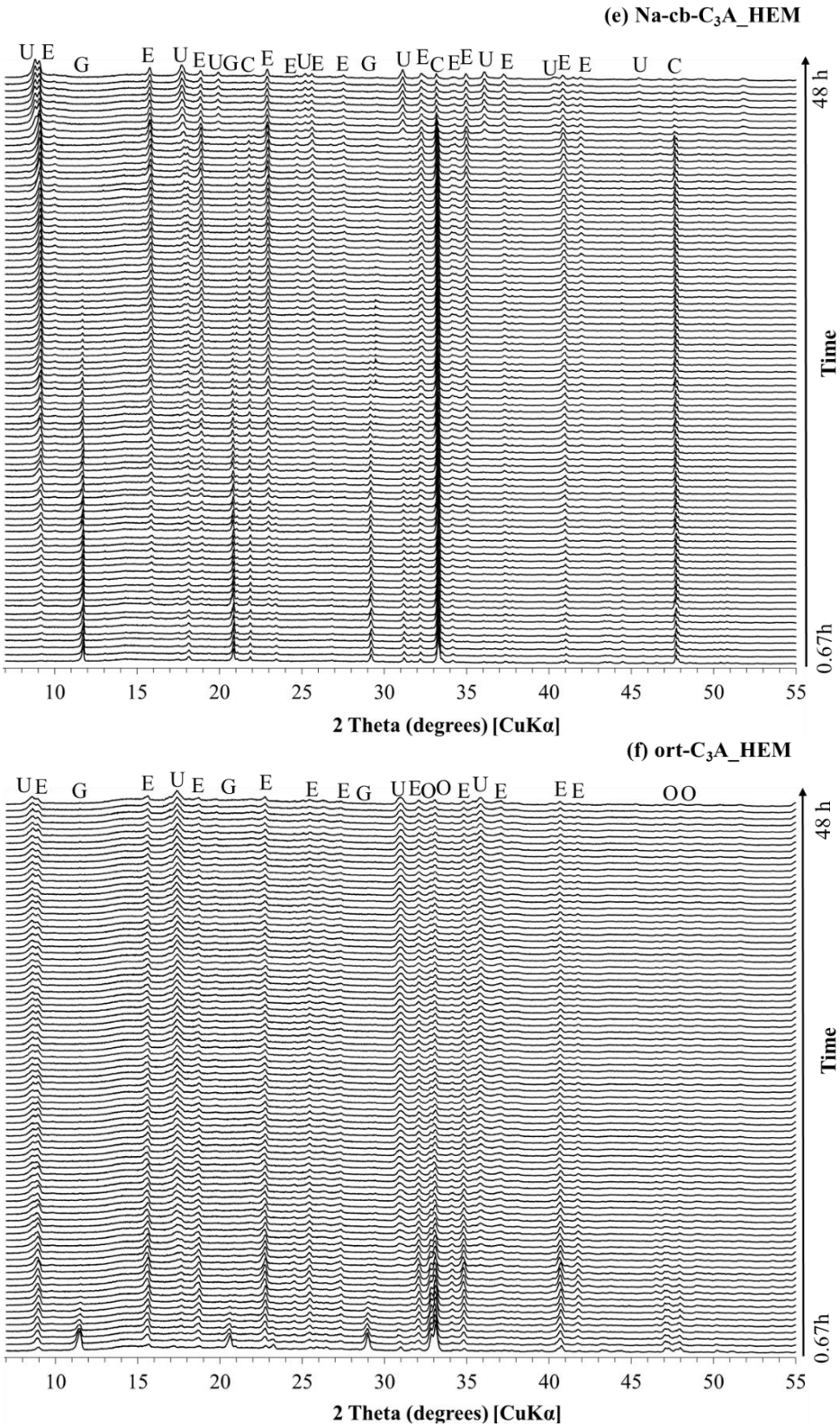

Figure C4 – *In-situ* XRD patterns of the mixes investigated: (a) cb-C_3A_GYP; (b) Na-cb-C_3A_GYP; (c) ort-C_3A_GYP; (d) cb-C_3A_HEM; (e) Na-cb-C_3A_HEM; (f) ort-C_3A_HEM. E: ettringite; G: gypsum; C: cb-C_3A; O: ort-C_3A; U: U-phase.

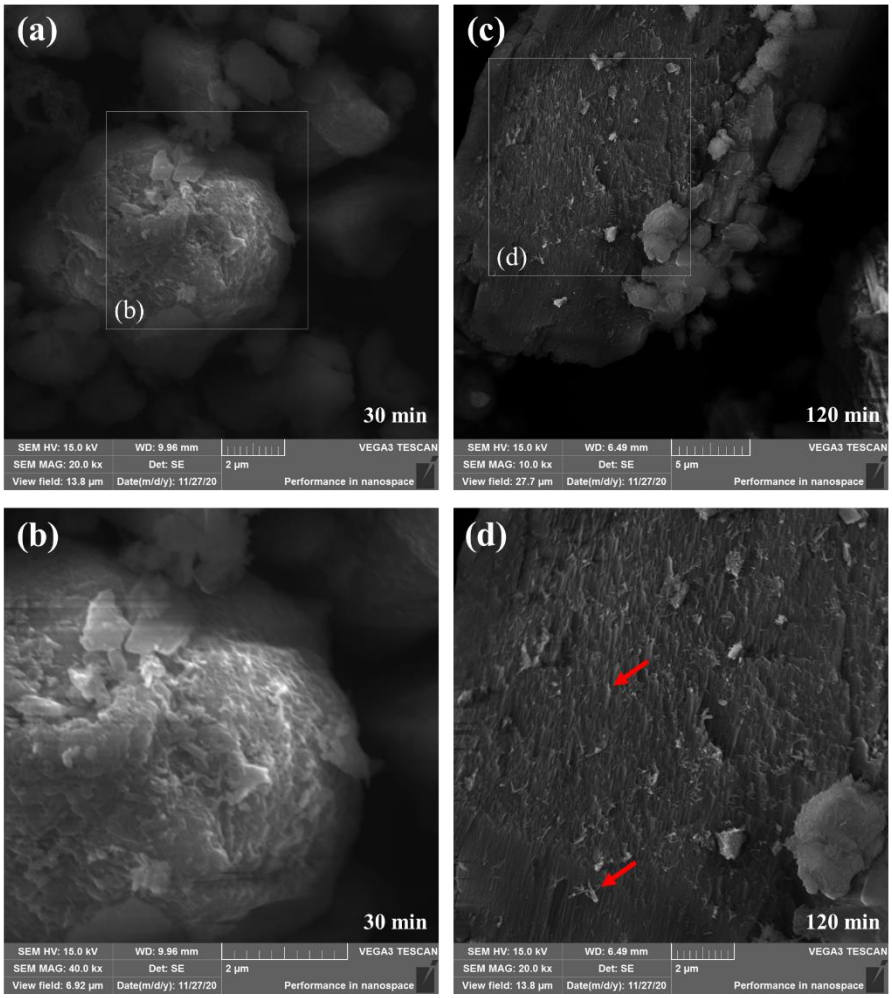

Figure C5 – SEM images of Na-cb-C_3A_GYP with 30 minutes of hydration [(a) ×20000; (b) ×40000] and 120 minutes of hydration [(c) ×10000; (d) ×20000]. The arrows indicate ettringite crystals.

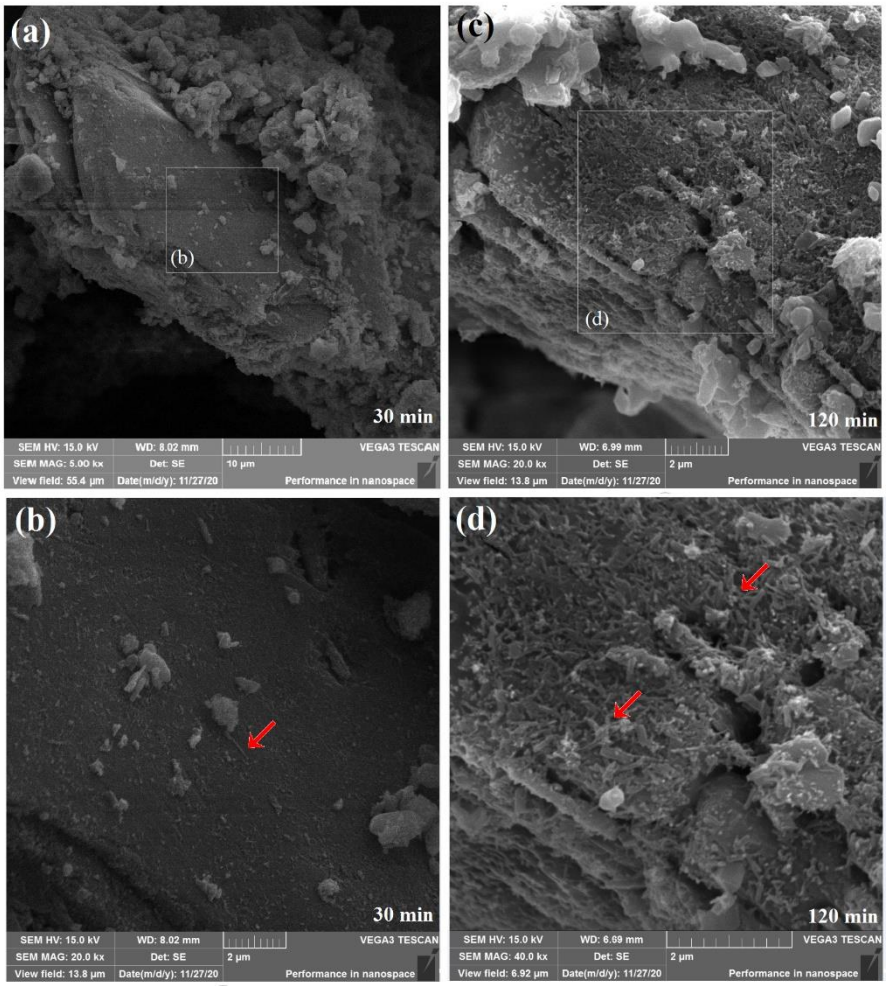

Figure C6 – SEM images of Na-cb-C_3A_GYP with 30 minutes of hydration [(a) ×5000; (b) ×20000] and 120 minutes of hydration [(c) ×20000; (d) ×40000]. The arrows indicate ettringite crystals.

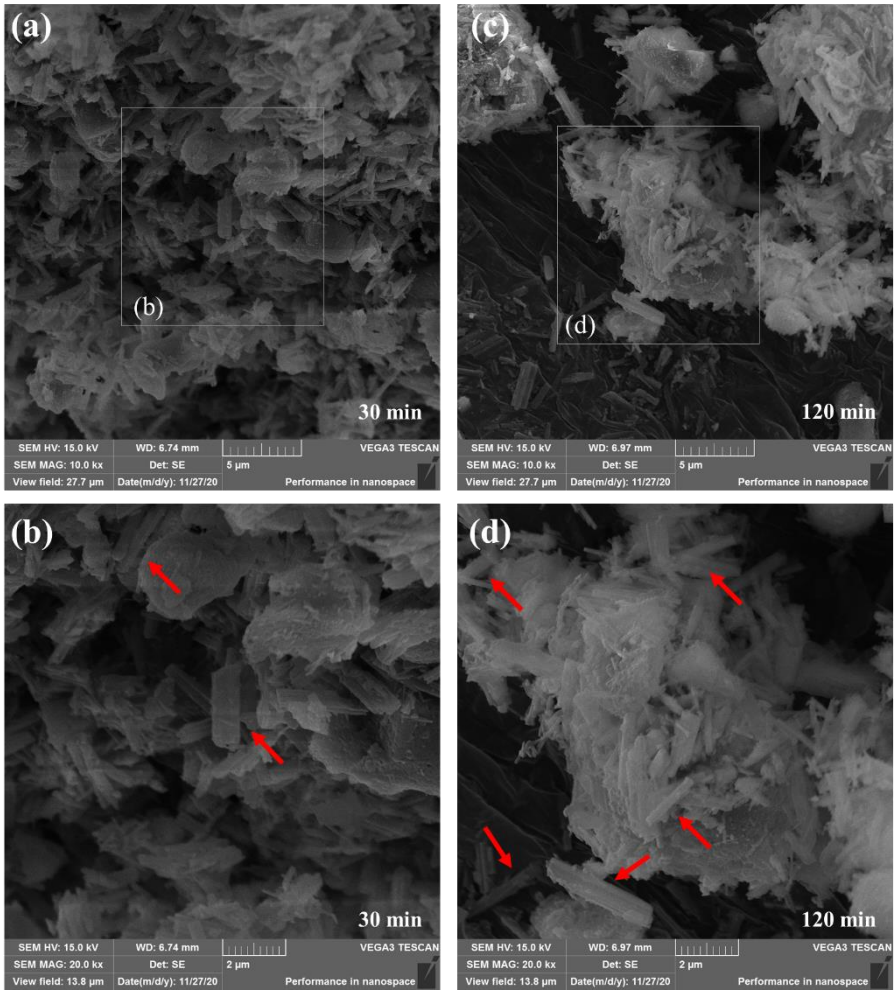

Figure C7 – SEM images of ort-C_3A_GYP with 30 minutes of hydration [(a) ×10000; (b) ×20000] and 120 minutes of hydration [(c) ×10000; (d) ×20000]. The arrows indicate ettringite crystals.

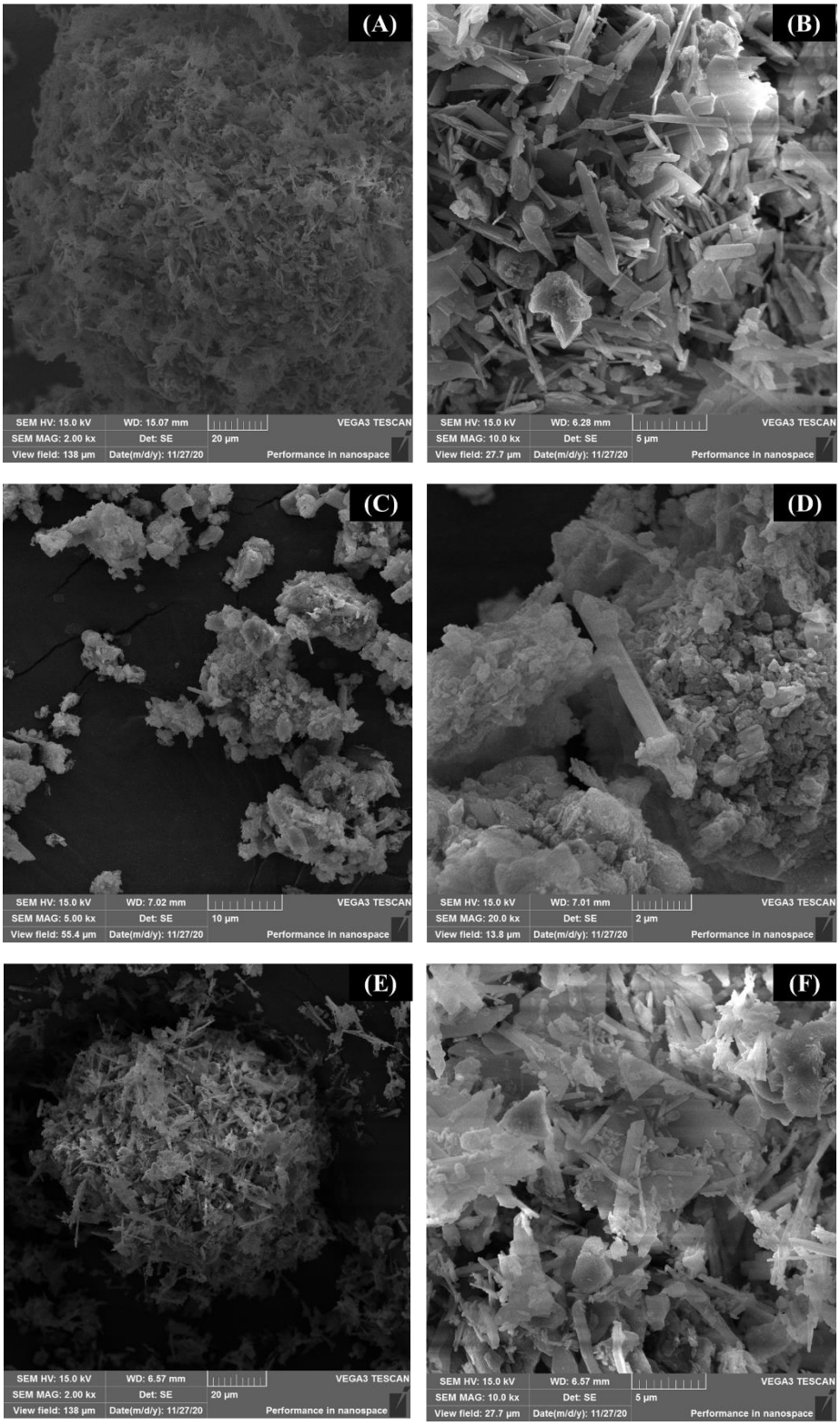

Figure C8 – SEM micrography of: (A) and (B) cb-C_3A-HEM, (C) and (D) Na-cb-C_3A_HEM, and (E) and (F) ort-C_3A_HEM pastes at 10 minutes of hydration.

REFERENCES

[1] D.A. Kulik, F. Winnefeld, A. Kulik, G.D. Miron, B. Lothenbach, CemGEMS – an easy-to-use web application for thermodynamic modeling of cementitious materials, RILEM Technical Letters. 6 (2021) 36–52. https://doi.org/10.21809/rilemtechlett.2021.140.

[2] B. Lothenbach, D.A. Kulik, T. Matschei, M. Balonis, L. Baquerizo, B. Dilnesa, G.D. Miron, R.J. Myers, Cemdata18: A chemical thermodynamic database for hydrated Portland cements and alkali-activated materials, Cement and Concrete Research. 115 (2019) 472–506. https://doi.org/10.1016/j.cemconres.2018.04.018.

[3] K. Post, H. Pollmann, PDF 00-044-0272, ICDD Grant-in-Aid, Friedrich-Alexander-Universität. (1992).

ANNEX D

Supplementary Material for Chapter 6:
Hydration and interactions between C_3S and C_3A polymorphs in the presence of different calcium sulfates

---

11 SUPPLEMENTARY MATERIAL FOR CHAPTER 6

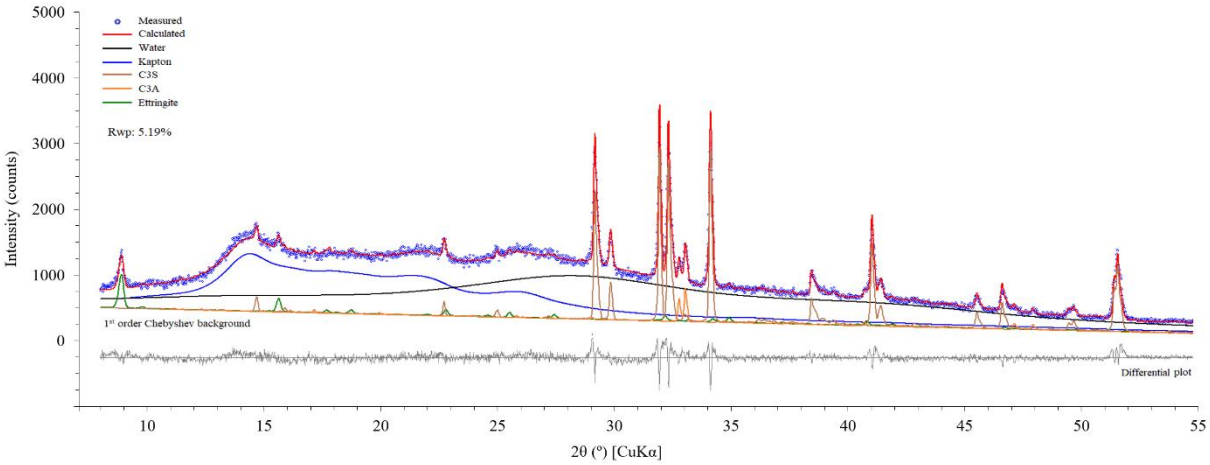

Figure D1. Example of fitted in-situ XRD pattern (for Al-C_3S_cb-C_3A_GYP at 0.5 hours of hydration).

Table D23. Chemical composition (wt.%) of the raw materials used, obtained by XRF.

Oxides	**C_3S**	**Al-C_3S**	**cb-C_3A**	**ot-C_3A**	**Gypsum**	**Hemihydrate**
CaO	72.18	72.55	60.89	56.58	34.04	34.04
SiO_2	25.11	25.37	0.43	0.18	0.95	0.95
Al_2O_3	-	0.81	35.52	36.70	0.09	0.09
MgO	0.95	0.50	0.11	0.09	0.81	0.81
Na_2O	-	-	0.03	3.98	-	-
Fe_2O_3	0.06	0.06	0.08	0.06	0.16	0.16
SO_3	0.02	-	0.02	0.03	46.05	46.05
LOI*	1.47	0.58	2.76	2.20	17.53	17.53
MAC (cm^2/g)**	96.24	96.82	84.96	80.91	63.11	69.67

*LOI: loss on ignition; **MAC: mass absorption coefficient.

Table D24. Mineralogical composition (wt.%) of the raw materials used.

Phase	**ICSD code**	**C_3S**	**Al-C_3S**	**cb-C_3A**	**ot-C_3A**	**Gypsum**	**Hemihydrate**
C_3S T1	4331	95.7	98.7	-	-	-	-
C_3S M1	*	-	-	-	-	-	-
C_3A cubic	1841	-	-	96.9	5.6	-	-
C_3A orthorhombic	1880	-	-	-	94.4	-	-
Gypsum	151692	-	-	-	-	96.1	97.2
Bassanite	69060	-	-	-	-	-	-
Calcite	73446	1.5	0.5	-	-	-	-
Dolomite	66333			-	-	-	2.4
Magnesite	40117	1.5	0.9	-	-	3.4	-
Portlandite	202220	1.3	-	-	-	-	-
Mayenite	261586	-	-	2.0	-	-	-
Lime	75786	-	-	1.1	-	-	-
Quartz	200721	-	-	-	-	0.5	0.4
Rwp (%)	-	10.7	11.4	13.3	14.7	11.7	11.3

*Noirfontaine et al., Zeitschrift Fur Kristallographie, 227 (2012), 102–112.

Table.D25. Mix proportions of the pastes investigated (wt.%)

Mix	**C_3S**	**Al-C_3S**	**cb-C_3A**	**ot-C_3A**	**Gypsum**	**Hemihydrate**	**Water**	**MAC (cm^2/g)***
C_3S_cb-C_3A_GYP	59.36	-	5.16	-	2.14	-	33.33	66.12
C_3S_ot-C_3A_GYP	59.36	-	-	5.16	2.14	-	33.33	65.91
Al-C_3S_cb-C_3A_GIP	-	59.36	5.16	-	2.14	-	33.33	66.46
Al-C_3S_ot-C_3A_GYP	-	59.36	-	5.16	2.14	-	33.33	66.25
C_3S_cb-C_3A_HEM	59.61	-	5.19	-	-	1.87	33.33	66.33
C_3S_ot-C_3A_HEM	59.61	-	-	5.19	-	1.87	33.33	66.12
Al-C_3S_cb-C_3A_HEM	-	59.61	5.19	-	-	1.87	33.33	66.67
Al-C_3S_ot-C_3A_HEM	-	59.61	-	5.19	-	1.87	33.33	66.46

*MAC: mass absorption coefficient.